Earth Observing System (EOS)
Aura Microwave Limb Sounder (MLS)

Version 6.0*x* Level-2 and Level-3 data quality and description document

Nathaniel J. Livesey[1], William G. Read[1], Paul A. Wagner[1*], Michelle L. Santee[1], Lucien Froidevaux[1*], Michael J. Schwartz[1], Alyn Lambert[1], Luis F. Millán[1], Frank Werner[1], Hugh C. Pumphrey[2*], Gloria L. Manney[3,4*], Ryan A. Fuller[1], Robert F. Jarnot[1], Brian W. Knosp[1], Christina Vuu[5]

1. Jet Propulsion Laboratory, California Institute of Technology
2. University of Edinburgh
3. NorthWest Research Associates
4. New Mexico Institute of Mining and Technology
5. Raytheon

* Retired

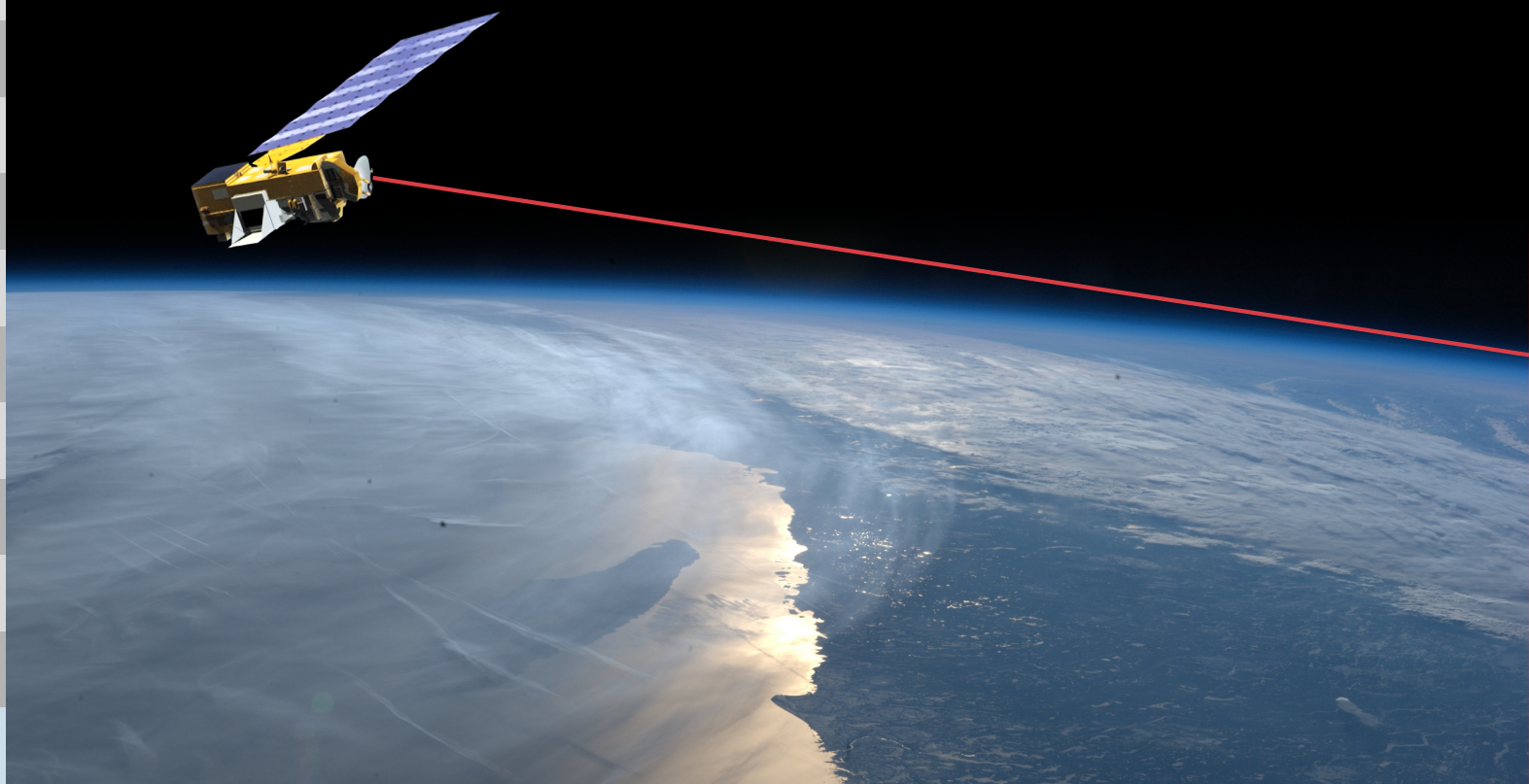

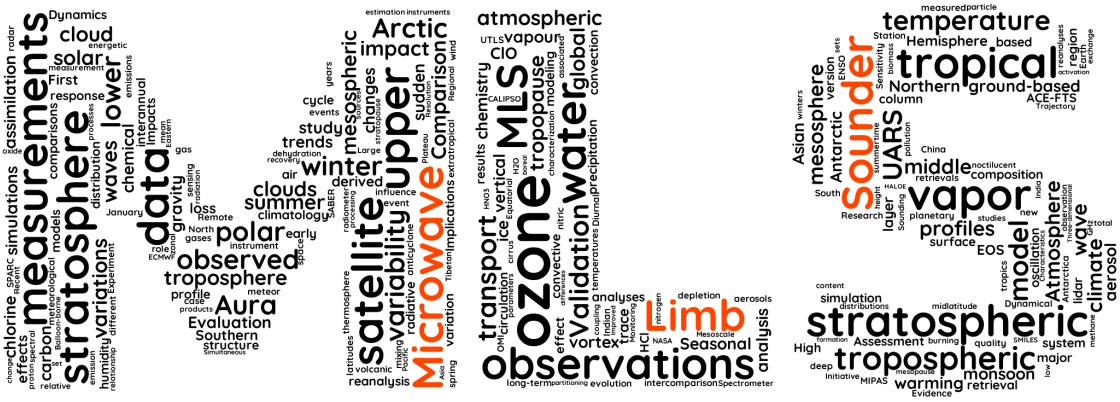

Design credit Luis Millán

Aura Microwave Limb Sounder (MLS) Version 6.0*x* Level-2 and Level-3 data quality and description document

Nathaniel J. Livesey[1], William G. Read[1], Paul A. Wagner[1*], Michelle L. Santee[1], Lucien Froidevaux[1*], Michael J. Schwartz[1], Alyn Lambert[1], Luis F. Millán[1], Frank Werner[1], Hugh C. Pumphrey[2*], Gloria L. Manney[3,4*], Ryan A. Fuller[1], Robert F. Jarnot[1], Brian W. Knosp[1], Christina Vuu[5]

1. Jet Propulsion Laboratory, California Institute of Technology
2. University of Edinburgh
3. NorthWest Research Associates
4. New Mexico Institute of Mining and Technology
5. Raytheon

[*] Retired

Version 6.0-1.0
March 26, 2026
doi: 10.5067/AURA/MLS/DOC/v6_dataqualitydocument

Jet Propulsion Laboratory
California Institute of Technology
Pasadena, California, 91109-8099

Work at the Jet Propulsion Laboratory, California Institute of Technology, was performed under contract with the National Aeronautics and Space Administration (80NM0018D0004).

Navigating this document

Each page of this document includes a navigation bar on the left-hand side. Clicking on "Help" takes you back to this page.

There is a one-page overview of the information in this document. You can return to it by clicking on the "Overview" tab in the navigation bar.

MLS data users are advised to read Chapter 1 first. The discussion includes a table summarizing key aspects of each MLS product that can be accessed from anywhere in the document by clicking on the "Table" tab in the navigation bar.

Chapter 3 describes each of the MLS "Level-2" data products individually. You can use the navigation bar to skip immediately to any of the product-specific sections.

Most sections include:

- A set of rules for screening out data not recommended for scientific use.
- A table summarizing the precision, accuracy, resolution, etc., for each product.

Clicking on the product name in the navigation bar takes you to the beginning of that section; clicking on the "S" and "T" symbols takes you directly to the screening rules and summary table, respectively, for that product.

Contents

Preface

One should perhaps be skeptical whenever it is stated from the outset that a large written work is intended to be a "living document". Such promises seem to be borne out only rarely, and the resulting documents grow stale sooner than hoped. In this particular case, however, whenever a new version of the MLS dataset has been generated in the last two decades, it has been accompanied by an updated edition of this document. These updates have always been written with the recognition that, even given the robustness and value of the MLS dataset, there continues to be scope for improvements. Previous editions of this document have been written during times in which the MLS team had plans and resources to pursue such improvements. This time, on the other hand, is different, as v6.0*x* will be the final version of MLS data of record, and thus this will be the final edition of this document (though we anticipate further minor updates to this edition before the end of the MLS project).

At the time of writing, the future for the Aura mission is unclear. From an engineering perspective, Aura operations can continue until August 2028, but other considerations may bring that end date forward. Some MLS team members have retired, and previous mechanisms for contacting them are no longer active. In the coming months and years, this will become true for other team members. Accordingly, statements made in earlier versions of this document that data users should "contact the MLS team with any questions" will become less helpful than they were before. The team intends to respond to queries sent to `mls-data@jpl.nasa.gov` for as long as feasible, ideally beyond the closeout of the MLS project. As a potential aid to contacting individuals at a later date, we list, at the bottom of this page, the ORCIDs for various MLS team members. That said, if ORCIDs become the only means for making contact, it should be understood that any assistance given at that juncture would likely be on an "as time allows" basis.

Proposed in 1988, launched in 2004, and continuing to operate at the time of writing in early 2026, the Aura MLS project represents nearly four decades of effort by countless talented and dedicated individuals. It has been a privilege for those of us continuing to work on the project to reap the rewards of all those efforts and serve as stewards of the unique and invaluable MLS dataset. It has also been a privilege and a true pleasure to witness the scientific discoveries that MLS observations have provided. We dedicate this document to all those involved in the MLS project in any capacity: those who developed the ground-breaking technologies that enabled the technique; those who had the vision and drive to propose Aura MLS for flight; those who designed, built, tested, and calibrated the instrument; those responsible for Aura mission and spacecraft development; those working on instrument and spacecraft operations; those developing and maintaining data processing algorithms and ground systems; those contributing to data validation; and, finally, to you — the world-wide community of scientists who have used and continue to use MLS data to advance our understanding of the Earth system. Our profound thanks!

The MLS Team

Froidevaux, Lucien: ORCID: 0000-0002-0681-1483
Fuller, Ryan A.: ORCID: 0000-0001-5785-9949
Knosp, Brian W.: ORCID: 0000-0002-2266-8883
Lambert, Alyn: ORCID: 0000-0003-3182-1824
Livesey, Nathaniel J.: ORCID: 0000-0001-8753-9153
Manney, Gloria L.: ORCID: 0000-0003-4489-4811
Millán, Luis F.: ORCID: 0000-0002-9509-9095
Pumphrey, Hugh C.: ORCID: 0000-0003-0747-1457
Read, William G.: ORCID: 0000-0001-8474-3490
Santee, Michelle L.: ORCID: 0000-0002-9466-7257
Schwartz, Michael J.: ORCID: 0000-0001-6169-5094
Werner, Frank: ORCID: 0000-0002-7141-0934

Where to find answers to key questions

This document serves two purposes. Firstly, it summarizes the quality of version 6.0*x* Aura MLS Level-2 and Level-3 data. Secondly, it conveys important information to the community of MLS data users on how those data are to be read and interpreted.

The MLS science team strongly encourages users of MLS data to thoroughly read the parts of the document relevant to their research interests. Chapter 1 should be read by all, as it describes essential general information. Chapter 2 is considered background material that may be of interest to some data users. Chapter 3 discusses individual MLS Level-2 data (profiles of geophysical quantities along the orbit track) in detail, product by product. Chapter 4 describes the MLS Level-3 data, which are averages of the quality-screened Level-2 products in various coordinate systems (maps, zonal means, etc.).

For convenience, this page provides answers, or pointers to answers, to anticipated questions.

Where do I get v6.0*x* MLS data?

All the MLS Level-2 and Level-3 data described here can be obtained from the NASA Goddard Space Flight Center Earth Science Data and Information Services Center (GES-DISC, `https://disc.gsfc.nasa.gov/`). In addition, selected products are available on the Zenodo archive (`https://zenodo.org/communities/aura-mls`).

What format are MLS data files in?

MLS Level-2 data are in HDF-EOS version 5 format (see Section 1.5, page 6). Level-3 data are in netCDF4 (see Section 4.2, page 179).

Which MLS data points should be avoided? How much should I trust the remainder?

These issues are described in Section 1.6 (starting on page 7), and on a product-by-product basis in Chapter 3. The key rules are:

- Only data within the appropriate pressure range (defined for each product in Chapter 3) should be used.
- Always consider the precision of the data, as reported in the `L2gpPrecision` field.
- Do not use any data points for which the precision is zero or a negative number, as that indicates poor information yield from MLS.
- Do not use data for any profile for which the corresponding entry in the integer `Status` array is an odd number.
- Data for profiles where `Status` is a non-zero even number should be approached with caution. See Section 1.6 on page 7, and the product descriptions in Chapter 3 for details on how to interpret the `Status` information.
- Do not use any data for profiles for which the corresponding entry in the `Quality` array is *smaller* than the threshold given in the section of Chapter 3 describing your product of interest.
- Do not use any data for profiles for which the corresponding value in the `Convergence` array is *larger* than the threshold given in the section of Chapter 3 describing your product of interest.
- Some products require additional screening to remove biases or outliers; see specific sections of Chapter 3 for details.
- Chapter 3 also provides information on the accuracy of each product.
- Data users are strongly encouraged to contact the MLS science team (`mls-data@jpl.nasa.gov`, or see the Preface for alternate means of contact) to discuss their anticipated usage of the data and are always welcome to ask further data quality questions.

Why do some species abundances show negative values, and how do I interpret these?

Some of the MLS measurements have a poor signal-to-noise ratio for individual profiles. Radiance noise can naturally lead to some negative values for these species. It is critical to consider such values in scientific study. Any analysis that involves taking some form of average will exhibit a high bias if the points with negative mixing ratios are ignored.

Document revision history

Version 6.0-1.0

First release of the v6.0*x* edition of this document, derived from the earlier edition for v5.0*x*, but with significant updates.

Chapter 1
Essential reading for users of MLS version v6.0*x* data

1.1 Scope and background for this document

This document describes the quality of the geophysical data products produced by version 6.0 of the data processing algorithms for the Earth Observing System (EOS) Microwave Limb Sounder (MLS) instrument on NASA's Aura spacecraft. The intended audience is those wishing to use Aura MLS data for scientific study.

This chapter, as its name implies, is considered essential background reading for all MLS data users. Chapter 2 provides additional optional background information, outlining the algorithms used to generate the "Level-2" data (geophysical products reported along the instrument track) from the input "Level-1" data (calibrated microwave radiance observations). The bulk of the document, in Chapter 3, provides information on each of the MLS standard Level-2 products. This includes quantification of resolution, precision, and accuracy, along with a description of data screening and usage rules and other caveats, notes on any anomalies, and, in some cases, selected comparisons to other datasets. Key aspects of each product are summarized in Table 1.1. Finally, Chapter 4 describes "Level-3" data products, derived from the Level-2 data. These provide easier access to collections of MLS observations (e.g., daily zonal means, monthly polar vortex averages) to facilitate additional studies using MLS data. Users of these Level-3 data should still read the Chapter 1 material and the product-specific information in Chapter 3 (though note that the quality screening rules detailed in Chapter 3 are applied as part of the generation of the Level-3 data).

The MLS v6.0*x* data have been preceded by versions v1.5*x*, v2.2*x*, v3.3*x*/v3.4*x*, v4.2*x*, and v5.0*x*. The v2.2*x* data are described in a series of validation papers published in the "Aura Validation" special issue of the *Journal of Geophysical Research*, with papers published in 2007 and 2008. This document updates some of the findings from those papers for v6.0*x*, compares a limited subset of available v6.0*x* results to some of the previous data versions, and gives more general information on the use of MLS data. As always, those wishing to use MLS data are advised to consult the MLS science team (see the Preface for contact details) concerning their intended use.

More information on the MLS instrument can be found in the document *An Overview of the EOS MLS Experiment* [*Waters et al.*, 2004]. A more general discussion of the microwave limb sounding technique and an earlier MLS instrument is given by *Waters et al.* [1999]. The theoretical basis for the Level-2 software is described by *Livesey and Snyder* [2004]. A crucial component of the Level-2 algorithms is the "Forward Model", which is described in detail by *Read et al.* [2004] and *Schwartz et al.* [2004]. The document *EOS MLS Retrieved Geophysical Parameter Precision Estimates* [*Filipiak et al.*, 2004] provides pre-launch estimates EOS MLS data precision. The impact of clouds on MLS measurements and the use of MLS data to infer cloud properties is described by *Wu and Jiang* [2004]. The above-listed documents are currently available from the MLS website (`https://mls.jpl.nasa.gov`) and the NASA Goddard Space Flight Center Earth Science Data and Information Services Center (GES-DISC, `https://disc.gsfc.nasa.gov/`). They have also been placed in the Zenodo archive; see the Bibliography entries in this document for full references and links. The Zenodo archive also contains a significant amount of other MLS-related information, including selected data products; see `https://zenodo.org/communities/aura-mls/`.

A subset of the information in those documents is also reported in a series of articles in the 2006 Aura special issue of the *IEEE Transactions on Geoscience and Remote Sensing*. Specifically, an overview of MLS is given by *Waters et al.* [2006], and the algorithms that produce the Level-2 data described here are reviewed by *Livesey et al.* [2006], *Read et al.* [2006], *Schwartz et al.* [2006], and *Wu et al.* [2006]. Other papers describe the calibration and performance of various aspects of the MLS instrument [*Jarnot et al.*, 2006; *Pickett*, 2006; *Cofield and Stek*, 2006] and the MLS ground data system [*Cuddy et al.*, 2006].

Table 1.1: Summary of key information for each MLS standard product in v6.0*x*. See Chapter 3 for details.

Product	Useful vertical range / hPa	Quality threshold [1]	Convergence threshold [2]	Notes	Product lead(s)
BrO	10–3.2	1.3	1.05	A,D,N	Luis Millán
CH3Cl	147–4.6	1.3	1.05	N,W	Michelle Santee
CH3CN	46–1.0	1.4	1.05	E,N,W	Michelle Santee
CH3OH	Generally unsuitable for scientific use				Michelle Santee
ClO	147–1.0	1.3	1.05	B,D,W	Michelle Santee
CloudTopPressure	770-85	N/A	N/A		Frank Werner
CO	100–0.001 215–146	1.5	1.03	C	Hugh Pumphrey Michael Schwartz
GPH	83–0.00046 261–100	0.2 0.9	1.03	O C,O	Michael Schwartz
H2O	83–0.001 316–100	0.7	2.0	O,T C,O,T	Alyn Lambert William Read
HCl	100–0.32	1.2	1.05	R,T,W	Lucien Froidevaux
HCN	See §3.12	0.2	2.0	E,N,T	Hugh Pumphrey
HNO3	215–1.5	See §3.13.7	See §3.13.7	C	Michelle Santee
HO2	22–0.046	N/A	1.1	A,D,N	Luis Millán
HOCl	10–2.2	1.2	1.05	A,N	Lucien Froidevaux
IWC	215–83	See §3.16.5	See §3.16.5	B,W	Alyn Lambert
IWP	N/A	See §3.17.5	See §3.17.5	B,W	Alyn Lambert
N2O	100–0.46	0.8	2.0	R,T	Alyn Lambert
O3 [3]	100–0.001 261–121	1.0	1.03	C	Lucien Froidevaux Michael Schwartz
OH	32–0.0032	N/A	1.1	D	Luis Millán
RHI [4]	316–0.001	See §3.21.6	See §3.21.6	C,O,T	William Read
SO2	215–10	0.95	1.03	E	William Read
Temperature [5]	83–0.00046 261–100	0.2 0.9	1.03	O C,O	Michael Schwartz

Notes:

A Users should consider using alternative versions of this product, generated using different algorithms. See Chapter 3.

B This product has significant biases in certain regions that should be considered or corrected for. See Chapter 3.

C Interference from clouds can affect this product at certain altitudes. See Chapter 3 for details.

D Biases in this product can be ameliorated (in selected conditions) by taking day/night differences. See Chapter 3.

E At some altitudes, this product contains biases of a magnitude that render the product useful only for the study of "enhancement events" (e.g., volcanic plumes, extreme fire pollution). See Chapter 3.

N This is a "noisy" product requiring significant averaging (e.g., monthly zonal mean). See Chapter 3 for details.

O This product contains significant outliers (e.g., spikes or oscillations) in some regions (typically from upper tropospheric clouds). These should be screened out as detailed in Chapter 3.

R The spectral region(s) used to retrieve this product has been revised at some point in response to a change in instrument behavior. Earlier MLS data versions relied on the original region.

T Care should be taken when considering long-term trends in measurements of this quantity. See Chapter 3.

W The radiances used to measure this product are also affected by atmospheric water vapor. During periods when MLS water vapor observations are unavailable, climatological water vapor profiles are assumed in retrievals of this product instead, introducing artifacts. See §1.10.2 and Chapter 3 for details.

[1] Only use profiles with `Quality` *greater* than this value.

[2] Only use profiles with `Convergence` *less* than this value.

[3] File also contains a swath giving the column abundance above the (MLS-defined) tropopause.

[4] Relative humidity with respect to ice computed from the MLS H_2O and Temperature data.

[5] File also contains a swath giving tropopause pressure (WMO definition) inferred from MLS temperatures.

1.2 Overview of the MLS dataset and v6.0*x*

1.2.1 Level-2 standard products

Chapter 3 describes the data quality for "Standard" products from the MLS instrument for v6.0*x*. The bulk of these are observations of vertical profiles of the abundance of BrO, CH_3Cl, CH_3CN, CH_3OH, ClO, CO, H_2O, HCl, HCN, HNO_3, HO_2, HOCl, N_2O, O_3, OH, and SO_2, along with temperature, geopotential height, relative humidity (deduced from the H_2O and temperature data), and cloud ice water content, all described as functions of pressure. Most of these profiles are output on a grid that has a vertical spacing of six surfaces per decade change in pressure (~2.5 km), thinning out to three surfaces per decade above 0.1 hPa. Exceptions include water vapor, temperature, ozone, and relative humidity, which are on a finer 12-per-decade grid from 1000 hPa to 1 hPa. Cloud ice water content is also reported on this finer grid, though those profiles do not extend to the stratosphere and mesosphere. The OH product maintains a six-per-decade grid spacing into the upper mesosphere. Horizontally, the profiles are spaced by 1.5° great-circle angle along the orbit, which corresponds to about 160 km along track. The true vertical and along-track horizontal resolution of the products is typically somewhat coarser than the reporting grid described here. The cross-track resolution of the MLS products is set by the horizontal width of the MLS antenna beam. This varies by observing frequency, and thus product, over the range from ~3 to ~13 km. For some of the products, the signal-to-noise ratio is too low to yield scientifically useful data from a single MLS profile observation. In these cases, some form of averaging (e.g., weekly maps, monthly zonal means, etc.) will be required to obtain more useful results. The remaining MLS standard products, cloud ice water path and cloud top pressure (a new product in v6.0*x*), are not vertically resolved.

1.2.2 Level-2 diagnostic products

In addition to the standard products, the MLS Level-2 data include many "diagnostic" products. The bulk of them are similar to the standard products, in that they represent vertical profiles of retrieved species abundances. However, the information on these diagnostic products has typically been obtained from a different spectral region than that used for the standard products. These diagnostic products are not discussed in this document. Further information on them is available from the MLS science team.

1.2.3 Level-3 products

Chapter 4 of this document details the MLS Level-3 products, introduced in v4.2*x*. These products are averages (and other statistics) of MLS Level-2 observations on various geophysical grids (maps, zonal averages, polar-vortex averages, etc.) at daily and monthly time resolution. The Level-3 data are generated from the Level-2 data, applying all the screening rules described for each product in Chapter 3.

1.2.4 Different versions within the v6.0*x* family

At the time of writing, the current version of the data processing software is version 6.03, producing files labeled `v06-03`. Any minor updates for bug fixes (typically related to a failure to process a specific day within the record, and having no impact on other days) or to reflect changes in input data such as the analysis fields used as a priori information for temperature will be referred to as v6.04, v6.05, etc. This version of the document is intended to be applicable to any v6.0*x* data files (we note that the bulk of the MLS 20-plus-year data record was processed with the earlier v6.01 software). Any substantial changes at a later date (e.g., due to a change in the MLS instrument performance) may necessitate a larger change in the data processing software and/or its configuration. These will be numbered v6.1*x* etc. and will be accompanied by an updated version of this document (though not necessarily immediately, depending on the circumstances dictating the update).

1.3 MLS data validation status

As discussed above, a complete set of MLS validation papers details the validation of the earlier v2.2*x* data. The majority of the v2.2*x* MLS data products have, accordingly, completed "Stage 3 Validation", defined[1] as:

[1] See `https://www.earthdata.nasa.gov/learn/earth-observation-data-basics/data-maturity-levels`

> *Product accuracy has been assessed. Uncertainties in the product and its associated structure are well quantified from comparison with reference in situ or other suitable reference data. Uncertainties are characterized in a statistically robust way over multiple locations and time periods representing global conditions. Spatial and temporal consistency of the product and with similar products has been evaluated over globally representative locations and periods. Results are published in the peer-reviewed literature.*

Subsequent work, including that described in this document, has further validated aspects of more recent versions of the MLS data for some products (notably ozone and water vapor), working towards establishing them as "Stage 4" validated, defined as:

> *Validation results for stage 3 are systematically updated when new product versions are released and as the time-series expands.*

Finalizing the validation of the v6.0*x* MLS dataset will be the focus of the MLS team during the remaining years of the project.

1.4 Differences between MLS v6.0*x* data and v5.0*x* data

The most significant changes between MLS v6.0*x* data and the previous v5.0*x* dataset are associated with the N_2O and Temperature products. There were also some updates to the way cloud impacts on MLS observations are flagged, and some new cloud metrics have been included. In addition to these specific modifications, changes in other products have resulted as an indirect response to the temperature changes detailed below. The threshold values of `Quality` and `Convergence` (see below) to be used in data screening have been reaffirmed or updated. As described in Section 1.10.2, additional screening rules have been devised for several products in light of a change in instrument operation strategy.

1.4.1 Changes to the N_2O product in v6.0*x*

As discussed by *Livesey et al.* [2021] (see also Section 1.10.2), the v5.0*x* algorithms included a correction for a long-term drift (of about 1.3% per decade) in the calibration of the MLS 190-GHz radiometer subsystem that started around 2010. This drift led to statistically significant drifts in comparisons between the MLS v4.2*x* observations of species measured by this radiometer and measurements by other instruments, notably for H_2O and N_2O. Although the correction applied in v5.0*x* ameliorated the drift in H_2O (at least in comparison to ACE-FTS observations), significant issues remained with the N_2O product. The v6.0*x* algorithms include a further correction aimed at addressing those issues (see Section 2.8 for more details). Note that only species measured by the 190-GHz radiometer are affected by the drift (specifically H_2O, N_2O, HCN, and upper stratospheric HNO_3). No other MLS products are directly impacted.

1.4.2 Changes to the Temperature product in v6.0*x*

MLS obtains information about atmospheric temperature profiles from two largely independent sources. Firstly, cases where optically thick limb paths are observed convey information on the temperature in the region where the atmosphere becomes opaque (nadir-viewing microwave radiometers measure atmospheric temperature in the same manner). Secondly, measurements of spectral line shape convey information about atmospheric pressure along the individual limb ray paths. By combining this pressure information with knowledge of limb ray path tangent altitudes (deduced from instrument and spacecraft pointing knowledge), temperature profiles can be derived by assuming atmospheric hydrostatic balance. Historically, these two approaches have given conflicting information, disagreeing by 5–6 K (which amounts to a difference of only ~2% in terms of instrument calibration, well within expectations and original instrument requirements). This discrepancy likely arises from uncertainties in the radiometric and spectral calibration of the MLS 118-GHz observations, measured pre-launch, although uncertainties in spectroscopic parameters may play a role too. In v5.0*x* and earlier versions, in order to reduce the biases these differences introduced in the retrieved temperature profiles, the MLS retrievals only considered information from each channel measuring the 118-GHz oxygen line (the

main source of MLS temperature information in the mid-stratosphere and above) over specific height ranges, in order to favor the first (optically thick) source of information over the second (line shape and hydrostatic balance). Although this approach reduced the magnitude of systematic (vertically oscillatory) biases in the MLS temperature product, the resulting profiles had poorer precision and vertical resolution than would be obtained if the radiances were used over the full vertical scan range. As part of the v6.0*x* development, the MLS team sought to resolve this issue.

In order to identify potential corrections to the MLS 118-GHz calibration information, a diagnostic retrieval experiment was constructed in which, rather than using observations of O_2 emission at 118-GHz to infer temperature (based on the well-known abundance of O_2), instead O_2 abundances were retrieved (with temperature profiles constrained to the values retrieved by MLS). These retrievals yielded estimates of O_2 abundances that were ~20% higher than the true value. Given that MLS observations of other species such O_3 and H_2O (which have spectral signals that are just as strong as that from O_2) typically agree with correlative observations to within ~10%, we concluded that there was indeed a significant calibration error in the 118-GHz radiometer (which, notably, employs a different class of receiver technology from that used for other MLS radiometers [*Waters et al.*, 2006]). Using the known O_2 concentration as a guide, several possible sources of error, including the MLS field-of-view width, radiometric non-linearities, instrument mirror spill-over factors, and the O_2 lineshape, were ruled out as main sources of the problem. It was ultimately determined that the spectral placement of specific channels and/or their individual shapes were the most likely leading contributors to calibration error (the impacts of these two factors are not distinguishable). A new set of channel shapes for MLS "Band 1", targeting the 118-GHz O_2 line, were developed to give a more realistic estimate of O_2 abundance from these diagnostic retrievals. These channel shape adjustments (which amounted to imposing a slope across each passband followed by a renormalization) were within the range of uncertainty in MLS pre-launch calibration data. Using these revised channel shapes in v6.0*x* resulted in better agreement between the two approaches to measuring atmospheric temperature. This in turn enabled use of all the Band-1 (118-GHz) MLS radiance signals, improving the precision and vertical resolution of the MLS temperature product in the vertical range from the mid-stratosphere to the mid-mesosphere, as discussed in more detail in Section 3.23.

1.4.3 Changes to flagging of cloud impacts in v6.0*x*

The MLS retrieval algorithms and software take steps to avoid using radiances that may have been contaminated by clouds (see Section 2.5). The v6.0*x* algorithms use the same approach as v5.0*x* in this regard. However, the MLS team has adopted a new philosophy for setting the flags (in the `Status` diagnostic, see below) that indicate possible cloud impacts on the retrieved composition and temperature profiles. In v5.0*x* and earlier versions, these flags were set based on an assessment of the potential cloudiness of a scene, using criteria that were decoupled from those used in the composition and temperature retrievals. For v6.0*x*, the flags are set purely on whether the retrievals avoided specific radiances because of potential cloud contamination. Put another way, in v5.0*x* and earlier versions, the cloud flag would indicate:

> *The region of the atmosphere measured here includes signatures of clouds that may have impacted the measurements.* (V5.0*x* and earlier versions)

whereas, in v6.0*x*, these flags should be interpreted as:

> *The MLS algorithms flagged some of the radiances in this region as being affected by clouds and did not use them in the retrieval of this composition/temperature profile, thus changing the character of the retrieved profile in some manner that sets it apart from those in scenes marked cloud-free.* (V6.0*x*)

This change has no practical implications for data users; it is noted here purely for completeness.

Table 1.2: Additional swaths in specific standard product files.

Product	Additional swaths	Notes
HNO3	HNO3-190, HNO3-240	Nitric acid from the 190- and 240-GHz radiometers
IWC	IWP	Partial Ice Water Path (this file has no a priori swath)
O3	O3 column	Ozone column above the tropopause given in the Temperature file
RHI	UTRHI, UTRHI-APriori	"Single layer" relative humidity (see Section 3.21)
Temperature	WMOTPPressure	Tropopause (WMO definition, based on MLS temperature)

1.5 Aura MLS Level-2 data file formats, contents, and quality information

All the MLS Level-2 data files described here are available from the NASA Goddard Space Flight Center Earth Science Data and Information Services Center (GES-DISC, see https://disc.gsfc.nasa.gov/). The standard and diagnostic products are stored in the EOS MLS *Level 2 Geophysical Product* (L2GP) files. These are standard HDF-EOS (version 5) files containing swaths in the Aura-wide standard format. For more information on this format see *Craig et al.* [2003]. Sample software for reading these files has been released as open source in various languages and is available at https://github.com/NASA-MLS/Level-2-readers. Alternatively, any standard HDF and NetCDF software or interfaces (e.g., in Python, Julia, etc.) can be used to read the files as regular HDF5/NetCDF4 files (the HDF-EOS "swaths" discussed below can be found in the HDFEOS/SWATHS group).

The standard products are stored in files named according to the convention

```
MLS-Aura_L2GP-<product>_v06-02-c01_<yyyy>d<ddd>.he5
```

where <product> is BrO, O3, Temperature, etc. The Level-2 data are produced on a one-day granularity (midnight to midnight, universal time) and named according to the observation date, where <yyyy> is the four-digit calendar year and <ddd> is the day number in that year (001 = 1 January).

These files contain the corresponding standard product in an HDF-EOS swath given the same name as the product, e.g., "H2O". With the exception of the IWC and CloudTopPressure files, each file also contains the a priori values for that product (see Section 1.8 for details) inside a second swath whose name ends with the substring "-APriori".

The L2GP HNO3, IWC, O3, RHI, and Temperature files are special in that they carry extra standard or non-standard products, as detailed in Table 1.2. Given that some L2GP files contain multiple swaths, it is important to ensure that the correct swath in the L2GP files is requested from the file. In the case where the "default" swath is requested (i.e., no swath name is supplied) most HDF software will access the one whose name falls earliest in ASCII order. This generally results in the desired swath being returned for all products. For example, for temperature, the standard "Temperature" product will be read in preference to the "WMOTPPressure" swath that gives tropopause pressures.

Each swath contains data fields L2gpValue and L2gpPrecision, which describe the value and precision (reported at 1σ) of the data, respectively. Data points for which L2gpPrecision is set negative or zero *should not be used*, as this flags that the resulting precision is worse than 50% of the a priori precision, indicating that the instrument and/or the algorithms have failed to provide enough useful information for that point (the rare exceptions to this rule are noted on a product-by-product basis in Chapter 3). In addition to these fields, fields such as latitude etc. describe geolocation information. The field time describes time, in the EOS standard manner, as the number of seconds (including leap seconds) elapsed since midnight universal time on 1 January 1993.

The L2GP-DGG ("Diagnostic products on a Geophysical Grid") file contains a large number of additional

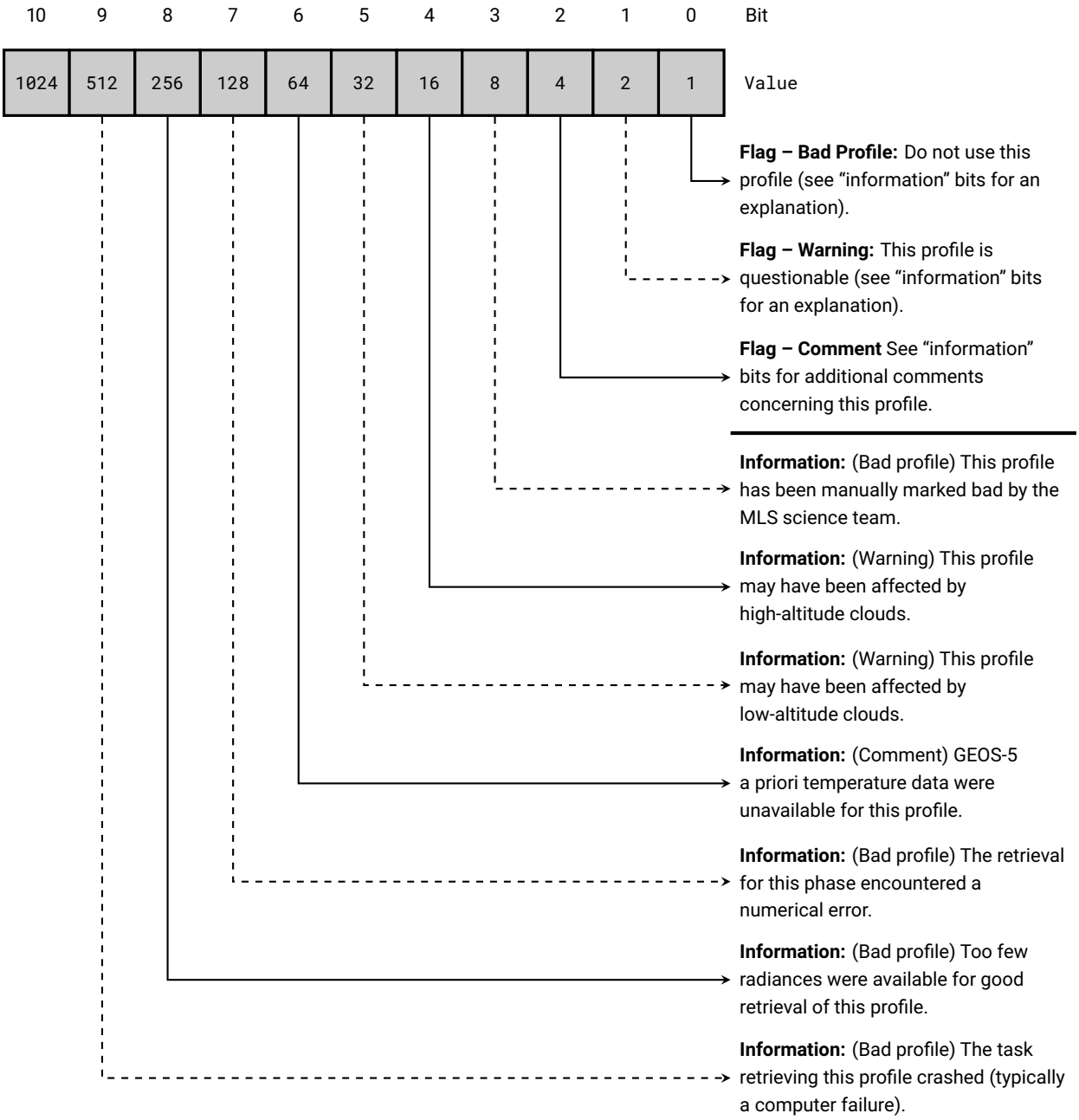

Figure 1.1: The meaning of the various bits in the `Status` field.

swath quantities. The vast majority of these are MLS diagnostic products that will be of little interest to most data users. A few that may be of interest to some users are detailed in Chapter 3.

1.6 Additional information given in the `Quality`, `Status`, and `Convergence` fields

In addition to the data and their estimated precisions, three data quality metrics are provided for every profile of each product. The first, called `Quality`, is a measure of the fit achieved by the Level-2 algorithms to the relevant radiances. Larger values of `Quality` generally indicate better radiance fits and therefore more trustworthy data. Values of `Quality` closer to zero indicate poorer radiance fits and therefore less trustworthy data. The value of `Quality` to be used as a "threshold" for rejecting data in scientific studies varies by product and

by version and is given in the discussions of each product in Chapter 3 (Table 1.1 summarizes the thresholds for most of the products).

The second quality metric is called `Status`. This is a 32-bit integer that acts as a binary bit field. Figure 1.1 describes the interpretation of the individual bits in more detail. The first three bits (bits 0, 1, and 2) are "flagging" bits. If the first bit ("bad profile") is set, it indicates that the corresponding profile *should not be used in any scientific study*. Accordingly, any profile for which `Status` is an odd number should not be used. The second bit ("warning") indicates that data in this profile are considered questionable for some reason, while the third ("comment") indicates that the data are noteworthy in some manner that does not rise to the level of a "warning". Higher-order bits give more information on the reasons behind the setting of the first three bits. So, for example, a value of `Status` of `18` (2+16) indicates that the data are questionable (2 ≡ bit 1) because of the possible presence of high-altitude clouds (16 ≡ bit 4).

The most commonly set information bits are the "low-altitude cloud" and "high-altitude cloud" bits. These indicate that the data have been marked as questionable because the Level-2 software took steps to avoid potential cloud contamination of the retrieved profile (clouds alone will never cause a profile to be marked as not to be used, i.e., with odd `Status`). Specifically, the "low-altitude cloud" flag notes that some radiances with tangent point pressures between 320 and 150 hPa were avoided due to potential cloud contamination. The "high-altitude cloud" flag indicates that some radiances in the 150 to 68 hPa tangent pressure range were avoided (in such cases, the low-cloud flag is automatically set in addition). The implications of this vary by product and, more importantly, by height. For example, situations of either "low-altitude cloud" or "high-altitude cloud" typically have very little impact on the quality of MLS measurements in the middle and upper stratosphere. Further details of the implications of these flags are given later in this document on a product-by-product basis.

The third diagnostic field, `Convergence`, describes how the fit to the radiances achieved by the retrieval algorithms compared to the degree of fit to be expected. This is quantified as the ratio of an aggregate χ^2 value to that predicted based on the assumption of a linear system [*Livesey et al.*, 2006]. Values around unity indicate good convergence, and the threshold values above which profiles should not be used are given on a product-by-product basis in Chapter 3 (as with `Quality`, these threshold values can vary between versions as well as by product).

1.7 An important note on negative values

Some of the MLS observations are "noisy" in nature. A consequence of this is that negative values may often be reported for species mixing ratios. It is important that such values *not be ignored or masked*. Ignoring such values will automatically introduce a positive bias into any averages made of the data as part of scientific analysis. Water vapor is retrieved using a logarithmic basis (both vertically and horizontally, as discussed in Section 1.9). Accordingly, no negative water vapor abundances are produced by v6.0*x*.

1.8 Averaging kernels for MLS v6.0*x* profiles

As is common for remote sounding instruments, consideration of the "Averaging Kernel" [e.g., *Rodgers*, 2000] can be useful in some scientific studies. However, the relatively high vertical resolution of the MLS observations (compared, for example, to those from nadir sounding composition instruments) allows for many scientifically useful studies to be undertaken without reference to the averaging kernels. This section reviews the role averaging kernels play in comparing MLS measurements to other observations and/or model fields and describes how to obtain representative kernels for the v6.0*x* data.

The averaging kernel matrix $\mathbf{A}$ relates the retrieved MLS profiles (given by the vector $\hat{\mathbf{x}}$) to the "true" atmospheric state (the vector $\mathbf{x}$) according to

$$\mathbf{A} = \frac{\partial \hat{\mathbf{x}}}{\partial \mathbf{x}}. \tag{1.1}$$

Rows of the $\mathbf{A}$ matrix accordingly describe the contributions of the true atmospheric profile to the given level in the retrieved profile. The figures later in this document show these rows as individual colored lines.

Given an independent observation or a model estimate of an atmospheric profile $\mathbf{x}$, the averaging kernels, in combination with the MLS a priori profile $\mathbf{x}_a$, can be used to linearly approximate the profiles that MLS would observe, were the true profile to be in the state given by $\mathbf{x}$, according to

$$\hat{\mathbf{x}} = \mathbf{x}_a + \mathbf{A}\left[\mathbf{x} - \mathbf{x}_a\right] \tag{1.2}$$

It is assumed here that the true profile uses the same vertical grid as the MLS data product in question (Section 1.9 discusses this issue further). Note that this linearization is about the a priori state, so the blurring by the averaging kernels is only of the difference between truth and a priori. The a priori profile for each MLS observation is available within each of the standard product files, in swaths named according to the product, with the suffix "`-APriori`" (i.e., "`Temperature-APriori`", "`O3-APriori`", etc.). In the case of water vapor, where a logarithmic interpolation is used for the profile, the calculations in Equation 1.2 should be performed in log space, i.e., with $\mathbf{x}$ and $\mathbf{x}_a$ containing the logarithm of the given H_2O mixing ratio (leaving the $\mathbf{A}$ matrix as supplied).

The MLS retrieval algorithms are "tomographic" in nature, in that they use information from multiple consecutive limb scans to simultaneously estimate the two-dimensional (along-track and vertical) state of the atmosphere over multiple Level-2 profiles (see Section 2.2). Formally, therefore, the MLS averaging kernels describe the smoothing in both the horizontal and the vertical directions. Archived two-dimensional averaging kernels capture this dependence, containing the partial derivatives of each level of a given profile to the truth at all levels of a block of eleven profiles centered on the location of the retrieved profile. These full kernels can be "collapsed" in the horizontal, to provide a single vertical averaging kernel for each product (similar to those provided for many nadir sounding instruments). This gives a matrix that corresponds to the single-profile view of the retrieval described in the preceding paragraph. Conversely, contributions from adjacent profiles to the retrieved values at each level may be collapsed in the vertical, to provide horizontal averaging kernels that capture the along-orbit-track resolution of the product. Chapter 3 includes plots of vertical and horizontal kernels for most of the standard products.

The MLS averaging kernels typically change little with latitude, season, or atmospheric state. Accordingly, two representative kernels are shown for each product, one for the tropics and one for polar winter conditions. These, and other, representative kernels are available to users, as described below. If variability in the averaging kernels is a concern, comparison of $\hat{\mathbf{x}}$ profiles obtained using multiple kernels (e.g., tropical and polar) can provide a quantitative estimate of the magnitude of differences introduced by kernel variations.

The representative vertical, horizontal, and 2-D averaging kernels have been archived for each MLS standard product on the MLS website and at Zenodo (`https://zenodo.org/records/18988586`). They are also directly attached to this document (see Appendix A). Two sets of kernels are provided, each comprising five files corresponding to five broad latitude bands. One set contains 1-D (horizontal and vertical) kernels, the other the full 2-D kernels, making ten files in all. Each file contains kernels (either 1-D or 2-D) for each of the MLS standard products for the given latitude band. Again, as the averaging kernels vary little with latitude, a file for a single latitude will generally be globally representative. These kernels were calculated from simulated MLS data for a single day (based on output from the SLIMCAT model for 20 February 1996). These files can be read as either NetCDF or HDF5 files, for which interfaces exist in many high-level analysis environments such as IDL, Python, and Matlab. These files contain multi-dimensional arrays, with dimensions named `RetrievalLevel`, `TruthLevel` and `TruthPhi`. The "`Phi`" terms are an along-track horizontal coordinate (geodetic great-circle angle) used in the MLS retrievals, within which profiles are spaced 1.5° apart.

In most cases, consideration of the 1-D vertical averaging kernels is likely sufficient to quantify the impact of the finite MLS resolution on a scientific study. In a column-major language (e.g., Matlab, IDL, Fortran), the 1-D vertical $\mathbf{A}$ matrix will be dimensioned [`RetrievalLevel`, `TruthLevel`], and the truth profiles should be multiplied by averaging kernels from the left (as in Equation 1.2, above). In a row-major language (e.g., C, Numpy), the order of dimensions in $\mathbf{A}$ is reversed, and the averaging kernels should be multiplied by truth

from the right. Horizontal averaging kernels (avkh) have size $n_{\text{lev}} \times 11$ in a column-major and $11 \times n_{\text{lev}}$ in a row-major environment. The side on which avkh has the 11-element dimension is the side against which truth profiles should be multiplied for all horizontal averaging kernels.

The 2-D averaging kernels give weights for every level of every nearby (within ±5) profile of truth, so in a row-major language are $11 \times n_{\text{lev}} \times n_{\text{lev}}$ and in column-major language are $n_{\text{lev}} \times n_{\text{lev}} \times 11$. To perform the convolution, blocks of eleven adjacent truth and a priori profiles centered on the retrieved profile location are unwrapped into length $n_{\text{lev}} \times 11$ vectors, $\mathbf{X}$ and $\mathbf{X}_a$. The 2-D averaging kernel, $\mathbf{A}_{2D}$, is reshaped into a two-dimensional matrix $n_{\text{lev}} \times (n_{\text{lev}} \times 11)$ and the retrieved state is estimated as

$$\hat{\mathbf{x}} = \mathbf{x}_a + \mathbf{A}_{2D}\left[\mathbf{X} - \mathbf{X}_a\right]. \tag{1.3}$$

Vertical averaging kernels for each product for 70°N and the equator are also available as text files, in the format used for previous MLS releases. These files are named according to

```
MLS-Aura_L2AK-<product>-<case>_v06-01_0000d000.txt
```

where <case> is Eq or 70N for the equator and 70°N, respectively (or Day and Night for OH, see Section 3.20). These files are available from the MLS web site at https://mls.jpl.nasa.gov/eos-aura-mls/data.php and as part of the same Zenodo record containing the NetCDF files (https://zenodo.org/records/18988586). The individual files contain comment lines (prefixed with a semicolon) describing their format. The first non-comment line gives the name of the product and the number of levels in the vertical profile. A list of the pressure levels in the profile (matching those in the L2GP files) is then given, followed by all the values of the averaging kernel matrix, with the row index (the level in the retrieved profile) varying most rapidly.

As discussed above, the MLS profile pressures are typically not the same as those of the observation or model dataset to which the comparison is being made. In many cases, particularly where the resolution of the other dataset is comparable to that of the MLS profiles, a simple interpolation is the most practical manner in which to transform the other dataset into the $\mathbf{x}$ profile space. However, we note that more formal approaches have been described [*Rodgers and Connor*, 2003] for the case where the comparison dataset is also remotely sounded and has an averaging kernel. In cases where the comparison dataset has high vertical resolution (e.g., sonde or lidar observations), an additional consideration is described in the following section.

1.9 Considerations for comparisons with high vertical resolution datasets

The MLS Level-2 data describe a piecewise linear representation of vertical profiles of mixing ratio (or temperature, GPH, etc.) as a function of pressure, with the tie points given in the L2GP files (in the case of water vapor, the representation is piecewise linear in log mixing ratio). This contrasts with some other instruments and model output datasets, which report profiles in the form of discrete layer means. This interpretation has important implications that may need to be considered when comparing profiles from MLS to those from other instruments or models, particularly those with higher vertical resolution.

It is clearly not ideal to compare MLS retrieved profiles with finer resolution data by simply sampling the finer profile at the MLS retrieval surfaces. One might expect that instead one should do some linear interpolation or layer averaging to convert the other dataset to the MLS grid. However, in the MLS case, where the state vector describes a profile at infinite resolution obtained by linearly interpolating from the fixed surfaces, it can be shown that the appropriate thing to do is to compare to a least-squares fit of the non-MLS profile to the lower-resolution MLS retrieval grid.

Consider a high-resolution profile described by the vector $\mathbf{z}_h$ and a lower-resolution MLS retrieved profile described by the vector $\mathbf{x}_l$. We can construct a linear interpolation in log pressure that interpolates the low-resolution information in $\mathbf{x}_l$ to the high-resolution grid of $\mathbf{z}_h$. We describe that operation by the (typically highly sparse) $n_h \times n_l$ matrix $\mathbf{H}$ such that

$$\mathbf{x}_h = \mathbf{H}\mathbf{x}_l \tag{1.4}$$

where $\mathbf{x}_h$ is the high-resolution interpolation of the low-resolution $\mathbf{x}_l$. (Each row of $\mathbf{H}$ contains the two interpolation weights corresponding to the MLS levels that bracket the high-resolution level, with all other elements in each row being zero.)

It can be shown that the best-estimate profile that an idealized MLS instrument could obtain, were the true atmosphere in the state described by $\mathbf{z}_h$, is given by

$$\mathbf{z}_l = \mathbf{W}\mathbf{z}_h \tag{1.5}$$

where

$$\mathbf{W} = \left[\mathbf{H}^{\mathrm{T}}\mathbf{H}\right]^{-1}\mathbf{H}^{\mathrm{T}} \tag{1.6}$$

In other words, $\mathbf{z}_l$ represents a least-squares linear fit to $\mathbf{z}_h$. This operation is illustrated by an example in Figure 1.2. Precision uncertainty on high-resolution measurements may be similarly converted to the MLS grid by applying

$$\mathbf{S}_l = \mathbf{W}\mathbf{S}_h\mathbf{W}^{\mathrm{T}} \tag{1.7}$$

where $\mathbf{S}_h$ is the covariance of the original high-resolution data (typically diagonal) and $\mathbf{S}_l$ is its low-resolution representation on the MLS pressure grid. Following this transfer of the high-resolution profile onto the state vector vertical grid, the profile can be multiplied by the averaging kernels, as described above, according to Equation 1.2.

In some cases, the application of this least-squares "smoothing" is as important, if not more important, than the application of the averaging kernels described above. This is particularly true when the averaging kernels are close to delta functions, indicating that the vertical resolution is comparable to the retrieved profile level spacing.

In the case of water vapor, where a logarithmic vertical basis is used, the $\mathbf{x}$ and $\mathbf{z}$ vectors should describe the logarithm of the mixing ratio.

1.10 A note on MLS 190-GHz observations, particularly from May 2024 onward

1.10.1 The post-2010 drift in the 190-GHz observations

In contrast with the MLS radiometers at 118, 240, and 640 GHz, which have exhibited no substantive changes in behavior in the two decades since launch, the MLS 190-GHz radiometer, used to measure H_2O, N_2O, HNO_3 in the upper stratosphere, and HCN, has shown clear signs of aging starting around 2010. This aging was first identified through its impact on the H_2O product. Specifically, differences between MLS v4.2*x* H_2O and coincident frostpoint sonde measurements showed a drift, with MLS tending towards larger values at a rate of around 6–15% per decade [*Hurst et al.*, 2016]. Comparisons to ACE-FTS solar occultation observations showed a similar, if smaller (about half the size), drift in H_2O and a concurrent drift in N_2O, with MLS N_2O drifting towards smaller abundances [*Livesey et al.*, 2021]. Extensive studies by the MLS team revealed that one consequence of the 190-GHz aging is a slow (~1.3% per decade) drift in a key calibration parameter. By accounting for the time-dependent nature of this calibration parameter in v5.0*x*, the statistically significant drifts in MLS/ACE-FTS H_2O comparisons were eliminated, though a drift remains compared to the frostpoint record [*Livesey et al.*, 2021]. This issue is discussed further in the product-specific sections of Chapter 3 for H_2O and N_2O.

1.10.2 Limited life for the MLS 190-GHz observations and current "duty-cycling" approach.

This aging also has implications for the total operating life expected from the 190-GHz radiometer. Therefore, to ensure as long a record as possible, since May 2024 the 190-GHz radiometer has been "duty cycled" to conserve its remaining lifetime. Initially, this subsystem was operated for about one week per calendar month, a cadence chosen to confidently enable observations to continue through the then-anticipated May 2026 end of Aura operations. In early 2026, however, in light of the potential for continued mission operations, the 190-GHz receiver duty cycle was reduced to ~4 days per calendar month (two complete days plus a partial

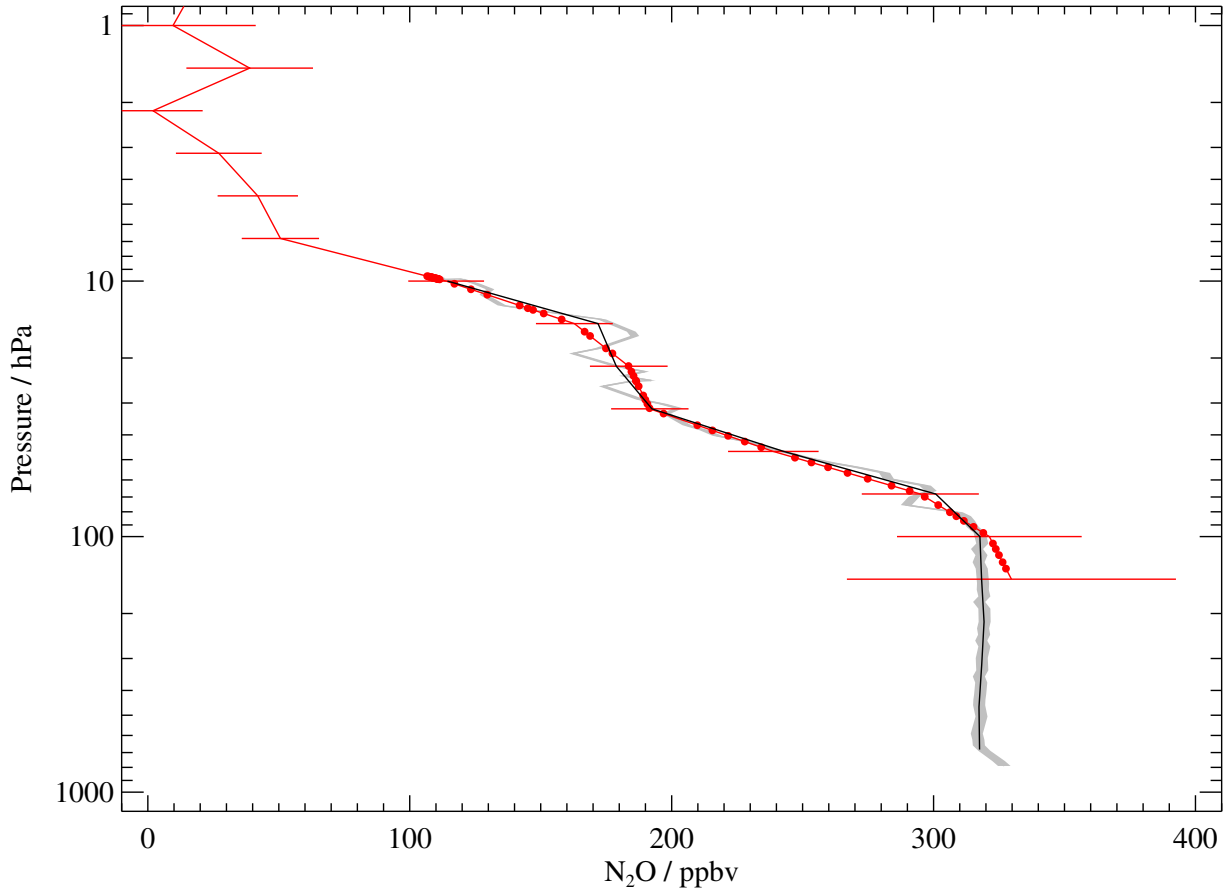

Figure 1.2: Comparisons of MLS (v1.5) N_2O observations with in situ balloon data (courtesy of J. Elkins). The raw balloon ("high-resolution") data ($\mathbf{z}_h$) are shown as the gray-shaded region (shading indicates precision). A coincident ("low-resolution") MLS profile $\mathbf{x}_l$ is shown in red, with the red error bars indicating precision. The red dots show the MLS data linearly interpolated to the balloon pressures using the **H** matrix (i.e., $\mathbf{x}_h$ from Equation 1.4). The black line shows the least-squares interpolation of the balloon data onto the MLS grid using the **W** matrix as described in the text (i.e., $\mathbf{z}_l$ from Equation 1.5). The black line therefore represents the closest possible match at this resolution to the original gray line and is the appropriate quantity to compare to the red MLS profile, as well as to be multiplied by the averaging kernels for formal comparison.

day on either side). At that pace, the 190-GHz subsystem can reasonably be expected to continue to operate reliably through the end of 2026 and likely beyond. Figure 1.3 details the schedule for MLS 190-GHz activation. With this duty cycling, MLS observations for H_2O, N_2O, HCN, and upper stratospheric HNO_3 are not available for several weeks each month.

The spectral regions used to measure some other species (notably CH_3Cl, CH_3CN, ClO, HCl, and cloud ice) are also affected by atmospheric water vapor. During periods when the 190-GHz radiometer is deactivated, climatological values of water vapor must be assumed in the retrievals of these other products. This introduces additional biases and variability in these other products during such periods, as discussed for each affected product in Chapter 3. Thus, although observations of these products on the affected days are still useful for purely morphological or qualitative purposes, they cannot be quantitatively compared to measurements taken on surrounding days or in previous years when the 190-GHz radiometer was operational. The biases also have potential implications for the calculation of long-term trends. Therefore, for quantitative studies using the affected products, we recommend against their use during periods when the 190-GHz radiometer is deactivated. We also note, however, that measurements taken during time periods since May 2024 when

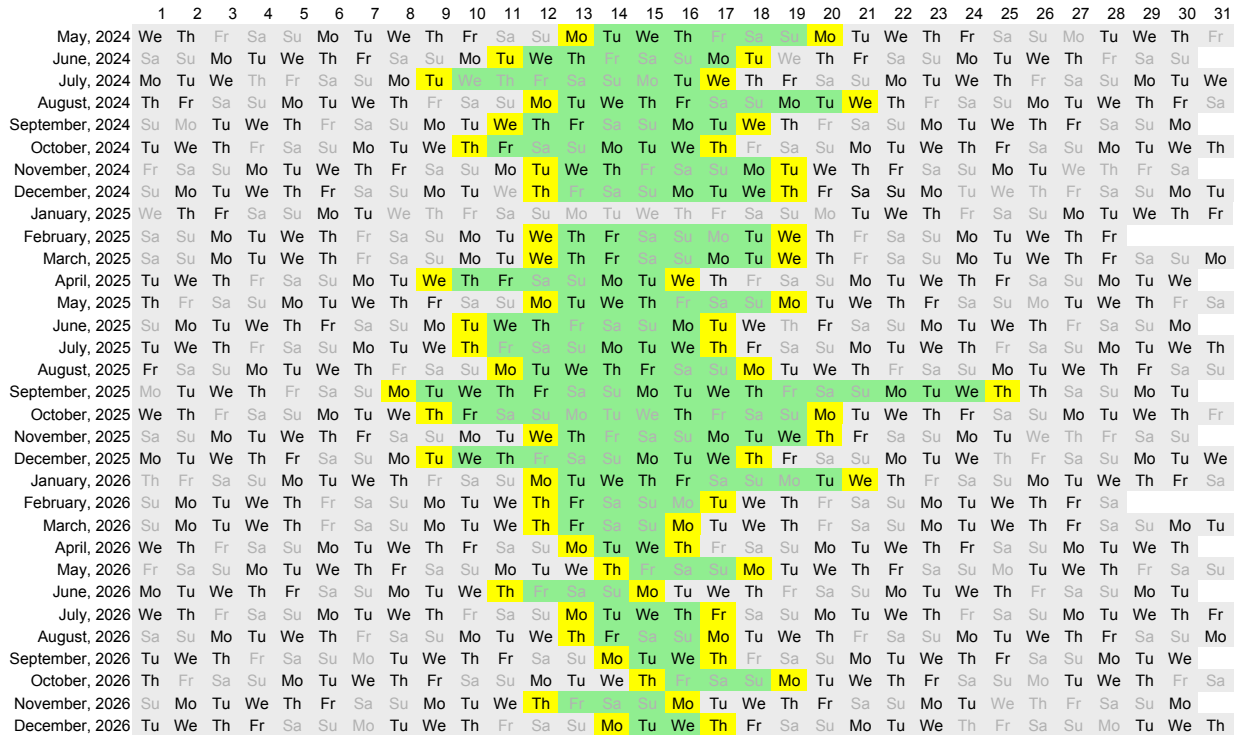

Figure 1.3: The schedule for past and planned (as of March 2026) operations of the MLS 190-GHz radiometer.

the 190-GHz radiometer is turned off can be intercompared. Again, see Chapter 3 for product-specific details. Finally, it should be recognized that the same guidance applies to the MLS v5.0*x* data in these periods, although there are no current plans to update the v5.0*x* edition of this document [*Livesey et al.*, 2022] to reflect this issue.

Chapter 2
Background reading for users of MLS data

2.1 Aura MLS radiance observations

Figures 2.1 and 2.2 show the spectral coverage of the MLS instrument. The instrument consists of seven radiometers observing emission in the 118-GHz ("R1A" and "R1B"), 190-GHz ("R2"), 240-GHz ("R3"), 640-GHz ("R4") and 2.5-THz ("R5H" and "R5V") regions. With the exception of the two 118-GHz devices, these are "double sideband" radiometers. This means that the observations from both above and below the local oscillator frequencies are combined and downconverted to form a ~20-GHz-bandwidth "intermediate frequency" signal. In the case of the 118-GHz radiometers (R1A and R1B), the signals from the upper sideband (those frequencies above the ~126-GHz local oscillator) are suppressed. These intermediate frequency signals are then split into separate "bands". The radiance levels within these bands are quantified by various spectrometers.

In operation, the instrument performs a continuous vertical scan of both the GHz antenna (for R1A, R1B, R2, R3, and R4) and THz antenna (for R5H and R5V) from the surface to about 90 km in a period of about 20 s. This is followed by about 5 s of antenna retrace and calibration activity. This ~25 s cycle is known as a *major frame* (MAF). During the ~20 s continuous scan, radiances are reported at ~1/6 s intervals, known as *minor frames* (MIFs). The scan timing is adjusted (through introduction of occasional "Leap MIFs" in selected MAFs) such that MLS performs exactly 240 scans during each orbit, with the latitudinal distribution of the scans being consistent from orbit to orbit.

2.2 Brief review of the theoretical basis

The Level 2 algorithms implement a standard *Optimal Estimation* retrieval approach [*Rodgers*, 1976, 2000] that seeks the "best" value for the "state vector" (the profiles of temperature and abundances) based on an optimal combination of the fit to the MLS radiance observations, a priori estimates of the state vector (from climatological information and, for temperature in the troposphere and lower stratosphere, analysis fields), and constraints on the smoothness of the result. This fit must often be arrived at in an iterative manner because of the non-linear nature of the Aura MLS measurement system.

An innovative aspect of the retrieval algorithms for Aura MLS [*Livesey and Read*, 2000; *Livesey et al.*, 2006] arises from taking advantage of the fact that the MLS instrument looks in the forward direction from the spacecraft. Figure 2.3 reviews the Aura MLS measurement geometry and shows that each radiance observation is influenced by the state of the atmosphere for several consecutive profiles. In the v6.0*x* Level 2 algorithms, as with earlier versions, the state vector consists of "chunks" of several profiles of atmospheric temperature and composition, which are then simultaneously retrieved from radiances measured in a similar number of MLS scans. Results from these chunks are joined together to give products at a granularity of one day (the chunks overlap in order to avoid edge effects).

The retrieval state vector consists of vertical profiles of temperature and composition on fixed pressure surfaces. Between these fixed surfaces, the retrieval algorithms (more specifically the "forward models" within the retrieval system, see below) assume that species abundances and temperature vary from surface to surface in a piecewise-linear fashion (except for the abundance of H_2O, which is assumed to vary linearly in the logarithm of the mixing ratio). This has important implications for the interpretation of the data, as was described in Section 1.9. In addition to these profiles, the pressure at the tangent point for the mid-point of each minor frame is retrieved, based on both radiance observations and knowledge of tangent point height, the latter computed from the MLS antenna position encoder readout and Aura spacecraft ephemeris and attitude information.

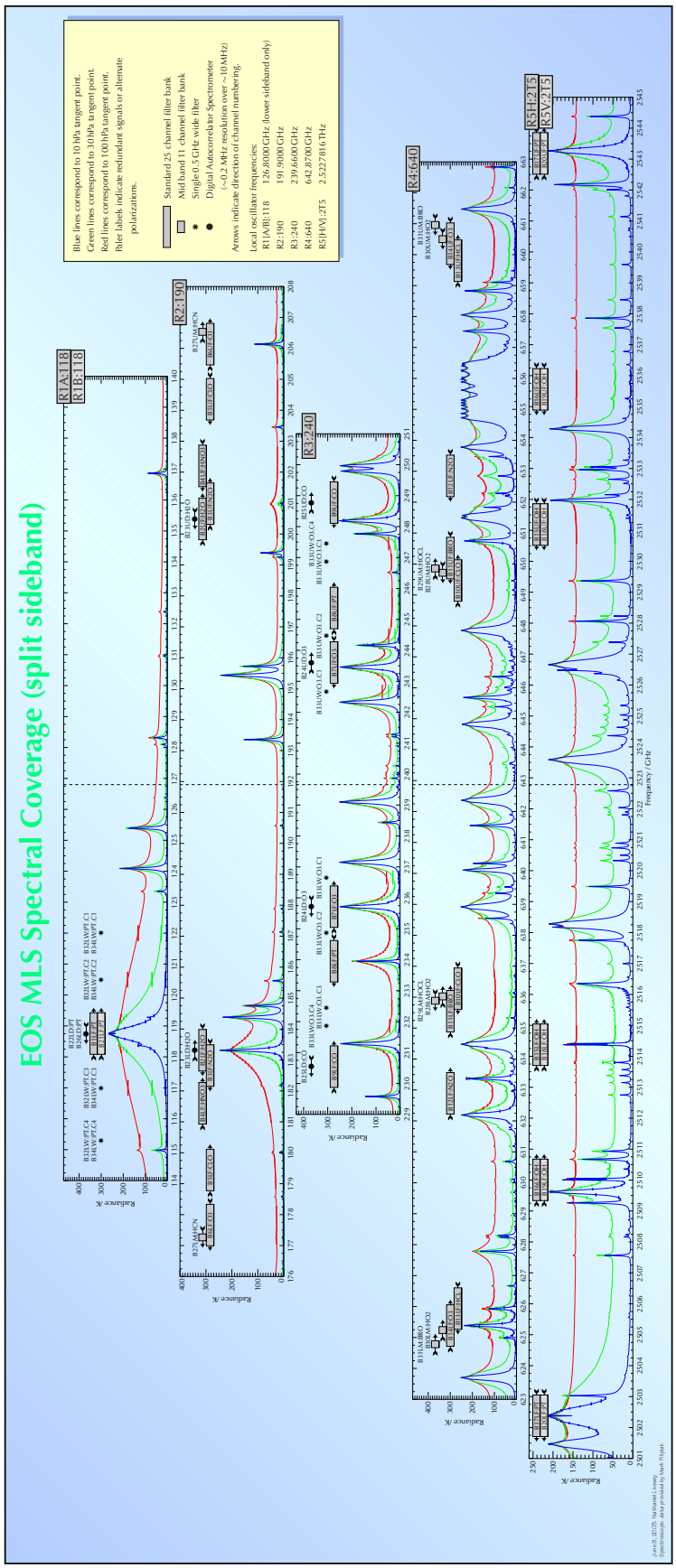

Figure 2.1: The five panels show the spectral regions covered by the MLS radiometers. The gray boxes and other symbols denote the position of the various "bands" observed within the spectral regions covered by each radiometer.

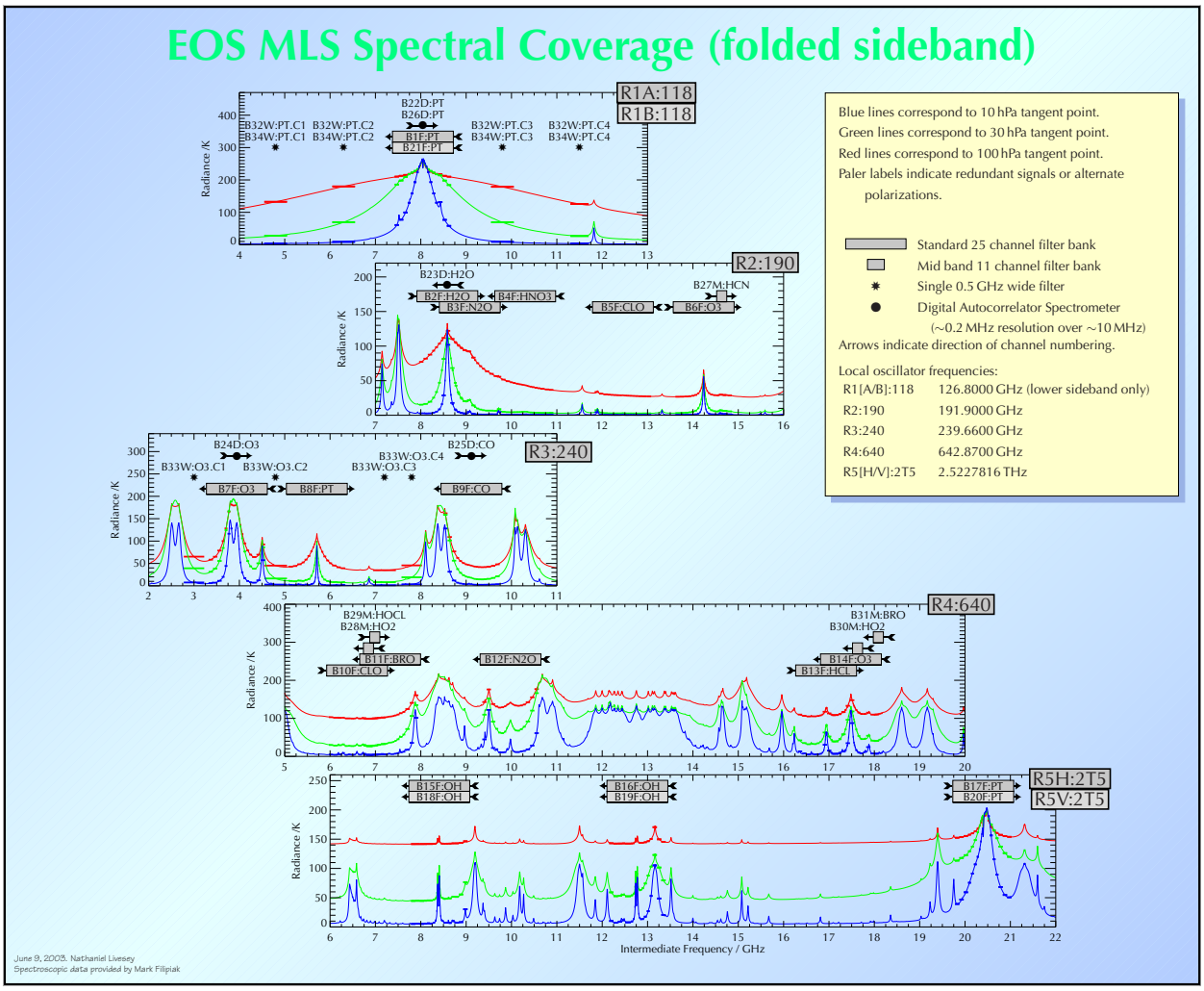

Figure 2.2: This is similar to figure 2.1, except that x-axes represent “intermediate frequency” (IF). The signal at each intermediate frequency represents a sum of the signals observed at that frequency both above (the “upper sideband”) and below (the “lower sideband”) the local oscillator. In the case of the 118-GHz receivers, the upper sideband signals are suppressed, giving a single-sideband IF signal.)

Most of the MLS data products are deduced from observations of spectral contrast, that is, variations in radiance as a function of frequency for a given limb pointing. Many of the systematic errors in the MLS measurement system manifest themselves as a spectrally flat or slowly spectrally varying error in radiance. This is true of effects arising both from the instrument (such as gain and offset during the limb scan) and from the “forward model” (such as knowledge of continuum emission and the impact of some approximations made in the forward model in order to increase its speed). In order to account for such effects, the v6.0*x* algorithms also retrieve spectrally flat (or slowly spectrally varying) corrections to the MLS radiances, either in terms of an additive radiance offset or an additive atmospheric extinction.

2.3 The “Core, Core-plus-Rn…” approach to the MLS retrievals

2.3.1 The need for separate “phases”

Many aspects of the MLS measurement system are close to being linear in nature. In other words, there is a near-linear relationship between changes in aspects of the atmospheric state and consequent changes in the MLS radiance observations. However, there are some components of the state vector whose impact on the

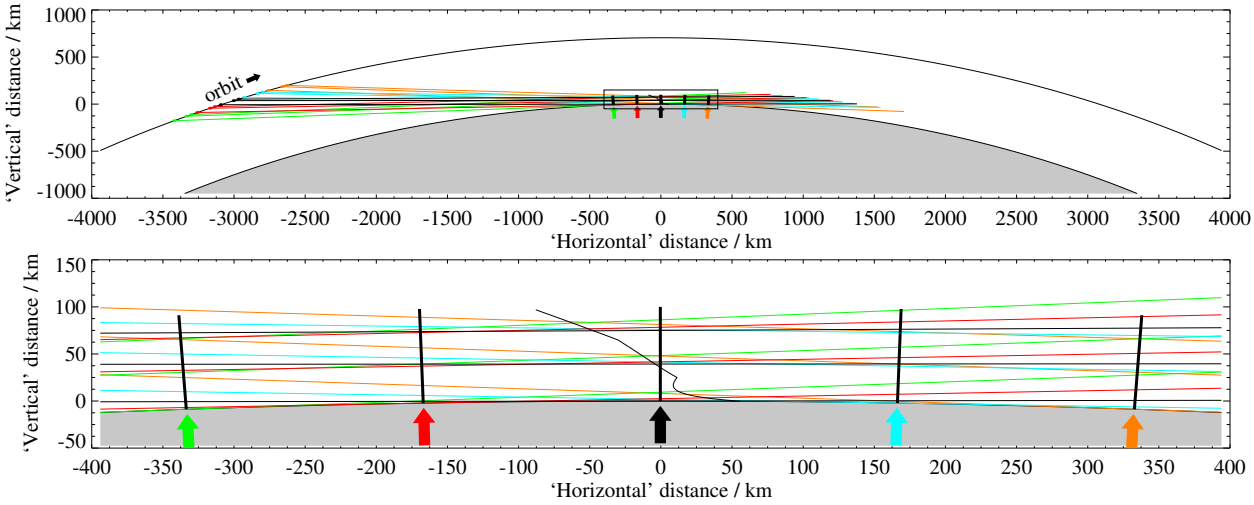

Figure 2.3: The top diagram shows a section of one orbit. Three of the 120 limb ray paths per scan are indicated by the “horizontal” lines. The lower diagram shows an expansion of the boxed region above. The straight radial lines denote the location of the retrieved atmospheric profiles. The limb ray scan closest to each profile is that whose color is the same as that of the arrow underneath. The thin black line under the central profile indicates the locus of the limb tangent point for this scan, including the effects of refraction.

radiances is non-linear. The most non-linear components are the limb-tangent-point pressures for each MIF. The impact of water vapor in the upper troposphere on the MLS radiance observations is also highly non-linear. Solving for these aspects of the state vector therefore requires several iterations. The computational effort involved in retrieval and forward models scales very rapidly (arguably as high as cubically) as a function of the size of the measurement system (i.e., the number of elements in the state and measurement vectors). Thus, it is desirable to simplify retrievals involving strongly non-linear variables to a small subset of the complete system, in order to cut down on the effort involved in retrievals that require many iterations. Given those considerations, most remote-sounding retrieval algorithms are split into *phases*. In the case of the MLS v6.0*x* retrievals, there are many such phases. The first group of phases (collectively known as “Core”) uses the 118-GHz and 240-GHz observations of O_2 and $O^{18}O$, respectively, to establish estimates for temperature and tangent pressure. Upper tropospheric 190-GHz radiances are used in these early phases to establish a first-order estimate of upper tropospheric humidity. The Core phases also include cloud screening computations (based on differences between observed and estimated clear-sky radiances). These identify minor frames where radiances in a given radiometer have been subject to significant (and poorly modeled) cloud scattering. Such minor frames are ignored in v6.0*x* processing of measurements from certain radiometers.

The Core phases are followed by phases such as `CorePlusR3` and `CorePlusR5`, where composition profiles are retrieved from a given radiometer. Sometimes (e.g., for `CorePlusR3`) these later phases continue to retrieve temperature and pressure, still using information from the 118-GHz radiometers, as in the Core phases. In other phases (e.g., the `CorePlusR2` and `CorePlusR4` families of phases), the 118-GHz information is neglected and temperature and pressure are constrained to the results from the earlier Core phases. This choice is made based on extensive testing aimed at maximizing the information yield from MLS while minimizing the impact of inevitable systematic disagreements among the different radiometers, introduced by uncertain spectroscopy and/or calibration knowledge.

Table 2.1 describes the phases in more detail. Many products (e.g., ozone) are produced in more than one phase. All the separate measurements of these species are produced as diagnostic quantities, typically labeled according to the spectral region from which they originated. For example, the ozone product obtained from the `CorePlusR2` retrieval is known in the v6.0*x* dataset as `O3-190`. In v6.0*x*, as with previous versions, in order

to reduce confusion for users of MLS data, the algorithms also output "standard products", which are typically copies of one of the products from the `CorePlusRn` phases. For example, the standard chlorine monoxide product is a copy of the `ClO-640` product. In the case of v6.0*x* nitric acid, the standard product represents a hybrid of the results from two phases. Details of which standard product is obtained from which phase are given in Table 2.2.

2.4 MLS forward models

At the heart of any optimal-estimation-based retrieval lies one or more "forward models". These are tasked with computing estimates of the radiances the instrument would measure when viewing an atmosphere described by a given state vector. The retrieval iteratively updates this state vector such that the corresponding forward model radiances agree satisfactorily with the measured radiances. The state vector updates made each iteration are driven by the "Jacobian" information (the derivative of the predicted radiance with respect to the estimated state, also known as "weighting functions") that is also computed by the forward model. The retrieval algorithms in v6.0*x* make use of a variety of different forward models. The most accurate is the so-called "full forward model" described in *Read et al.* [2004] and *Schwartz et al.* [2004]. This is a hybrid line-by-line and channel-averaged model that computes radiances on appropriate grids of frequency and limb tangent pressure that are then convolved with the MLS frequency and angular responses. This model is generally rather time consuming, although for some comparatively "clean" spectral regions the computational burden is small enough that the full forward model was used in early versions of the operational retrievals. In the years since the Aura launch, computational capabilities have improved significantly, enabling use of the full forward model for all MLS channels in more recent MLS data versions.

For some of the MLS channels, a simpler "linearized forward model" can be used to estimate radiances, or more typically just the Jacobian information, with the radiances still being computed by the full forward model. The linearized model invokes a simple first-order Taylor series to estimate radiances as a function of the deviation of the state from one of several pre-selected representative states. The inputs to this model are pre-computed radiances and derivatives corresponding to the pre-selected states, generated by stand-alone runs of the full forward model.

In addition, a "cloud forward model" can be invoked to model the effects of scattering from cloud particles in the troposphere and lower stratosphere [*Wu and Jiang*, 2004]. This model was used in the simulation of radiances based on known model atmospheres for the v6.0*x* testing but is not invoked in the v6.0*x* retrieval algorithms, as discussed below.

2.5 The handling of clouds in MLS retrievals

While MLS observations are insensitive to aerosols and thin clouds, the particle sizes and number densities associated with strong deep convective clouds can lead to scattering of the signals at the millimeter-scale wavelengths observed by MLS. Broadly speaking, this scattering redirects some fraction of the ambient radiation in the cloudy region towards the MLS antenna. This ambient radiation will be a mix of "bright" upwelling radiances and "dark" signals downwelling from cold space. Thus, for high-altitude optically thin limb views, where small radiance signals are seen in cloud-free situations, cloud scattering will increase the observed radiances. On the other hand, for low-altitude limb views, characterized by large radiances in cloud-free scenes, clouds in the line-of-sight will act to suppress the observed radiances, as some of the observed signal will originate from downwelling signatures of cold space scattered into the beam.

The MLS v6.0*x* algorithms can reliably retrieve composition in moderately cloudy cases (i.e., those having small limb radiance perturbations). In the case of the `CorePlusR3` retrieval this is handled by retrieving a frequency-squared-dependent extinction (including background atmospheric absorption from N_2, H_2O, and unknown emitters). In the other retrieval phases, by contrast, a spectrally flat radiance baseline term is used. Thick clouds can affect the MLS radiances beyond the modeling capability of this approach, mainly through scattering processes. In such situations, the affected radiances are excluded from the retrievals, or their influence is down-weighted.

Table 2.1: The phases that form the v6.0*x* retrieval algorithms.

Phase	Target species[1]	Measurements	Comment
InitPTan	T, pTan (GHz), GPH	R1A & R1B (118 GHz)	Initial estimate of P/T, lower limit 261 hPa
InitR2	H_2O, N_2O, CH_3CN, HCN, ClO, HNO_3, O_3, SO_2	R2 (190 GHz)	Initial trace gas estimator, lower limit 100 hPa
R3InitRHi	RHi, T_{cir}	R3 (240 GHz)	Retrieves RHi profile from 316 hPa and up, used mostly for "near field" cloud detection and to compute R3 T_{cir}
CloudDetector	none	R3 (240 GHz)	Determines cloud impacted radiance usage for R2 (190 GHz), R3 (240 GHz) and R4 (640 GHz)
FinalPTan	T, pTan (GHz), GPH	R1A & R1B (118 GHz), R3 (240 GHz)	Best P/T retrieval, lower limit 261 hPa
InitLowCloud	T_{cir}	All radiometers	Computes cloud-induced radiance terms (T_{cir})
InitRHi	UT RHi	R2 (190 GHz)	Retrieve RHi in a ~6 km-layer centered 400–600 hPa. Uses only saturated radiances
InitUTH	Upper tropospheric H_2O	R2 (190 GHz)	Low vertical resolution (6/decade) H_2O retrieval
CorePlusR3	T, pTan (GHz), GPH, O_3[2], CO, HNO_3, SO_2, RHi	R1A & R1B (118 GHz), R3 (240 GHz)	Retrievals down to 316 hPa
OzoneOnly	O_3, CO	R3 (240 GHz)	Retrievals down to 316 hPa optimized for O_3 product
CorePlusR2	H_2O, N_2O, HNO_3, ClO, O_3, HCN, CH_3CN, SO_2, pTan (GHz)	R1A & R1B (118 GHz), R2 (190 GHz)	H_2O retrieved down to 316 hPa, other species 100 hPa (note no T, GPH, pTan retrieval)
Hydrogen Cyanide	HCN, O_3, HNO_3	R2 (190 GHz)	Retrievals down to 100 hPa
CorePlusR4AB14	ClO, BrO, HO_2, HOCl, HCl, O_3, HNO_3, CH_3CN, SO_2, CH_3Cl	R4 (640 GHz)	Retrievals down to 147 hPa
Methanol	CH_3OH, ClO, BrO, HO_2, HOCl, HNO_3, SO_2, CH_3Cl	R2 (190 GHz) and R4 (640 GHz)	Retrievals down to 147 hPa
CorePlusR4AB13	HCl, O_3, SO_2	R4 (640 GHz)	Retrievals down to 147 hPa. This phase is only executed when MLS Band 13 is operating
CorePlusR4B	N_2O, SO_2	R4 (640 GHz)	Retrievals down to 147 hPa. This phase is only executed when MLS Band 12 is operating
HighCloud	Cloud induced radiance, IWC, IWP	—	Generates cloud ice (IWC, IWP) products
CorePlusR5	T, pTan (GHz, THz), GPH, OH, O_3	R1A & R1B (118 GHz), R5H and R5V (2.5 THz)	Retrievals down to 68 hPa (147 hPa for Temperature). This phase is only executed when the MLS THz module is operating
GPHOnly	GPH	—	Offsets CorePlusR3 GPH to match GEOS-5 at 100 hPa

[1] Tangent pressure and Geopotential height have been abbreviated to pTan (GHz/THz) and GPH respectively. Minor state vector components such as "baseline" and/or "extinction" have been omitted unless they are the specific focus of the phase. Temperature, IWC, H_2O, RHi are "high resolution" (12 surfaces per decade change in pressure from 1000 hPa to 1 hPa) unless otherwise stated. O_3 is low resolution except for the Core+R3 phase.

[2] On high vertical resolution grid

Table 2.2: The origin of each of the "standard products" from v6.0*x*. (Cloud top pressure is generated using a separate program.)

Product	Origin	Spectral region
BrO	`CorePlusR4AB14`	640 GHz
CH_3Cl	`CorePlusR4AB14`	640 GHz
CH_3CN	`CorePlusR4AB14`	640 GHz
CH_3OH	`Methanol`	640 GHz
ClO	`CorePlusR4AB14`	640 GHz
CO	`CorePlusR3`	240 GHz
GPH	`GPHOnly`	118 & 240 GHz
H_2O	`CorePlusR2`	190 GHz
HCl	`CorePlusR4AB14`	640 GHz
HCN	`HydrogenCyanide`	190 GHz
HNO_3	`CorePlusR2` (15 hPa and less) `CorePlusR3` (larger than 15 hPa)	190 GHz 240 GHz
HO_2	`CorePlusR4AB14`	640 GHz
HOCl	`CorePlusR4AB14`	640 GHz
IWC	`HighCloud`	240 GHz
IWP	`HighCloud`	240 GHz
N_2O	`CorePlusR2`	190 GHz
O_3	`OzoneOnly`	240 GHz
OH	`CorePlusR5`	2.5 THz
RHi	Computed from Temperature and H_2O	190 GHz
SO_2	`CorePlusR3`	240 GHz
Temperature	`CorePlusR3`	118 & 240 GHz

Table 2.3: MLS frequency channels and thresholds for the cloud flag.

Radiometer	Cloud channel	USB/LSB frequency / GHz	Low threshold	High threshold
R1A:118	B32W:PT.C4	115.3 (LSB only)	$T_{cir} < -4$ K	none
R1B:118	B34W:PT.C4	115.3 (LSB only)	$T_{cir} < -4$ K	none
R2:190	B5F:ClO.C1	178.8 / 204.9	$T_{cir} < -20$ K	$T_{cir} > 10$ K
R3:240	B8F:PT	233.4–234.5 / 244.8–245.9	none	$^2 > 30$
R4:640	B11F:BrO.C23	635.9 / 649.8	$T_{cir} < -10$ K	none

The first aspect of handling clouds in v6.0*x* is therefore the flagging of radiances that are believed to be significantly contaminated by cloud effects. In the `CorePlusR2`, `CorePlusR3`, and `CorePlusR4[…]/Methanol` phases, cloud flagging is based on determining the highest-altitude limb view contaminated by cloud signals and rejecting all radiances below that targeted altitude. Cloud radiance scattering narrows the line shape for any molecule. The $O^{18}O$ line measured by MLS "Band 8" is a convenient signal to use for cloud detection as (1) the concentration of $O^{18}O$ is well known, (2) its signal is at a relatively high frequency, making it more susceptible to cloud scattering effects than many (but not all) other MLS signals, and (3) the line never goes opaque at any altitude, making it sensitive to tangent pressure into the upper troposphere.

The detection of cloud scattering is based on recognition of a poor lineshape fit (typically manifested as the measured linewidth being unphysically narrow compared to the calculated width) or unexpected signal enhancements/depressions in MLS channels used for sounding the upper troposphere and lower stratosphere when viewing low in the atmosphere (limb tangent altitudes below ~10 km). The cloud detection calculation uses estimates of tangent pressure and temperature obtained from a combination of the 118-GHz Band 1 measurements (unaffected by clouds) and tangent point altitude information obtained from instrument/spacecraft pointing knowledge. This tangent pressure and temperature profile information, combined with an estimate of relative humidity from a previous retrieval phase, is used to compute the radiances in the most optically thin MLS channel (Channel 3 of Band-33) expected in a clear-sky scene. Those estimated clear-sky radiances are compared to the actual radiances measured in that channel, with the difference giving a vertical profile of estimated cloud-induced radiances (T_{cir}). Clear-sky radiances are also computed for the $O^{18}O$ signal measured in Band-8 and are then used to compute vertical profiles of a χ^2 metric, again comparing the radiances expected in a cloud-free atmosphere to those actually measured. The T_{cir} and χ^2 metrics are used to deduce the highest limb view (if any) affected by cloud scattering (the specific criteria are that Band-8 $\chi^2 > 10$ or $T_{cir} < -15$ K indicate a cloud in the field of view); radiances from limb views lower in the atmosphere than this highest cloud detection view are not used in the composition retrievals.

The other aspect of cloud handling in v6.0*x* is the estimation of cloud ice water content (IWC) and ice water path (IWP) products from the final T_{cir} computed by the retrieval in the `HighCloud` phase. More information on these products and their derivation is given in Sections 3.16 and 3.17. For details of a cloud top pressure product that is new in v6.0*x*, see Section 3.7.

2.6 The quantification of systematic uncertainty in MLS data

A major component of the validation of MLS data is the quantification of the various sources of systematic uncertainty. These can arise from instrumental issues (e.g., radiometric calibration, field of view characterization), spectroscopic uncertainty, and approximations in the retrieval formulation and implementation. Comprehensive quantification of these uncertainties has been performed for v6.0*x* MLS products, updated from that described in the MLS validation papers (which were based on v2.2*x*). The individual sections of Chapter 3 detail the results of this quantification for each product.

For each identified source of systematic uncertainty, its impact on MLS measurements of radiance (or

pointing where appropriate) has been quantified and modeled. These modeled impacts correspond to either 2σ estimates of uncertainties in the relevant parameter(s) or an estimate of their maximum reasonable error(s) based on instrument knowledge and/or design requirements. Accordingly, the numbers reported for each product in Chapter 3 reflect 2σ estimates of potential systematic error.

For most of the uncertainty sources, the impact on MLS standard products has been quantified by running perturbed radiances through the MLS data processing algorithms. Other (typically smaller) uncertainty sources have been quantified by simple perturbation calculations.

Although the term "systematic uncertainty" is often associated with consistent biases and/or scaling errors, many sources of "systematic" error in the MLS measurement system give rise to additional scatter. For example, an error in the ozone spectroscopy, while being a constant bias on the fundamental parameter, will have an impact on the retrievals of species with weaker signals (e.g., CO) that is dependent on the amount and morphology of atmospheric ozone. By performing end-to-end simulations of the impacts of systematic errors, it is possible to quantify the extent to which such uncertainties either "cancel-out" (e.g., a truly constant bias will not impact a trend calculation) or "average down" (e.g., the impact of ozone-spectroscopy-related errors in MLS CO may be reduced by averaging in some circumstances). A comprehensive consideration of such issues is beyond the scope of most scientific investigations using MLS data. For ease of usage, the results of the MLS systematic error quantification studies are summarized in Chapter 3 simply as "accuracy". More details on the accuracy quantification for each product are given in the respective v2.2*x* MLS validation papers. In addition, Appendix A of *Read et al.* [2007] gives more specific details of the perturbations used in those quantifications.

2.7 A brief note on the Quality field

As described in Section 1.6, the Quality field in the L2GP files gives a measure of the fit achieved between the observed MLS radiances and those computed by the forward model given the retrieved MLS profiles. Quality is computed from a χ^2 statistic for all the radiances considered to have significantly affected the retrieved species (i.e., those close to the relevant spectral lines), normalized by dividing by the number of radiances. Quality is simply the reciprocal of this statistic (a metric chosen such that low values of "quality", corresponding to large χ^2, indicate poor fits).

Ideally, the typical values of these normalized χ^2 statistics will be around one, indicating that radiances are typically fitted to around their noise levels. Quality will therefore also ideally have a typical value of one. For some species, however, because of uncertain knowledge of spectroscopy and/or instrument calibration, the v6.0*x* algorithms are known to be consistently unable to fit some observed radiances to within their predicted noise. In many of these cases, the noise reported on the radiances has been "inflated" to allow the retrieval more leeway in fitting to radiances known to be challenging. As the noise level is the denominator in the χ^2 statistic, these species will have typical χ^2 statistics that are less than one and thus typical values of Quality higher than one. Accordingly, differences in Quality from one species to another do not reflect the species' relative validity, nor do version-to-version increases in Quality for a given product necessarily indicate improvements.

2.8 Changes in v6.0*x* retrievals of N_2O

As discussed in Section 1.4.1, in the v6.0*x* algorithms changes were made to the manner in which N_2O is retrieved from radiances measured by the MLS 190-GHz radiometer. MLS observes N_2O by measuring a spectral line that (particularly in the folded-sideband MLS measurements) is spectrally close to, but 25 times weaker than, the H_2O line at 183 GHz. The sideband fraction fix developed for the CorePlusR2 products in v5.0*x* (see Sections 3.10 and 3.18, as well as *Livesey et al.* [2021]) clearly improved H_2O (and O_3 measurements made by the 190-GHz radiometer) but, for unknown reasons, degraded N_2O. As an unsatisfying workaround for this issue, N_2O in v5.0*x* was retrieved from a separate phase where the sideband fractions were based on the prelaunch calibration value (in contrast with H_2O, which was retrieved using a corrected value for this fraction), with a correction for the drift. This phase also unrealistically assumed no contribution to the 190-GHz

signals from continuum emission. With the exception of drift correction, these changes were empirically derived and non-physical [*Livesey et al.*, 2021]. For v6.0*x* N_2O we opted to instead determine a correction for the 190-GHz radiances based on N_2O information obtained from the stronger and less interference-prone 640-GHz line (measurements from which were available from launch through August 2013). Using a subset of the days for which 640-GHz N_2O measurements are available, we examined the spectral and scan-angle-dependent form of the correction needed to improve the agreement between the 190- and 640-GHz N_2O products. In order to reduce the dependence on specifics of the MLS scan etc., we opted to characterize the correction as a function of the total integrated radiance measured across the 190-GHz band, as a proxy for limb tangent pressure and other parameters. With this correction in place, a separate phase for retrieving N_2O is no longer needed, and the standard N_2O product is again retrieved concurrently with H_2O and HNO_3 (for pressure ≤ 14.7 hPa) from the CorePlusR2 phase, as in v4.2*x* and previous versions. The root of the issue is that the interference between the strong H_2O line and the weak N_2O signature is not modeled well enough to provide an accurate N_2O retrieval (e.g., to within 10%), especially in the lower stratosphere and upper troposphere.

Chapter 3
MLS Level-2 data — product-specific information

3.1 Overview of species-specific discussion

This chapter describes each MLS v6.0*x* "standard product" in more detail. An overview is given of the expected resolution, precision, and accuracy of the data. The resolution is characterized by the averaging kernels described in Section 1.8. Precision is quantified through a combination of the precision estimated by the MLS v6.0*x* algorithms, through reference to the systematic uncertainty budget described in Section 2.6, and through study of the actual MLS data (e.g., quantification of the observed scatter in regions where little natural variability is anticipated, or examination of differences between observations of the same region of the atmosphere measured on successive orbits).

The systematic uncertainty reported is generally based on the study described in Section 2.6. However, in some cases, larger disagreements are seen between MLS and correlative observations than these quantifications would imply. In such cases the discrepancy is noted and the uncertainty quoted reflects these disagreements.

3.1.1 A note on the averaging kernel plots

The averaging kernels shown in this chapter describe both the horizontal (along track) and vertical (pressure) resolution of the MLS v6.0*x* data. While the averaging kernels vary somewhat from profile to profile, their variation is sufficiently small that these samples can be considered representative for all profiles. Estimates of the horizontal and vertical resolution of the product, defined by the full width at half maximum of the kernels, are also given in tables for each product.

3.2 Bromine monoxide (BrO)

Swath name: BrO

Useful range: 10–3.2 hPa (day/night differences needed)

Product lead: Luis Millán <Luis.F.Millan@jpl.nasa.gov>

3.2.1 Introduction

MLS observes BrO emission lines within the 640-GHz radiometer. The spectral signature of BrO in the MLS radiances is very small, leading to a very poor signal-to-noise ratio on individual MLS observations. Significant averaging (e.g., monthly zonal means) is required to obtain scientifically useful results. Large biases of between 12 and 40 pptv (typical BrO abundances range from 5 to 15 pptv) are seen in the data. These biases can be minimized by taking day/night differences. For pressures of 4.6 hPa and greater, nighttime BrO is negligible; however, for smaller pressures, nighttime BrO needs to be taken into account. Table 3.2.1 summarizes the precision, accuracy, and resolution of the MLS v6.0*x* BrO product. The accuracy assessment is based on v2.2*x* data, as described in the validation paper [*Kovalenko et al.*, 2007].

The v6.0*x* "standard" BrO product (as with earlier versions) contains systematic biases and horizontal oscillations that present a larger challenge than for other species. Those interested in using MLS BrO in scientific studies are strongly advised to contact the MLS team before embarking on their research. An algorithm to retrieve daily zonal means of BrO by first averaging the radiances has been developed by the MLS team [*Millán et al.*, 2012]. This dataset and associated documentation is available from the GSFC DISC with the product short name "ML3DZMBRO".

3.2.2 Vertical Resolution

Figure 3.2.1 shows that the vertical resolution for the v6.0*x* MLS BrO is about 5.5 km in the 10 to 4.6 hPa pressure region, degrading to 6 km at 3.2 hPa.

3.2.3 Precision

The expected precision in a retrieved profile is calculated from radiance noise and reported for each retrieved data point. The value of the expected precision is flagged negative or zero if it is worse than 50% of the value of the a priori precision. Figure 3.2.2 compares the expected precision (thick line) on an individual MLS BrO measurement with that deduced from observations of scatter in nighttime observations (expected to be zero). Also shown are the expected precisions for daily, monthly, and yearly 10° zonal means. For the minimal averaging recommended, a monthly 10° zonal mean, which corresponds to about 3,000 measurements, the precision is about ±4 ppt. See Table 3.2.1 for more details.

3.2.4 Accuracy

The accuracy of the MLS BrO product is summarized in Table 3.2.1. The effect of each identified source of systematic error on MLS measurements of radiance has been quantified and modeled [*Read et al.*, 2007]. These quantified effects correspond to either 2σ estimates of uncertainties in each MLS product, or an estimate of the maximum reasonable uncertainty based on instrument knowledge and/or design requirements. More discussion is given in *Kovalenko et al.* [2007]. While that paper described v2.2*x* BrO, findings are expected to be applicable also to v6.0*x*. The potential systematic bias in MLS BrO measurements can be as high as about ±40 ppt at 10 hPa, decreasing to about ±12 pptv at 3.2 hPa. The systematic bias is dramatically reduced by subtracting the nighttime signal from the daytime signal. Taking the day/night difference reduces the systematic biases to ±12 pptv at 10 hPa and ±8 pptv at 3.2 hPa. If the MLS BrO data is used at 3.2 hPa, the day/night difference value will need to be adjusted to compensate for the non-negligible nighttime BrO. We note that this method of taking day/night differences is not applicable for polar summer / winter during periods of continuous sunlight / darkness.

3.2.5 Data screening

Pressure range: 10–3.2 hPa

Values outside this range are not recommended for scientific use.

Averaging required: Significant averaging (such as monthly zonal means) is required to obtain useful data for scientific studies.

Diurnal differences: For use in any scientific study, day/night or ascending/descending differences should be used to alleviate biases.

Note that, for 3.2 hPa, the expected non-zero nighttime abundances of BrO need to be taken into account.

Estimated precision: Only use values for which the estimated precision is a positive number.

Values where the a priori information has a strong influence are flagged with negative or zero precision and should not be used in scientific analyses (see Section 1.5).

Status flag: Only use profiles for which the `Status` field is an even number.

Odd values of `Status` indicate that the profile should not be used in scientific studies. See Section 1.6 for more information on the interpretation of the `Status` field.

Clouds: Profiles identified as being affected by clouds can be used with no restriction.

Quality: Only profiles whose `Quality` field is greater than 1.3 should be used.

Convergence: Only profiles whose `Convergence` field is less than 1.05 should be used.

3.2.6 Artifacts

Significant biases exist in the BrO data, as discussed above. Day/night (or ascending/descending) differences must be used to reduce these biases. At 3.2 hPa, nighttime BrO needs to be taken into account [*Kovalenko et al.*, 2007].

A systematic horizontal (i.e., profile-to-profile) oscillation has been discovered in the MLS v6.0*x* (and earlier) standard BrO product. This presents a significant challenge to the interpretation of the BrO observations. Users are strongly advised to contact the MLS team before embarking on research involving the MLS standard BrO product. As noted above, an alternative zonal-mean BrO dataset produced by the MLS team is available from the GSFC DISC (product short name "ML3DZMBRO").

3.2.7 Review of comparisons with other data sets

We have calculated total bromine, Br_y, from MLS measurements of BrO using a photochemical model and compared that value with Br_y similarly inferred from balloon-borne measurements of BrO; good agreement is seen [*Kovalenko et al.*, 2007; *Millán et al.*, 2012].

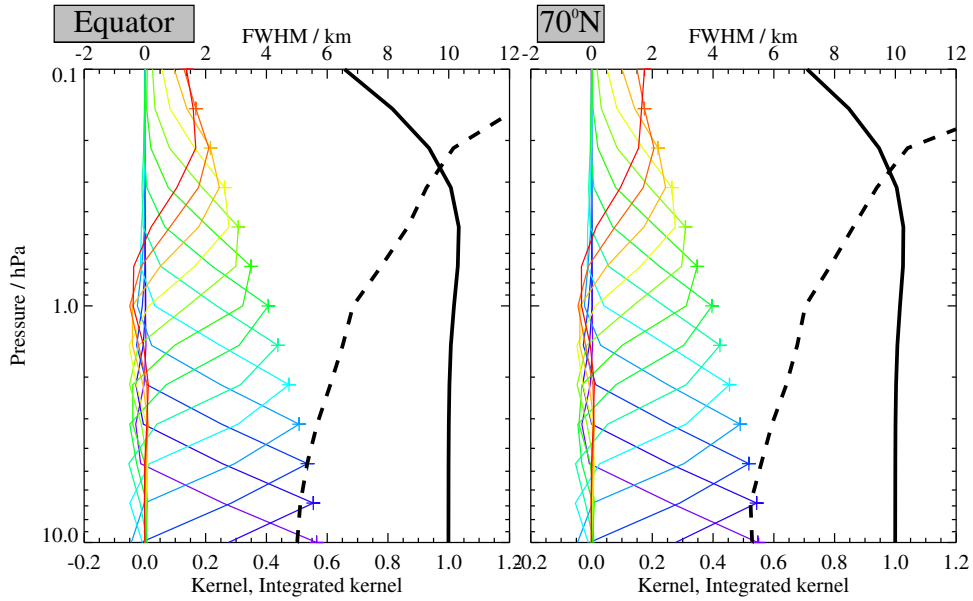

Figure 3.2.1: Typical vertical averaging kernels for the MLS v6.0*x* BrO data at the equator (left) and at 70°N (right); variation in the averaging kernels is sufficiently small that these are representative of typical profiles. Colored lines show the averaging kernels as a function of MLS retrieval level, indicating the region of the atmosphere from which information is contributing to the measurements on the individual retrieval surfaces, which are denoted by plus signs in corresponding colors. The dashed black line indicates the vertical resolution, determined from the full width at half maximum (FWHM) of the averaging kernels, approximately scaled into kilometers (top axes). The solid black line shows the integrated area under each kernel; values near unity imply that the majority of information for that MLS data point has come from the measurements, whereas lower values imply substantial contributions from a priori information. The low signal to noise for this product necessitates the use of significant averaging (e.g., monthly zonal mean), making horizontal averaging kernels largely irrelevant.

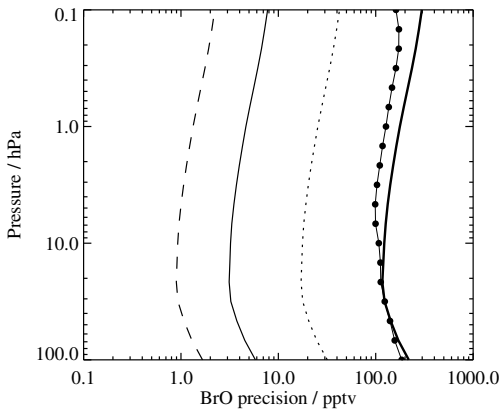

Figure 3.2.2: Comparison of the MLS v6.0*x* BrO precision as estimated from scatter in the retrieved data (circles) with that expected from the retrieval (thick line), for a single profile. Also shown is the expected precision for the day/night difference of 10° zonal-mean profiles averaged over a day (dotted line), a month (thin line) and a year (dashed line).

Table 3.2.1: Summary of Aura MLS v6.0*x* BrO characteristics

Pressure	Vertical resolution	Precision[a]	Day/night difference accuracy[b]	Comments
hPa	km	pptv	pptv	
2.2 and less	–	–	–	Unsuitable for scientific use
3.2	6	±5	±6	Need to account for non-negligible nighttime BrO
4.6	5.5	±4	±8	Use day–night difference
6.8	5.5	±4	±9	Use day–night difference
10	5.5	±4	±10	Use day–night difference
150–15	–	–	–	Unsuitable for scientific use
1000–215	–	–	–	Not retrieved

[a]The precision quoted is for a 10° monthly zonal mean

[b]Because of large biases in the data, the daytime and nighttime BrO data are unsuitable for scientific use, so day/night differences must be used. Note that day/night differences are not useful for polar winter and summer, where BrO does not undergo a diurnal variation.

3.3 Methyl chloride (CH_3Cl)

Swath name: CH3Cl

Useful range: 147–4.6 hPa

Product lead: Michelle Santee <Michelle.L.Santee@jpl.nasa.gov>

3.3.1 Introduction

As is the case for ClO, the standard CH_3Cl product is derived from radiances measured by the radiometer centered near 640 GHz. The v2.2*x* MLS ClO measurements were characterized by a substantial (~0.1–0.4 ppbv) negative bias at retrieval levels below (i.e., pressures larger than) 22 hPa. *Santee et al.* [2008] suggested that contamination from an interfering species such as CH_3Cl, which has lines in two wing channels of the 640-GHz band used to measure ClO, could have given rise to the bias; they showed results from precursory v3 algorithms in which CH_3Cl was also retrieved that demonstrated significant reduction in the bias in lower stratospheric ClO. Further refinements in the v3.3*x*/v3.4*x* algorithms yielded not only an improved ClO product, but also a reliable retrieval of CH_3Cl. The quality and reliability of the v3.3*x*/v3.4*x* MLS CH_3Cl measurements were assessed in detail by *Santee et al.* [2013].

Limb radiances measured by the MLS 640-GHz radiometer are also affected by water vapor. As noted in Section 1.10.2, as of May 2024, the MLS 190-GHz radiometer, which is used to measure water vapor, is operated only intermittently. When that radiometer is turned off and H_2O measurements are not available, a priori information for H_2O (based on climatological values) is used in the CH_3Cl retrievals, adversely affecting their quality; further details are given in Section 3.3.8. The MLS v6.0*x* CH_3Cl data are scientifically useful over the range 147 to 4.6 hPa. A summary of the estimated precision, resolution (vertical and horizontal), and systematic uncertainty of the v6.0*x* CH_3Cl measurements as a function of altitude is given in Table 3.3.1.

3.3.2 Differences between v5.0*x* and v6.0*x*

Throughout most of the lower stratosphere, the CH_3Cl retrieval has changed very little (by less than ±10%) between v5.0*x* and v6.0*x* (Figures 3.3.1 and 3.3.2). Mixing ratios are slightly larger (by up to 10–20%) in v6.0*x* at 147 hPa in the tropics. Larger (>30%, both positive and negative) differences are present at 15 hPa and lower pressures in the polar regions.

3.3.3 Resolution

The resolution of the retrieved data can be described using "averaging kernels" [e.g., *Rodgers*, 2000]; the two-dimensional nature of the MLS data processing system means that the kernels describe both vertical and horizontal resolution. Values of the integrated kernel near unity indicate that the majority of information for that level has come from the measurements themselves and not the a priori; Figure 3.3.3 shows that the measurements dominate at pressures greater than 3.2 hPa, above which level the integrated kernel drops below 0.5. Smoothing, imposed on the retrieval system in both the vertical and horizontal directions to enhance retrieval stability and precision, degrades the inherent resolution of the measurements. Thus, although CH_3Cl measurements are reported at six pressure levels per decade change in pressure (spacing of ~2.7 km), the vertical resolution of the v6.0*x* CH_3Cl data as determined from the full width at half maximum of the rows of the averaging kernel matrix shown in Figure 3.3.3 is ~4–6 km in most of the lower stratosphere, degrading to ~8–10 km at and above (i.e., at pressures less than) 15 hPa. The averaging kernels are fairly symmetric, and for the most part they peak at their nominal position. However, overlap in the averaging kernels for the 100 and 147 hPa retrieval surfaces indicates that the 147 hPa retrieval does not provide as much independent information as is given by retrievals at higher altitudes. Figure 3.3.3 also shows horizontal averaging kernels, from which the along-track horizontal resolution is determined to be ~600 km at 147 hPa, ~500 km from 100 to 22 hPa, and ~600–900 km at and above 15 hPa. The cross-track resolution, set by the width of the field of view of the 640-GHz radiometer, is ~3 km. The along-track separation between adjacent retrieved profiles

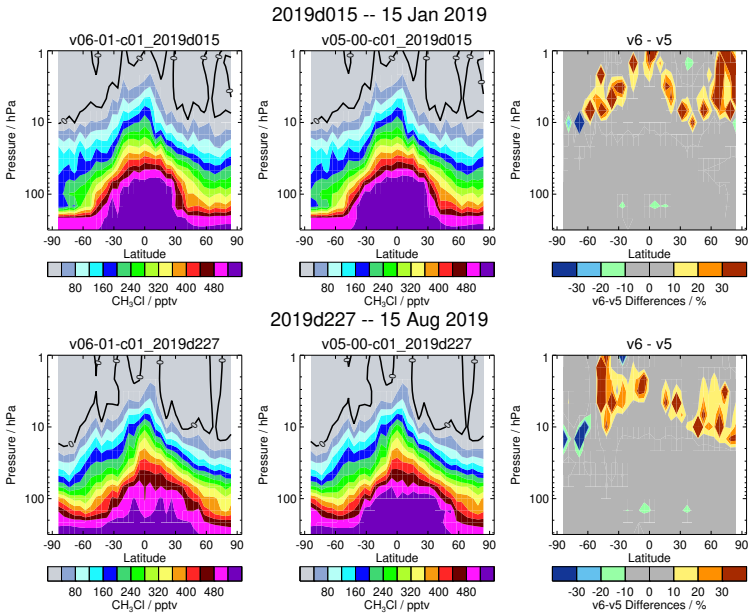

Figure 3.3.1: Zonal mean pressure-latitude cross sections of MLS CH_3Cl, for (left) v6.0*x*, (middle) v5.0*x*, and (right) their differences (v6.0*x* minus v5.0*x*, in percent). Results are shown for two representative days in different seasons. The black curves overlaid on the abundance panels (left and middle) mark the zero contour. No quality screening of the data has been performed.

is 1.5° great circle angle (~165 km), whereas the longitudinal separation of MLS measurements, set by the Aura orbit, is 10°–20° over low and middle latitudes, with much finer sampling in the polar regions.

3.3.4 Precision

The precision of the MLS CH_3Cl data is estimated empirically by comparing profiles measured at the intersections of ascending (mainly day) and descending (mainly night) portions of the orbit. Under ideal conditions (i.e., a quiescent atmosphere), the standard deviation about the mean differences between such matched profile pairs provides a measure of the precision of the individual data points. In practice, however, real changes in the atmosphere may occur over the 12 h interval between the intersecting measurement points, in which case the observed scatter provides an upper limit on the estimate of precision, assuming that the a priori has a negligible influence on the retrieval (a reasonable assumption at least at pressures greater than 3.2 hPa). The precision estimates were found to be essentially invariant with time; results for a representative year of data are shown in Figure 3.3.4. Mean differences between paired crossing profiles are ~10 pptv or less except at the lowest three levels, where they reach ~15–20 pptv. Given the large number of data points being compared, these ascending−descending differences are substantially larger than the standard error of the mean, implying the presence of significant systematic biases. These biases likely arise from the cumulative effect of various factors in the retrieval system that can vary diurnally or along the orbit, such as interferences from temperature or other atmospheric constituents (e.g., H_2O and ClO), or thermal emissions from the MLS antenna.

The observed standard deviation values are ~100–140 pptv throughout the vertical range over which the data are recommended for scientific use (see Section 3.3.5 below). The precision reported for each data point by the Level 2 data processing system exceeds the observationally determined precision throughout the vertical range (Figure 3.3.4), indicating that the vertical smoothing (regularization) applied to stabilize the retrieval system and improve the precision has a non-negligible influence. Because the reported precisions take into account occasional variations in instrument performance, the best estimate of the precision of an individual data point is the value quoted for that point in the L2GP files, but it should be borne in mind that

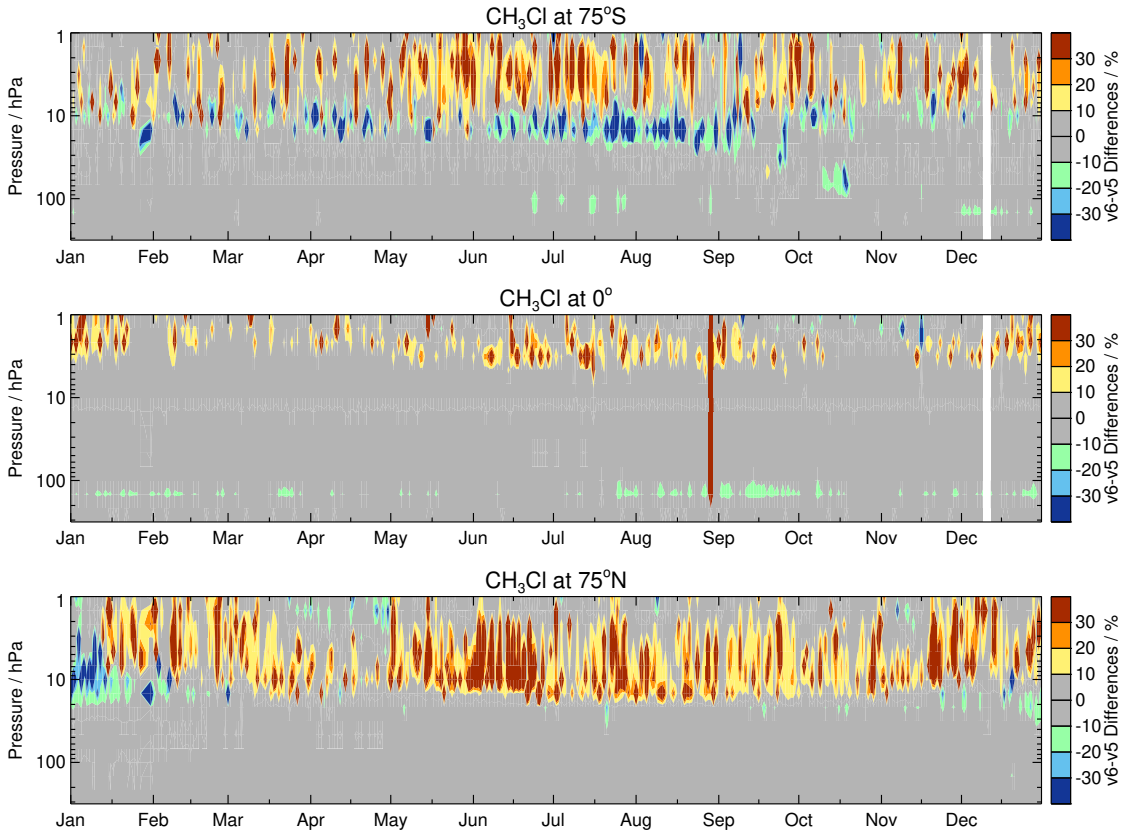

Figure 3.3.2: Time series for a representative year (2019) of v6.0*x* minus v5.0*x* MLS CH_3Cl (percent differences), for (top) 75°S, (middle) the equator, and (bottom) 75°N. No quality screening of the data has been performed.

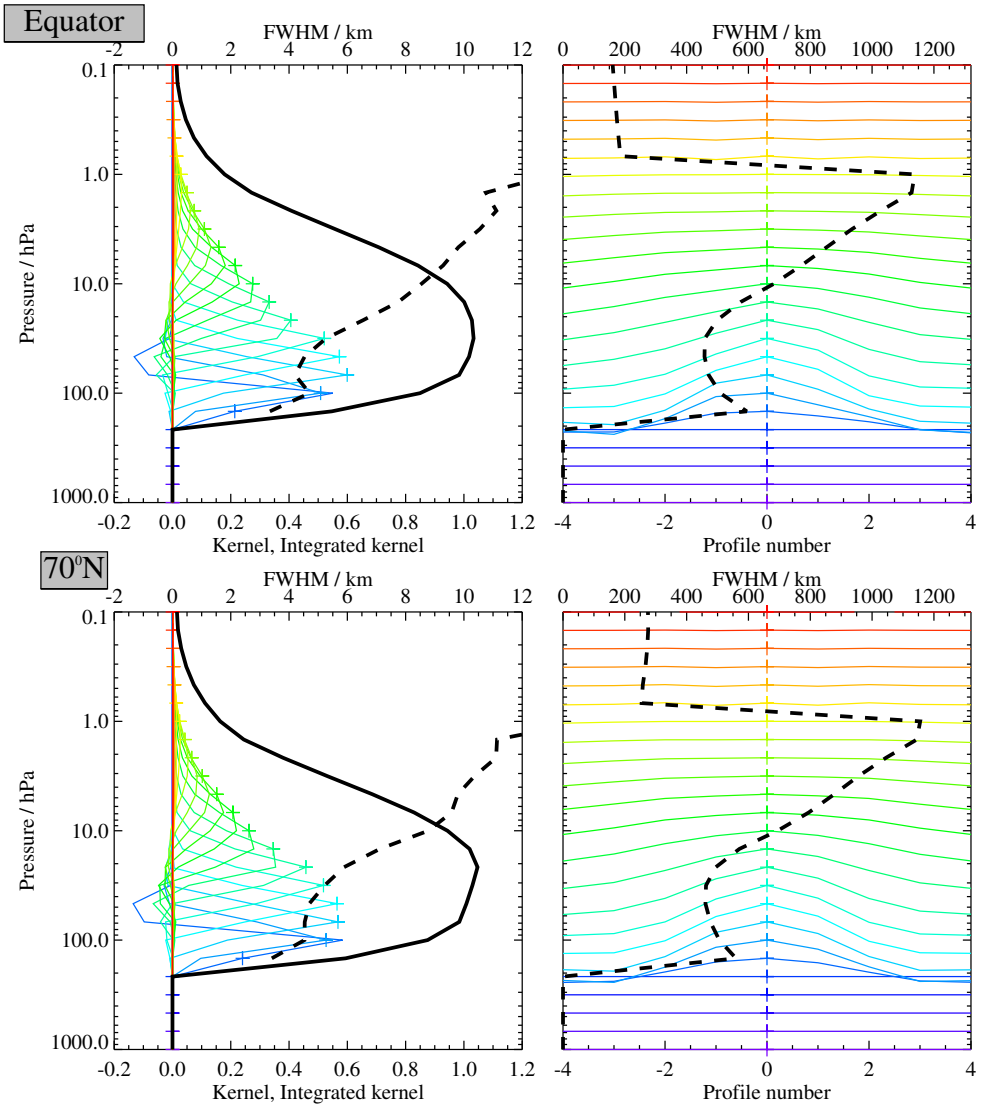

Figure 3.3.3: Typical two-dimensional (vertical and horizontal along-track) averaging kernels for the MLS v6.0*x* CH_3Cl data at the equator (upper) and at 70°N (lower); variation in the averaging kernels is sufficiently small that these are representative of typical profiles. Colored lines show the averaging kernels as a function of MLS retrieval level, indicating the region of the atmosphere from which information is contributing to the measurements on the individual retrieval surfaces, which are denoted by plus signs in corresponding colors. The dashed black line indicates the resolution, determined from the full width at half maximum (FWHM) of the averaging kernels, approximately scaled into kilometers (top axes). (Left) Vertical averaging kernels (integrated in the horizontal dimension for five along-track profiles) and resolution. The solid black line shows the integrated area under each kernel (horizontally and vertically); values near unity imply that the majority of information for that MLS data point has come from the measurements, whereas lower values imply substantial contributions from a priori information. (Right) Horizontal averaging kernels (integrated in the vertical dimension) and resolution. The horizontal averaging kernels are shown scaled such that a unit averaging kernel amplitude is equivalent to a factor of 10 change in pressure.

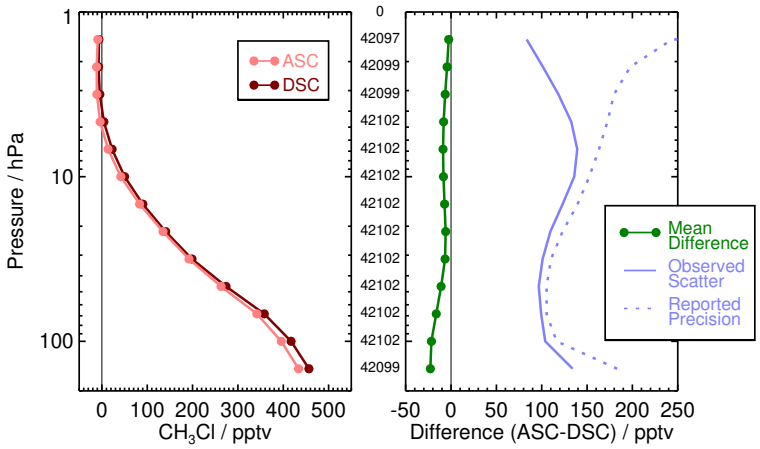

Figure 3.3.4: (left) Ensemble mean profiles for ascending (light red) and descending (dark red) orbit matching pairs of MLS v6.0*x* CH_3Cl profiles averaged over a representative year of data (2019). Symbols indicate MLS retrieval pressure levels. (right) Mean differences (ascending minus descending) in pptv (green solid line). Also shown are the standard deviations about the mean differences (light blue solid line) and the root sum square (RSS) of the precisions calculated by the retrieval algorithm for the two sets of profiles (light blue dotted line). The observed scatter about the mean differences and the reported precision values have been scaled by $1/\sqrt{2}$ (to convert from standard deviations of differences into standard deviations of individual data points); hence the light blue solid line represents the statistical repeatability of the MLS measurements, and the light blue dotted line represents the expected 1 precision for a single profile. The thin black lines mark zero in each panel. The number of crossing pairs of measurements being compared at each pressure level is noted in the space between the panels.

this approach slightly overestimates the actual measurement noise. The estimates reported here represent the precisions at each pressure level of a single profile; precision can generally be improved by averaging, with the precision of an average of N profiles being $1/\sqrt{N}$ times the precision of an individual profile.

3.3.5 Range

Although CH_3Cl is retrieved (and reported in the L2GP files) over the range 147 to 0.001 hPa, on the basis of the degradation in resolution and expected precision, the reduction in independent information contributed by the measurements, and the results of simulations using synthetic data as input radiances to test the closure of the retrieval system, the data are not deemed reliable at retrieval pressures less than 4.6 hPa. Despite the overlap in the averaging kernels for the 147 and 100 hPa surfaces discussed above, the simulations show that the retrieved CH_3Cl values track the variations in the "truth" field at both levels. Moreover, the retrievals (of real data) at 147 hPa display significant features not seen at 100 hPa (not shown) that are believed to represent actual atmospheric variations. Thus, we recommend that the v6.0*x* CH_3Cl data may be used for scientific studies between 147 and 4.6 hPa (inclusive), although the reduced sensitivity at the extremes of this range, as well as the relatively coarse vertical resolution of the retrieved profiles, should be borne in mind.

3.3.6 Accuracy

The effects of various sources of systematic uncertainty (e.g., instrumental issues, spectroscopic uncertainty, and approximations in the retrieval formulation and implementation) on the MLS v6.0*x* CH_3Cl measurements were quantified through a comprehensive set of retrievals of synthetic radiances; see *Santee et al.* [2013] for details of a similar analysis conducted on MLS v3.3*x*/v3.4*x* CH_3Cl data. The overall systematic uncertainty, or accuracy, is calculated by combining (RSS) the contributions from both the expected biases and the additional scatter each source of uncertainty may introduce into the data. In aggregate, the factors considered in these simulations are estimated to give rise to total systematic uncertainty in the MLS v6.0*x* CH_3Cl data ranging from approximately 50 to 250 pptv, depending on the level (see Table 3.3.1).

3.3.7 Review of comparisons with other datasets

Extensive comparisons of MLS v3.3*x*/v3.4*x* CH_3Cl with measurements from a variety of instruments (balloon-borne, aircraft, and satellite) were presented by *Santee et al.* [2013]. Comparisons of v6.0*x* CH_3Cl with correlative data have not been conducted but are expected to yield results similar to those for previous versions.

3.3.8 Data screening

Pressure range: 147–4.6 hPa

Values outside this range are not recommended for scientific use.

Estimated precision: Only use values for which the estimated precision is a positive number.

Values where the a priori information has a strong influence are flagged with negative or zero precision and should not be used in scientific analyses (see Section 1.5).

Status flag: Only use profiles for which the `Status` field is zero.

We recommend that all profiles with nonzero values of `Status` be discarded, because of the potential impact of cloud artifacts at lower levels. Note, however, that rejecting in their entirety all profiles with nonzero `Status` may be unnecessarily severe at and above (i.e., at pressures equal to or smaller than) 46 hPa, where clouds have negligible impact; thus otherwise good-quality profiles with nonzero but even `Status` values may be used without restriction at those levels as long as they are removed at larger pressures. See Section 1.6 for more information on the interpretation of the `Status` field.

Quality: Only profiles whose `Quality` field is greater than 1.3 should be used.

In a typical month this threshold for `Quality` (unchanged from v5.0*x*) discards few (0.3% or less) of the CH_3Cl profiles; note that it potentially discards some "good" data points while not necessarily identifying all "bad" ones.

Convergence: Only profiles whose `Convergence` field is less than 1.05 should be used.

In a typical month this threshold for `Convergence` (unchanged from v5.0*x*) discards few (0.1% or less) of the CH_3Cl profiles, most (but not all) of which are filtered out by the other quality control measures.

Additional screening on H_2O `Status`: As noted earlier, CH_3Cl retrieval quality is degraded at some levels when the 190-GHz radiometer is turned off and H_2O measurements are not available. In these circumstances, biases in the retrieved CH_3Cl values as large as 5% at 68–100 hPa and 20% at 147 hPa are seen. These artifacts are not removed by the standard CH_3Cl data filtering protocols. Thus, while the CH_3Cl data on affected days are still useful for purely morphological or qualitative purposes, they cannot be quantitatively compared to measurements taken on surrounding days or in previous years when the 190-GHz radiometer was operational. The biases also have potential implications for the calculation of long-term trends. Therefore, for quantitative studies using CH_3Cl data at those retrieval levels, an additional screening step is recommended, whereby the `Status` field in the colocated H_2O profile is examined to remove affected CH_3Cl retrievals. That is, only CH_3Cl profiles for which the `Status` flags of the corresponding H_2O profiles are an even number should be used in quantitative studies relying on CH_3Cl measurements in the 68–147 hPa range (at lower pressures / higher altitudes, all CH_3Cl data points passing the standard quality screening measures may be used). We also note, however, that measurements taken during time periods since May 2024 when the 190-GHz radiometer is turned off can be intercompared.

3.3.9 Artifacts

- Significant ascending−descending differences imply the presence of systematic biases at the bottom three retrieval pressure levels. However, various analyses performed separately on sets of ascending-only and descending-only measurements suggest that, although significant, these biases will have little or no impact on most scientific conclusions based on the MLS CH_3Cl measurements.

- As discussed in Section 3.3.8, considerable biases in CH_3Cl values are present at some levels when coincident measurements from the 190-GHz radiometer are not available and H_2O a priori information is used in the CH_3Cl retrieval. Depending on the specific goals of any study based on these measurements, additional CH_3Cl data quality filtering may be necessary for days when the 190-GHz radiometer is off.

3.3.10 Desired improvements should another data version be produced

Specific achievable improvements in the CH_3Cl retrieval remain to be determined.

Table 3.3.1: Summary of Aura MLS v6.0*x* CH_3Cl Characteristics

Pressure hPa	Resolution[a] V × H km	Single-Profile Precision[b] pptv	Accuracy[c] pptv	Known Artifacts or Other Comments
3.2–0.001	—	—	—	Unsuitable for scientific use
4.6	10 × 900	±140	±50	
10–6.8	9 × 800	±140	±50	
15	8 × 600	±140	±50	
21	6.5 × 500	±100	±70	
68–32	5 × 500	±100	±120	
100	4.5 × 500	±100	±200	
147	3.5 × 600	±140	±250	
1000–215	—	—	—	Not retrieved

[a]Vertical and along-track horizontal resolutions, the cross-track resolution is ~3 km.
[b]Precision on individual profiles, determined from observed scatter in the data in a region of minimal atmospheric variability.
[c]Values should be interpreted as 2σ estimates of the probable magnitude.

3.4 Methyl cyanide (CH_3CN)

Swath name: CH3CN

Useful range: 46–1.0 hPa

Product lead: Michelle Santee <Michelle.L.Santee@jpl.nasa.gov>

3.4.1 Introduction

In v6.0*x*, as in v5.0*x*, the standard CH_3CN product is taken from radiances measured by the radiometer centered near 640 GHz. The CH_3CN retrieval is largely unchanged in v6.0*x* over the altitude range of most interest for this species. Although the data have not been validated extensively, the v6.0*x* CH_3CN retrievals are deemed to be scientifically useful over the range 46 to 1 hPa, except in the winter polar regions, where they may exhibit large biases below (i.e., at pressures greater than) 10 hPa. Data retrieved at pressures greater than 46 hPa may be used with caution in certain circumstances (e.g., as a marker of pollution injected into the upper troposphere / lower stratosphere, UTLS). Limb radiances measured by the MLS 640-GHz radiometer are affected by water vapor (and other species) in addition to CH_3CN. As noted in Section 1.10.2, as of May 2024, the MLS 190-GHz radiometer, which is used to measure water vapor, is operated only intermittently. When that radiometer is turned off and H_2O measurements are not available, a priori information for H_2O (based on climatological values) is used in the CH_3CN retrievals, adversely affecting their quality; further details are given in Section 3.4.8. A summary of the estimated precision, resolution (vertical and horizontal), and systematic uncertainty of the v6.0*x* CH_3CN measurements as a function of altitude is given in Table 3.4.1.

3.4.2 Differences between v5.0*x* and v6.0*x*

Except near the top of the retrieval range (where the data are generally of less interest), the CH_3CN retrieval has changed very little between v5.0*x* and v6.0*x*. Differences are within ±10% throughout all seasons in most regions (Figures 3.4.1 and 3.4.2). Larger (>30%, mostly negative) differences are occasionally seen around 10 hPa in both polar regions.

3.4.3 Resolution

The resolution of the retrieved data can be described using "averaging kernels" [e.g., *Rodgers*, 2000]; the two-dimensional nature of the MLS data processing system means that the kernels describe both vertical and horizontal resolution. Values of the integrated kernel near unity indicate that the majority of information for that level has come from the measurements themselves and not the a priori; Figure 3.4.3 shows that the measurements dominate throughout most of the vertical range. Smoothing, imposed on the retrieval system in both the vertical and horizontal directions to enhance retrieval stability and precision, degrades the inherent resolution of the measurements. Thus, although CH_3CN measurements are reported at six pressure levels per decade change in pressure (spacing of ~2.7 km), the vertical resolution of the v6.0*x* CH_3CN data as determined from the full width at half maximum of the rows of the averaging kernel matrix shown in Figure 3.4.3 degrades from ~4.5 km at 147 hPa to ~5–6.5 km in the lower stratosphere, and then further worsens to ~7–8 km in the upper stratosphere. Substantial overlap in the averaging kernels for the 100 and 147 hPa retrieval surfaces (which both peak at 100 hPa) indicates that the 147 hPa retrieval does not provide as much independent information as is given by retrievals at higher altitudes. Figure 3.4.3 also shows horizontal averaging kernels, from which the along-track horizontal resolution is determined to be ~400–700 km over most of the vertical range. The cross-track resolution, set by the width of the field of view of the 640-GHz radiometer, is ~3 km. The along-track separation between adjacent retrieved profiles is 1.5° great circle angle (~165 km), whereas the longitudinal separation of MLS measurements, set by the Aura orbit, is 10°–20° over low and middle latitudes, with much finer sampling in the polar regions.

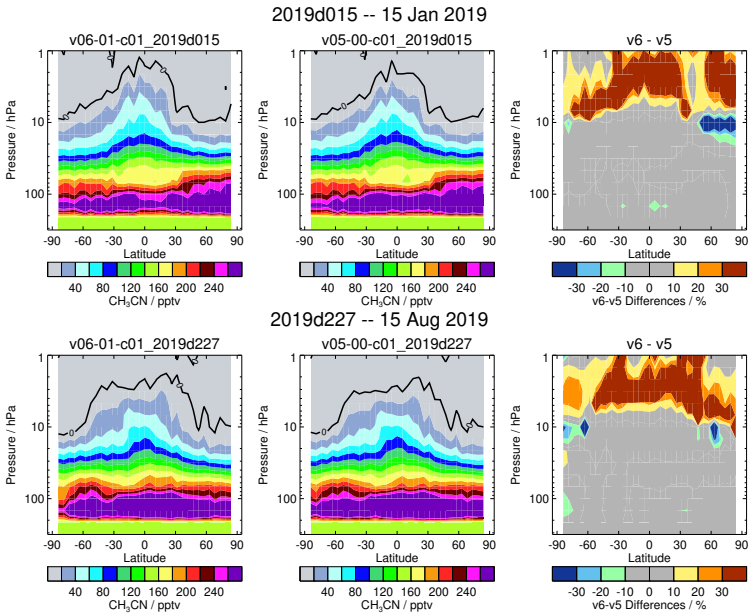

Figure 3.4.1: Zonal mean pressure-latitude cross sections of MLS CH_3CN, for (left) v6.0*x*, (middle) v5.0*x*, and (right) their differences (v6.0*x* minus v5.0*x*, in percent). Results are shown for two representative days in different seasons. The black curves overlaid on the abundance panels (left and middle) mark the zero contour. No quality screening of the data has been performed.

3.4.4 Precision

The precision of the MLS CH_3CN data is estimated empirically by comparing profiles measured at the intersections of ascending (mainly day) and descending (mainly night) portions of the orbit. Under ideal conditions (i.e., a quiescent atmosphere), the standard deviation about the mean differences between such matched profile pairs provides a measure of the precision of the individual data points. In practice, however, real changes in the atmosphere may occur over the 12 h interval between the intersecting measurement points, in which case the observed scatter provides an upper limit on the estimate of precision, assuming that the a priori has a negligible influence on the retrieval (a reasonable assumption throughout the retrieval range for CH_3CN). The precision estimates were found to be essentially invariant with time; results for a representative year of data are shown in Figure 3.4.4. Mean differences between paired crossing profiles are negligible, indicating the absence of significant systematic ascending / descending biases.

The observed standard deviation values are 50 pptv or less throughout most of the vertical domain, increasing to ~120 pptv at 147 hPa and ~100 pptv at 1 hPa. The precision reported for each data point by the Level 2 data processing system exceeds the observationally determined precision throughout the vertical range (Figure 3.4.4), indicating that the vertical smoothing (regularization) applied to stabilize the retrieval system and improve the precision has a non-negligible influence. Because the reported precisions take into account occasional variations in instrument performance, the best estimate of the precision of an individual data point is the value quoted for that point in the L2GP files, but it should be borne in mind that this approach slightly overestimates the actual measurement noise. The estimates reported here represent the precisions at each pressure level of a single profile; precision can generally be improved by averaging, with the precision of an average of N profiles being $1/\sqrt{N}$ times the precision of an individual profile.

3.4.5 Range

Although CH_3CN is retrieved (and reported in the L2GP files) over the range 147 to 0.001 hPa, on the basis of the degradation in resolution and expected precision, the lack of independent information contributed by the measurements, the results of simulations using synthetic data as input radiances to test the closure of

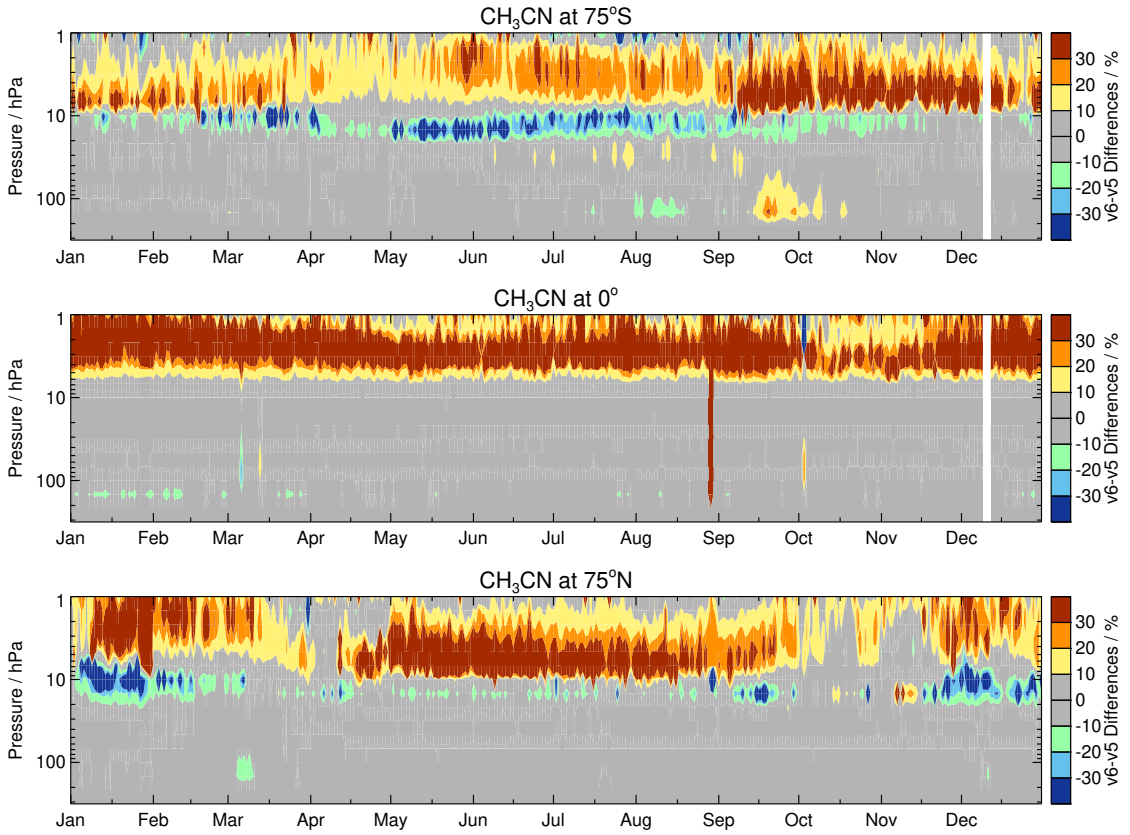

Figure 3.4.2: Time series for a representative year (2019) of v6.0*x* minus v5.0*x* MLS CH_3CN (percent differences), for (top) 75°S, (middle) the equator, and (bottom) 75°N. No quality screening of the data has been performed.

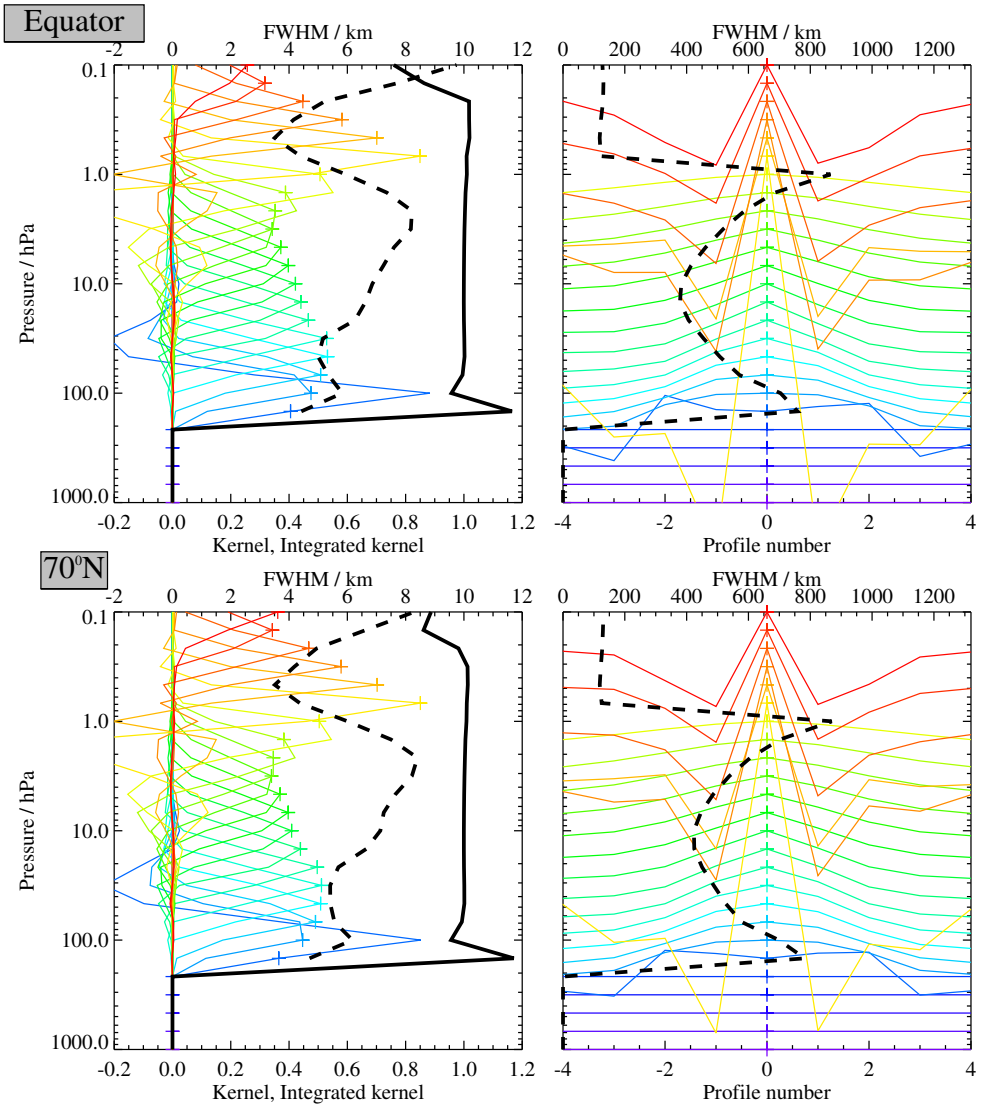

Figure 3.4.3: Typical two-dimensional (vertical and horizontal along-track) averaging kernels for the MLS v6.0*x* CH_3CN data at the equator (upper) and at 70°N (lower); variation in the averaging kernels is sufficiently small that these are representative of typical profiles. Colored lines show the averaging kernels as a function of MLS retrieval level, indicating the region of the atmosphere from which information is contributing to the measurements on the individual retrieval surfaces, which are denoted by plus signs in corresponding colors. The dashed black line indicates the resolution, determined from the full width at half maximum (FWHM) of the averaging kernels, approximately scaled into kilometers (top axes). (Left) Vertical averaging kernels (integrated in the horizontal dimension for five along-track profiles) and resolution. The solid black line shows the integrated area under each kernel (horizontally and vertically); values near unity imply that the majority of information for that MLS data point has come from the measurements, whereas lower values imply substantial contributions from a priori information. (Right) Horizontal averaging kernels (integrated in the vertical dimension) and resolution. The horizontal averaging kernels are shown scaled such that a unit averaging kernel amplitude is equivalent to a factor of 10 change in pressure.

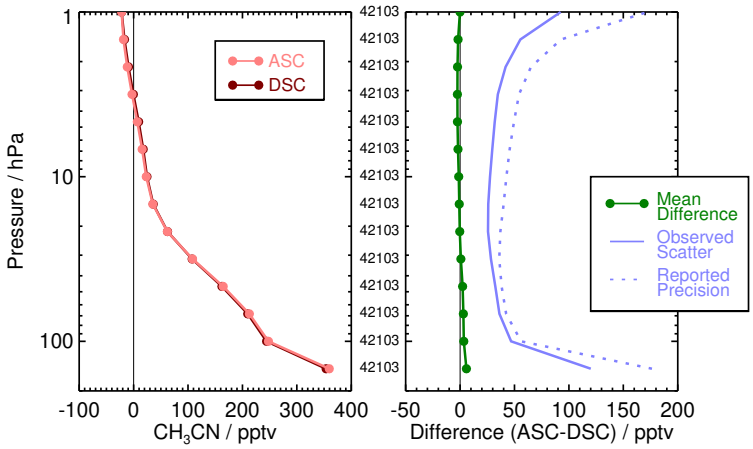

Figure 3.4.4: (left) Ensemble mean profiles for ascending (light red) and descending (dark red) orbit matching pairs of MLS v6.0*x* CH_3CN profiles averaged over a representative year of data (2019). Symbols indicate MLS retrieval pressure levels. (right) Mean differences (ascending−descending) in pptv (green solid line). Also shown are the standard deviations about the mean differences (light blue solid line) and the root sum square (RSS) of the precisions calculated by the retrieval algorithm for the two sets of profiles (light blue dotted line). The observed scatter about the mean differences and the reported precision values have been scaled by $1/\sqrt{2}$ (to convert from standard deviations of differences into standard deviations of individual data points); hence the light blue solid line represents the statistical repeatability of the MLS measurements, and the light blue dotted line represents the expected 1precision for a single profile. The thin black lines mark zero in each panel. The number of crossing pairs of measurements being compared at each pressure level is noted in the space between the panels.

the retrieval system, and the inconsistency of the morphology of the retrieved profiles with expectation, the CH_3CN data are not deemed reliable at the extremes of the retrieval range. For example, positive biases are particularly large at high latitudes at altitudes below (i.e., pressures larger than) 10 hPa. In addition, the data display unrealistic sharp latitudinal gradients at around ±30° at 147–68 hPa (see the "concave" shape of the contours in this region in Figure 3.4.1). Thus we recommend that v6.0*x* CH_3CN be used for scientific studies only at the levels between 46 and 1 hPa. However, although the 147, 100, and 68 hPa retrievals are not generally recommended, they may be scientifically useful in some circumstances. The large-scale longitudinal variations within the tropics are probably robust. Similarly, confined regions of significant enhancement at 147 hPa unaccompanied by comparably enhanced values at 100 hPa may reflect real atmospheric features. Indeed, many of the "hotspots" apparent in MLS CH_3CN measurements in the UTLS closely track similar enhancements in other pollution markers measured by MLS, such as CO and CH_3Cl. The v6.0*x* CH_3CN data at the lowest retrieval levels (147–68 hPa) should only be used in consultation with the MLS science team.

3.4.6 Accuracy

The effects of various sources of systematic uncertainty (e.g., instrumental issues, spectroscopic uncertainty, and approximations in the retrieval formulation and implementation) on the MLS v6.0*x* CH_3CN measurements were quantified through a comprehensive set of retrievals of synthetic radiances. The overall systematic uncertainty, or accuracy, is calculated by combining (RSS) the contributions from both the expected biases and the additional scatter each source of uncertainty may introduce into the data. In aggregate, the factors considered in these simulations are estimated to give rise to total systematic uncertainty in the MLS v6.0*x* CH_3CN data ranging from approximately 20 to more than 100 pptv, depending on the level (see Table 3.4.1).

3.4.7 Review of comparisons with other datasets

Detailed quantification of differences from correlative data sets has not been performed, but preliminary comparisons suggest that the MLS CH_3CN measurements are biased substantially high in the UTLS relative to airborne [*Singh et al.*, 2003], balloon-borne [*Kleinböhl et al.*, 2005], and ACE-FTS satellite [*Harrison and Bernath*, 2013] CH_3CN measurements, as do results from a two-dimensional chemistry transport model and

(noncoincident) CH_3CN retrievals from the predecessor MLS instrument on the Upper Atmosphere Research Satellite (UARS) [*Livesey et al.*, 2001] (not shown). Furthermore, as noted above, the zonal-mean morphology of the Aura MLS CH_3CN at the lowest levels does not agree well with that either observed from space (by UARS MLS and ACE-FTS) or predicted by the model. In the middle and upper stratosphere, v4.2*x* MLS CH_3CN measurements were shown to be consistent with those from the Superconducting Submillimeter-Wave Limb-Emission Sounder (SMILES), which operated aboard the International Space Station for 6 months in 2009/2010 [*Fujinawa et al.*, 2020]. Absolute differences between coincident CH_3CN profiles from the two instruments were <25 ppt (20–80%) in the range 15–5 hPa, increasing to 35 ppt (260%) at 1.6 hPa.

3.4.8 Data screening

Pressure range: 46–1.0 hPa

Values outside this range are not recommended for scientific use. The CH_3CN data at 147–68 hPa may be useful under certain circumstances but should not be analyzed in scientific studies without significant discussion with the MLS science team.

Estimated precision: Only use values for which the estimated precision is a positive number.

Values where the a priori information has a strong influence are flagged with negative or zero precision and should not be used in scientific analyses (see Section 1.5).

Status flag: Only use profiles for which the `Status` field is zero.

We recommend that all profiles with nonzero values of `Status` be discarded, because of the potential impact of cloud artifacts at lower levels. Note, however, that rejecting in their entirety all profiles with nonzero `Status` may be unnecessarily severe at and above (i.e., at pressures equal to or smaller than) 46 hPa, where clouds have negligible impact; thus otherwise good-quality profiles with nonzero but even `Status` values may be used without restriction at those levels as long as they are removed at larger pressures. See Section 1.6 for more information on the interpretation of the `Status` field.

Quality: Only profiles whose `Quality` field is greater than 1.4 should be used.

In a typical month this threshold for `Quality` (unchanged from v5.0*x*) discards few (0.2% or less) of the CH_3CN profiles; note that it potentially discards some "good" data points while not necessarily identifying all "bad" ones.

Convergence: Only profiles whose `Convergence` field is less than 1.05 should be used.

In a typical month this threshold for `Convergence` (unchanged from v5.0*x*) discards few (0.2% or less) of the CH_3CN profiles, many (but not all) of which are filtered out by the other quality control measures.

Additional screening on H_2O `Status`: As noted earlier, CH_3CN retrieval quality is degraded at some levels when the 190-GHz radiometer is turned off and H_2O measurements are not available. In these circumstances, biases in the retrieved CH_3CN values as large as 30% are seen at 100 and 147 hPa. These artifacts are not removed by the standard CH_3CN data filtering protocols. Thus, while the CH_3CN data on affected days may still be useful for purely morphological or qualitative purposes, they cannot be quantitatively compared to measurements taken on surrounding days or in previous years when the 190-GHz radiometer was operational. The biases also have potential implications for the calculation of long-term trends. It should be borne in mind that CH_3CN data are not typically recommended for scientific use at retrieval levels below (i.e., pressures greater than) 46 hPa. However, for quantitative studies using CH_3CN data at the lower retrieval levels (e.g., in cases of convective injection of pollutants into the UTLS), an additional screening step is recommended, whereby the `Status` field in the colocated H_2O profile is examined to remove affected CH_3CN retrievals. That is, only CH_3CN profiles for which the `Status` flags of the corresponding H_2O profiles are an even number should be used in quantitative studies relying on CH_3CN measurements at 100–147 hPa (at lower pressures / higher altitudes, all CH_3CN data points passing the standard quality screening measures may be used). We also note,

however, that measurements taken during time periods since May 2024 when the 190-GHz radiometer is turned off can be intercompared.

3.4.9 Artifacts

- The measurements exhibit a substantial high bias throughout the UTLS, particularly in the polar regions.
- Over the range 147–68 hPa, the retrievals are characterized by unphysical sharp latitudinal gradients at around ±30°.
- As discussed in Section 3.4.8, considerable biases in CH_3CN values are present at some levels when coincident measurements from the 190-GHz radiometer are not available and H_2O a priori information is used in the CH_3CN retrieval. Depending on the specific goals of any study based on these measurements, additional CH_3CN data quality filtering may be necessary for days when the 190-GHz radiometer is off.

3.4.10 Desired improvements should another data version be produced

Specific achievable improvements in the CH_3CN retrieval remain to be determined.

Table 3.4.1: Summary of Aura MLS v6.0*x* CH_3CN Characteristics

Pressure hPa	Resolution[a] V × H km	Single-Profile Precision[b] pptv	Accuracy[c] pptv	Known Artifacts or Other Comments
0.68–0.001	—	—	—	Unsuitable for scientific use
1.0	6 × 900	±100	±10	Consult with MLS science team
1.5	7.5 × 700	±50	±15	Consult with MLS science team
3.2–2.2	8.5 × 600	±50	±20	Consult with MLS science team
6.8–4.6	7.5 × 450	±50	±25	Consult with MLS science team
15–10	7 × 400	±50	±20	Consult with MLS science team
22	6 × 450	±50	±40	Consult with MLS science team
32	5.5 × 500	±50	±55	Consult with MLS science team
68–46	5.5 × 600	±50	±35	Consult with MLS science team
100	6 × 700	±50	±60	Consult with MLS science team
147	4.5 × 800	±120	±110	Consult with MLS science team
1000–215	—	—	—	Not retrieved

[a]Vertical and along-track horizontal resolutions; cross-track horizontal resolution is ~3 km.
[b]Precision on individual profiles, determined from observed scatter in the data in a region of minimal atmospheric variability.
[c]Values should be interpreted as 2σ estimates of the probable magnitude.

3.5 Methanol (CH_3OH)

Swath name: CH3OH

Useful range: Contact the MLS science team before contemplating use (only useful over 147–100 hPa, with caution).

Product lead: Michelle Santee <Michelle.L.Santee@jpl.nasa.gov>

3.5.1 Introduction

The standard CH_3OH product is taken from radiances measured by the radiometer centered near 640 GHz. However, as the methanol spectral signature in this region is very similar to that of ClO, additional measurements from the 190-GHz radiometer (which has channels sensitive to ClO but not CH_3OH) are used to decouple the CH_3OH and ClO information. Consequently, the intermittent operation of the 190-GHz radiometer since May 2024 (see Section 1.10.2) has affected the availability of CH_3OH measurements. CH_3OH was a new product in v4.2*x*; its quality has never been fully validated, and the scientific utility of the v6.0*x* MLS CH_3OH measurements remains to be determined. A summary of the estimated precision, resolution (vertical and horizontal), and systematic uncertainty of the v6.0*x* CH_3OH measurements as a function of altitude is given in Table 3.5.1.

3.5.2 Differences between v5.0*x* and v6.0*x*

CH_3OH abundances at 100 and 147 hPa were reduced considerably between v4.2*x* and v5.0*x* in the tropics, and they are further reduced in v6.0*x* at most latitudes (Figures 3.5.1 and 3.5.2), with v6.0*x* − v5.0*x* differences frequently exceeding 60% in magnitude. This change likely represents a mild improvement, as preliminary comparisons with correlative measurements and model results had suggested that CH_3OH mixing ratios in previous versions were generally too high. Over the range 68–10 hPa, differences between the two versions are much smaller (typically within ±10%).

3.5.3 Resolution

The resolution of the retrieved data can be described using "averaging kernels" [e.g., *Rodgers*, 2000]; the two-dimensional nature of the MLS data processing system means that the kernels describe both vertical and horizontal resolution. Values of the integrated kernel near unity indicate that the majority of information for that level has come from the measurements themselves and not the a priori; Figure 3.5.3 shows that the measurements dominate throughout most of the vertical range. Smoothing, imposed on the retrieval system in both the vertical and horizontal directions to enhance retrieval stability and precision, degrades the inherent resolution of the measurements. Thus, although CH_3OH measurements are reported at six pressure levels per decade change in pressure (spacing of ~2.7 km), the vertical resolution of the v6.0*x* CH_3OH data as determined from the full width at half maximum of the rows of the averaging kernel matrix shown in Figure 3.5.3 is ~3.5 km at 147 hPa and ~5 km at 100 hPa. Figure 3.5.3 also shows horizontal averaging kernels, from which the along-track horizontal resolution is determined to be ~150–350 km. The cross-track resolution, set by the width of the field of view of the 640-GHz radiometer, is ~3 km. The along-track separation between adjacent retrieved profiles is 1.5° great circle angle (~165 km), whereas the longitudinal separation of MLS measurements, set by the Aura orbit, is 10°–20° over low and middle latitudes, with much finer sampling in the polar regions.

3.5.4 Precision

The precision of the MLS CH_3OH data is estimated empirically by comparing profiles measured at the intersections of ascending (mainly day) and descending (mainly night) portions of the orbit. Under ideal conditions (i.e., a quiescent atmosphere), the standard deviation about the mean differences between such matched profile pairs provides a measure of the precision of the individual data points. In practice, however, real changes

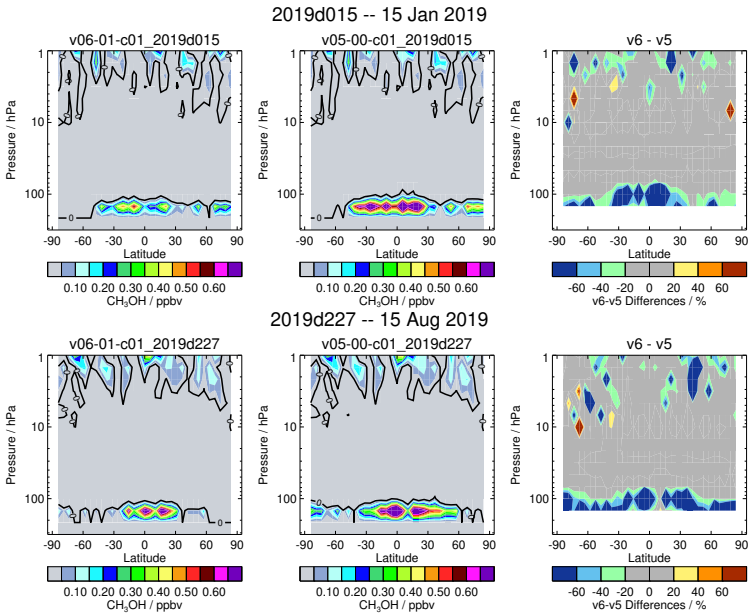

Figure 3.5.1: Zonal mean pressure-latitude cross sections of MLS CH_3OH, for (left) v6.0*x*, (middle) v5.0*x*, and (right) their differences (v6.0*x* minus v5.0*x*, in percent). Results are shown for two representative days in different seasons. The black curves overlaid on the abundance panels (left and middle) mark the zero contour. No quality screening of the data has been performed.

in the atmosphere may occur over the 12 h interval between the intersecting measurement points, in which case the observed scatter provides an upper limit on the estimate of precision, assuming that the a priori has a negligible influence on the retrieval (a reasonable assumption throughout the retrieval range for CH_3OH). The precision estimates were found to be essentially invariant with time; results for a representative year of data are shown in Figure 3.5.4. For the most part, differences between paired crossing profiles are small, implying the absence of significant systematic ascending / descending biases. The observed standard deviation is <1 ppbv at 100 hPa and ~1.2 ppbv at 147 hPa. At the lowest retrieval levels, the observationally determined precision exceeds that reported for each data point by the Level 2 data processing system, but the two estimates agree well at 46 hPa and smaller pressures. The estimates reported here represent the precisions at each pressure level of a single profile; precision can generally be improved by averaging, with the precision of an average of N profiles being $1/\sqrt{N}$ times the precision of an individual profile.

3.5.5 Range

The MLS science team should be consulted before embarking on research using the CH_3OH product. CH_3OH is retrieved (and reported in the `L2GP` files) over the range 147 to 0.001 hPa. However, zonal mean mixing ratios are negative everywhere at retrieval pressures less than 100 hPa, as well as at middle and high latitudes at 100 hPa. Thus, with rare exceptions (such as during extreme events), the v6.0*x* CH_3OH data are considered potentially useful for scientific studies only at 147 hPa and at low latitudes at 100 hPa.

3.5.6 Accuracy

The effects of various sources of systematic uncertainty (e.g., instrumental issues, spectroscopic uncertainty, and approximations in the retrieval formulation and implementation) on the MLS v6.0*x* CH_3OH measurements were quantified through a comprehensive set of retrievals of synthetic radiances. The overall systematic uncertainty, or accuracy, is calculated by combining (RSS) the contributions from both the expected biases and the additional scatter each source of uncertainty may introduce into the data. In aggregate, the factors considered in these simulations are estimated to give rise to total systematic uncertainty in the MLS v6.0*x* CH_3OH data of approximately 1–1.5 ppbv (see Table 3.5.1).

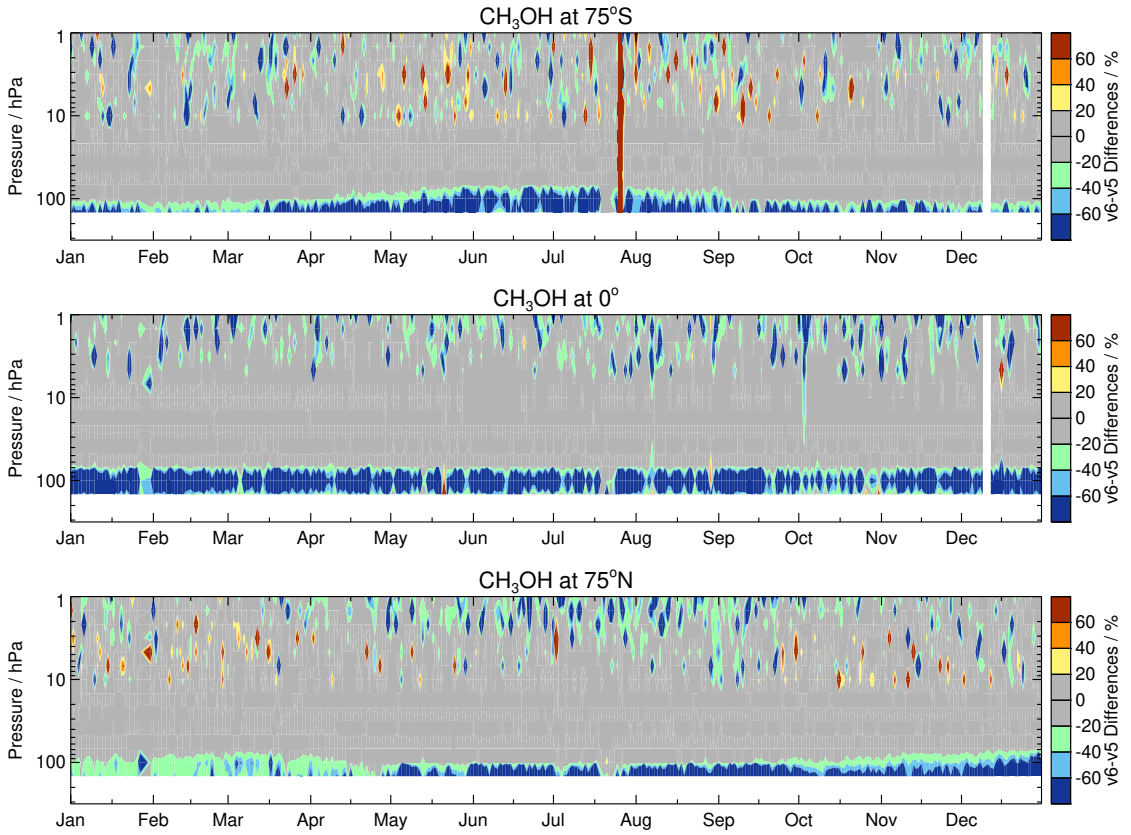

Figure 3.5.2: Time series for a representative year (2019) of v6.0*x* minus v5.0*x* MLS CH_3OH (percent differences), for (top) 75°S, (middle) the equator, and (bottom) 75°N. No quality screening of the data has been performed.

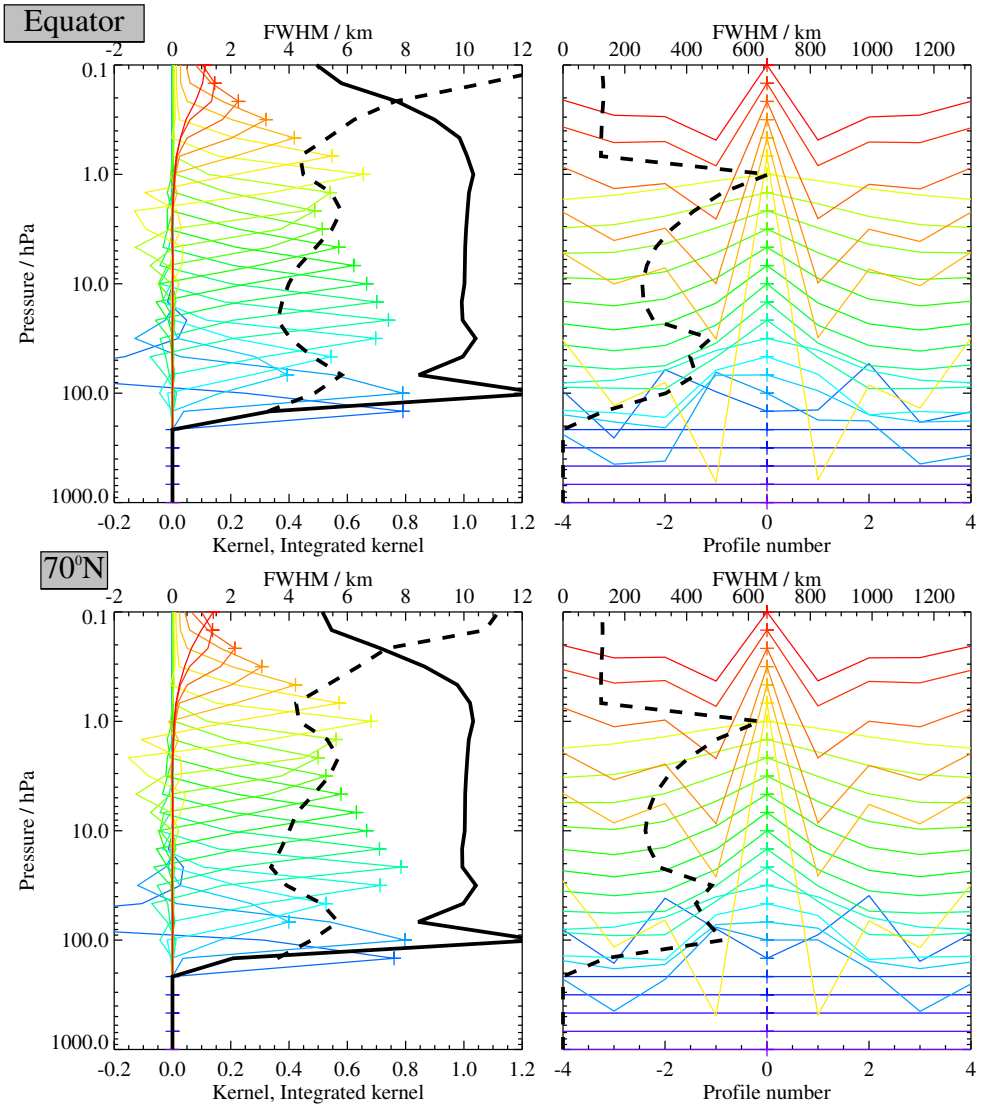

Figure 3.5.3: Typical two-dimensional (vertical and horizontal along-track) averaging kernels for the MLS v6.0*x* CH_3OH data at the equator (upper) and at 70°N (lower); variation in the averaging kernels is sufficiently small that these are representative of typical profiles. Colored lines show the averaging kernels as a function of MLS retrieval level, indicating the region of the atmosphere from which information is contributing to the measurements on the individual retrieval surfaces, which are denoted by plus signs in corresponding colors. The dashed black line indicates the resolution, determined from the full width at half maximum (FWHM) of the averaging kernels, approximately scaled into kilometers (top axes). (Left) Vertical averaging kernels (integrated in the horizontal dimension for five along-track profiles) and resolution. The solid black line shows the integrated area under each kernel (horizontally and vertically); values near unity imply that the majority of information for that MLS data point has come from the measurements, whereas lower values imply substantial contributions from a priori information. (Right) Horizontal averaging kernels (integrated in the vertical dimension) and resolution. The horizontal averaging kernels are shown scaled such that a unit averaging kernel amplitude is equivalent to a factor of 10 change in pressure.

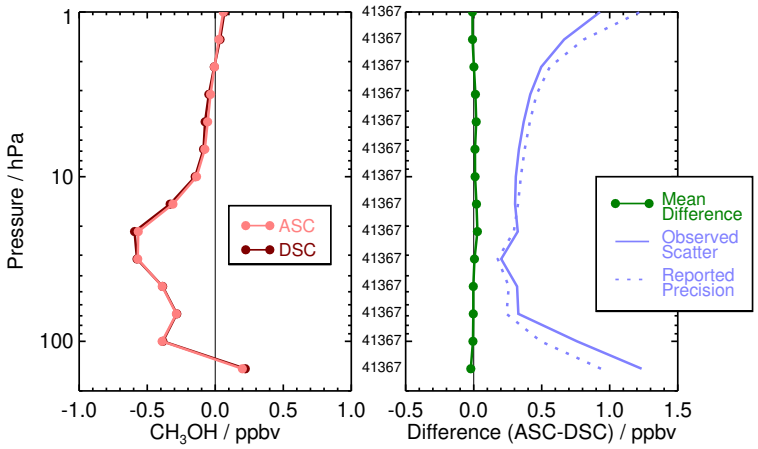

Figure 3.5.4: (left) Ensemble mean profiles for ascending (light red) and descending (dark red) orbit matching pairs of MLS v6.0*x* CH_3OH profiles averaged over a representative year of data (2019). Symbols indicate MLS retrieval pressure levels. (right) Mean differences (ascending minus descending) in pptv (green solid line). Also shown are the standard deviations about the mean differences (light blue solid line) and the root sum square (RSS) of the precisions calculated by the retrieval algorithm for the two sets of profiles (light blue dotted line). The observed scatter about the mean differences and the reported precision values have been scaled by $1/\sqrt{2}$ (to convert from standard deviations of differences into standard deviations of individual data points); hence the light blue solid line represents the statistical repeatability of the MLS measurements, and the light blue dotted line represents the expected 1 precision for a single profile. The thin black lines mark zero in each panel. The number of crossing pairs of measurements being compared at each pressure level is noted in the space between the panels.

3.5.7 Review of comparisons with other datasets

Detailed comparisons with correlative data sets have not been undertaken, but preliminary comparisons with version 3 ACE-FTS data suggested that the v4.2*x* MLS values may have been biased substantially high at 147 hPa (not shown). As noted above, CH_3OH abundances at 147 hPa have been reduced considerably in v6.0*x* and thus may be in better agreement with ACE-FTS data.

3.5.8 Data screening

Do not use: The v6.0*x* CH_3OH data should only be used in consultation with the MLS science team.

3.5.9 Artifacts

- A complete assessment of artifacts in the v6.0*x* CH_3OH measurements has not been performed, but it is known that zonal mean mixing ratios are negative everywhere at retrieval pressures less than or equal to 68 hPa, as well as at middle and high latitudes at 100 hPa.

3.5.10 Desired improvements should another data version be produced

Specific achievable improvements in the CH_3OH retrieval remain to be determined.

Table 3.5.1: Summary of Aura MLS v6.0*x* CH_3OH Characteristics

Pressure hPa	Resolution[a] V × H km	Single-Profile Precision[b] ppbv	Accuracy[c] ppbv	Known Artifacts or Other Comments
68–0.001	—	—	—	Unsuitable for scientific use
100	5 × 350	±1	±1	Consult with MLS science team
147	3.5 × 150	±1.2	±1.5	Consult with MLS science team
1000–215	—	—	—	Not retrieved

[a]Vertical and along-track horizontal resolutions; cross-track horizontal resolution is ∼3 km.
[b]Precision on individual profiles, determined from observed scatter in the data in a region of minimal atmospheric variability.
[c]Values should be interpreted as 2σ estimates of the probable magnitude.

3.6 Chlorine Monoxide (ClO)

Swath name: `ClO`

Useful range: 147–1.0 hPa

Product lead: Michelle Santee <`Michelle.L.Santee@jpl.nasa.gov`>

3.6.1 Introduction

As in previous versions, in v6.0*x* the standard ClO product is derived from radiances measured by the radiometer centered near 640 GHz. ClO is also retrieved using radiances from the 190-GHz radiometer, but those data have poorer precision and larger biases and are not used in the standard ClO product. The quality and reliability of the version 2 (v2.2*x*) Aura MLS ClO measurements were assessed in detail by *Santee et al.* [2008]. The ClO product was significantly improved in v3.3*x*/v3.4*x* [*Livesey et al.*, 2013]; in particular, the substantial (∼0.1–0.4 ppbv) negative bias present in the v2.2*x* ClO values at retrieval levels below (i.e., pressures larger than) 22 hPa was mitigated to a large extent, primarily through retrieval of CH_3Cl, which was a new MLS product in v3.3*x*/v3.4*x*.

Limb radiances measured by the MLS 640-GHz radiometer are affected by water vapor (and other species) in addition to ClO. As noted in Section 1.10.2, as of May 2024, the MLS 190-GHz radiometer, which is used to measure water vapor, is operated only intermittently. When that radiometer is turned off, 190-GHz ClO retrievals are not available. Moreover, in the absence of H_2O measurements, a priori information for H_2O (based on climatological values) is used in the 640-GHz ClO retrievals, adversely affecting their quality; further details are given in Section 3.6.9. The MLS v6.0*x* ClO data are scientifically useful over the range 147 to 1 hPa. A summary of the estimated precision, resolution (vertical and horizontal), and systematic uncertainty of the v6.0*x* ClO measurements as a function of altitude is given in Table 3.6.1.

3.6.2 Differences between v5.0*x* and v6.0*x*

Zonal-mean differences between v5.0*x* and v6.0*x* ClO are generally small (less than ±10%) in the lower stratosphere during winter at high latitudes in both hemispheres, where ClO is often strongly enhanced in the sunlit polar vortices (Figures 3.6.1 and 3.6.2). The two versions are also in very close agreement near the broad secondary peak in the ClO profile centered around 2–3 hPa (see also Figure 3.6.3). Outside of those regions, low ClO abundances lead to larger percent differences between the two versions. For example, large positive v6.0*x* − v5.0*x* differences are seen at 1 hPa, where an unphysical kink in the v5.0*x* global-mean profile has been ameliorated in v6.0*x* (Figure 3.6.1). Similarly, large negative v6.0*x* − v5.0*x* differences are found at the bottom of the retrieval range (Figures 3.6.1 and 3.6.2). In particular, the substantial positive bias at low latitudes at 100 and 147 hPa present in v5.0*x* has been reduced in v6.0*x*, while the negative bias at middle and high latitudes at those levels has been slightly exacerbated (Figures 3.6.3 and 3.6.4).

In addition to the standard product (derived from the 640-GHz radiances), Figure 3.6.3 includes results for the ClO product retrieved from the 190-GHz radiances. As was the case in v5.0*x*, the two v6.0*x* ClO products agree fairly well in the middle and upper stratosphere. The very large negative bias in `ClO-190` at its lowest retrieval levels (68–100 hPa) has been reduced in v6.0*x*; thus the two ClO products correspond more closely in the lower stratosphere now than they did in v5.0*x*. Nevertheless, as was the case in previous versions, both ClO products continue to display non-negligible biases that need to be corrected before the data can be used in detailed quantitative studies. The biases in the v6.0*x* 640-GHz ClO data are quantified and further compared to those in v5.0*x* in Section 3.6.6.

3.6.3 Resolution

The resolution of the retrieved data can be described using "averaging kernels" [e.g., *Rodgers*, 2000]; the two-dimensional nature of the MLS data processing system means that the kernels describe both vertical and

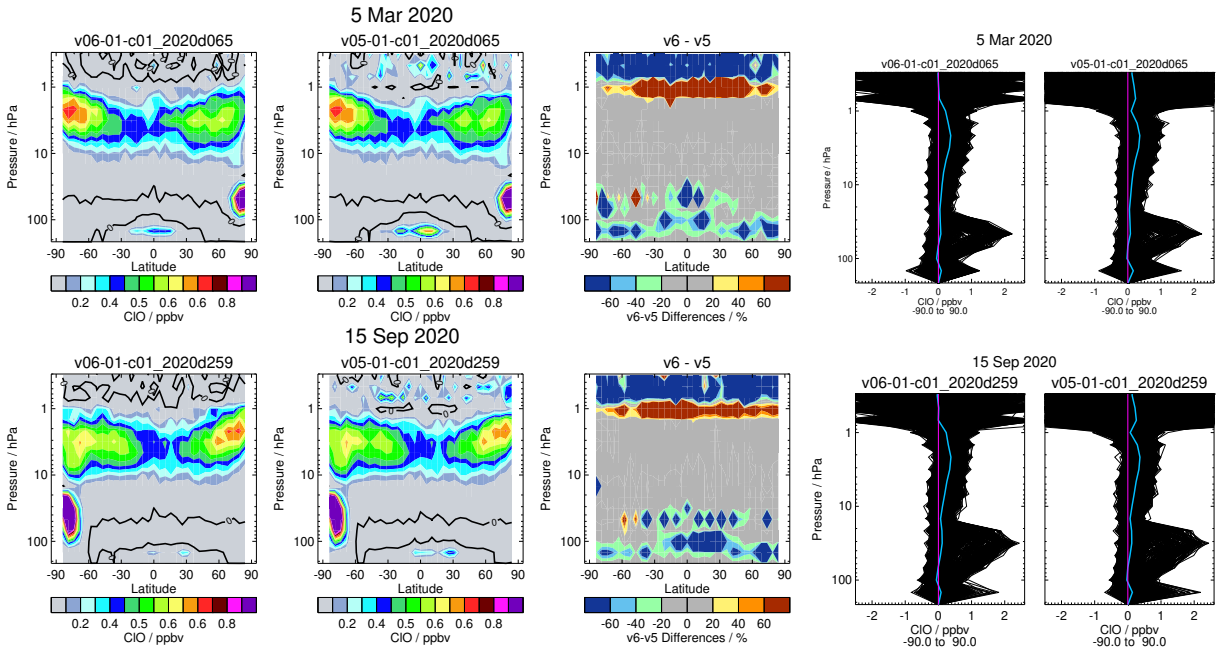

Figure 3.6.1: (left-hand panels) Zonal mean pressure-latitude cross sections of MLS daytime (ascending) ClO, for (left) v6.0*x*, (middle) v5.0*x*, and (right) their differences (v6.0*x* minus v5.0*x*, in percent). The black curves overlaid on the abundance panels (left and middle) mark the zero contour. No bias corrections or quality screening have been applied. (right-hand panels) Black lines show all profiles (day and night) measured on the given day, and the cyan line depicts the global mean profile; the pink line marks zero. Results for days with strong ClO enhancement in the winter polar region are shown for (top panels) the Northern Hemisphere and (bottom panels) the Southern Hemisphere.

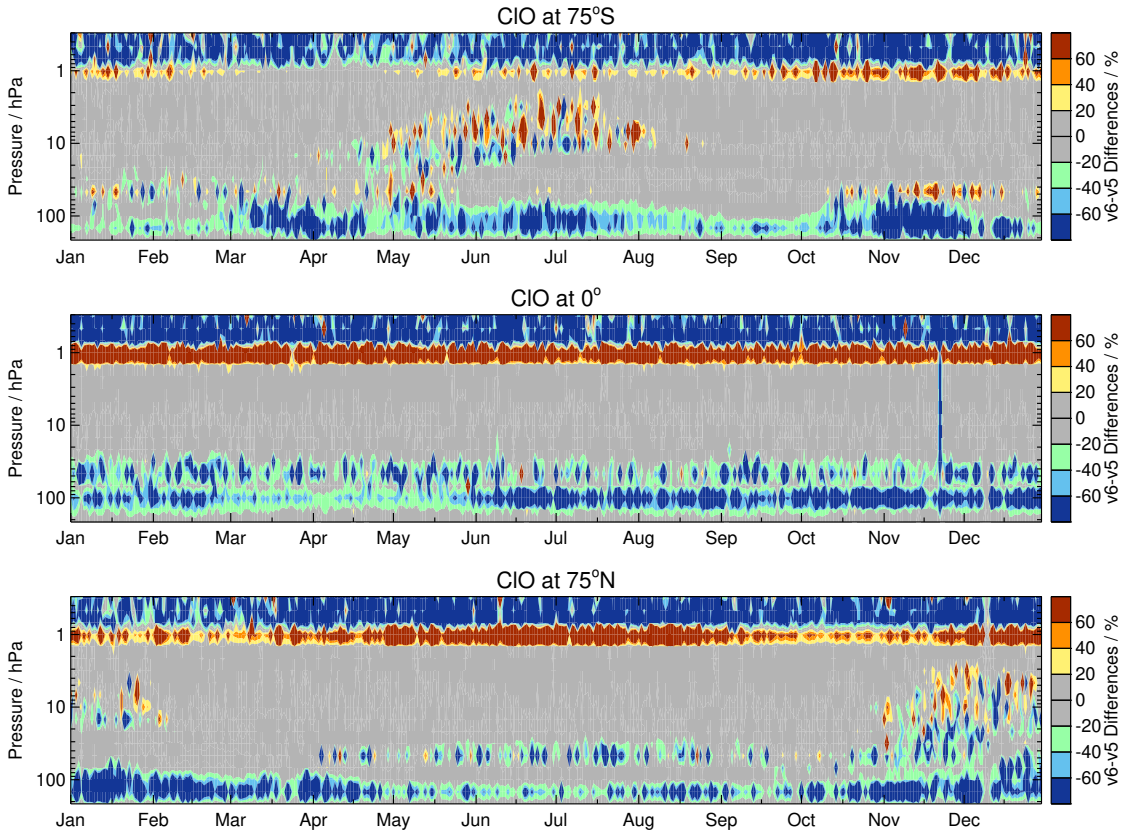

Figure 3.6.2: Time series for a representative year (2020) of v6.0*x* minus v5.0*x* MLS ClO (percent differences), for (top) 75°S, (middle) the equator, and (bottom) 75°N. No bias corrections or quality screening have been applied.

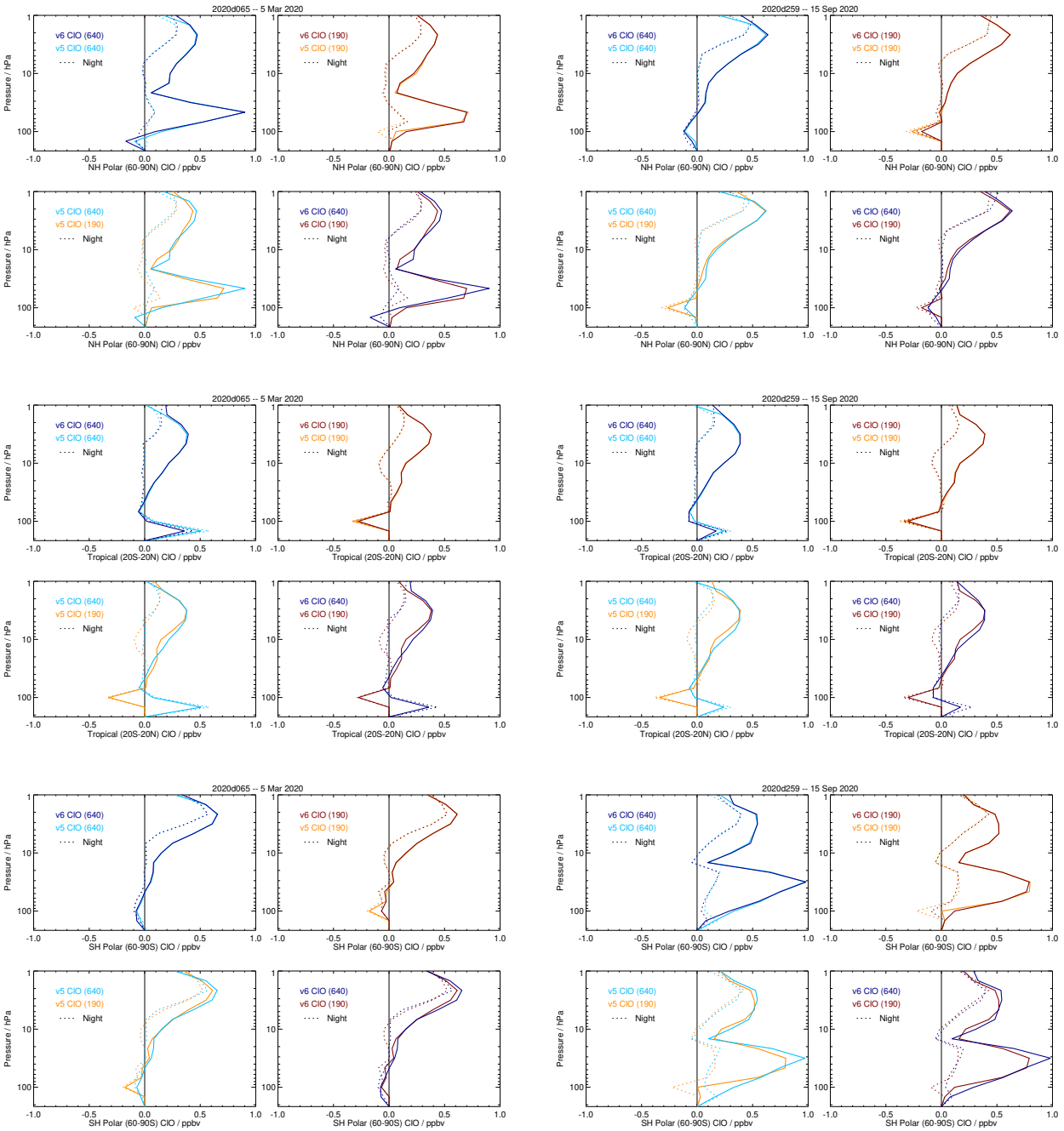

Figure 3.6.3: MLS v6.0*x* (dark colors) and v5.0*x* (light colors) profiles of `ClO-640` (blues) and `ClO-190` (reds) averaged over the Northern Hemisphere polar (top set), tropical (middle set), and Southern Hemisphere polar (bottom set) regions for days with strong ClO enhancement during winter in the Northern (left side) and Southern (right side) Hemispheres. Each set of plots contains four panels, comparing v6.0*x* and v5.0*x* `ClO-640` retrievals, v6.0*x* and v5.0*x* `ClO-190` retrievals, v5.0*x* `ClO-640` and `ClO-190` retrievals, and v6.0*x* `ClO-640` and `ClO-190` retrievals. Solid lines show ascending (mainly daytime) and dashed lines show descending (mainly nighttime) averages. No bias corrections or quality screening have been applied.

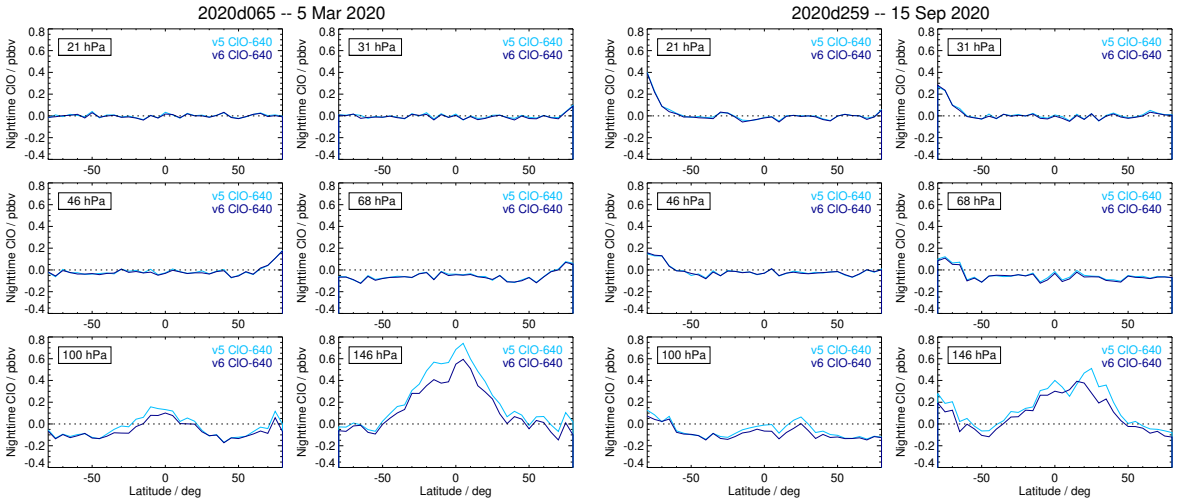

Figure 3.6.4: Nighttime v6.0*x* (dark blue) and v5.0*x* (light blue) MLS ClO data as a function of latitude for the six lowest retrieval pressure surfaces (21–147 hPa) for days with strong ClO enhancement during winter in the Northern (left) and Southern (right) Hemispheres. No bias corrections or quality screening have been applied.

horizontal resolution. Smoothing, imposed on the retrieval system in both the vertical and horizontal directions to enhance retrieval stability and precision, degrades the inherent resolution of the measurements. Thus, although ClO measurements are reported at six pressure levels per decade change in pressure (spacing of ~2.7 km), the vertical resolution of the v6.0*x* ClO data as determined from the full width at half maximum of the rows of the averaging kernel matrix shown in Figure 3.6.5 is ~3–4.5 km throughout the vertical range over which data are recommended for scientific use (with a mean of ~3.3 km). The averaging kernels are sharply peaked at all levels, even at 147 hPa, where the kernel indicates that the retrieval has sensitivity to ClO abundances higher in the atmosphere (particularly 100 hPa). Nevertheless, the 147 hPa surface provides independent information. Figure 3.6.5 also shows horizontal averaging kernels, from which the along-track horizontal resolution is determined to be ~300–500 km over most of the vertical range. The cross-track resolution, set by the width of the field of view of the 640-GHz radiometer, is ~3 km. The along-track separation between adjacent retrieved profiles is 1.5° great circle angle (~165 km), whereas the longitudinal separation of MLS measurements, set by the Aura orbit, is 10°–20° over low and middle latitudes, with much finer sampling in the polar regions.

3.6.4 Precision

The precision of the MLS ClO measurements is estimated empirically by computing the standard deviation of the descending (i.e., nighttime) profiles in the 20°-wide latitude band centered around the equator. For this region and time of day, natural atmospheric variability should be negligible relative to the measurement noise. As shown in Figure 3.6.6, the observed scatter in the data has changed very little in v6.0*x*, ranging from ~0.1 ppbv over the interval 100–3 hPa to ~0.3 ppbv at 147 and 1 hPa. The smoothing of the retrieval is turned off above 1 hPa, and as a consequence the precision worsens steeply above this level. The scatter in the data is essentially invariant with time, as seen by comparing the results for the different days 10 years apart shown in Figure 3.6.6.

The single-profile precision estimates cited here are, to first order, independent of latitude and season, but of course the scientific utility of individual MLS profiles (i.e., signal-to-noise) varies with ClO abundance. Outside of the lower stratospheric winter polar vortices, within which ClO is often strongly enhanced, the single-profile precision exceeds typical ClO mixing ratios, necessitating the use of averages for scientific studies. Precision can generally be improved by averaging, with the precision of an average of N profiles being $1/\sqrt{N}$

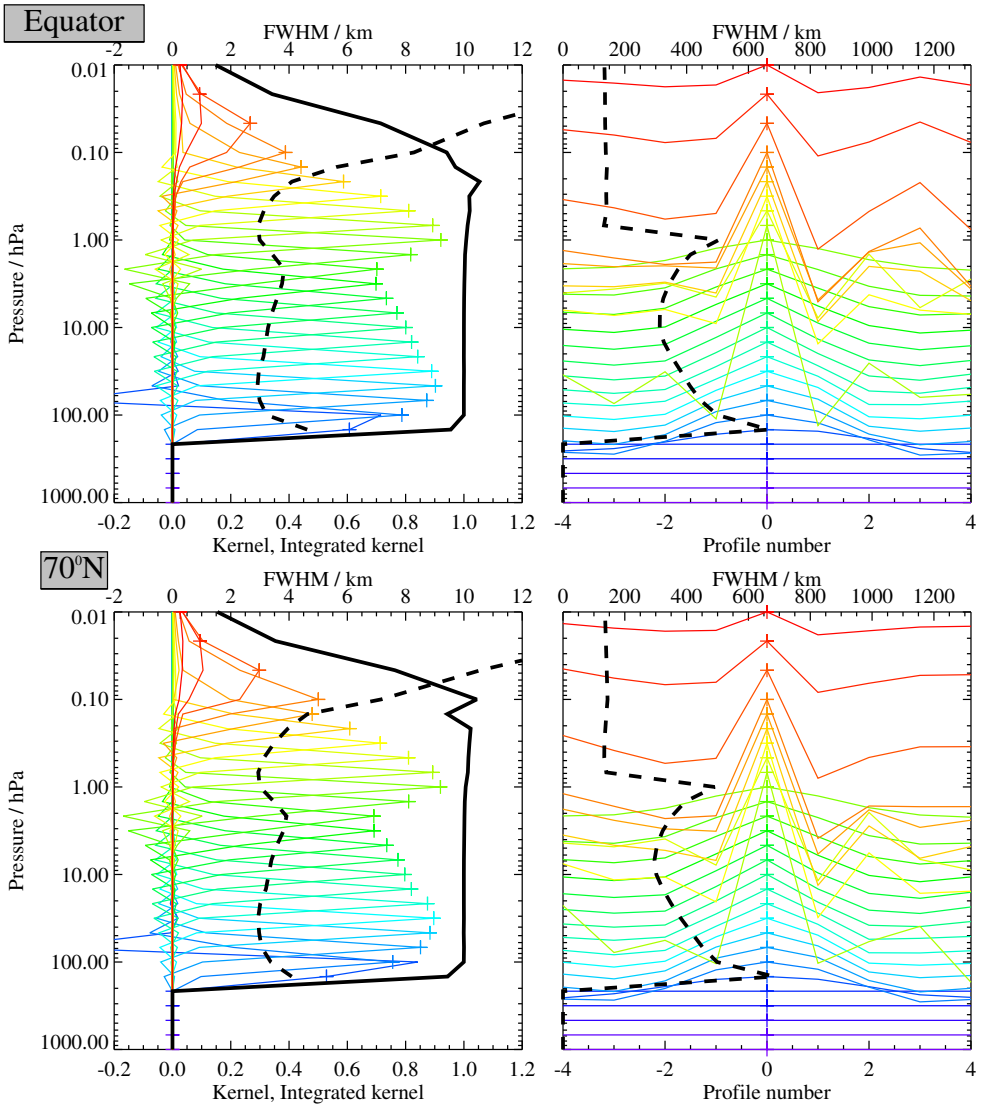

Figure 3.6.5: Typical two-dimensional (vertical and horizontal along-track) averaging kernels for the MLS v6.0*x* ClO data at the equator (upper) and at 70°N (lower); variation in the averaging kernels is sufficiently small that these are representative of typical profiles. Colored lines show the averaging kernels as a function of MLS retrieval level, indicating the region of the atmosphere from which information is contributing to the measurements on the individual retrieval surfaces, which are denoted by plus signs in corresponding colors. The dashed black line indicates the resolution, determined from the full width at half maximum (FWHM) of the averaging kernels, approximately scaled into kilometers (top axes). (Left) Vertical averaging kernels (integrated in the horizontal dimension for five along-track profiles) and resolution. The solid black line shows the integrated area under each kernel (horizontally and vertically); values near unity imply that the majority of information for that MLS data point has come from the measurements, whereas lower values imply substantial contributions from a priori information. (Right) Horizontal averaging kernels (integrated in the vertical dimension) and resolution. The horizontal averaging kernels are shown scaled such that a unit averaging kernel amplitude is equivalent to a factor of 10 change in pressure.

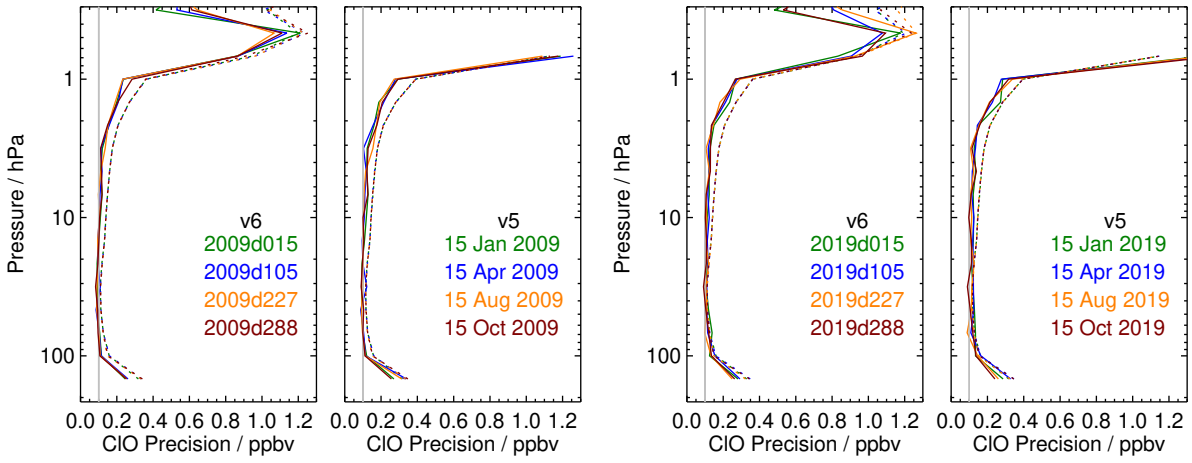

Figure 3.6.6: Precision of the (left-hand panels in each set) v6.0*x* and (right-hand panels) v5.0*x* MLS ClO measurements for four representative days in different seasons in two representative years (see legend). Solid lines depict the observed scatter in nighttime (descending) measurements obtained in a narrow equatorial band (see text); dotted lines depict the theoretical precision estimated by the retrieval algorithm. The light gray vertical line marks 0.1 ppbv, the estimated single-profile precision over most of the recommended vertical range in both versions.

times the precision of an individual profile.

The observational determination of the precision is compared in Figure 3.6.6 to the theoretical precision values reported by the Level 2 data processing algorithms. The predicted precision exceeds the observed scatter, particularly above 15 hPa, indicating that the vertical smoothing (regularization) applied to stabilize the retrieval and improve the precision has a non-negligible influence on the results at these levels. Because the theoretical precisions take into account occasional variations in instrument performance, the best estimate of the precision of an individual data point is the value quoted for that point in the L2GP files, but it should be borne in mind that this approach slightly overestimates the actual measurement noise.

3.6.5 Accuracy

The effects of various sources of systematic uncertainty (e.g., instrumental issues, spectroscopic uncertainty, and approximations in the retrieval formulation and implementation) on the MLS v6.0*x* ClO measurements were quantified through a comprehensive set of retrievals of synthetic radiances; see *Santee et al.* [2008] for details of a similar analysis conducted on MLS v2.2*x* ClO data. The overall systematic uncertainty, or accuracy, is calculated by combining (RSS) the contributions from both the expected biases and the additional scatter each source of uncertainty may introduce into the data. In aggregate, the factors considered in these simulations are estimated to give rise to a total systematic uncertainty in the MLS v6.0*x* ClO data ranging from approximately 0.01 to 0.4 ppbv, depending on the level (see Table 3.6.1), slightly better at some levels than the corresponding accuracy estimates for v5.0*x* ClO data. These values for the overall uncertainty in v6.0*x* ClO do not take into account the known biases in MLS ClO data at the lowest retrieval levels discussed in the following subsection.

3.6.6 Quantification and correction of biases in v6.0*x*

As noted in Section 3.6.2, substantial biases are present in the standard v6.0*x* ClO data at the lowest retrieval levels. To investigate in more detail the magnitude of and temporal variations in the bias in the v6.0*x* MLS ClO data, we show in Figure 3.6.7 monthly zonal means of MLS nighttime ClO measurements for pressure levels 147–46 hPa. Each panel represents a calendar month; nighttime data taken during that month over the period 2005–2024 have been binned and averaged in 5°-wide latitude bands between ±85°. Figure 3.6.8 is the same kind of plot but encompasses all of the MLS nighttime ClO data (i.e., the climatological annual mean over

2005–2024) for pressure levels 147–10 hPa. To guide the eye, the global-mean annual-mean bias calculated over the climatological period is indicated for each pressure level (horizontal solid lines in the respective colors). Figures 3.6.4, 3.6.7, and 3.6.8 show that the magnitude, and at 100 and 147 hPa even the sign, of the bias varies with latitude as well as pressure. At 46 hPa the two versions track one another closely, with the negligible negative bias present in v5.0*x* essentially unchanged in v6.0*x*, whereas at 68 hPa the small negative bias in v6.0*x* is slightly larger than that in v5.0*x*, particularly at low latitudes (Figure 3.6.4). At 100 hPa, the small positive bias in the tropics in v5.0*x* has been considerably reduced in v6.0*x* (Figure 3.6.4; this is especially evident in the climatological mean, not shown), but the moderate negative bias at higher latitudes in both hemispheres has grown slightly. Similarly, at 147 hPa the large positive bias at low and middle latitudes has diminished, whereas the negative bias in the polar regions has worsened slightly; nevertheless, the global-mean annual-mean bias at 147 hPa is smaller than it was in v5.0*x* (not shown). In contrast to the strong altitude and latitude dependence of the ClO bias evident in these plots, Figure 3.6.7 reveals only modest month-to-month variability in most places.

In many cases the ClO bias can be essentially eliminated by subtracting daily gridded or zonal-mean nighttime values from daytime measurements, and where feasible that is often the preferred bias-correction approach. However, it is not practical to take day−night differences under conditions of continuous daylight in the summer or continuous darkness in the winter at high latitudes. Moreover, under certain circumstances during the mid-winter period of peak ClO enhancement inside the lower stratospheric polar vortices, non-negligible ClO abundances can be present even in darkness, masking the negative bias. In this case, computing day−night differences considerably reduces the apparent degree of observed chlorine activation. Consequently, for studies of polar chemical processing and chlorine partitioning, it is instead recommended that an estimate of the bias be subtracted from the individual measurements at each affected retrieval level. Attempts to estimate the bias through approaches other than examination of nighttime ClO measurements (e.g., via correlations with potentially interfering species, which themselves may vary strongly with season) have so far met with little success. Thus the bias is estimated from the analysis depicted in Figure 3.6.8. Although monthly varying bias estimates might be desirable, as noted above seasonal variations are small, and it is not possible to directly quantify the bias in the polar regions during much of the year. Interannual variations and longer-term trends (not shown) in the magnitude of the bias are also small (especially in comparison to the uncertainty in the bias estimates and the v6.0*x* ClO data themselves; see Section 3.6.5). For these reasons, and to simplify application of the ClO bias correction for MLS data users, we report 20-yr climatological bias estimates that vary latitudinally and altitudinally but not temporally; such bias corrections should be adequate for most studies. The bias values, which are reported on a 5° grid, must be interpolated to the MLS Level 2 measurement locations being considered and subtracted from the ClO mixing ratios (daytime or nighttime) at those locations. The bias correction must be performed *before* interpolation to a different vertical coordinate (e.g., potential temperature). An ASCII file containing the estimated ClO bias values is embedded in the PDF file for this document; instructions for extracting this file are given in Appendix A.2. The file is also available from the MLS website at `https://mls.jpl.nasa.gov/data/MLS-Aura_ClO-BiasCorrection_v06.txt` and from Zenodo at `https://zenodo.org/records/18988847`.

3.6.7 Review of comparisons with other data sets

Extensive comparisons of MLS v2.2*x* ClO data with measurements from a variety of different platforms (ground-based, balloon-borne, aircraft, and satellite) were presented by *Santee et al.* [2008]. A subset of those comparisons with v3.3*x*/v3.4*x* ClO data were reported by *Livesey et al.* [2013]. Comparisons of v6.0*x* ClO with correlative measurements have not been conducted but are expected to yield results similar to those for previous versions.

3.6.8 Data screening

Pressure range: 147–1.0 hPa

Values outside this range are not recommended for scientific use.

Estimated precision: Only use values for which the estimated precision is a positive number.

Values where the a priori information has a strong influence are flagged with negative or zero precision and should not be used in scientific analyses (see Section 1.5).

Status flag: Only use profiles for which the `Status` field is zero.

We recommend that all profiles with nonzero values of `Status` be discarded, because of the potential impact of cloud artifacts at lower levels. Note, however, that rejecting in their entirety all profiles with nonzero `Status` may be unnecessarily severe at and above (i.e., at pressures equal to or smaller than) 46 hPa, where clouds have negligible impact; thus otherwise good-quality profiles with nonzero but even `Status` values may be used without restriction at those levels as long as they are removed at larger pressures. See Section 1.6 for more information on the interpretation of the `Status` field.

Quality: Only profiles whose `Quality` field is greater than 1.3 should be used.

In a typical month this threshold for `Quality` (unchanged from v5.0*x*) discards few (0.2% or less) of the ClO profiles; note that it potentially discards some "good" data points while not necessarily identifying all "bad" ones.

Convergence: Only profiles whose `Convergence` field is less than 1.05 should be used.

In a typical month this threshold for `Convergence` (unchanged from v5.0*x*) discards few (0.2% or less) of the ClO profiles, many (but not all) of which are filtered out by the other quality control measures.

Additional screening on H_2O `Status`: As noted earlier, the quality of the 640-GHz ClO retrievals is degraded at some levels when the 190-GHz radiometer is turned off and H_2O measurements are not available. In these circumstances, biases in the retrieved ClO values as large as 0.05 ppbv (>50% at some latitudes) are seen over 68–100 hPa. These artifacts are not removed by the standard ClO data filtering protocols. Thus, while the ClO data on affected days are still useful for purely morphological or qualitative purposes, they cannot be quantitatively compared to measurements taken on surrounding days or in previous years when the 190-GHz radiometer was operational. The biases also have potential implications for the calculation of long-term trends. Therefore, for quantitative studies using ClO data at those retrieval levels, an additional screening step is recommended, whereby the `Status` field in the colocated H_2O profile is examined to remove affected ClO retrievals. That is, only ClO profiles for which the `Status` flags of the corresponding H_2O profiles are an even number should be used in quantitative studies relying on ClO measurements in the 68–147 hPa range (at lower pressures / higher altitudes, all ClO data points passing the standard quality screening measures may be used). We also note, however, that measurements taken during time periods since May 2024 when the 190-GHz radiometer is turned off can be intercompared.

3.6.9 Artifacts

- As discussed in Section 3.6.6, non-negligible biases are present in both daytime and nighttime v6.0*x* ClO mixing ratios at and below (i.e., pressures larger than) 68 hPa. Outside of the winter polar lower stratosphere, the bias can be eliminated by subtracting daily gridded or zonal-mean nighttime values from daytime measurements. Under conditions of ClO enhancement inside the polar vortices, however, the bias should be corrected by subtracting from the individual measurements at each affected retrieval level the altitude- and latitude-dependent bias estimates. An ASCII file containing the estimated ClO bias values is embedded in the PDF file for this document; instructions for extracting this file are given in Appendix A.2. This file is also available from the MLS web page at `https://mls.jpl.nasa.gov/data/MLS-Aura_ClO-BiasCorrection_v06.txt` and from Zenodo at `https://zenodo.org/records/18988847`.
- Care must be taken in interpreting the ClO measurements immediately following severe pyrocumulonimbus (pyroCbs) events, which can rapidly loft polluted air from the surface and deposit it in the

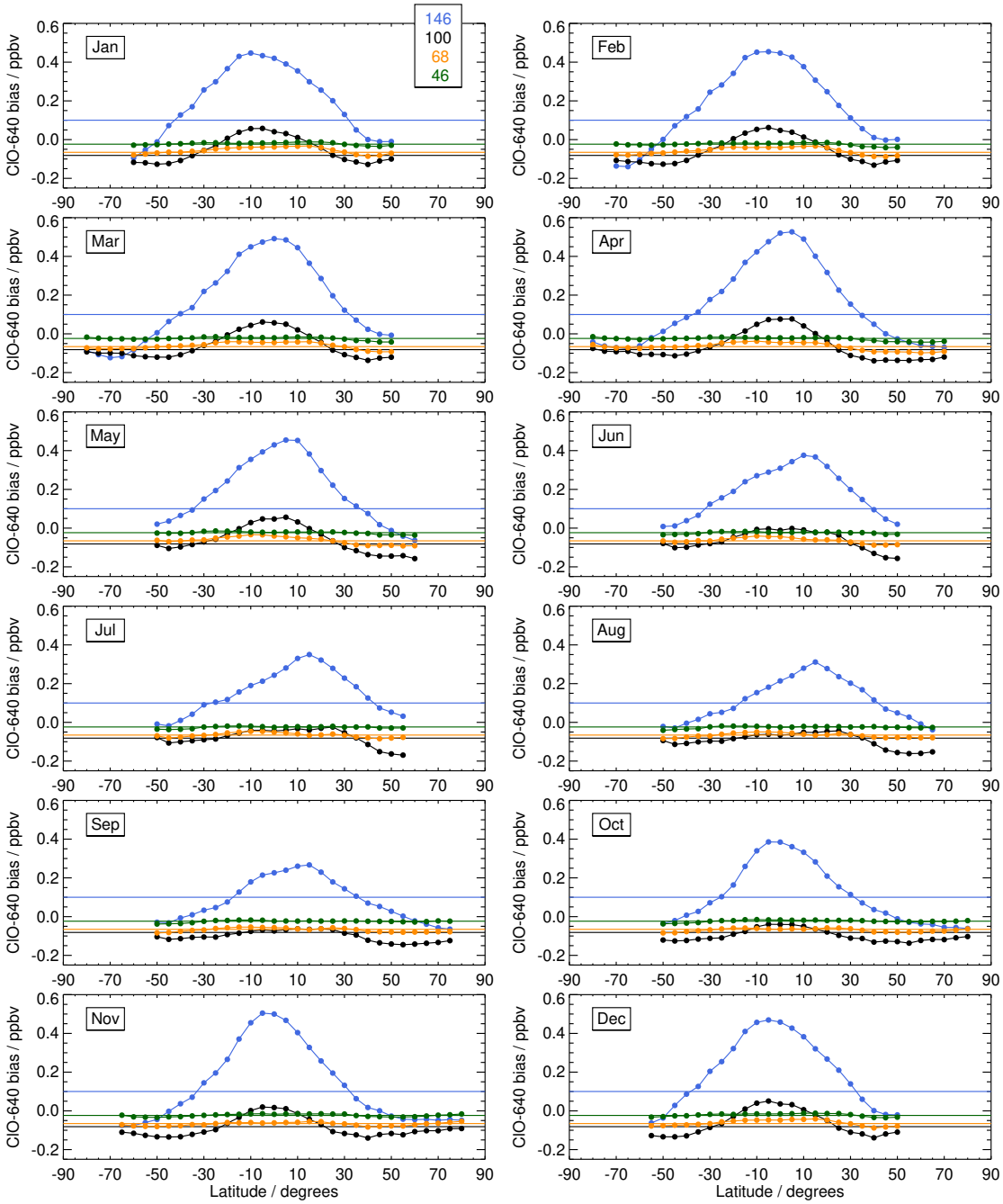

Figure 3.6.7: Estimates of the bias in MLS v6.0*x* ClO data in 5°-wide geographic latitude bands on the 147, 100, 68, and 46 hPa MLS retrieval pressure surfaces (see legend). Each panel shows climatological (2005–2024) monthly zonal means of MLS nighttime (solar zenith angle > 100°) ClO measurements (filled circles). The horizontal lines denote the global-mean annual-mean bias estimates over the climatological period at each level. To ensure that ClO was not enhanced, consideration was restricted to latitudes equatorward of 50°S for the days between 1 May and 1 November and to latitudes equatorward of 50°N for the days between 1 December and 1 April. The recommended data quality filtering procedures were applied to calculate the biases in the ClO data.

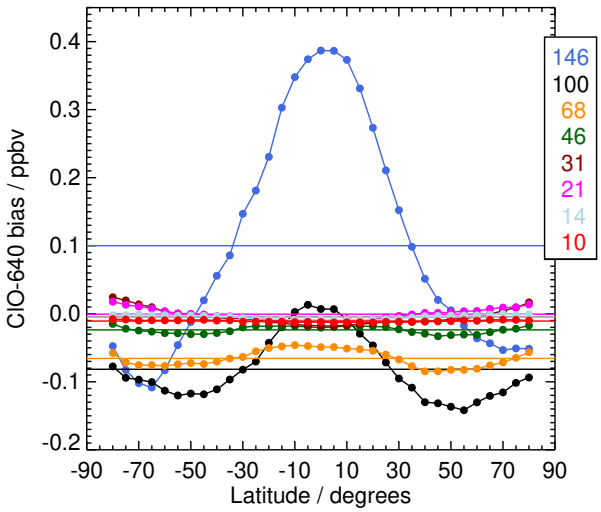

Figure 3.6.8: Estimates of the bias in MLS v6.0*x* nighttime (solar zenith angle > 100°) ClO data in 5°-wide geographic latitude bands on MLS retrieval pressure surfaces from 147 to 10 hPa (see legend) calculated over 2005–2024. The horizontal lines denote the global-mean annual-mean bias estimates over the climatological period at each level. To ensure that ClO was not enhanced, consideration was restricted to latitudes equatorward of 50°S for the days between 1 May and 1 November and to latitudes equatorward of 50°N for the days between 1 December and 1 April. The recommended data quality filtering procedures were applied to calculate the biases in the ClO data.

lower stratosphere. Air masses characterized by enhanced abundances of biomass burning pollutants may appear to also contain elevated levels of ClO, but such apparent enhancements are artifacts induced by contamination of the ClO retrieval from methanol (CH_3OH), a product of wildfires that has a similar spectral signature in the MLS band used to measure ClO.

- As discussed in Section 3.6.8, considerable biases in ClO values are present at some levels when coincident measurements from the 190-GHz radiometer are not available and H_2O a priori information is used in the 640-GHz ClO retrieval. Depending on the specific goals of any study based on these measurements, additional ClO data quality filtering may be necessary for days when the 190-GHz radiometer is off.

3.6.10 Desired improvements should another data version be produced

Further work to diagnose and eliminate the persistent biases at the lowest retrieval levels (147–68 hPa) will be undertaken should an opportunity to produce an updated MLS data version arise.

Table 3.6.1: Summary of Aura MLS v6.0*x* ClO Characteristics

Pressure hPa	Resolution[a] V × H km	Single-Profile Precision[b] ppbv	Accuracy[c] ppbv	Known Artifacts or Other Comments
0.68–0.001	—	—	—	Unsuitable for scientific use
1.0	3 × 500	±0.3	±0.02	
1.5	3.5 × 400	±0.1	±0.02	
3.2–2.2	4 × 350	±0.1	±0.02	
6.8–4.6	3.5 × 300	±0.1	±0.03	
15–10	3.5 × 300	±0.1	±0.04	
22	3 × 350	±0.1	±0.05	
46–32	3 × 400	±0.1	±0.15	
68	3 × 450	±0.1	±0.2	Latitude-dependent bias[d]
100	3.5 × 500	±0.1	±0.3	Latitude-dependent bias[d]
147	4.5 × 650	±0.3	±0.4	Latitude-dependent bias[d]
1000–215	—	—	—	Not retrieved

[a]Vertical and along-track horizontal resolutions; cross-track horizontal resolution is ~3 km.

[b]Precision on individual profiles, determined from observed scatter in nighttime (descending) data in a region of minimal atmospheric variability.

[c]Values should be interpreted as 2σ estimates of the probable magnitude and, at the higher pressures, are the uncertainties after subtraction of the known bias.

[d]Correct for the bias by subtracting from the individual measurements at this level the latitude-dependent bias estimates (see Section 3.6.6).

3.7 Cloud Top Pressure (CloudTopPressure)

Swath name: CldTopP

Useful range: 770–85 hPa

Units: hPa

Product Lead: Frank Werner <Frank.Werner@jpl.nasa.gov>

3.7.1 Introduction

This product is new in v6.0*x* and is described in more detail by *Werner et al.* [2021]. Note that the model setup has been updated since that initial description was published. More specifically, we increased the complexity of the feedforward neural network used for cloud masking, and the cloud top pressure predictions are now provided by a Gradient Boosted Decision Tree model, with noticeably improved performance.

The two machine learning models have been trained on aggregated cloud properties reported by Aqua's Moderate Resolution Imaging Spectroradiometer (MODIS) around colocated MLS tangent points. This data set is comprised of 162,117 cloud and clear sky scenes sampled on 208 days between 2005 and 2020. The model input is a vector of 1,710 MLS brightness temperatures, sampled at 15 different tangent altitudes and as many as 13 spectral channels within 10 different MLS bands. The model first predicts a binary cloudiness flag for a $1^\circ \times 1^\circ$ latitude $\times$ longitude box around each MLS tangent point. If the observation is flagged to be cloudy, the model subsequently predicts the average cloud top pressure within that box. The *Werner et al.* [2021] study describes the model setup, training, and evaluation in extensive detail.

This new cloud top pressure product differs from most other MLS products, because it is not a profile quantity. Instead, it is a single scalar value that aims to add additional interpretability to each MLS tangent point. It should be interpreted as follows: "If there were colocated MODIS cloud top property observations available for an individual MLS profile location, then this is a reliable prediction of what the average MODIS-retrieved cloud top pressure would have been in the immediate vicinity of that MLS profile." A fill value of −999.99 is assigned to samples where the model predicts clear sky conditions.

3.7.2 Precision

In contrast to most other MLS products, for which the precision can be computed from the solution covariance matrix after the optimal estimation retrieval, the machine learning predictions do not provide diagnostic variables that can be used for uncertainty estimates. Instead, we derived the root–mean–square deviation between the model predictions and colocated MODIS retrievals from an independent test data set, resulting in an uncertainty of 71 hPa. Each precision is initially set to that value. Subsequently, two tests are performed for each sample: (1) Is the predicted cloud top pressure within the range encountered in the full training data set (we allow for some extrapolation on either side); and (2) Are the input radiances within the range observed in the full training data set (again, the range is slightly extended on either side). If either of these tests fails, then the precision is set to a fill value of −999.99. These values indicate samples where the cloud top pressure reported by the model is not reliable.

3.7.3 Accuracy

Similar to the precision, we can use the comparison between predicted and observed cloud top pressures from an independent test data set, which is shown in Figure 3.7.1. For this independent test data set the correlation coefficient r exceeds 0.86, with a root-mean-square deviation of ≈ 71 hPa. The median deviation indicates a small positive bias of < 1.5 hPa. Looking at the difference between predicted and observed cloud top pressures, about half of the data points lie within the full width at half maximum (FWHM) of ≈ 42 hPa.

3.7.4 Data screening

Pressure range (770–85 hPa): Values outside this range are not recommended for scientific use.

Estimated precision: Only use values for which the estimated precision is a positive number. If positive, the precision value is based on the root-mean-square deviation between predictions and colocated MODIS cloud top pressures from an independent test data set. These samples were not involved in the training procedure.

3.7.5 Artifacts

The current version of the algorithm relies on radiances from MLS radiometers centered at 190, 250, and 640 GHz. Whenever any of those radiometers are turned off, or MLS sampled radiances that are outside the range observed in the extensive training data set, the algorithm produces fill values of −999.99 for the cloud top pressure predictions and the associated precisions for all samples is set to −999.99.

3.7.6 Comparisons with other datasets

Please refer to the detailed analysis by *Werner et al.* [2021], which provides statistical comparisons of cloud properties with MODIS, as well as maps of example cloud scenes.

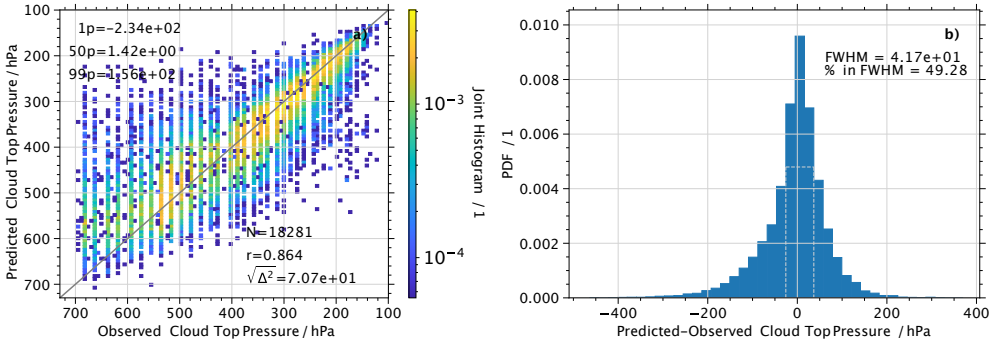

Figure 3.7.1: Left: Joint histogram of predicted and observed MODIS cloud top pressure from an independent test data set. Number of data points (*N*), correlation coefficient (*r*), and root-mean-square deviation are provided, as well as the 1st, 50th, and 99th percentile of the deviation between predictions and observations. Right: Histogram of deviations between predicted and observed cloud top pressures. The FWHM is indicated by the white dashed lines, and the percentage of data points within the FWHM is given in the panel.

3.8 Carbon monoxide (CO)

Swath name: CO

Useful range: 215–0.001 hPa

Product leads: Hugh C. Pumphrey (stratosphere/mesosphere), Michael J. Schwartz (troposphere)

Contact: Michael J. Schwartz <Michael.J.Schwartz@jpl.nasa.gov>

3.8.1 Introduction

Carbon monoxide (CO) is retrieved from radiance measurements of two bands in the MLS 240-GHz radiometer. Details are given by *Pumphrey et al.* [2007] and *Livesey et al.* [2008].

3.8.2 Differences between v6.0*x* and v5.0*x*

The v6.0*x* CO product is almost identical to the v5.0*x* product, and both are very similar to v4.2*x* in the upper troposphere and stratosphere, with improvement in some cases relative to v4.2*x* in the mesosphere and mesopause region resulting from the use of a more computationally expensive, nonlinear forward model for radiances near the 230-GHz line center. Small differences between v6.0*x* and v5.0*x* CO in the upper stratosphere result from changes in the temperature and pointing retrieval, as discussed in Section 3.23.

In the upper mesosphere, v6.0*x* and v5.0*x* CO are less tightly constrained to the a priori than was v4.2*x* CO (a priori precision is 1.5× larger at 0.046 hPa and 2× larger at and above 0.01 hPa than it was in v4.2*x*). Horizontal smoothing of v6.0*x* and v5.0*x* has been tightened at and above 0.01 hPa to maintain retrieval stability, but this change has no appreciable impact on the sharpness of horizontal features seen in preliminary validation. The top of the vertical range of the retrieval remains 0.00046 hPa, and profiles are recommended for scientific use up to 0.001 hPa.

Figure 3.8.1 shows scatter plots of data-quality-screened v5.0*x* vs. v6.0*x* CO from 215 hPa to 0.01 hPa during 2009, showing that the two versions are almost identical. High outlier values of CO along the 1:1 lines of panels for 216–46.4 hPa in Figure 3.8.1 are measurements within the plume from the "Black Saturday" Australian wildfires and confirm the consistency of the v6.0*x* and v5.0*x* retrievals in the upper troposphere and lower stratosphere, even when unusally high values are retrieved.

The calculation of cloud flags bits in the product status has changed significantly in v6.0*x*, as is discussed in Section 2.5. V6.0*x* CO has approximately twice as many profiles marked as possibly influenced by low cloud than v5.0*x*, and no profiles flagged as influenced by only high clouds; however, neither of those flags is used in the recommended screening of CO.

3.8.3 Impact of November 2025 MLS instrument configuration change on mesospheric CO data

In the mesosphere, the spectral lines measured by MLS are very narrow compared to their width at lower altitudes, with the Doppler-broadened mesospheric 230-GHz CO line being only ~400 kHz full width at half maximum. MLS includes four high-spectral-resolution (128 96-kHz-wide channels) digital autocorrelator spectrometers (DACS) targeting O_2, H_2O, O_3, and CO (MLS Bands 22 to 25, respectively). Prior to 20 November 2026, Band 25 (B25) provided 6 MHz of 96-kHz-resolution spectra around the center of the 230-GHz CO line to the v6.0*x* (and all previous) retrievals. This DACS was repurposed for geomagnetic field studies using the Zeeman-split O_2 line. Starting with v06.03, information on mesospheric CO is instead obtained from a single, unresolved, 6-MHz-wide channel (Channel 13, at the center of filterbank spectrometer Band 9 (B9.C13)) that covers the same bandwidth as the DACS. Figure 3.8.2 shows the impact of the degradation in spectral resolution between v06.01 and v06.03 on the CO retrieval. The upper panels show zonal-mean profiles from the degraded retrieval (v06.03, blue), the retrieval using the DACS (v06.01, red), and the a priori (yellow). In the southern hemisphere, both retrievals have similarly high values relative to a priori above 0.0046 hPa. The lower row of panels in Figure 3.8.2 shows that retrieval single-profile estimated precisions (dashed lines)

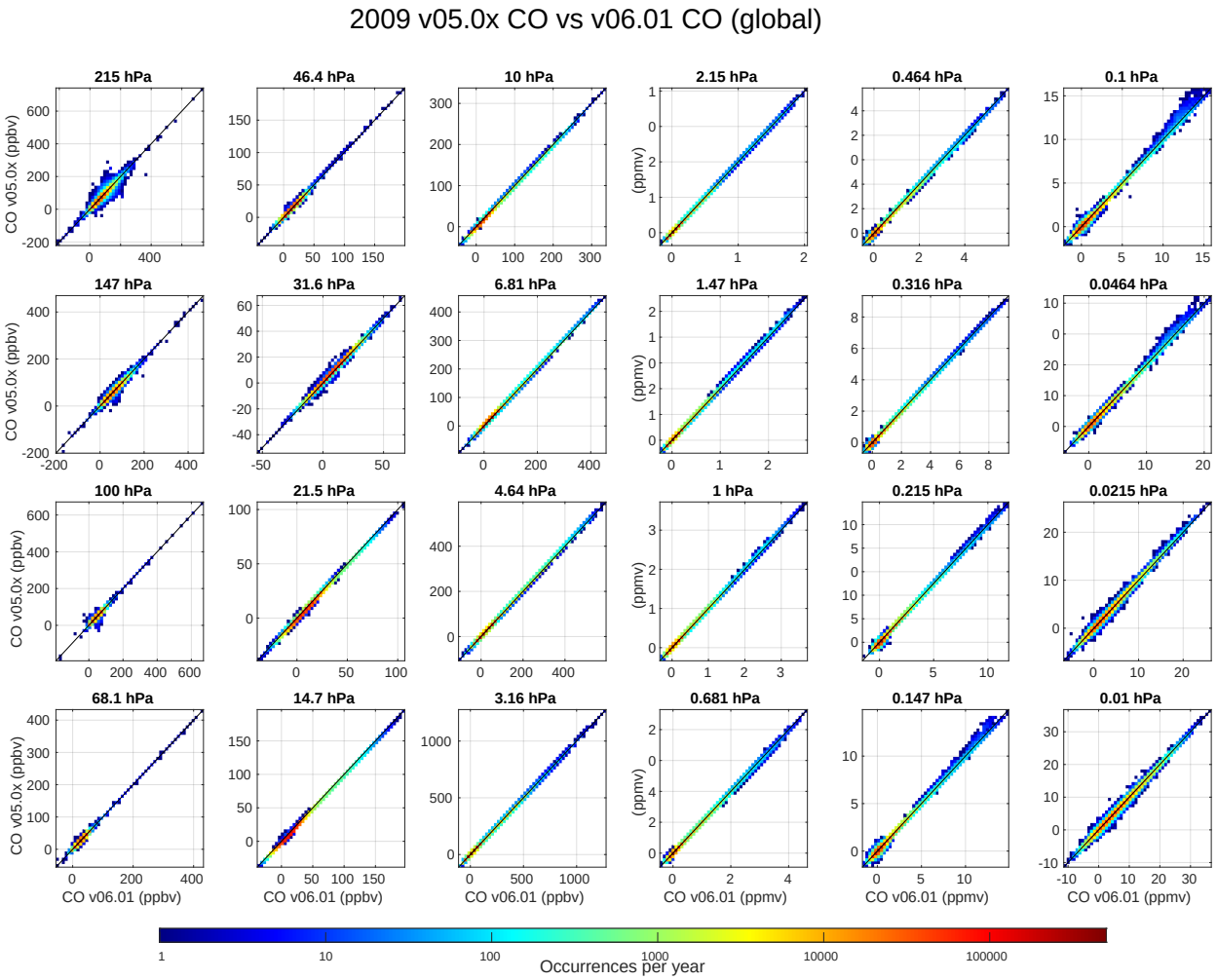

Figure 3.8.1: Joint histograms of v5.0*x* CO and v6.0*x* CO for 2009 data show the general consistency of the two versions. The color scale is logarithmic, with red points along the 1:1 line corresponding to pairs of values that are identical in the two versions.

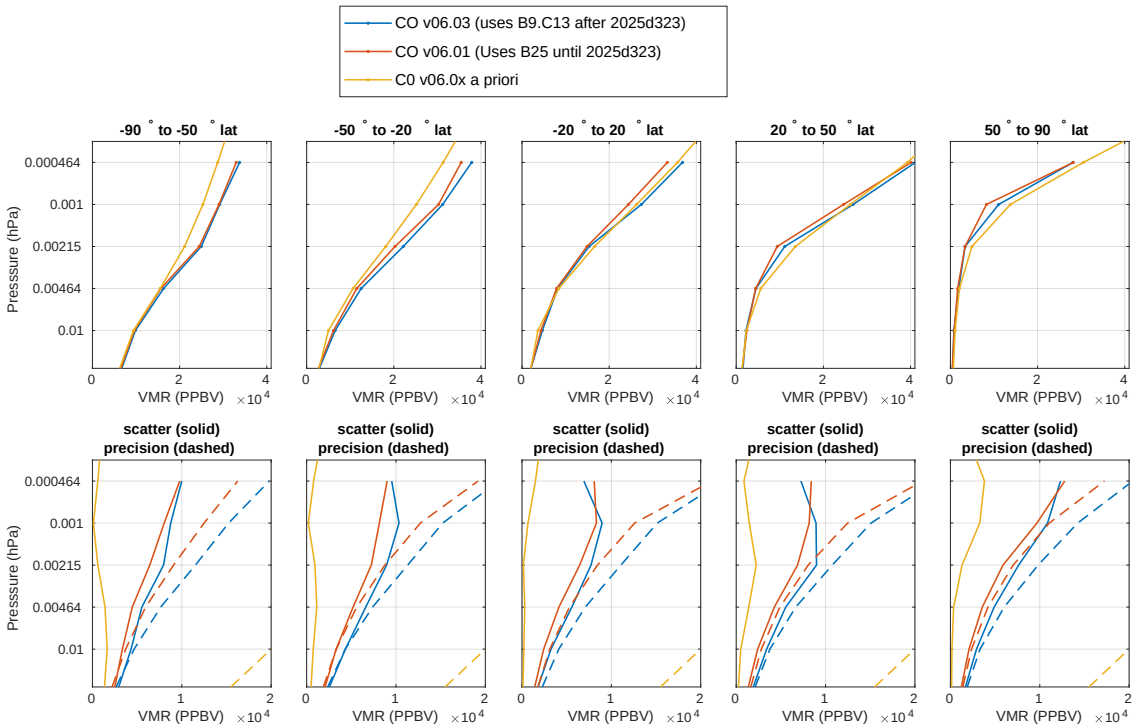

Figure 3.8.2: Top row shows zonal averages of the highest levels of the MLS v06.01 (red) and v06.03 (blue) CO retrieved values, the former using high-resolution digital autocorrelator radiances covering the CO line center (Band 25) and the latter using a single 6-MHz channel covering the same spectrum (Band 9 Channel 13). The a priori CO profile is shown in yellow. The lower row of panels are zonal averages of the standard deviations (solid) and estimated precisions (dashed) with the same color scheme. Data are from 2025d196.

at pressures lower than 0.01 hPa are generally 10–30% poorer (larger) for the retrieval using `B9.C13` rather than the `B25` DACS and that there is ~15% more variability in the v06.03 retrieval (using `B9.C13`) than in the v06.01 retrieval (using the `B26` DACS).

3.8.4 Resolution

Figure 3.8.3 shows the horizontal and vertical averaging kernels for v6.0*x* MLS CO. Estimated vertical and horizontal resolutions are essentially identical to those of v5.0*x* and v4.2*x*. The vertical resolution is in the range 3.5–5 km from the upper troposphere to the lower mesosphere, degrading to 6–7 km in the upper mesosphere. Down to the 215 hPa level, the vertical averaging kernels are sharply peaked at the level being retrieved, but while the 316-hPa measurement contains a contribution from 316 hPa, it has a larger contribution from 215 hPa and a negative contribution around 100 hPa of similar magnitude to that at 316 hPa. The retrieved value at 316 hPa is thus more an extrapolation of the profile higher in the UTLS than it is an independent measurement at 316 hPa, and it is not recommended for scientific use. The horizontal resolution is about 200 km in the mesosphere, degrading slowly to 300 km with decreasing height in the stratosphere and more rapidly to about 460 km at 100 hPa and 690 km at 215 hPa.

3.8.5 Precision

The MLS data are supplied with an estimated precision (the field `L2gpPrecision`), which is the *a posteriori* precision as returned by the optimal estimation. The precision of the v6.0*x* CO is nearly identical to that of v5.0*x*, and very similar to that of v4.2*x*. Reported precision is greater than the scatter observed in the data in regions of low natural variability. This can be seen in the middle (low-latitude) panels of the second row of Figure 3.8.4, where the black solid line (scatter about the zonal mean) has smaller values than the black dashed lines (precisions). Where the estimated precision is greater than 50% of the a priori precision the data will be influenced by the a priori to an undesirably large extent. In such cases, `L2gpPrecision` is set to be negative (or zero in some cases) to indicate that the data should not be used.

Note that the random errors (precisions) are larger than 100% of the mixing ratio for much of the vertical range, meaning that significant averaging (e.g., daily zonal mean or weekly map) is typically needed to make use of the data.

3.8.6 Accuracy

The estimated accuracy is summarized in Table 3.8.1. In the middle atmosphere, the accuracies are estimated by comparisons with the ACE-FTS instrument; see *Pumphrey et al.* [2007] for further details. The MLS v2.2*x* CO data at 215 hPa showed high (factor of ~2) biases compared to other observations. The morphology, however, was generally realistic [*Livesey et al.*, 2008]. In v6.0*x* (as in v5.0*x*), this bias has been essentially eliminated through a change in the approach to modeling the background radiance upon which the CO spectral line sits and a small reduction in the number of MLS spectral channels considered in the retrieval. Tropospheric (215–100 hPa) accuracies in Table 3.8.1 are 2σ estimates obtained by propagating parameter uncertainties through a model of the measurement system, and they are unchanged from those calculated for v5.0*x*.

3.8.7 Data screening

Pressure range: 215–0.001 hPa.

Values outside this range are not recommended for scientific use. Data at 0.00046 hPa represent a total column at and at pressures lower than that pressure level. Scientific use of these 0.00046 hPa data may be possible, but consultation with the MLS team is advised.

Estimated precision: Only use values for which the estimated precision is a positive number.

Values where the a priori information has a strong influence are flagged with negative or zero precision and should not be used in scientific analyses (see Section 1.5).

Status flag: Only use profiles for which the `Status` field is an even number.

Odd values of `Status` indicate that the profile should not be used in scientific studies. See Section 1.6 for more information on the interpretation of the `Status` field.

Clouds: Clouds have no impact for pressures of 31 hPa or less. v6.0*x*, v5.0*x*, and v4.2*x* CO are much less susceptible to cloud-induced artifacts than was v3.3*x*/v3.4*x*, so screening of the CO product is considerably simplified compared to that recommended for v3.3*x*/v3.4*x*, needing only application of the standard `Quality` and `Convergence` rules as described below. The low-cloud `Status` bit, which was set for 0.2% of profiles in v5.0*x*, is set for 0.6% of profiles in v6.0*x*, but this flag is not recommended as a source of information for data screening.

Quality: Only use profiles with `Quality` greater than 1.5.

Profiles with `Quality` less than or equal to 1.5 comprise 0.7% of all data, and ~2% of profiles in the tropics. At 215 hPa in the tropics, the rejected profiles have mixing ratios that are, on average, 7% higher than other tropical values, and the occurrence rates of high outliers with mixing ratios greater than 150 ppbv is about twice that of the rest of the tropical ensemble. At pressures of 100 hPa and smaller, the utility of the `Quality` threshold for screening is less clear, but its use is still recommended.

Convergence: Only profiles whose `Convergence` field is less than 1.03 should be used.

This `Convergence` criterion rejects fewer than 0.1% of profiles, as almost all of the retrievals in the phase that produces v6.0*x* CO converge to their target.

3.8.8 Artifacts

- Positive systematic error of 20–50% throughout the mesosphere, as was the case for v5.0*x*.
- Negative systematic error of 50–70% near 30 hPa, as was the case for v5.0*x*.
- Retrieved profiles are rather jagged, especially between 1 hPa (48 km) and 0.1 hPa (64 km). The greater smoothing applied in v6.0*x*, v5.0*x*, v4.2*x*, and v3.3*x*/v3.4*x* compared to v2.2*x* reduced this problem considerably but has not eliminated it entirely.
- The tendency for negative values to occur at the level below a large positive value that was present in v4.2*x* is somewhat reduced in v6.0*x* and v5.0*x*.
- Upper-tropospheric v6.0*x* CO retrieved values still show some anomalous sensitivity to thick clouds associated with deep convection. The screening procedure based upon `Quality` and `Convergence` described above is generally effective in removing these artifacts.
- Negative outliers in upper tropospheric CO have been observed in volcanic plumes, such as that from the eruption of Sarychev in June of 2009. These are likely the result of interference from spectral lines of a gas-phase plume component and could be a subject for further analysis and validation.

3.8.9 Review of comparisons with other datasets

In the upper troposphere, comparisons with various in situ CO observations (NASA DC-8, WB-57, and the MOZAIC dataset) indicate that the *earlier* MLS v2.2*x* 215 hPa CO product was biased high by a factor of ~2. As in v4.2*x* and v5.0*x*, this bias is largely eliminated in v6.0*x*.

In the mesosphere, comparisons of the earlier v2.2*x* MLS CO with ODIN-SMR and ACE-FTS suggest a positive bias: 30%–50% against ACE-FTS, 50%–100% against SMR. Near 31 hPa, the MLS values are lower than SMR and ACE-FTS by at least 70%. MLS CO values have not changed much between v2.2*x* and v6.0*x* in the middle atmosphere, so these comparisons may mostly be considered valid for v6.0*x*. What change there was between v2.2*x* and later versions consists of a slight lowering of the MLS values, bringing them slightly towards the ACE-FTS data; 20% is now a better estimate of the MLS-ACE bias in much of the middle atmosphere (compared to 30% with v2.2*x*). Further validation of the v6.0*x* retrieval above 0.01 hPa is needed.

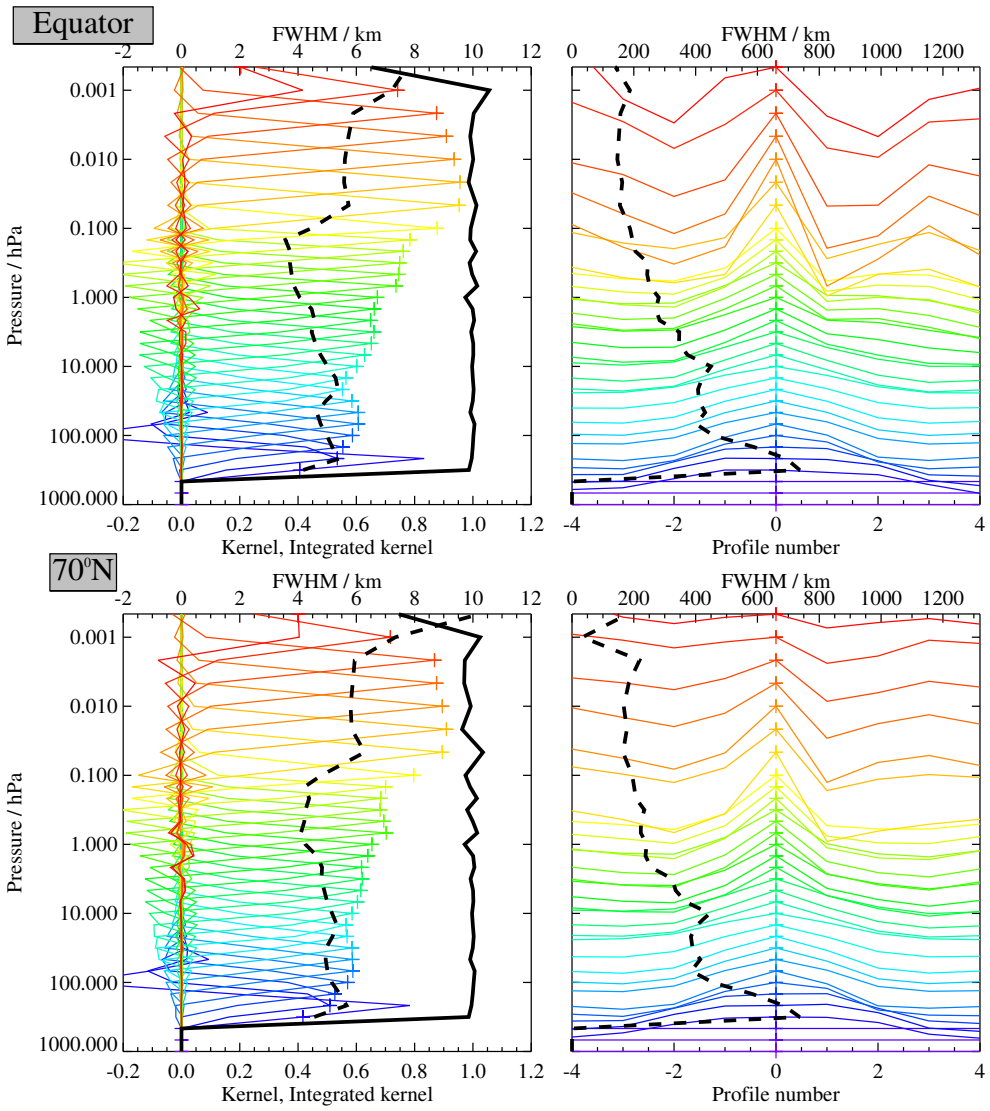

Figure 3.8.3: Typical two-dimensional (vertical and horizontal along-track) averaging kernels for the MLS v6.0*x* CO data at the equator (upper) and at 70°N (lower); variation in the averaging kernels is sufficiently small that these are representative of typical profiles. Colored lines show the averaging kernels as a function of MLS retrieval level, indicating the region of the atmosphere from which information is contributing to the measurements on the individual retrieval surfaces, which are denoted by plus signs in corresponding colors. The dashed black line indicates the resolution, determined from the full width at half maximum (FWHM) of the averaging kernels, approximately scaled into kilometers (top axes). (Left) Vertical averaging kernels (integrated in the horizontal dimension for five along-track profiles) and resolution. The solid black line shows the integrated area under each kernel (horizontally and vertically); values near unity imply that the majority of information for that MLS data point has come from the measurements, whereas lower values imply substantial contributions from a priori information. (Right) Horizontal averaging kernels (integrated in the vertical dimension) and resolution. The horizontal averaging kernels are shown scaled such that a unit averaging kernel amplitude is equivalent to a factor of 10 change in pressure.

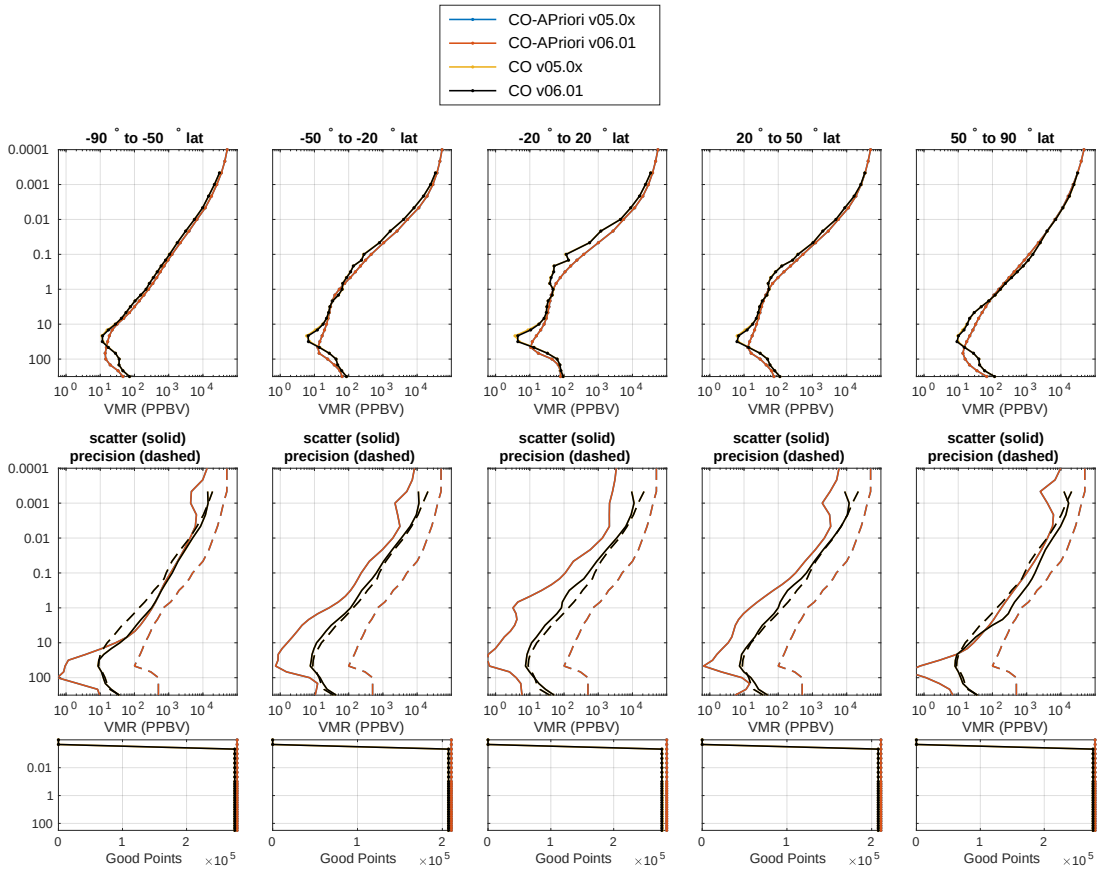

Figure 3.8.4: The top row shows 2009 zonal means of v6.0*x* and v5.0*x* retrieved mixing ratios and their a priori values, with the v6.0*x* retrieved mixing ratio lines (black) lying on top of the v5.0*x* mixing ratio lines (yellow) and the v6.0*x* a priori mixing ratio line (red) lying on top of the v5.0*x* a priori lines (blue) throughout. The middle row shows the zonal scatter about these zonal means (solid lines) and corresponding estimated precisions (dashed lines). The bottom row shows that the number of good profiles drops to zero only at the highest retrieval levels (0.00046 hPa and lower pressures), where retrieved precision exceeds half of the a priori precision.

Table 3.8.1: Summary of Aura MLS v6.0*x* CO Characteristics

Pressure hPa	Resolution[a] V × H km	Single-Profile Precision ppbv	Accuracy	Comment
< 0.001	—	—	—	Not retrieved
0.00046	—	—	—	Unsuitable for scientific use
0.001	7.2 × 200	12000	validation needed	possibly use, with caution
0.0022	5.9 × 200	8700	validation needed	possibly use, with caution
0.0046	5.8 × 200	6000	+20% to +50%	
0.01	5.9 × 200	3400	+20% to +50%	
0.046	5.9 × 200	1000	+20% to +50%	
0.14	3.8 × 200	640	+20% to +50%	
1	4.1 × 250	120	+20% to +50%	
10	5.0 × 440	16	±10%	
31	4.9 × 400	9	−70% to −50%	
100	4.9 × 450	14	±23 ppbv and ±30% [b]	
147	5.1 × 570	16	±32 ppbv and ±30% [b]	
215	5.4 × 690	19	±53 ppbv and ±30% [b]	
316	—	—	—	Unsuitable for scientific use
>316	—	—	—	Not retrieved

[a] Vertical and along-track horizontal resolutions; cross-track horizontal resolution is ~7 km.
[b] Estimated 215–100 hPa systematic uncertainty is the root sum square of the additive and multiplicative terms.

3.9 Geopotential Height (GPH)

Swath name: GPH

Useful range: 261–0.00046 hPa

Units: m

Product lead: Michael J. Schwartz <Michael.J.Schwartz@jpl.nasa.gov>

3.9.1 Introduction

Geopotential height (GPH) is retrieved, along with temperature and the related assignment of tangent pressures to limb views, primarily from bands near O_2 spectral lines at 118 GHz and 234 GHz. The v6.0*x* GPH product is generally similar to the GPH products of earlier versions, including the v2.2*x* product that is described by *Schwartz et al.* [2008], except that each profile is offset vertically in v6.0*x*, as it was in v5.0*x*, so that its value at 100 hPa matches that of a global assimilation model. For v6.0*x*, this reference level value is taken from GEOS-5.29.4 "Goddard Earth Observing System for Instrument Teams" (GEOS-IT). In v4.2*x* and earlier versions, the absolute reference for GPH was inferred from the spacecraft orbit/attitude system and the instrument scan model. Throughout the rest of this section, "GEOS-5" without additional qualification refers to GEOS-IT.

The heights of surfaces of constant geopotential are a property of the Earth's gravitational field and do not depend upon atmospheric conditions. Geopotential differences between surfaces are equal to the integral with height of the gravitational acceleration, g. GPH is the geopotential difference from the Earth's surface geopotential to a given location, scaled by the mean-sea-level gravitational acceleration, g_0, to give units of height.

MLS products, including GPH and temperature, are reported on pressure surfaces, but pressure, temperature, and height depend upon one another through assumed hydrostatic balance and the gas law:

$$\frac{1}{g_o}\int g\,dh = \frac{R}{Mg_o}\int T\,dP/P, \tag{3.1}$$

where M is the molar mass of air and R is the gas constant. If we assume that we know the molar-mass profile of the atmosphere (which begins to vary significantly from its dry-air surface value in the mesosphere due to height-dependent changes in the mixing ratios of O_2 and N_2), then the retrieval of a temperature profile on fixed pressure surfaces also determines GPH differences between those surfaces, and so determines the complete GPH profile to within an additive constant. Absolute pointing cannot be inferred from radiometric information and must be obtained from a priori information. In v4.2*x* and earlier versions, the spacecraft orbit/attitude system and instrument scan model provided this information, but there were systematic, annually repeating biases in the inferred 100-hPa reference altitude that were large compared to expected error in GPH from assimilations such as GEOS-5. In v6.0*x*, 100-hPa GPH from the GEOS-IT analysis is used as the reference height instead of values inferred from the instrument scan model.

Table 3.9.1 summarizes v6.0*x* measurement precision, modeled accuracy, and observed biases. The following sections provide details.

3.9.2 Differences between v6.0*x* and previous versions

Both v6.0*x* and v5.0*x* GPH products are taken from the `CorePlusR3` retrieval phase (along with a number of standard products that depend upon radiances from the 240-GHz radiometer). The GEOS-IT 100-hPa GPH, used by v6.0*x* as its reference level, and GEOS-FPIT 100-hPa GPH, used by v5.0*x*, typically differ by less than 10 m, so differences caused by the choice of reference level are negligible.

The Earth Gravitational Model 1996 (EGM96) geoid defines zero height for GEOS-5 GPH, v6.0*x* GPH (which inherits this definition from GEOS-5), and v5.0*x* GPH. Earlier versions of MLS GPH used the WGS84

ellipsoid that is used in the MLS forward model ray tracing. The impact of this difference is discussed in the v4.2*x* edition of this document [*Livesey et al.*, 2020].

In v5.0*x* and v6.0*x*, the fill value for missing GPH data (the geopotential heights themselves) has been changed to -1×10^{15} m. The value of −999.99 m used for missing GPH data in earlier versions of MLS GPH is within the range of valid GPH values that might be found at the bottom of a retrieval. The fill value for missing geolocation data (latitude, longitude, etc.) remains −999.99, consistent with that used for other products.

Figure 3.9.1(a) shows biases in v6.0*x* minus v5.0*x* GPH that result from biases in v6.0*x* minus v5.0*x* temperature, shown in 3.23.2(b). Relative to v5.0*x*, v6.0*x* has a low temperature bias of ∼−2 K at 1 hPa, a high bias of as much as +3 K in the lower mesosphere, and a slightly low bias at higher levels. The v6.0*x* minus v5.0*x* GPH biases approach −20 m at 1 hPa, exceed +100 m in the tropical middle mesosphere, and decline in magnitude at higher levels.

3.9.3 Comparison to GEOS-5 Analysis

Figure 3.9.1(b) shows that biases between v6.0*x* and GEOS-IT GPH, which are zero by definition at 100 hPa, grow through the stratosphere due to the persistent ∼1 K low bias in v6.0*x* temperature with respect to GEOS-IT. In the lower and middle stratosphere, GEOS-IT assimilates numerous high-quality data sets, and it is likely that it is more accurate than MLS, so the differences shown in the lower parts of Figure 3.9.1(b) are likely due to error in MLS GPH, not in GEOS-IT. GEOS-IT is not well constrained by data in the mesosphere, so it is likely a less reliable correlative data set above 1 hPa.

A latitudinally and seasonally varying bias between MLS v4.2*x* GPH and GEOS-5 GPH was the subject of extensive discussion in the v4.2*x* edition of the MLS data quality document [*Livesey et al.*, 2020]. Some of this annually repeating "bias" may result from annually repeating geophysical information captured by MLS that is not in the GEOS-5 analysis. However, the large ascending/descending differences are almost certainly not primarily diurnal effects. The fidelity with which these patterns annually repeat suggests that they may result from thermal distortions of the spacecraft/instrument that vary annually due to the eccentricity of the Earth's orbit, or from orbit/attitude errors from the star trackers that provide the spacecraft-attitude information. The same star fields are viewed each year at the same date and orbit position.

Elimination of this bias was a primary motivation for the adoption of GEOS-5 100-hPa GPH as an absolute reference height. The GEOS-IT operational products are available in time to be used in routine v6.0*x* MLS processing and also provide the temperature a priori for the retrieval. At 100 hPa, the model of the near-real-time system is good enough that the differences that would accrue by waiting for a reanalysis with additional assimilated data (e.g., MERRA-2) are generally negligible compared to the GPH biases that were present in v4.2*x*.

In v6.0*x* (as in v5.0*x*), each profile is offset in height so that the 100-hPa GPH reference level matches that of the GEOS-5 GPH. Differences between GEOS-5 GPH and v6.0*x* GPH at other retrieval levels are the accumulated differences between GEOS-5 and MLS temperatures as these differences are integrated (as in Equation 3.1) away from 100 hPa. The 100-hPa GPH produced by the MLS v6.0*x* retrieval algorithm is stored as a diagnostic swath in the "DGG" file before is is overwritten with GEOS-5 values.

3.9.4 Vertical resolution

The GPH profile is vertically integrated temperature, so its vertical resolution is not well defined. The vertical resolution of the underlying temperature given in Section 3.23 is repeated in Table 3.9.1.

3.9.5 Precision

MLS v6.0*x* GPH precision is summarized in Table 3.9.1. Precision is the random component of measurements that will average down if a measurement is repeated. The retrieval algorithms produce an estimate of GPH precision only for the 100-hPa reference level, as this is the only element included in the MLS "state vector." In v6.0*x*, this level is replaced by the GEOS-5 100-hPa GPH, and so has no random error from MLS radiance noise, leading to the 0 m precision reported for 100 hPa in Table 3.9.1. Precisions at other standard-product profile levels (summarized in the second column of Table 3.9.1) are calculated from the profiles of temperature

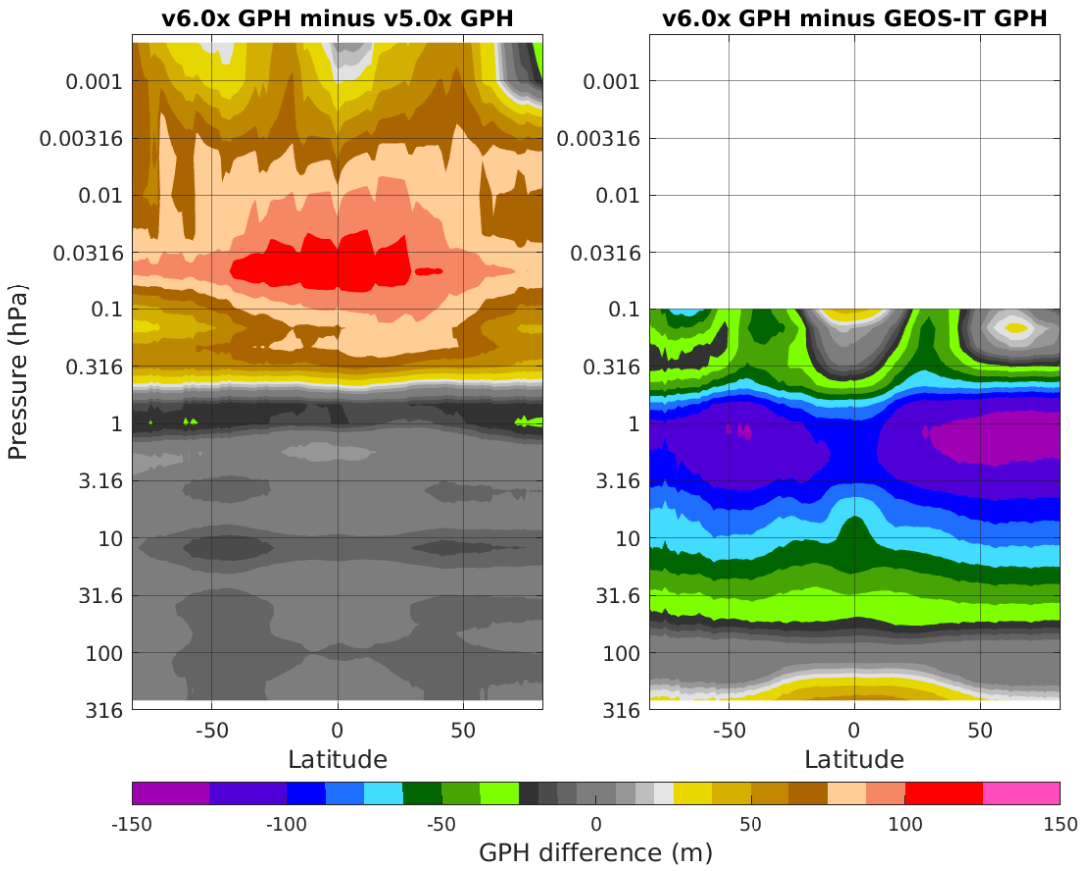

Figure 3.9.1: (a) The zonal-mean difference between v6.0*x* and v5.0*x* MLS GPH. (b) The difference between v6.0*x* and GEOS-IT GPH. In both cases, the 2021 annual averages are shown and are typical of the record.

precisions. v6.0*x* GPH precision is improved (smaller) in the upper stratosphere and mesosphere compared to that of v5.0*x* due to improvements in the temperature retrieval precision, with typical reductions exceeding 15% (e.g. 38 m vs. 46 m at 0.1 hPa) in the lower mesosphere. Typical estimated precisions remain smaller than 20 m up to 1 hPa and degrade to ~100 m at 0.01 hPa. Off-diagonal elements of the temperature/GPH error covariance matrix are neglected in this GPH-precision-profile calculation, but resulting errors are believed to be small.

3.9.6 Accuracy

The v6.0*x* GPH accuracy has been modeled through consideration of a variety of sources of systematic error, much as v2.2*x* GPH accuracy was modeled, as discussed by *Schwartz et al.* [2008]. Results of these calculations are given in the fourth column of Table 3.9.1. Substantial biases believed to originate in satellite pointing data and/or time-varying biases in the instrument pointing system have been removed through the use of GEOS-5 100-hPa GPH as an absolute GPH reference rather than information from the satellite attitude and instrument scan model. Of the remaining error sources considered, modeled amplifier non-linearity has the largest impact, just as is the case with the calculation for temperature.

"Observed accuracy" in Table 3.9.1 is an estimate of the bias based upon comparisons with analyses and with other previously validated satellite-based measurements.

3.9.7 Known Artifacts

GPH in v5.0*x* and earlier versions had large artifacts, reaching ~3500 m in amplitude, in the orbit following "inclination adjustment maneuvers" (IAMs), which are done to keep Aura in the "A-Train" constellation of satellites. Starting in v5.0*x*, IAM-related biases were eliminated by the use of GEOS-5 100-hPa GPH as an absolute reference.

3.9.8 Data screening

GPH should be screened in much the same way as is temperature:

Pressure range: 261–0.00046 hPa.

Values outside this range are not recommended for scientific use.

Estimated precision: Only use values for which the estimated precision is a positive number.

Values where the a priori information has a strong influence are flagged with negative or zero precision and should not be used in scientific analyses (see Section 1.5). For the hydrostatic integration calculations that compute GPH above and below the 100-hPa reference level, GPH precision is set negative at any level where the temperature precision is negative. Furthermore, the output GPH precision remains negative for all levels beyond (i.e., further above or further below), even if the temperature precision becomes positive again.

Status flag: Only use profiles for which the `Status` field is an even number.

Odd values of `Status` indicate that the profile should not be used in scientific studies. See Section 1.6 for more information on the interpretation of the `Status` field.

Clouds: Thick clouds are believed have some impact on v6.0*x* GPH measurements in the upper troposphere (261–100 hPa). If a user wants to prioritize minimization of the impact of clouds on GPH in the troposphere, GPH may be screened using the ice water content (IWC) product, rejecting profiles between 261 and 100 hPa for which the 215 hPa value of IWC is greater than 0.005 g/m^3.

Quality: Only use profiles with `Quality` greater than 0.2 for the 83 hPa level and smaller pressures, and profiles with `Quality` greater than 0.9 at pressures of 100 hPa and larger.

Convergence: Only profiles whose `Convergence` field is less than 1.03 should be used.

Use of this threshold typically discards less than 0.1% of profiles and is primarily a safeguard against profiles with extremely poor convergence.

Table 3.9.1: Summary of MLS GPH product.

Pressure hPa	Resolution[a] V × H km	Single-Profile Precision m	Modeled accuracy[b] m	Observed accuracy[c] m	Comments
<0.00046	—	—	—	—	Unsuitable for scientific use
0.00046	13 × 316	±190	4200	—	More validation needed
0.001	12 × 280	±170	700	450	
0.01	11 × 250	±100	250	100	
0.1	6 × 170	±38	250	100	
1	5 × 165	±18	120	100	
10	4.1 × 165	±11	30	100	
100	4.6 × 165	±0[d]	20	20	
261	3.8 × 167	±8	30	50	
1000–316	—	—	—	—	Unsuitable for scientific use

[a]Vertical and along-track horizontal resolutions; cross-track horizontal resolution is ∼13 km. The GPH profile is vertically integrated temperature, so its vertical resolution is not well defined. The vertical resolution of the underlying temperature retrieval is repeated here.

[b]Not including pointing contribution.

[c]Validation is based upon SABER and GEOS-5 comparisons with MLS v2.2*x* and should be updated.

[d]The retrieval's 100-hPa GPH value is fixed to that of the GEOS-IT, so radiometric noise has no contribution to precision at this level. GPH precision accumulates radiometric noise as retrieved temperature is integrated while moving away from 100 hPa, either higher or lower in pressure.

3.10 Water Vapor (H_2O)

Swath name: H20

Useful range: 316–0.001 hPa

Product lead: Alyn Lambert (stratosphere/mesosphere) <alyn.lambert@jpl.nasa.gov>
William Read (troposphere) <william.g.read@jpl.nasa.gov>

3.10.1 Introduction

The standard water vapor product is taken from the 190-GHz "CorePlusR2" retrieval. The vertical grid for H_2O is 12 levels per decade change in pressure (LPD) for 1000–1 hPa, 6 LPD for 1.0–0.1 hPa, and 3 LPD for 0.1–10^{-5} hPa. The horizontal grid is every 1.5° along the orbit track. H_2O is unusual among MLS products in that the retrieval calculations assume that the logarithm of the volume mixing ratio (VMR), and not mixing ratio itself, varies linearly with log-pressure between grid points; however, H_2O is still retrieved in VMR (not log VMR) just as is the case for the other MLS constituents. This means that, when interpolating MLS measurements to other locations (along track and/or vertically), such interpolation should be performed linearly on the logarithm of the H_2O concentration (VMR).

The recommended vertical range for MLS v6.0*x* H_2O is 316–0.001 hPa. The uppermost retrieved level, 0.00046 hPa, is not vertically resolved from the levels above it and should be regarded as a measure of the total column water vapor at and above 0.001 hPa. The 0.00046-hPa data may be usable for some studies when interpreted in this manner, but only in consultation with the MLS science team. The MLS H_2O data between 1000 and 383 hPa are taken from a retrieval of relative humidity with respect to ice (RHi), converted to specific humidity using the Goff-Gratch vapor pressure over ice equation. This RHi retrieval is not vertically resolved, and all levels between 1000 and 383 hPa are assumed to have the same RHi. See Section 3.21 for more information. H_2O data for pressures less than or equal to 0.000215 hPa are filled with a priori values.

Validation of MLS v2.2*x* water vapor is presented by *Read et al.* [2007] and *Lambert et al.* [2007]. This section reiterates the key information from those studies and updates them for v6.0*x*. Table 3.10.1 gives a summary of MLS v6.0*x* H_2O precision, resolution, and accuracy.

3.10.2 Changes from v4.2*x* to v5.0*x* and v6.0*x*

Modifications to the H_2O retrievals in v6.0*x*

A defect in MLS v4.2*x* and prior versions was that H_2O exhibited a rather low bias (20–50%) around 2–3 km below the tropopause [*Read et al.*, 2022]. Also, v4.2*x* likely underestimated the H_2O seasonal cycle at 147 hPa in the tropics. These two issues are related, as the tropopause height has a strong seasonal cycle in the tropics, and the dry bias at a given height will be modulated accordingly. This acted to flatten the seasonal cycle in retrieved 147 hPa H_2O in earlier MLS versions. Additionally, as discussed in Section 1.10.1, it is clear that the MLS 190-GHz radiometer that measures H_2O (and other species, notably N_2O, HCN, and upper stratospheric HNO_3) is slowly drifting, due to aging of this instrument subsystem. A possible drift in the MLS H_2O was first noted by *Hurst et al.* [2016]. An in-depth investigation into potential causes for all these issues [*Livesey et al.*, 2021] has shown the most likely contributors to be:

1. A slow (~2%-per-decade) drift in the 190-GHz "sideband fraction" (the relative sensitivity of the radiometer to signals on either side of the 190-GHz "local oscillator" tone),
2. An offset between the pre-launch-measured value of that sideband fraction and the post-launch value (likely due to a difference in instrument operating temperature between the two environments and the radiometer being more temperature sensitive than designed), and
3. A bias (within the uncertainty estimated for pre-launch instrument alignment measurements) in the assumed pointing offset between the 190-GHz radiometer and other MLS radiometers.

The v5.0*x* algorithms implemented a correction for these issues, including a time-dependent (on a month-by-month basis) sideband fraction estimate derived internally from the MLS observations. Importantly, as described in more detail by *Livesey et al.* [2021], this time-dependent correction to the sideband fraction makes no reference to correlative measurements of stratospheric water vapor from satellite or balloon observations, although improved agreement with such correlative measurements builds confidence in the validity of the correction.

The same correction is applied in a more-or-less identical manner in v6.0*x*. The key difference is that the v5.0*x* sideband fraction estimate for each month relied on having v4.2*x* data available for that month. For v6.0*x*, the sideband fraction estimation is performed in a stand-alone manner, typically using the fraction from the previous calendar month as a starting point. The differences between the two methods are negligibly small, on the order of less than 0.01% in the correction. Of note is that v4.2*x* processing was halted on 31 May 2024, but v5.0*x* processing continues to the present day. For data from 1 June 2024 onward, the v5.0*x* processing has used the same sideband fraction estimates employed in v6.0*x* rather than relying on the discontinued v4.2*x*.

The extent to which the time-dependent sideband fraction continues to ameliorate drifts in recent years in the MLS v6.0*x* H_2O (and N_2O) is under investigation. We note that recent studies [*Zhang et al.*, 2025; *Tinney and Randel*, 2026] have found a decreasing trend in MLS v5.0*x* water vapor near and below the tropopause that appears to be at odds with other data records and model predictions. Initial assessment by the MLS team shows that v4.2*x*, v5.0*x*, and v6.0*x* all exhibit such a trend (though this trend is weaker in v6.0*x*). Further study is needed to assess the validity of this apparent negative trend.

Another difference between v5.0*x* and v6.0*x* is that limb tangent pressure is no longer retrieved from the H_2O linewidth in v6.0*x*. Instead, the tangent pressure estimated from the O_2 measurements in an earlier phase of processing is used. This change alleviated issues on two fronts:

1. There is a small drift (equivalent to a ∼20 m change in altitude over the mission lifetime) between the tangent pressures retrieved from the `CorePlusR3` and `CorePlusR2` phases.
2. In the immediate aftermath of the January 2022 Hunga eruption, for measurements in the core of the volcanic plume, the tangent pressures retrieved from the `CorePlusR2` phase deviated by the equivalent of ∼1 km in altitude from those retrieved in the `CorePlusR3` phase, as a result of the unprecedented (in the satellite era) levels of H_2O and large abundances of SO_2 in the atmosphere at that time. This failure to retrieve realistic tangent pressure information invalidates all the results from the `CorePlusR2` phase in such profiles. Thus, users were directed to use v4.2*x* retrievals of H_2O from 15 January to 8 February 2022 [*Millán et al.*, 2022] in preference to v5.0*x*. This issue is fixed in v6.0*x*.

The cause of the 20 m drift between the two tangent pressure estimates is not fully understood but may originate from subtle aspects of the method used to estimate the 190-GHz sideband fraction drift in v5.0*x* discussed above. One further change between v5.0*x* and v6.0*x* that impacts the H_2O product results from efforts to place the retrievals of N_2O on a more robust footing, as described in more detail in Sections 1.4.1 and 2.8.

V5.0*x* and previous versions exhibit a vertical kink in H_2O at 10 and 8.3 hPa, first noted by *Niemeier et al.* [2023] and *Millán et al.* [2024]. This kink originates from the a priori profile used in the retrieval. The a priori combines (a) the results of a preliminary low-vertical-resolution retrieval (from the `InitUTH` phase) for pressures greater than (i.e., altitudes below) 10 hPa with (b) a climatological H_2O profile for pressures smaller than (i.e., altitudes above) 10 hPa. This transition introduces a kink in the a priori profile, which is then echoed in the retrieved profile, owing to the vertical smoothing (Tikhonov regularization) used in the retrieval. To eliminate this artifact, the v6.0*x* retrievals vertically smooth the transition in the a priori profiles over the range from 17.8 to 6.8 hPa.

As for v5.0*x*, humidity data for the region of the atmosphere below the 316 hPa MLS retrieval level are derived from a retrieval of RHI over a single broad layer (using low-limb-viewing MLS wing channel radiances);

a similar approach is employed by NOAA nadir-viewing operational humidity sounders such as TOVS. As noted by *Read et al.* [2007], the v2.2*x* RHI retrievals in this surface-to-mid-troposphere region were likely to be ~30% too high, based on comparisons with AIRS. The accuracy of the low-altitude RHI retrieval is highly sensitive to the assumed transmission efficiency of the MLS optics system. In v3.3*x*/v3.4*x* and thereafter, the transmission efficiency assumed in the retrievals was adjusted empirically (within the uncertainty range established from MLS pre-launch calibration) to give better agreement with AIRS RHI in the tropical mid-troposphere. This retrieval is used as an a priori and constraint for humidity at the levels below the bottom of the H_2O retrieval range.

The number of "good" H_2O profiles has declined slightly over the mission life. A typical day has 3495 available profiles and, depending on the season, the fraction of these that pass the quality screening runs in the range 95–99%, corresponding to 35–175 profiles being rejected per day. Most of these rejections are caused by poor radiance fits (`Quality` < 0.7). The v4.2*x* record shows a gradual increase in the number of rejections over the mission life, with an additional ~25 profiles per day rejected in the 2024 timeframe. The changes in v5.0*x* reduced this growth to only 8 profiles per day. For v6.0*x*, this difference in the number profiles rejected between the start of the mission and recent data has increased slightly to 10 profiles per day.

Impacts of these changes on the MLS H_2O dataset

The v6.0*x* H_2O product agrees with v5.0*x* to within 2% in the bulk of the stratosphere and in the mesosphere. Lower down, v6.0*x* is 2–3% wetter than v5.0*x* at 68 hPa, 5–10% wetter at 83 and 100 hPa, 5–10% drier at 121 and 178 hPa, and 5–10% wetter over 215–316 hPa. Also, at 10–8.3 hPa, v6.0*x* is smoother than v5.0*x* as a result of changes to the manner in which the a priori profile is constructed as discussed above.

Figure 3.10.1 compares prior MLS H_2O versions to v5.0*x* for various latitude bins. Notable differences in earlier versions include the removal of a kink that was present in v2.2*x* at 32/26 hPa. This kink was caused by a linewidth error and was fixed in version v3.3*x*/v3.4*x*. In v2.2*x*, H_2O was retrieved on a fine 12 LPD grid from the bottom of the retrieval range to 22 hPa. V3.3*x*/v3.4*x* extended that region up to 1 hPa. V4.2*x* saw improvements in cloud screening and in the lower-resolution initial H_2O phase that is used to initialize values and profile shape smoothing for the final high-resolution phase. These changes improved agreement with simulated data at the 316–215 hPa levels. The change in sideband fraction in v5.0*x* leads to a 5–10% reduction in H_2O in the stratosphere and above. The combined changes in sideband fraction and assumed radiometer alignment result in a moistening of the levels 2 km below the tropopause, which is nominally 147 hPa in the tropics, 215 hPa at midlatitudes, and 261 hPa at high latitudes. The extremely low values retrieved at 215 hPa at high latitudes seen in previous versions appear to be less dry in v5.0*x* and v6.0*x*.

The third panel in Figure 3.10.1 shows the mean estimated single-profile precision and the measured variability (which reflects a combination of instrument noise and atmospheric variability). The estimated precisions generally vary little with height in the lower stratosphere. In the upper troposphere, however, the estimated precision roughly scales by the amount of H_2O. At these altitudes, higher concentrations of H_2O are typically accompanied by larger (i.e., worse) estimated precision (in VMR). That said, when considered as a percentage of concentration, the precision value declines somewhat. Taken together, the large dynamic range of possible humidity in the upper troposphere and the non-linear behavior of the instrument response to these concentrations, are the main motivation for choosing a logarithmic representation for H_2O in the retrievals. Differences in precision between v2.2*x* and later versions result from the use of a coarser retrieval grid above 22 hPa and a different value of the H_2O linewidth.

Figure 3.10.2 compares all versions v2.2*x* to v6.0*x* over the range from 10 to 0.0001 hPa over all latitudes. As expected, H_2O abundances from v5.0*x* and v6.0*x* are lower than those in all other versions except v2.2*x*, which assumed an erroneous H_2O linewidth. Also shown is the increased a priori precision being used for v5.0*x* and v6.0*x* at pressures smaller than 0.0046 hPa, modified in order to make H_2O at the 0.001 and 0.00046 hPa levels usable. V5.0*x* and v6.0*x* used a non-linear radiative transfer model in place of an approximate linear model for the highly spectrally resolved digital autocorrelator spectrometer (DACS) signals. This leads to some differences in the uppermost levels. Given that a more accurate model is being used, these differences

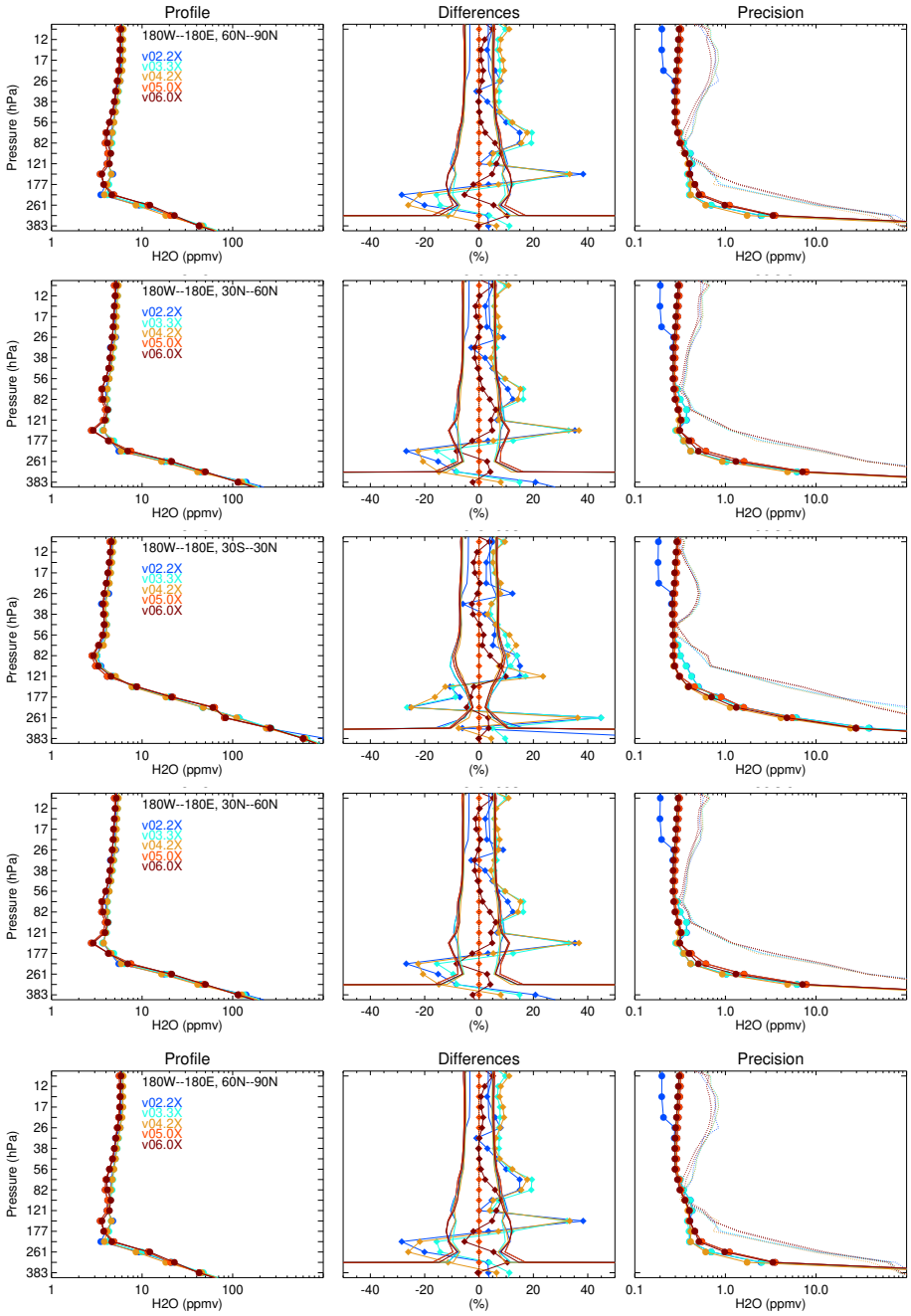

Figure 3.10.1: A comparison of MLS v2.2*x* (blue), v3.3*x*/v3.4*x* (cyan), v4.2*x* (mustard), v5.0*x* (orange), and v6.0*x* (dark red) water vapor for January-February-March 2005 in five latitude bands. Comparisons for other time periods (not shown) are similar. Left panels show mean profiles, center panels show the mean differences relative to v5.0*x* (colored lines with diamonds) surrounded by each version's estimated precision (colored lines with no symbols), and right panels show the estimated retrieval precision (solid lines with bullets) and measured variability (which includes atmospheric variability about the mean; dotted lines).

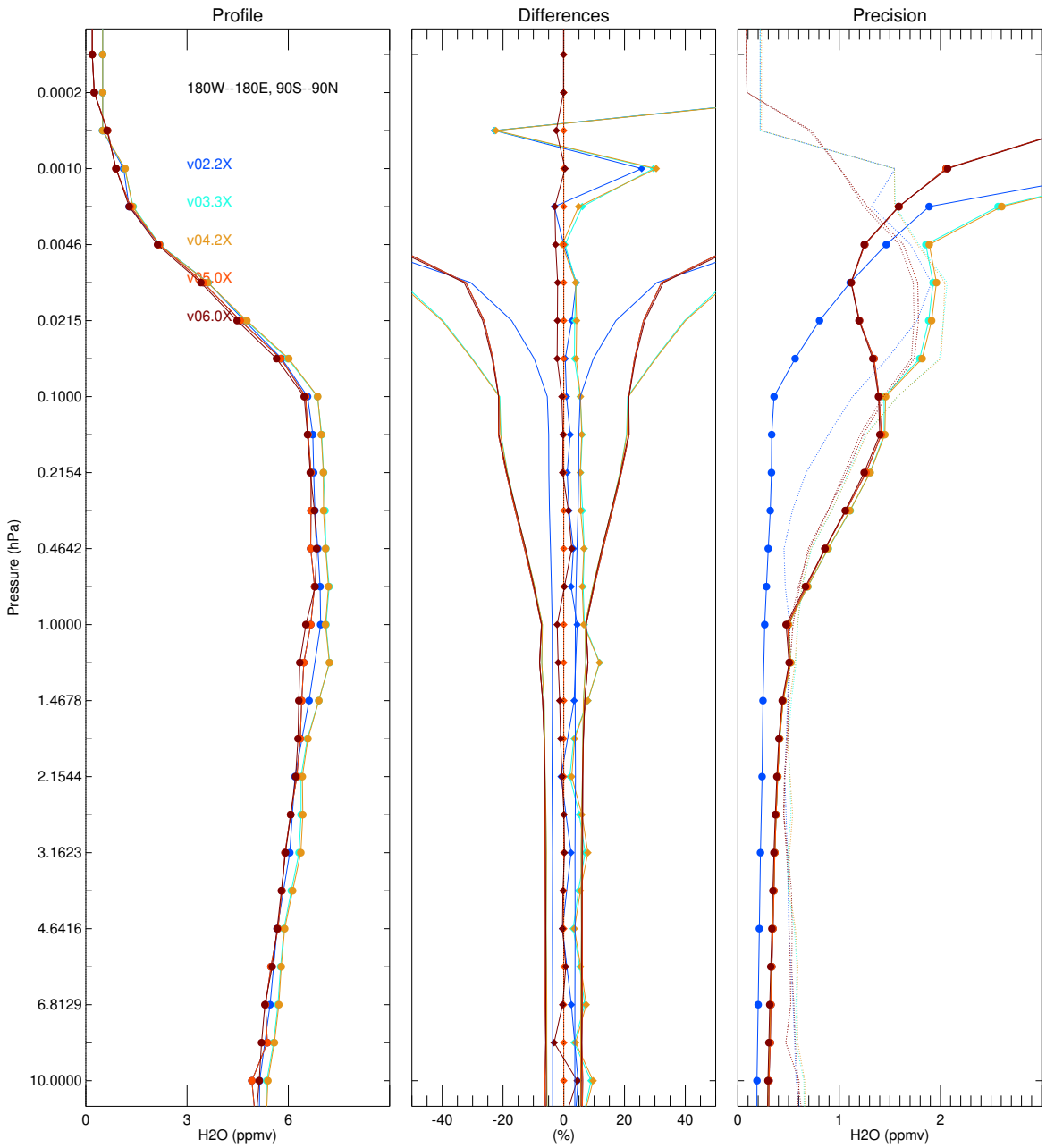

Figure 3.10.2: An all-latitudes comparison of v2.2*x* (blue), v3.3*x*/v3.4*x* (cyan), v4.2*x* (mustard), v5.0*x* (orange), and v6.0*x* (dark red) water vapor for January-February-March 2005 showing levels in the middle stratosphere up to the mesosphere. Other time periods are similar. The left panel compares mean profiles, the center shows the mean difference relative to v5.0*x* (diamonds), and the right panel shows the estimated retrieval precision (solid and bullets), measured variability (dotted), which includes atmospheric variability about the mean, and the a priori precision (dashed and small diamonds) profile.

are expected to represent improvements in the accuracy of the product.

Figures 3.10.3 and 3.10.4 show a comparison of H_2O zonal means from v2.2*x*, v3.3*x*/v3.4*x*, v4.2*x*, v5.0*x*, and v6.0*x* retrievals for 316–8.3 hPa and 6.8–0.00046 hPa, respectively. In the stratosphere, v6.0*x* values are similar to those in v5.0*x* and usually lower than those in prior versions, thanks to the sideband adjustment. V5.0*x* also shows increased 147 hPa humidity in the tropics, with further increases at 215 hPa in midlatitudes, and yet more increases at 261 hPa at high latitudes. In the mesosphere, $p < 1$ hPa, all versions show similar abundances up to the uppermost level, 0.001 hPa. At 0.00046 hPa, the v5.0*x* and v6.0*x* column estimates agree; earlier versions output the a priori at this level.

3.10.3 Resolution

The spatial resolution is obtained from examination of the averaging kernel matrices shown in Figure 3.10.5. The vertical resolution for H_2O is in the range 1.3–3.6 km from 316–0.22 hPa and degrades to 6–11 km for pressures smaller than 0.22 hPa. The along-track horizontal resolution is ~170–350 km for pressures greater than 4.6 hPa and degrades to 400–740 km at smaller pressures. The resolutions shown in Table 3.10.1 are averages of the equatorial and 70°N values given in Figure 3.10.5. The horizontal cross-track resolution is 9 km, the width of the MLS 190-GHz field of view for all pressures. The longitudinal separation of the MLS measurements is 10°–20° over middle and lower latitudes, with much finer sampling in polar regions. The instrument nominally scans to 0.001 hPa; therefore the retrieved value at 0.00046 hPa is not vertically resolved and is effectively a column measurement from 0.001 hPa to the spacecraft, with the H_2O profile values for $p \leq 0.000215$ hPa fixed at a priori values.

3.10.4 Precision

Table 3.10.1 summarizes the estimated precision of the MLS v6.0*x* H_2O data. For pressures ≥ 100 hPa, the precisions quoted are the 1σ scatter about the mean of coincident comparison differences, which are larger than the formal retrieval precisions estimated by the Level 2 software [*Read et al.*, 2007]. For $p \leq 83$ hPa, the precisions are the 1σ scatter of coincident ascending/descending MLS profile differences [*Lambert et al.*, 2007]. The individual Level 2 precisions are set to negative values or zero in situations when the retrieved precision is larger than 50% of the a priori precision – an indication that the data are biased toward the a priori value.

3.10.5 Accuracy

The values for accuracy are based on a full systematic error analysis performed on the MLS measurement system, as described (for v2.2*x*) by *Read et al.* [2007] and *Lambert et al.* [2007]. The results are shown in Table 3.10.1. For pressures between 316 and 178 hPa, comparisons between AIRS v7 and MLS v6.0*x* show agreement within 20% in the zonal mean (with MLS usually drier for low concentrations and wetter for high concentrations) equatorward of 40°, with MLS having a dry bias at higher latitudes. Comparisons to AIRS indicate that the accuracy estimates in Table 3.10.1 for pressures between 316 and 178 hPa may be pessimistic, but they are retained here to indicate the theoretical range. For the pressure range 178–83 hPa, the quoted values come directly from the systematic error analysis performed on the MLS measurement system.

3.10.6 A note about the water vapor averaging kernels

In general, averaging kernels are most applicable to linear and moderately non-linear retrieval problems. The MLS H_2O retrievals are mostly linear, except when the atmosphere approaches opaqueness at the frequencies observed by MLS. This occurs when the limb tangent of the instrument field of view is less than 10 km above the Earth's surface and the atmosphere is moist. In such cases the measurements are very nonlinear, and often the averaging kernel calculations for the lowest retrieved levels are numerically unstable and unrepresentative of the actual MLS measurement system. This is the case, for example, for the 316 hPa and 262 hPa equatorial kernels shown in Figure 3.10.5. Analysis of simulated MLS observations indicates that application of the averaging kernel provides little benefit to analyses involving the 316 hPa and 262 hPa levels, and accordingly we recommend not applying the (unrepresentative) kernels at those levels.

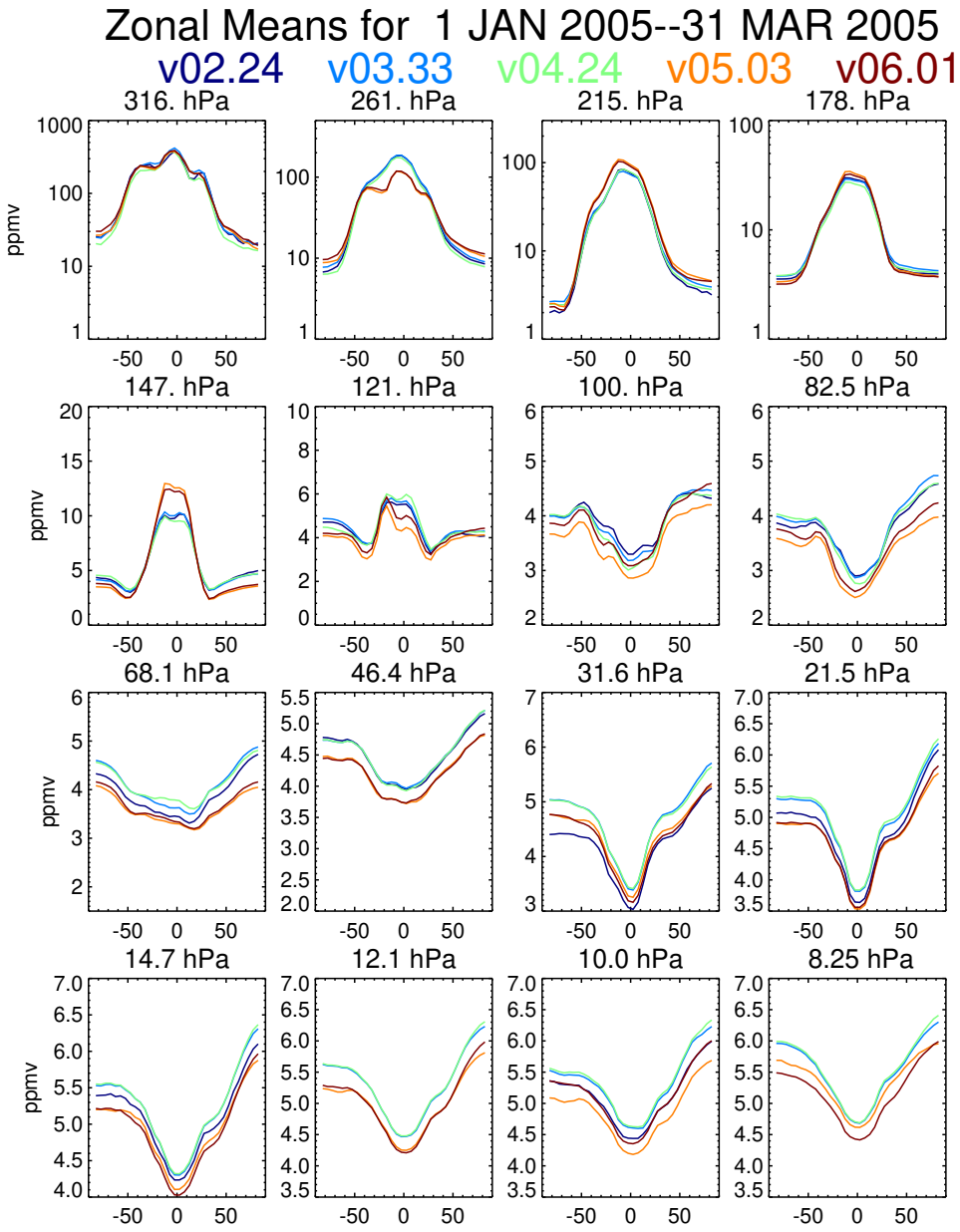

Figure 3.10.3: A comparison of v2.2*x* (dark blue), v3.3*x*/v3.4*x* (blue), v4.2*x* (green), v5.0*x* (orange), and v6.0*x* (red) water vapor zonal means for January-February-March 2005. Each panel represents results for a specific pressure level, ranging from 316 hPa to 8.3 hPa.

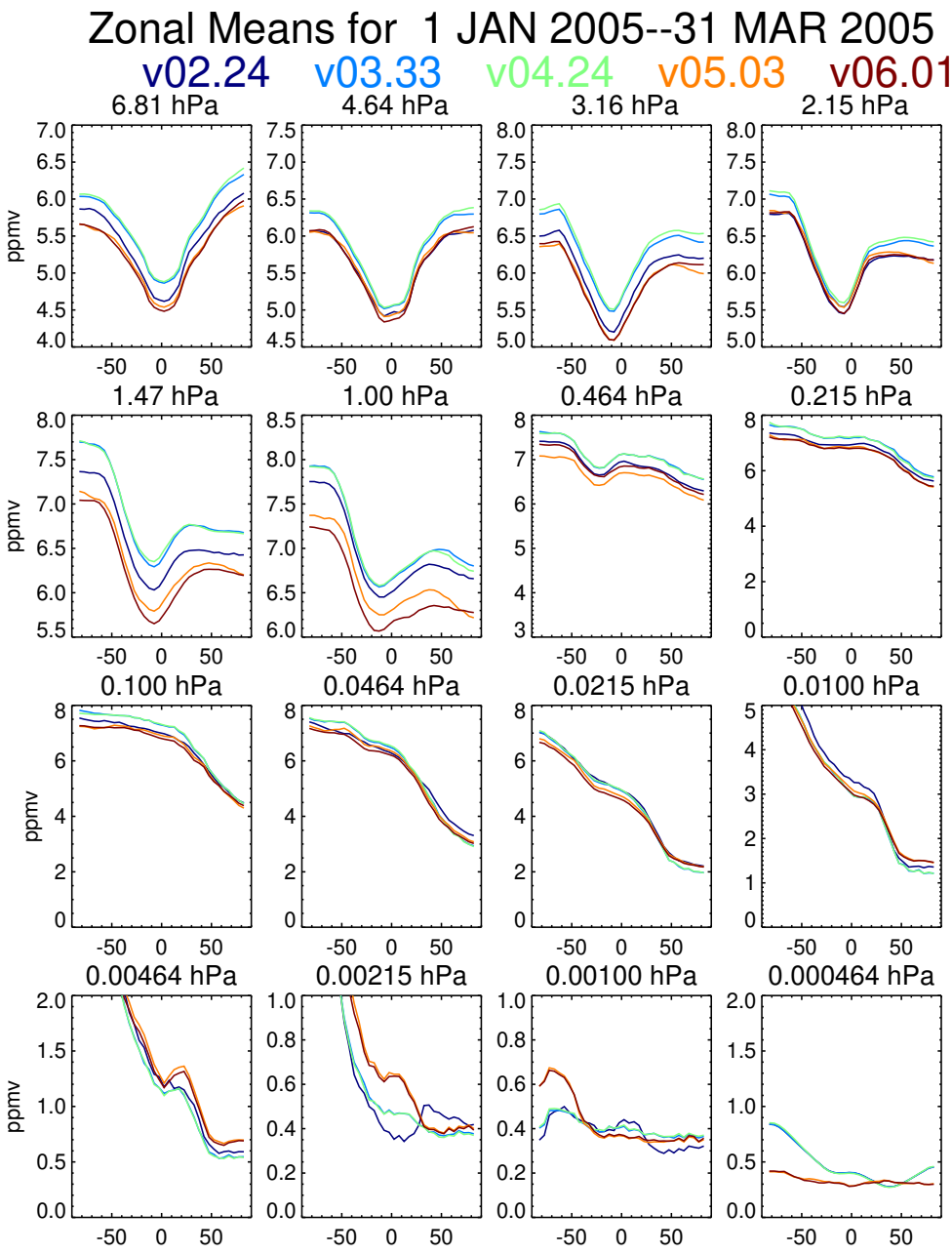

Figure 3.10.4: As Figure 3.10.3 but for 6.8 hPa to 0.00046 hPa.

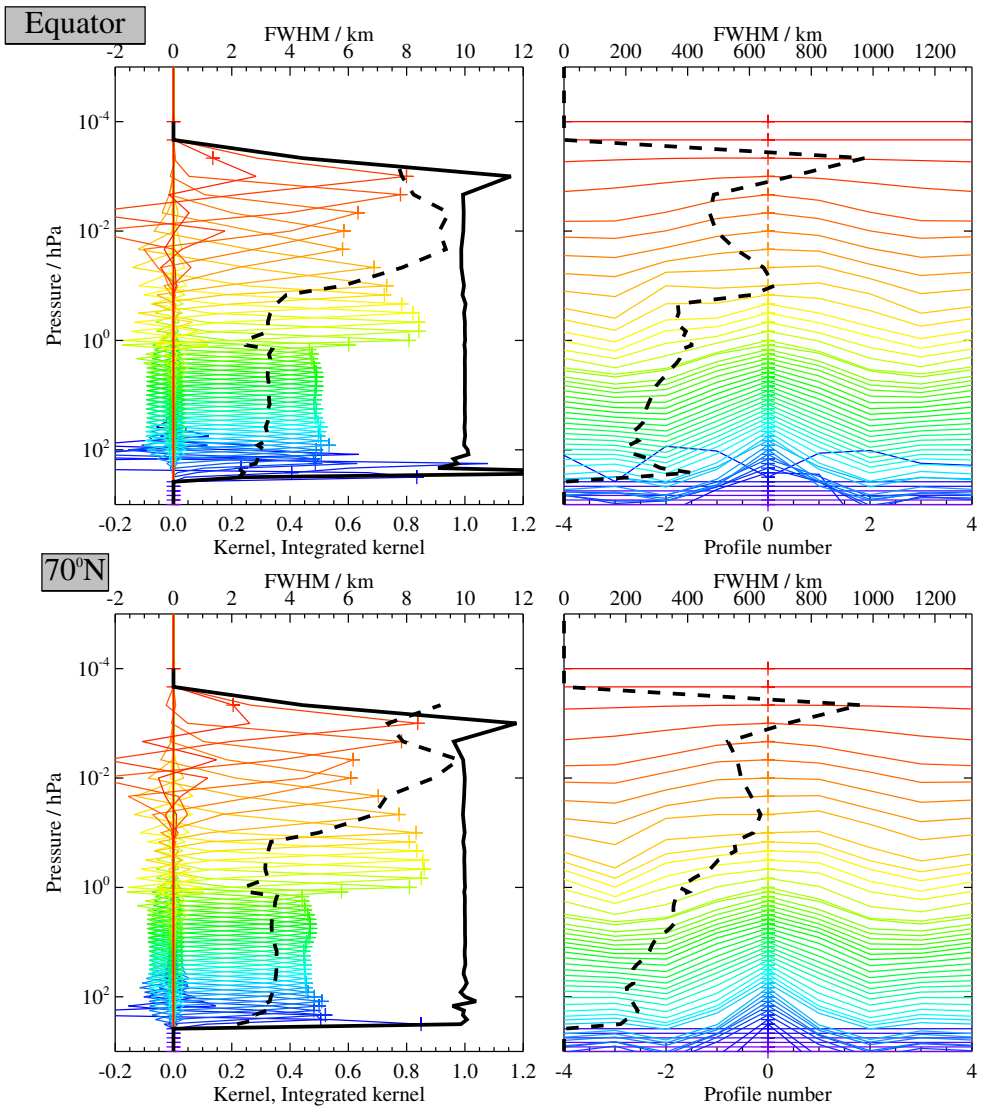

Figure 3.10.5: Typical two-dimensional (vertical and horizontal along-track) averaging kernels for the MLS v6.0*x* H_2O data at the equator (upper) and at 70°N (lower); variation in the averaging kernels is sufficiently small that these are representative of typical profiles. Colored lines show the averaging kernels as a function of MLS retrieval level, indicating the region of the atmosphere from which information is contributing to the measurements on the individual retrieval surfaces, which are denoted by plus signs in corresponding colors. The dashed black line indicates the resolution, determined from the full width at half maximum (FWHM) of the averaging kernels, approximately scaled into kilometers (top axes). (Left) Vertical averaging kernels (integrated in the horizontal dimension for five along-track profiles) and resolution. The solid black line shows the integrated area under each kernel (horizontally and vertically); values near unity imply that the majority of information for that MLS data point has come from the measurements, whereas lower values imply substantial contributions from a priori information. (Right) Horizontal averaging kernels (integrated in the vertical dimension) and resolution. The horizontal averaging kernels are shown scaled such that a unit averaging kernel amplitude is equivalent to a factor of 10 change in pressure.

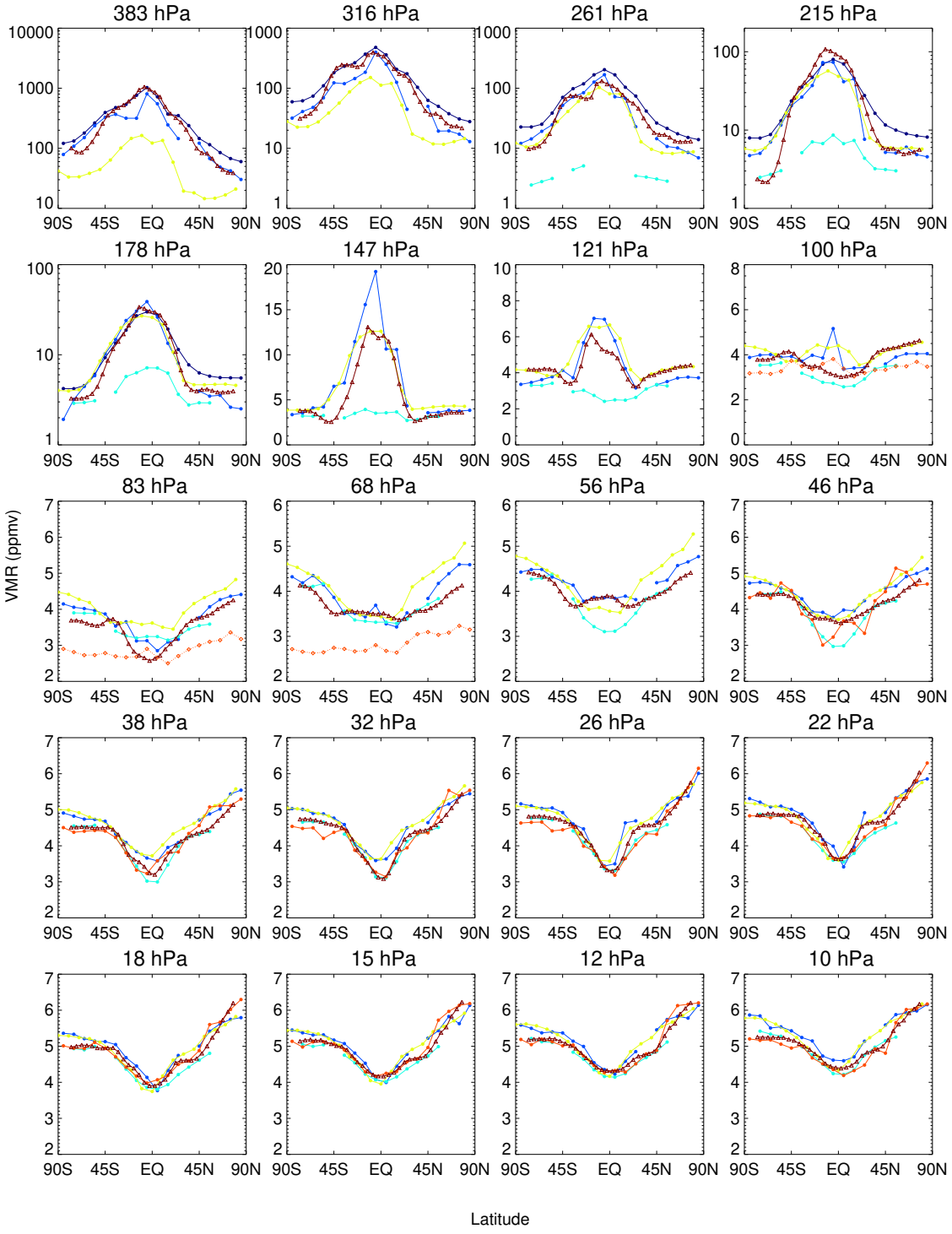

Figure 3.10.6: A comparison of zonal-mean MLS v6.0*x* (dark red) water vapor for January-February-March 2005 with other satellite observations. Each panel represents a pressure surface. The satellites are: AIRS v7 (dark blue), ACE-FTS v3.5 (light blue), MIPAS IMK v4 (yellow-green), HALOE v19 (cyan), Odin SMR 544-GHz continuum product (orange open diamonds), and Odin SMR line-resolved product (orange solid bullets).

3.10.7 Review of comparisons with other datasets

Figure 3.10.6 shows a zonal-mean comparison between several satellite H_2O data sets, including MLS v6.0*x*, AIRS v7, ACE-FTS v3.5, MIPAS IMK v4, HALOE v19, Odin SMR continuum H_2O, and Odin SMR line-resolved H_2O. Good agreement is found for the stratospheric levels at 32 hPa and at smaller pressures (higher altitudes). More significant departures are seen at 121–38 hPa, with some differences in latitudinal structure. Averaging kernels were not applied here because the nominal resolutions of these data sets are similar. However, each data set will exhibit its own vertical smoothing and a priori dependencies that contribute to the differences, particularly around the tropopause where the water vapor profile changes sharply. The patterns are more similar for the upper tropospheric levels (316–147 hPa).

Figures 3.10.7 and 3.10.8 show improvements in MLS comparisons to AIRS (v7) observations in both v6.0*x* and v5.0*x*. The very moist regions over the tropics in versions v4.2*x*–v6.0*x* are drier than they were in v2.2*x* and v3.3*x*/v3.4*x* for pressures greater than 250 hPa, in better agreement with AIRS.

Apart from the differences noted above, the MLS v6.0*x* H_2O is similar to the v5.0*x*, v4.2*x*, v3.3*x*/v3.4*x*, and v2.2*x* products; the latter are described and validated by *Read et al.* [2007] and *Lambert et al.* [2007]. In the time since those studies, the MLS and AIRS teams have both released newer versions of their data records showing reduced humidities. MLS v4.2*x* was further studied in the second SPARC Water Vapor Assessment (WAVAS-II) activity [*Read et al.*, 2022; *Khosrawi et al.*, 2018; *Kiefer et al.*, 2023; *Lossow et al.*, 2017, 2019].

3.10.8 Data screening

Pressure range: 316–0.001 hPa.

Values outside this range are not recommended for scientific use. Data at 0.00046 hPa represent a total column at and above that pressure level. Scientific use of these 0.00046 hPa data may be possible but requires consultation with the MLS team.

Estimated precision: Only use values for which the estimated precision is a positive number.

Values where the a priori information has a strong influence are flagged with negative or zero precision and should not be used in scientific analyses (see Section 1.5).

Status flag: Only use profiles for which the `Status` field is an even number.

Odd values of `Status` indicate that the profile should not be used in scientific studies. See Section 1.6 for more information on the interpretation of the `Status` field.

Clouds: Profiles flagged as being affected by high or low clouds (i.e., with `Status` bits corresponding to values of 16 and 32 set) can continue to be used. See Section 3.10.9 for more details.

Quality field: Only profiles with a value of the `Quality` *greater* than 0.7 should be used in scientific studies.

The quality threshold is deliberately set low because it is not a very good discriminator of poor profiles except when quality is well below the mean value; therefore, we recommend the "additional screening to avoid outliers," as described below.

Convergence field: Only profiles with a value of the `Convergence` *less* than 2.0 should be used in scientific studies.

Additional screening to avoid outliers: After applying the `Status`, `Quality`, and `Convergence` screening described above, some unphysical profiles remain in the MLS v6.0*x* H_2O dataset. These are characterized by unrealistically low water vapor mixing ratios in the upper troposphere and stratosphere. The cause of this behavior is the use of the logarithmic basis, which excludes negative values. Sometimes the retrieval minimizer seeks a negative value at a given level (which is almost always accompanied by severe vertical profile oscillations). Such values are not allowed, and therefore an optimal fit to the measurement signal is not achieved. H_2O profiles having values less than 0.101 ppmv at pressures of 1 hPa or greater should not be used. Profiles with acceptable `Status`, `Quality`, and `Convergence` having

values less than 0.101 ppmv at pressures less than 1 hPa are acceptable and occur frequently, because the water vapor concentration in the mesosphere is often less than the measurement precision, and although negative values are preferable, they are not realizable due to the logarithmic basis definition being used.

3.10.9 Artifacts

There is a minimum concentration at which MLS H_2O measurements at a given level become unreliable, given in Table 3.10.1 under the "Minimum Value" column. The lowest allowable H_2O value is 0.1 ppmv.

Clouds in the field of view degrade the data in unpredictable ways. The methods used to identify and reject radiances affected by clouds occasionally fail, leading to instances of `Quality` < 0.7. Cloud radiative scattering distorts the spectral lineshape, causing poor fits and low-quality values. However, not all MLS signals are obviously affected. Coincident comparisons of MLS cloud-flagged H_2O (`Status` bits corresponding to values of 16 or 32 set, considering only profiles with acceptable values of `Quality`) with AIRS data show a small mean bias of 10% but exhibit a 50% increase in variability for the individual differences. Users should therefore be aware that, although the overall biases for measurements inside clouds are similar to those for clear sky, individual profiles affected by clouds will exhibit greater variability about the true atmospheric humidity than those not marked as being cloud-influenced.

As discussed in Section 3.10.2 (and 1.10.2), the MLS 190-GHz radiometer is slowly drifting. While v6.0*x* (as with v5.0*x*) applies a correction for this drift, some signature of it remains, particularly in comparison to frostpoint hygrometer observations.

In the mesosphere, the random error (precision) is often larger than the retrieved value and therefore negative concentrations are possible and proper. However, the logarithmic definition of the H_2O basis precludes retrieval of negative values, with the minimum lowest allowed concentration being 0.1 ppmv. Therefore, arithmetic means of multiple MLS H_2O profiles that include values of 0.1 ppmv will be biased high. A better representation of averages at these altitudes is given by the median.

The top of the MLS limb scan range is nominally around 0.001 hPa. Therefore, although a retrieved value is now reported at 0.00046 hPa, it is not a vertically resolved measurement but rather a column amount from 0.001 hPa to the spacecraft altitude, under the constraint that concentrations at all levels above (i.e., pressures smaller than) 0.00046 hPa are fixed at a priori values. Accordingly, should there be a large H_2O event at altitudes above that level, it would be retrieved as an enhancement at 0.00046 hPa, but its true vertical location above 0.00046 hPa would be unknown.

3.10.10 Desired improvements should another data version be produced

While many defects in v4.2*x* and earlier versions have been addressed, there is scope for further investigation and improvements. The degree to which issues associated with the 190-GHz drift are ameliorated by the time-dependent sideband fraction merits further study. In particular, the validity of the negative water vapor trend observed by MLS in the upper troposphere, noted above, should be assessed. The retrievals of smaller water vapor values than those in other satellite data records (see Figure 3.10.6) at high latitudes (poleward of 50°) in the upper troposphere (pressures greater than 178 hPa) should also be investigated. Finally, it may be possible to extend the vertically resolved portion of the H_2O profile further down into the mid-troposphere (to altitudes below the current 316 hPa lower limit) at high latitudes.

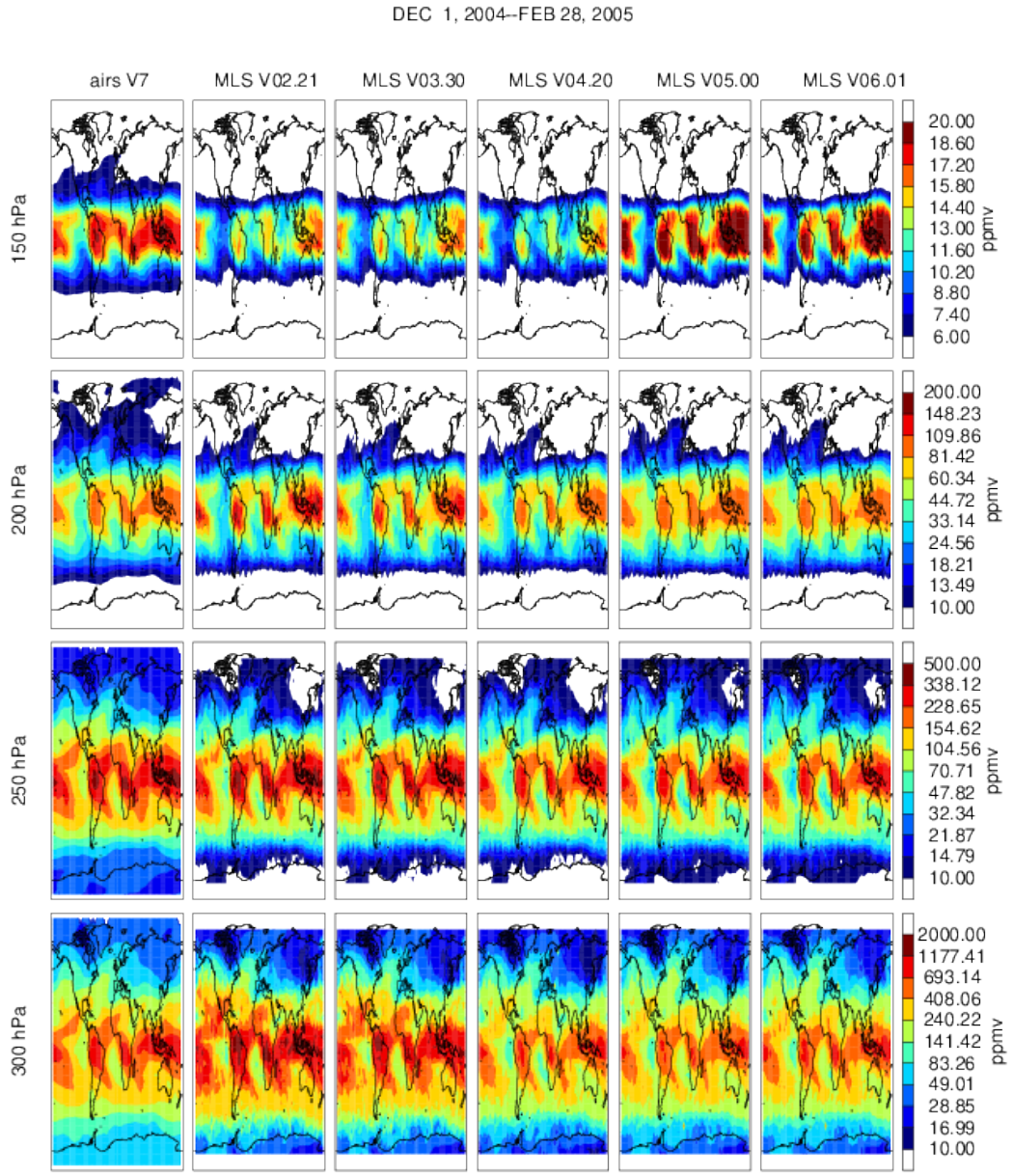

Figure 3.10.7: Mapped H_2O fields from AIRS v7 and MLS v2.2*x*, v3.3*x*/v3.4*x*, v4.2*x*, v5.0*x*, and v6.0*x* at pressures between 300 and 150 hPa for December-January-February 2004/2005. Note that the AIRS measurement is suitable only for cases where H_2O is greater than 10 ppmv.

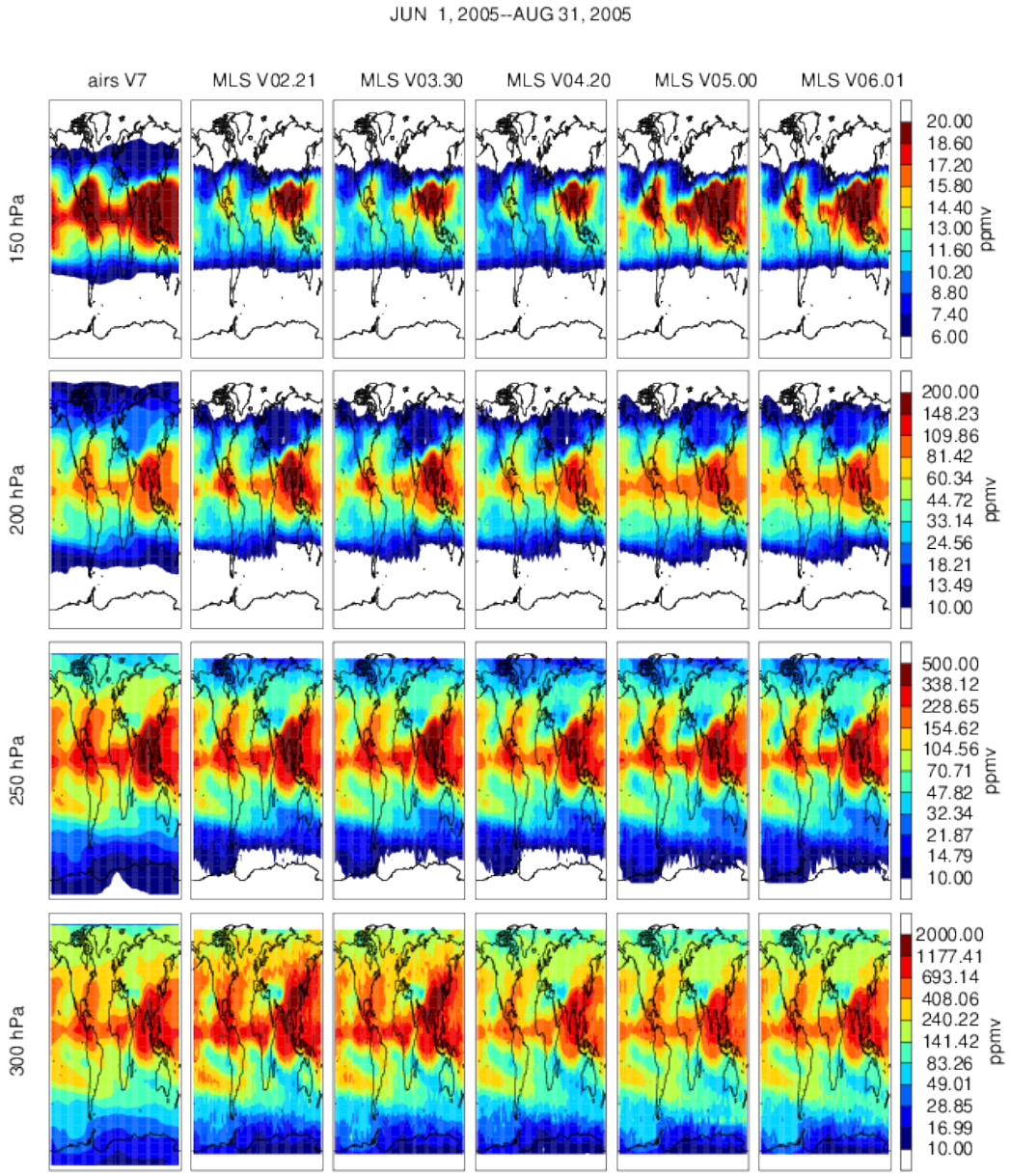

Figure 3.10.8: As Figure 3.10.8 but for June-July-August 2005.

Table 3.10.1: Summary of Aura MLS v6.0*x* H_2O Characteristics.

Pressure hPa	Resolution[a] V × H km	Single-Profile Precision %	Accuracy %	Minimum Value[b] ppmv	Comments
≤0.00022	—	—	—	—	Unsuitable for scientific use
0.0005	NVR[c] × 650	738	ND[d]	0.1	Column ($p \leq 0.001$ hPa)
0.001	7.1 × 650	305	63	0.1	
0.002	7.8 × 430	117	78	0.1	
0.005	9.4 × 340	55	39	0.1	
0.010	8.3 × 310	35	26	0.1	
0.022	7.3 × 300	32	27	0.1	
0.046	7.0 × 250	30	26	0.1	
0.10	4.8 × 210	29	17	0.1	
0.22	3.3 × 200	24	12	0.1	
0.46	3.2 × 200	15	9	0.1	
1.0	2.5 × 270	8	8	0.1	
2.2	3.6 × 260	7	9	0.1	
4.6	3.5 × 245	7	8	0.1	
10	3.6 × 240	7	8	0.1	
22	3.8 × 220	7	8	0.1	
46	3.8 × 210	7	9	0.1	
68	3.7 × 185	7	15	0.1	
83	3.6 × 185	7	18	0.1	
100	3.5 × 190	7	18	0.1	
121	3.5 × 200	6	29	0.1	
147	3.1 × 200	5	48	0.1	
178	3.3 × 205	3	49	3	
215	2.8 × 205	2	60	3	Low bias for latitudes > ±60°
261	2.8 × 190	3	80	4	Low bias for latitudes > ±60°
316	1.3 × 168	7	167	7	Low bias for latitudes > ±60°. Occasionally erroneous small (< 1 ppmv) and large fliers in the tropics, usually in clouds
> 316	—	—	—	—	Unsuitable for scientific use

[a] Vertical and along-track horizontal resolutions; cross-track horizontal resolution is ~9 km.
[b] Minimum H_2O is an estimate of the minimum H_2O concentration measurable by v6.0*x* MLS.
[c] Not vertically resolved (NVR)
[d] Not determined (ND)

3.11 Hydrogen Chloride (HCl)

Swath name: HCl

Useful range: 100–0.32 hPa

Product lead: Lucien Froidevaux

Contact: Michelle Santee <Michelle.L.Santee@jpl.nasa.gov>

3.11.1 Introduction

Multiple MLS bands measure the spectral signature of HCl around 624–626 GHz. Starting in February 2006, the MLS band designed to target HCl (specifically the HCl^{35} isotopologue), `R4:640.B13F:HCl`, known as "Band 13", began to exhibit symptoms of aging and was deactivated to conserve life. This aging is likely due to a radiation susceptibility issue for a batch of transistors that was identified shortly before launch. Useful observations of HCl are still made with the adjacent band (`R4:640.B14F:O3`, "Band 14"), which, as can be seen from Figures 2.1 and 2.2, also observes the HCl^{35} line (and a smaller line for the HCl^{37} isotopologue). The Band 14 radiances are used to produce the v6.0*x* standard HCl product (as was the case for most earlier MLS data versions).

In order to avoid undesirable discontinuities in the v6.0*x* HCl dataset, the Band 13 radiances are not considered in the retrieval of the standard HCl product, even on days for which it was active. For days prior to the 16 February 2006 deactivation of Band 13 and the few subsequent days when Band 13 has been (or may be) reactivated, the v6.0*x* algorithms also produce a second HCl product (in the `HCl-640-B13` swath in the `L2GP-DGG` file) for which the Band 13 radiances are used. Complete days with Band 13 on after 15 February 2006 are: 15 March 2006 (2006d074), 14 April 2006 (2006d104), 6–8 January 2009 (2009d006 through 2009d008), and 24–27 January 2010 (2010d024 through 2010d027). Based on the channel counts and channel noise characteristics during the three-day turn-on period in late January 2010, the remaining lifetime of Band 13 is estimated to be a few days to a few weeks at most. Band 13 has narrower channels than Band 14; thus the `HCl-640-B13` product has slightly better precision and vertical resolution in the upper stratosphere and mesosphere than the standard HCl product, enhancing its value for quantification of trends in that region. For this reason, the MLS team plans to reactivate Band 13 one last time before the end of the Aura mission.

As the arrangement of channels in Band 14 is not optimized to measure the HCl line, particularly at altitudes in the upper stratosphere where the line is narrow compared to the channel width, upper stratospheric trends from the (uninterrupted from 2004 to present) Band 14 retrievals are not reliable, showing HCl decreases that are too small compared to estimates from Band 13 data (Figure 3.11.1) as well as from ACE-FTS HCl data (not shown). Scientific usage of the MLS standard (Band 14) HCl dataset should therefore be restricted to the lower stratosphere, where variations in the two HCl products agree more closely. Band 14 retrievals are appropriate for use in studies of seasonal and latitudinal changes in HCl (e.g., during polar winter/spring), as well as for longer-term trend studies in the lower stratosphere (e.g., *Mahieu et al.* [2014]), despite some differences compared to model-derived trends as discussed by *Froidevaux et al.* [2019].

Limb radiances measured by the MLS 640-GHz radiometer are affected by water vapor (and other species) in addition to HCl. As noted in Section 1.10.2, as of May 2024, the MLS 190-GHz radiometer, which is used to measure water vapor, is operated only intermittently. When that radiometer is turned off and H_2O measurements are not available, a priori information for H_2O (based on climatological values) is used in the HCl retrievals, adversely affecting their quality; further details are given in Section 3.11.7. Detailed validation of the MLS v2.2*x* HCl product and comparisons with other data sets were presented by *Froidevaux et al.* [2008b]; based on the overall small changes in HCl data since v2.2*x*, the conclusions of that study should remain essentially unchanged for v6.0*x*. Table 3.11.1 summarizes the estimated resolution, precision, and accuracy of the v6.0*x* MLS HCl measurements as a function of pressure.

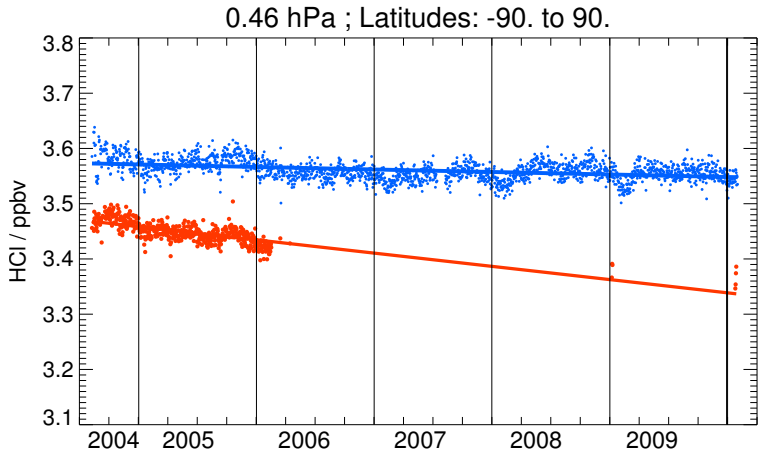

Figure 3.11.1: Daily zonal averages for MLS HCl at 0.46 hPa from mid-August 2004 through January 2010, for the originally targeted Band 13 measurements (red points; available only occasionally since February 2006 to conserve lifetime) and the Band 14 data (blue points). The lines are simple linear fits through the daily data points; differences are apparent in this region of the atmosphere, where the information obtained from Band 14 HCl data is not reliable enough for trend quantification.

3.11.2 Changes from v5.0*x*

There are no significant changes in the v6.0*x* HCl retrieved values compared to those in v5.0*x*. Figure 3.11.2 shows zonal mean pressure-latitude cross sections of v6.0*x* and v5.0*x* and their differences for a typical month (April 2009) for the standard HCl product. For pressures larger than or equal to 0.22 hPa, the average differences between the two data versions are typically less than about 0.05 ppbv (or 1–2%). These average changes are easily within the estimated accuracy values (see Table 3.11.1). There is still an unrealistic high bias in HCl at 147 hPa in the tropics, so values at this pressure are not recommended within the 40°S to 40°N latitude range. The precision (single-profile random uncertainty) estimates provided in the Level 2 files are essentially unchanged from those in v5.0*x*.

3.11.3 Resolution

Typical (rounded off) values for resolution are provided in Table 3.11.1. Based on the width of the averaging kernels shown in Figure 3.11.3, the vertical resolution for the standard HCl stratospheric product is ~3 km (2.7 km at best in the lower stratosphere), or about double the 640-GHz radiometer vertical field-of-view width at half maximum; the vertical resolution degrades to 4–6 km in the lower mesosphere. The along-track resolution is ~200 to 350 km for pressures of 2 hPa or more and ~500 km in the lower mesosphere. The cross-track resolution is set by the 3-km width of the MLS 640-GHz field of view. The longitudinal separation of MLS measurements, set by the Aura orbit, is 10°–20° over middle and lower latitudes, with much finer sampling in polar regions.

3.11.4 Precision

The estimated single-profile precision of MLS HCl reported by the Level 2 software varies from ~0.2 to 0.6 ppbv in the stratosphere (see Table 3.11.1), with poorer precision obtained in the lower mesosphere. The v6.0*x* precision has not changed significantly from that in v5.0*x*. The Level 2 precision values are often only slightly smaller than the observed scatter in the data, as evaluated from a narrow latitude band centered around the equator where atmospheric variability is often weaker than elsewhere, or as obtained from a comparison between ascending and descending coincident MLS profiles. The scatter in MLS data and in simulated MLS retrievals (using noise-free radiances) becomes smaller than the theoretical precision (given in the Level 2 files) in the upper stratosphere and mesosphere, where a priori and smoothing constraints have a larger impact. The HCl precision values increase rapidly (i.e., precision worsens) at pressures less than 0.2 hPa and are generally flagged negative (or zero) at pressures less than 0.1 hPa, indicating increasing influence from the a priori and thus poorer measurement sensitivity and reliability.

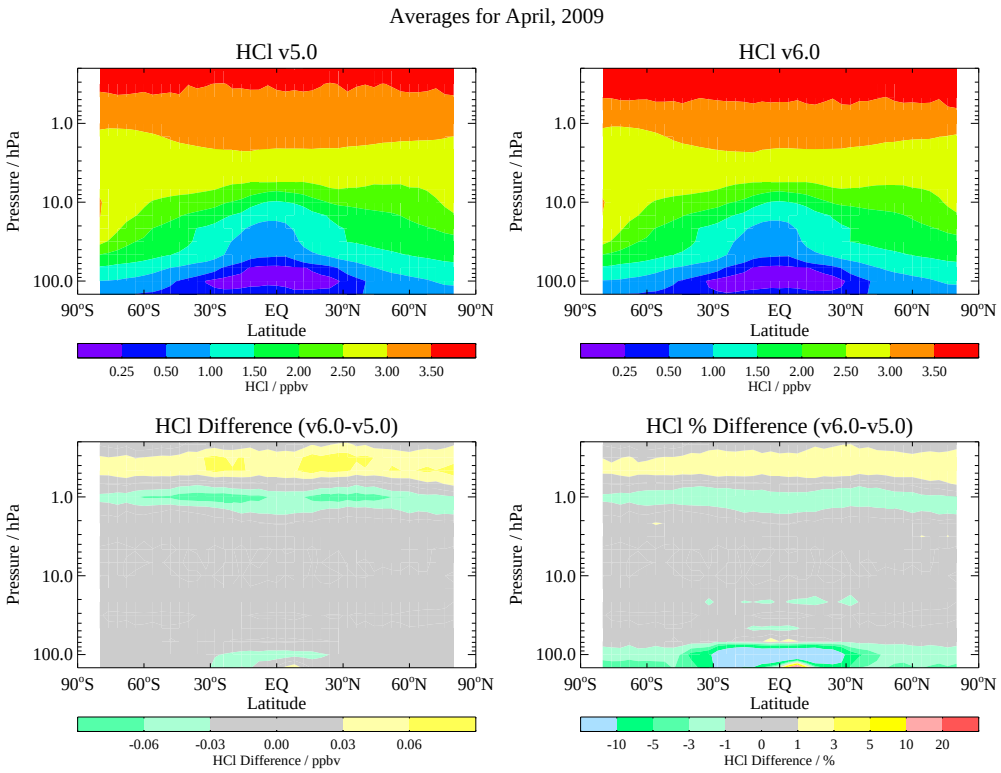

Figure 3.11.2: Zonal mean pressure-latitude cross sections of MLS HCl for April 2009 for v5.0*x* (top left), v6.0*x* (top right), and their differences (v6.0*x* minus v5.0*x*) in ppbv (bottom left) and percent (bottom right).

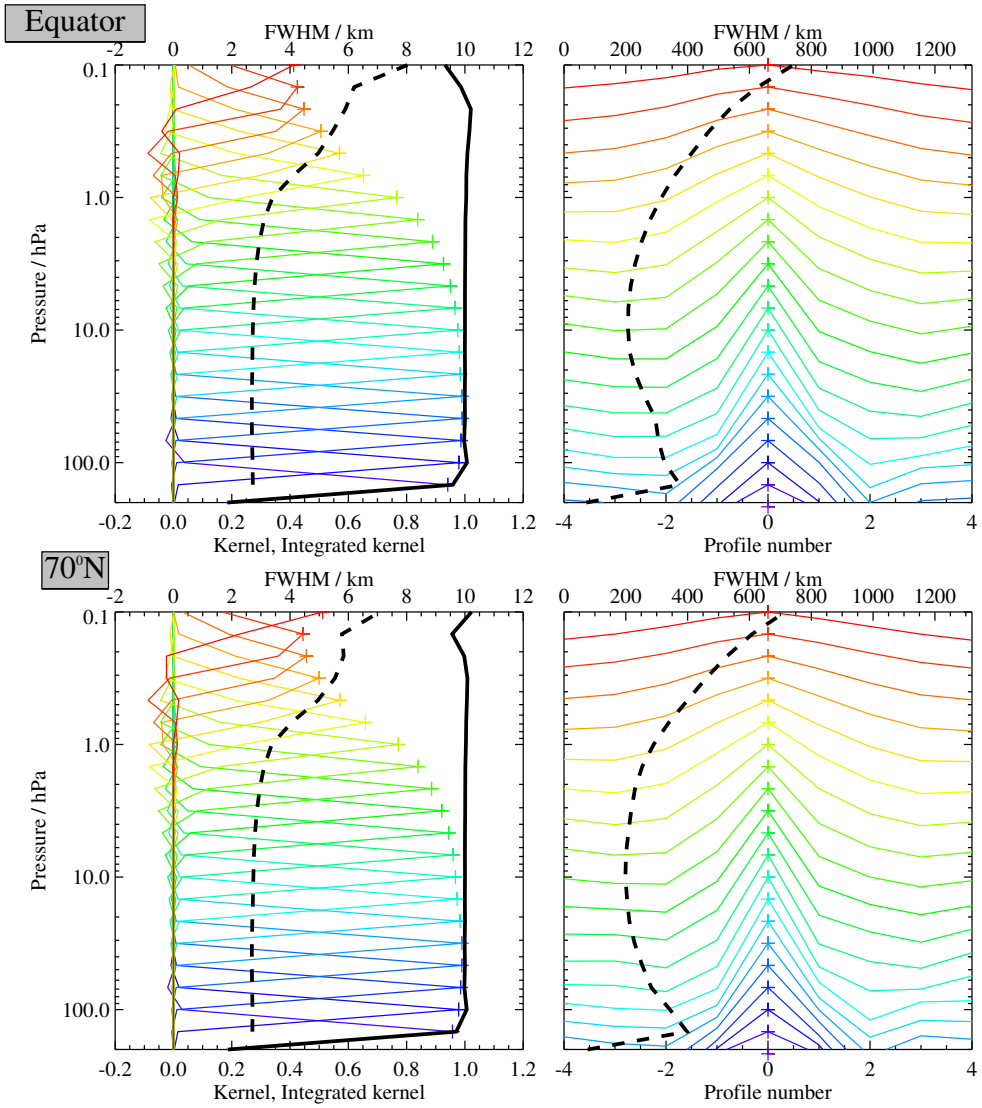

Figure 3.11.3: Typical two-dimensional (vertical and horizontal along-track) averaging kernels for the MLS v6.0*x* HCl data at the equator (upper) and at 70°N (lower); variation in the averaging kernels is sufficiently small that these are representative of typical profiles. Colored lines show the averaging kernels as a function of MLS retrieval level, indicating the region of the atmosphere from which information is contributing to the measurements on the individual retrieval surfaces, which are denoted by plus signs in corresponding colors. The dashed black line indicates the resolution, determined from the full width at half maximum (FWHM) of the averaging kernels, approximately scaled into kilometers (top axes). (Left) Vertical averaging kernels (integrated in the horizontal dimension for five along-track profiles) and resolution. The solid black line shows the integrated area under each kernel (horizontally and vertically); values near unity imply that the majority of information for that MLS data point has come from the measurements, whereas lower values imply substantial contributions from a priori information. (Right) Horizontal averaging kernels (integrated in the vertical dimension) and resolution. The horizontal averaging kernels are shown scaled such that a unit averaging kernel amplitude is equivalent to a factor of 10 change in pressure.

3.11.5 Accuracy

The effects of various sources of systematic uncertainty (e.g., instrumental issues, spectroscopic uncertainty, and approximations in the retrieval formulation and implementation) on the MLS v6.0*x* HCl measurements were quantified through a comprehensive set of retrievals of synthetic radiances; see *Froidevaux et al.* [2008b] for details of a similar analysis conducted on MLS v2.2*x* HCl data. Several error sources (particularly those related to radiometric calibration components) contribute significantly to the total error, which is given for various pressure levels in Table 3.11.1 (values are intended to represent 2σ estimates of the probable magnitude). Given the trend issues affecting the standard (Band 14) HCl product in the upper stratosphere and lower mesosphere, we estimate an accuracy for v6.0*x* (as for v5.0*x*) of no better than about 0.3 ppbv (or 10%) in that region. For the lower stratosphere, based on the better agreement between the Band 13 and Band 14 retrievals as well as some trend studies (for the standard product), we use the accuracy estimates derived from the formal systematic error analysis.

3.11.6 Review of comparisons with other datasets

Froidevaux et al. [2008b] compared v2.2*x* MLS HCl measurements to those from other satellite, balloon, and aircraft sensors and found generally good agreement. HCl values from both MLS and ACE-FTS are generally larger (by about 10–15%) than those from HALOE, especially at upper stratospheric altitudes. MLS HCl at 147 hPa was shown to be biased high at low to middle latitudes compared to WB-57 aircraft in situ (CIMS) measurements; while this is still true in v6.0*x*, MLS HCl data at this pressure level are potentially useful for scientific studies at high latitudes.

3.11.7 Data screening

Pressure range: 100–0.32 hPa

Values outside this range are not recommended for scientific use. MLS HCl values at 147 hPa are biased high, at least at low to middle latitudes (equatorward of about 40°), and thus they are not recommended. In addition, although the top of the recommended vertical range is 0.32 hPa, users are reminded about the issues relating to HCl trend estimates in the upper stratosphere and lower mesosphere discussed earlier; average profiles in that region should only be used for studies that do not involve trends (or whose accuracy requirements are less stringent than about 0.3 ppbv or 10%).

Estimated precision: Only use values for which the estimated precision is a positive number.

Values where the a priori information has a strong influence are flagged with negative or zero precision and should not be used in scientific analyses (see Section 1.5).

Status flag: Only use profiles for which the `Status` field is an even number.

Odd values of `Status` indicate that the profile should not be used in scientific studies. See Section 1.6 for more information on the interpretation of the `Status` field.

Quality field: Only profiles with a value of the `Quality` field *greater* than 1.2 should be used.

This criterion removes the profiles with the poorest radiance fits, typically less than 0.1% of the daily profiles. For HCl (as for other 640 GHz MLS products), this screening correlates well with the poorly converged sets of profiles (see below); we recommend the use of both the `Quality` and the `Convergence` fields for data screening.

Convergence field: Only profiles with a value of the `Convergence` field *less* than 1.05 should be used.

For the vast majority of profiles (99% or more for most days), this field has values below 1.05. However, on occasion sets of profiles (typically one or more groups of ten profiles, retrieved as a "chunk") have the `Convergence` field set to larger values; such profiles should be discarded.

Clouds: Thick clouds can induce significant artifacts (mainly in the tropics, statistically), with total systematic errors potentially as large as 0.5 ppbv at 100 hPa and even larger at 147 hPa. The large positive HCl bias at 147 hPa at low and middle latitudes likely arises in part from unknown or improperly modeled

systematic error sources and not just from clouds. At other pressures, the potential impact on HCl from clouds is small or negligible.

Additional screening on H_2O `Status`: As noted earlier, HCl retrieval quality is degraded at some levels when the 190-GHz radiometer is turned off and H_2O measurements are not available. In these circumstances, biases in the retrieved HCl values can reach more than 3% at 68 hPa, with some biases as large as 50 to 100% or more at 100 to 147 hPa, although the latter level is not recommended at extra-polar latitudes. These artifacts are not removed by the standard HCl data filtering protocols. Thus, while the HCl data on affected days are still useful for purely morphological or qualitative purposes, they cannot be quantitatively compared to measurements taken on surrounding days or in previous years when the 190-GHz radiometer was operational. The biases also have potential implications for the calculation of long-term trends. Therefore, for quantitative studies using HCl data at those retrieval levels, an additional screening step is recommended, whereby the `Status` field in the colocated H_2O profile is examined to remove affected HCl retrievals. That is, only HCl profiles for which the `Status` flags of the corresponding H_2O profiles are an even number should be used in quantitative studies relying on HCl measurements in the 68–147 hPa range (at lower pressures / higher altitudes, all HCl data points passing the standard quality screening measures may be used). We also note, however, that measurements taken during time periods since May 2024 when the 190-GHz radiometer is turned off can be intercompared.

3.11.8 Artifacts

- We do not recommend the use of the MLS HCl standard product in the upper stratosphere and lower mesosphere, especially for trend studies, for reasons discussed above.
- The HCl values at 147 hPa are biased high and generally not recommended at low to middle latitudes (equatorward of about 40°) but may be usable at high latitudes. Please consult with the MLS team for further information.
- Users should screen out the non-converged and poorest-quality HCl profiles, as such profiles (typically less than 0.2% of the data) tend to behave unlike the majority of the other MLS retrievals. See the criteria listed above.
- As discussed in Section 3.11.7, biases in HCl values are present at some levels when coincident measurements from the 190-GHz radiometer are not available and H_2O a priori information is used in the HCl retrieval. Depending on the specific goals of any study based on these measurements, additional HCl data quality filtering may be necessary for days when the 190-GHz radiometer is off.

Table 3.11.1: Summary of Aura MLS v6.0*x* HCl Characteristics

Pressure hPa	Resolution[a] V × H km	Single-Profile Precision[b] ppbv	Accuracy[c] ppbv	Comments
0.22–0.001	—	—	—	Unsuitable for scientific use
0.32	5.5 × 450	0.7	0.3	Unsuitable for trend studies
0.5	5 × 400	0.6	0.3	Unsuitable for trend studies
1	3.5 × 300	0.5	0.3	Unsuitable for trend studies
2	3 × 250	0.4	0.3	Unsuitable for trend studies
5	3 × 200	0.3	0.3	Unsuitable for trend studies
10	3 × 200	0.2	0.2	
22	3 × 250	0.2	0.2	
46	3 × 300	0.2	0.2	
68	3 × 300	0.2	0.2	
100	3 × 350	0.3	0.2	
147	3 × 400	0.4	0.4	High bias at low lats (use with caution elsewhere)
1000–215	—	—	—	Unsuitable for scientific use

[a] Vertical and along-track horizontal resolutions; cross-track horizontal resolution is ~3 km.
[b] Precision (1σ) for individual profiles.
[c] 2σ estimate from systematic uncertainty characterization tests (but see text for estimates at pressures lower than 10 hPa).

3.12 Hydrogen Cyanide (HCN)

Swath name: HCN

Useful range: 68–32 hPa (qualitative studies), 21–0.1 hPa (no restrictions)

Product lead: Hugh C. Pumphrey

Contact: Luis Millán <Luis.F.Millan@jpl.nasa.gov>

3.12.1 Introduction

MLS observes HCN emission lines within the 190-GHz radiometer. The spectral signature of HCN in the MLS radiances is weak, a relatively strong smoothing constraint is required to obtain meaningful retrievals, and averaging (e.g., weekly zonal means) is recommended.

Table 3.12.1 summarizes the precision, accuracy, and resolution of the MLS HCN product. The MLS v6.0*x* HCN data are scientifically useful over the range 21 to 0.1 hPa. At 68–32 hPa, the data may still be usable with caution for qualitative studies. More details on the HCN measurement may be found in *Pumphrey et al.* [2006].

3.12.2 Differences between earlier versions and v6.0*x*

No changes specific to the HCN retrieval were made between v2.2*x* and v3.3*x*/v3.4*x*. For v4.2*x*, a new phase was introduced in which HCN is retrieved using only Bands 6 and 27, rather than all of R2; this phase is also used in v6.0*x*. The v4.2*x* HCN had obvious biases in the lower stratosphere, but they were far less severe than in v2.2*x* and v3.3*x*/v3.4*x*, both of which had large regions with negative mixing ratios. In v5.0*x* and v6.0*x*, the biases appear to be further reduced; the changes between v5.0*x* and v6.0*x* are small. Between 10 and 3 hPa, v5.0*x* and v6.0*x* HCN values are somewhat lower than those in all prior versions.

Figure 3.12.2 shows that the precisions in v6.0*x* are essentially unchanged from earlier versions. The retrieved mixing ratios change very little in the region where use was recommended for earlier versions. Mixing ratios are considerably different between all five earlier versions in the lower stratosphere. However, the profile shape in v6.0*x* appears less unrealistic than in any prior version.

3.12.3 Vertical resolution

The HCN signal is fairly small, so a rather strong smoothing constraint has to be applied to ensure that the retrieval is at all useful. As Figure 3.12.1 shows, the vertical resolution is about 8–9 km between 68–1 hPa, degrading to more than 12 km at 0.1 hPa. The horizontal resolution along the measurement track is between 2 and 4 profile spacings.

3.12.4 Precision

Figure 3.12.2 shows the estimated precision (values of the field `L2gpPrecision`), together with the observed standard deviation in an equatorial latitude band where the natural variability of the atmosphere is small. The observed scatter is smaller than the estimated precision due to the effects of retrieval smoothing.

3.12.5 Accuracy

There is no formal validation of the MLS HCN product because HCN had extremely large systematic errors in the lower stratosphere when initial validation efforts were undertaken (for v2.2*x* and v3.3*x*/v3.4*x*). In v5.0*x* and v6.0*x*, the errors are reduced over those in v4.2*x* in some places but are somewhat worse in others, while being far better than in earlier versions. Some comparisons with ACE-FTS data are shown in Figure 3.12.3. At 21 hPa and smaller pressure levels the two instruments agree well, with MLS v5.0*x* and v6.0*x* agreeing better with ACE-FTS than v4.2*x* (Figure 3.12.3a, c). These values are consistent with the current understanding of HCN chemistry. Comparisons with historical measurements suggest an accuracy no worse than 50%.

In the 68–32 hPa range at the tropics, the two instruments agree well, except for a small, nearly constant systematic bias (e.g., Figure 3.12.3b). In this pressure range at middle and high latitudes, however, the MLS

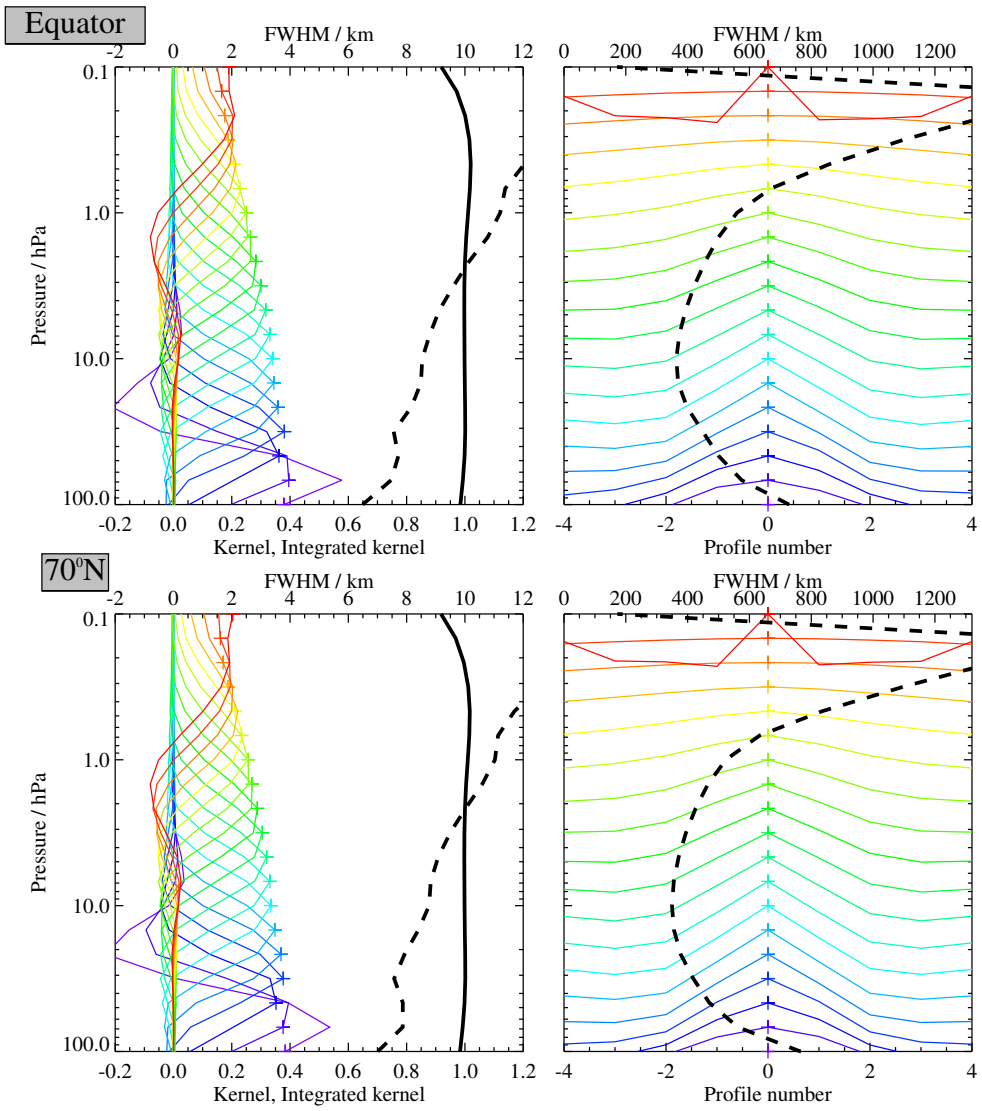

Figure 3.12.1: Typical two-dimensional (vertical and horizontal along-track) averaging kernels for the MLS v6.0*x* HCN data at the equator (upper) and at 70°N (lower); variation in the averaging kernels is sufficiently small that these are representative of typical profiles. Colored lines show the averaging kernels as a function of MLS retrieval level, indicating the region of the atmosphere from which information is contributing to the measurements on the individual retrieval surfaces, which are denoted by plus signs in corresponding colors. The dashed black line indicates the resolution, determined from the full width at half maximum (FWHM) of the averaging kernels, approximately scaled into kilometers (top axes). (Left) Vertical averaging kernels (integrated in the horizontal dimension for five along-track profiles) and resolution. The solid black line shows the integrated area under each kernel (horizontally and vertically); values near unity imply that the majority of information for that MLS data point has come from the measurements, whereas lower values imply substantial contributions from a priori information. (Right) Horizontal averaging kernels (integrated in the vertical dimension) and resolution. The horizontal averaging kernels are shown scaled such that a unit averaging kernel amplitude is equivalent to a factor of 10 change in pressure.

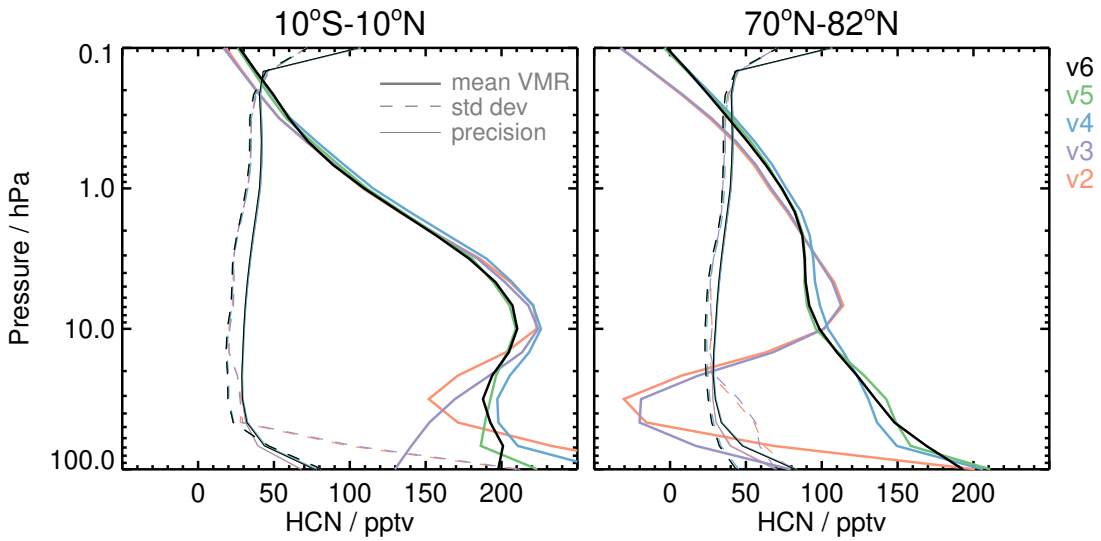

Figure 3.12.2: Estimated precision (`L2gpPrecision`, thin lines) and observed standard deviation (dashed lines) for MLS v6.0*x* (black), v5.0*x* (green), v4.2*x* (blue), v3.3*x*/v3.4*x* (purple) and v2.2*x* (red) HCN. The data shown are for 10° S to 10° N (left) and 70° N–82° N (right) for 28 January 2005. Mean volume mixing ratio (VMR) profiles are shown for comparison. Between 3 and 10 hPa, v6.0*x* and v5.0*x* depart from the three earlier versions. Below 10 hPa, profiles from all five versions are different, but those in v2.2*x* and v3.3*x*/v3.4*x* are less realistic than in v4.2*x*, v5.0*x*, and v6.0*x*.

data differ considerably from ACE-FTS (e.g., Figure 3.12.3d), displaying larger biases that are not constant in time. That said, the seasonal and interannual variability shows many similarities between the two instruments. Thus, the MLS data in the lower stratosphere can be used with caution for qualitative studies, although comparison with ACE-FTS data is advisable.

3.12.6 Data screening

Pressure range: 68–0.1 hPa

Data in the 68 to 32 hPa range may be used, with caution, for qualitative studies. Data in the 21 to 0.1 hPa range can be used for scientific studies.

Estimated precision: Only use values for which the estimated precision is a positive number.

Values where the a priori information has a strong influence are flagged with negative or zero precision and should not be used in scientific analyses (see Section 1.5).

Status flag: Only use profiles for which the `Status` field is an even number.

Odd values of `Status` indicate that the profile should not be used in scientific studies. See Section 1.6 for more information on the interpretation of the `Status` field.

Clouds: Clouds have no impact; profiles with non-zero even values of `Status` are suitable for use.

As HCN is only generally recommended in regions unaffected by clouds, profiles which have either, both, or neither of the cloud flags set may be used.

Quality: Only profiles whose `Quality` field is greater than 0.2 should be used.

Values of `Quality` are usually near 1.5; occasional lower values do not seem correlated with unusual profiles, but we suggest as a precaution that only profiles with `Quality` > 0.2 be used. Typically this will eliminate only 1–2% of profiles.

Convergence: Only profiles whose `Convergence` field is less than 2.0 should be used.

This should eliminate any chunks that failed to converge (typically only 1–2% of the total).

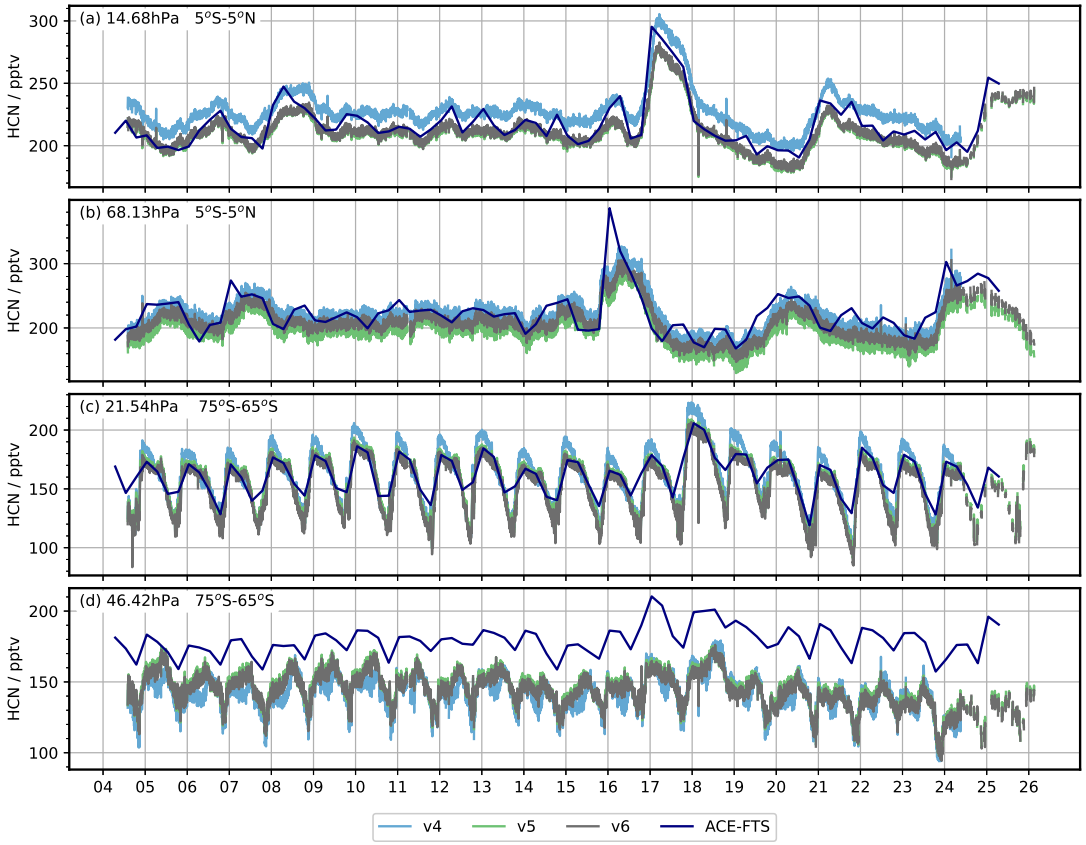

Figure 3.12.3: Daily time series of HCN at selected latitudes and pressure levels from MLS versions v4.2*x*, v5.0*x*, and v6.0*x*, with seasonal ACE-FTS version 5.3 for comparison.

Table 3.12.1: Summary of Aura MLS v6.0*x* HCN Characteristics

Pressure hPa	Resolution[a] V × H km	Single-Profile Precision[b] pptv	Accuracy pptv	Comments
< 0.1	—	—	—	Unsuitable for scientific use
1–0.1	12 × 600	50	5	
21–1	9 × 400	40	15	
68–21	8 × 500	40	60	Use with caution for qualitative studies
100	8 × 600	50	130	Unsuitable for scientific use
> 100				Not Retrieved

[a]Vertical and along-track horizontal resolutions; cross-track horizontal resolution is ~9 km.
[b]The precision shown is the estimated precision (`L2gpPrecision`); the observed scatter is about 80% of this value.

3.12.7 Artifacts

There are no obvious artifacts within the 21–0.1 hPa recommended pressure range. At 68–32 hPa, the data may be usable with caution for qualitative studies, and comparison with ACE-FTS measurements is recommended.

3.13 Nitric Acid (HNO_3)

Swath name: HNO3

Useful range: 215–1.5 hPa (1.0 hPa under enhanced conditions)

Product lead: Michelle Santee <Michelle.L.Santee@jpl.nasa.gov>

3.13.1 Introduction

The standard HNO_3 product is a hybrid constructed by merging retrievals based on radiances from different radiometers: at pressures equal to or greater than 22 hPa, the standard product is derived from the 240-GHz retrievals, whereas above that level (i.e., at lesser pressures), it is derived from the 190-GHz retrievals. Consequently, the intermittent operation of the 190-GHz radiometer since May 2024 (see Section 1.10.2) has affected the availability of HNO_3 data in the middle and upper stratosphere. The quality and reliability of the Aura MLS v2.2*x* HNO_3 measurements were assessed in detail by *Santee et al.* [2007]. V3.3*x*/v3.4*x* HNO_3 was greatly improved over that in v2.2*x*; in particular, a low bias through much of the stratosphere (especially evident at pressures greater than or equal to 100 hPa) was largely eliminated. However, the v3.3*x*/v3.4*x* 240-GHz HNO_3 was adversely impacted by clouds [*Livesey et al.*, 2013], leading to a noisy HNO_3 product in the upper troposphere / lower stratosphere (UTLS). The adverse cloud impacts were substantially mitigated in v4.2*x* [*Livesey et al.*, 2020]. For the most part, HNO_3 mixing ratios did not change dramatically in v5.0*x*, nor have they changed substantially in v6.0*x*. A summary of the estimated precision, resolution (vertical and horizontal), and systematic uncertainty of the v6.0*x* HNO_3 measurements as a function of altitude is given in Table 3.13.1.

3.13.2 Differences between v5.0*x* and v6.0*x*

Throughout most of the lower stratosphere, the HNO_3 retrieval has changed very little between v5.0*x* and v6.0*x*. Figure 3.13.1 shows zonal mean pressure-latitude cross sections of v6.0*x* and v5.0*x* and their differences on selected days for the standard HNO_3 product, which as noted above is composed from the `HNO3-240` and the `HNO3-190` retrievals in the lower and upper parts of the profile, respectively. Figure 3.13.2 displays the variations in those differences over the annual cycle for a representative year. Differences are generally less than ±10%; low HNO_3 abundances lead to larger percent differences between the two versions at and below (i.e., pressures larger than) 100 hPa in the tropics and in the upper stratosphere at all latitudes. Figure 3.13.3 shows northern polar cap, tropical, and southern polar cap mean profiles for the two data versions for both the 240-GHz and the 190-GHz retrievals throughout the entire vertical domain, with the "join" level for the hybrid product (22 hPa) marked by the horizontal line. For both HNO_3 data products, the shapes of the zonal-mean profiles are very similar in the two data versions throughout the vertical range (compare dark and light blue curves in the upper left-hand panels and red and orange curves in the upper right-hand panels of each set).

Mean profiles computed from measurements taken during the ascending (mainly daytime, solid lines) and descending (mainly nighttime, dashed lines) portions of the orbit are distinguished in Figure 3.13.3; as expected since HNO_3 is not strongly diurnally varying at these altitudes, no substantial differences are seen between day and night values in the upper troposphere / lower stratosphere for the 240-GHz retrievals or the middle and upper stratosphere for the 190-GHz retrievals in either version. Figure 3.13.3 also compares the behavior of the two HNO_3 products in both versions (lower panels of each set); again, since neither the 240-GHz nor the 190-GHz retrievals changed very much in v6.0*x*, the agreement between `HNO3-240` and `HNO3-190` is largely unchanged in v6.0*x*.

3.13.3 Resolution

The resolution of the retrieved data can be described using "averaging kernels" [e.g., *Rodgers*, 2000]; the two-dimensional nature of the MLS data processing system means that the kernels describe both vertical and

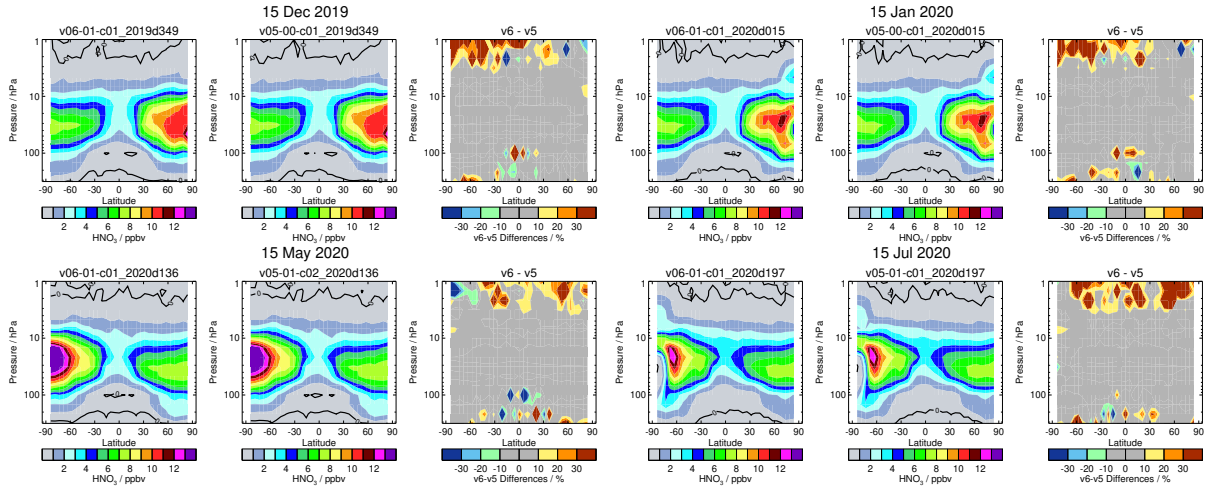

Figure 3.13.1: Zonal mean pressure-latitude cross sections of MLS HNO_3 for four selected days during Arctic (top row) and Antarctic (bottom row) winter under high-HNO_3 (left side) and denitrified (right side) conditions. Each set of plots contains (left) v6.0*x*, (middle) v5.0*x*, and (right) their differences (v6.0*x* minus v5.0*x*, in percent). The black curves overlaid on the abundance panels (left and middle of each set) mark the zero contour. No quality screening of the data has been performed.

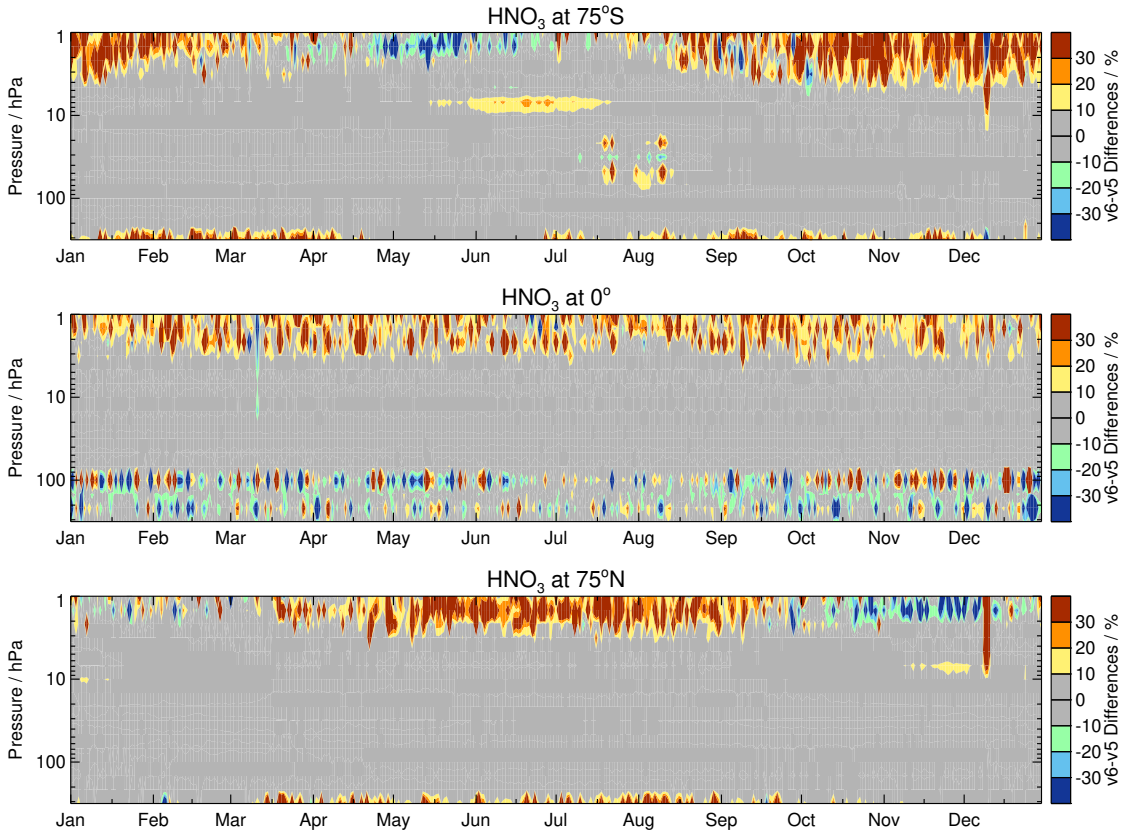

Figure 3.13.2: Time series for a representative year (2020) of v6.0*x* minus v5.0*x* MLS HNO_3 (percent differences), for (top) 75°S, (middle) the equator, and (bottom) 75°N. No quality screening of the data has been performed.

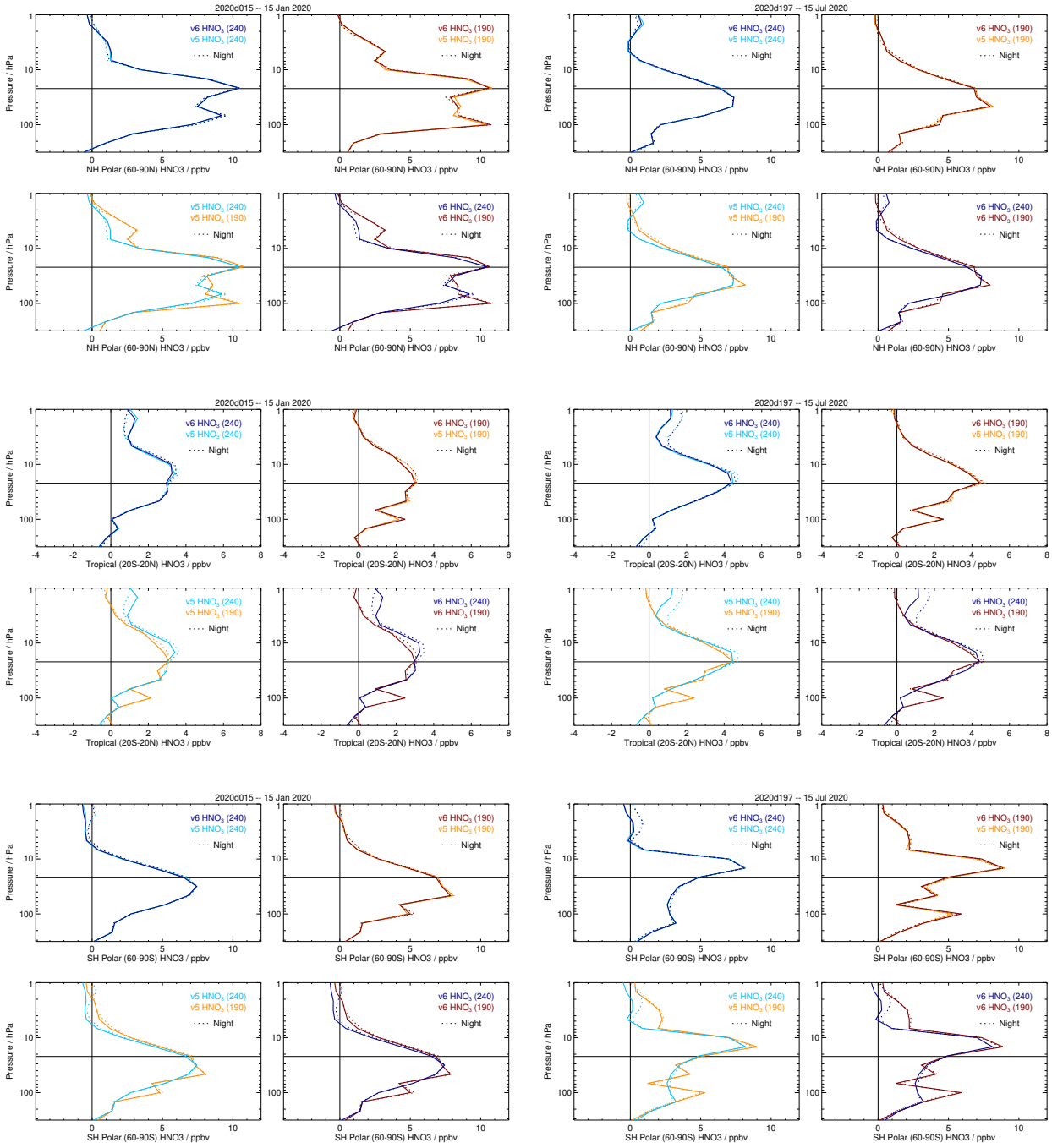

Figure 3.13.3: MLS v6.0*x* (dark colors) and v5.0*x* (light colors) profiles of `HNO3-240` (blues) and `HNO3-190` (reds) averaged over the Northern Hemisphere polar (top set), tropical (middle set), and Southern Hemisphere polar (bottom set) regions for a representative day during winter in the Northern (left side) and Southern (right side) Hemispheres. Each set of plots contains four panels, comparing v6.0*x* and v5.0*x* `HNO3-240` retrievals, v6.0*x* and v5.0*x* `HNO3-190` retrievals, v5.0*x* `HNO3-240` and `HNO3-190` retrievals, and v6.0*x* `HNO3-240` and `HNO3-190` retrievals. Solid lines show ascending (mainly daytime) and dashed lines show descending (mainly nighttime) averages. No quality screening of the data has been performed. For completeness, full profiles are shown in all panels, but the standard HNO_3 product is derived from the `HNO3-240` retrievals at and at pressures greater than 22 hPa (marked by the horizontal black line) and from the `HNO3-190` retrievals at lower pressures.

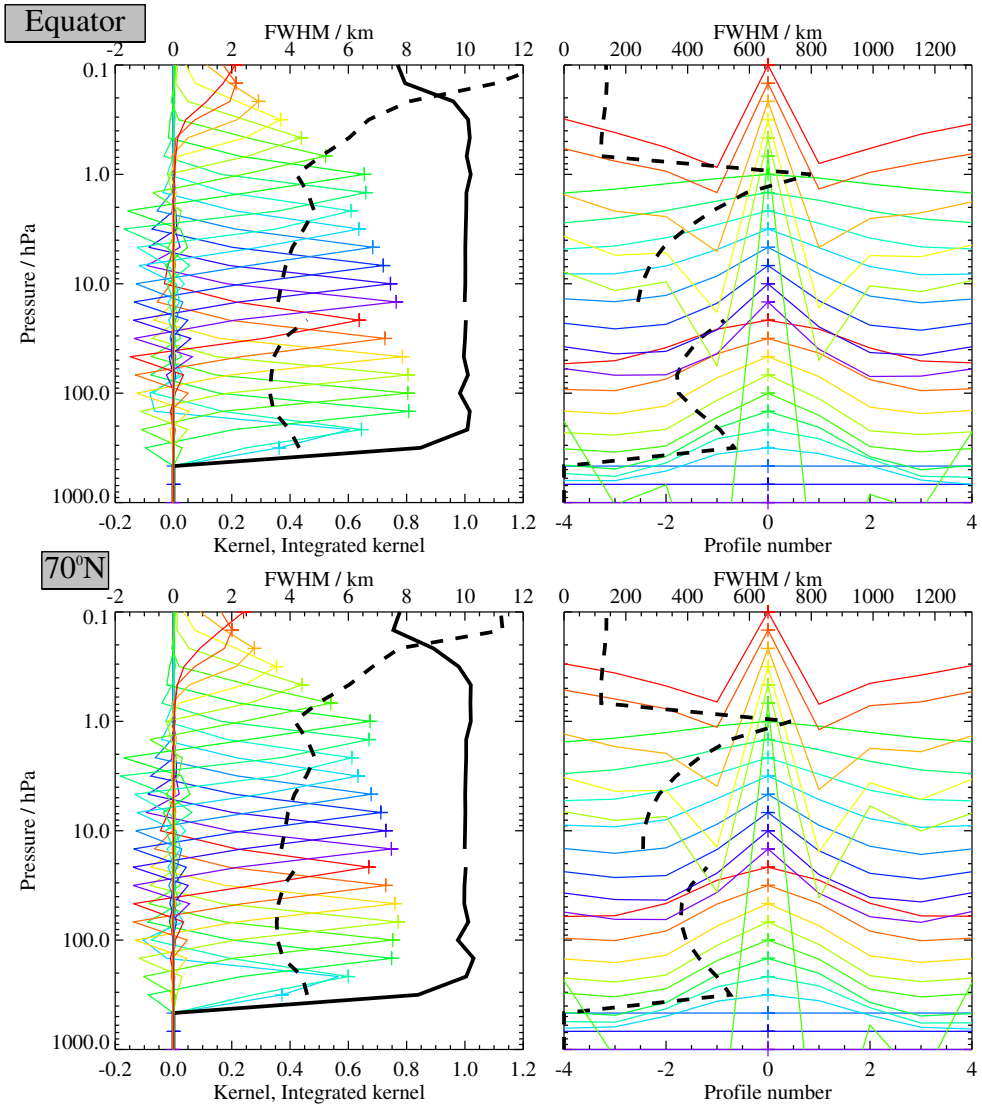

Figure 3.13.4: Typical two-dimensional (vertical and horizontal along-track) averaging kernels for the MLS v6.0*x* HNO_3 data at the equator (upper) and at 70°N (lower); variation in the averaging kernels is sufficiently small that these are representative of typical profiles. Colored lines show the averaging kernels as a function of MLS retrieval level, indicating the region of the atmosphere from which information is contributing to the measurements on the individual retrieval surfaces, which are denoted by plus signs in corresponding colors. The dashed black line indicates the resolution, determined from the full width at half maximum (FWHM) of the averaging kernels, approximately scaled into kilometers (top axes). (Left) Vertical averaging kernels (integrated in the horizontal dimension for five along-track profiles) and resolution. The solid black line shows the integrated area under each kernel (horizontally and vertically); values near unity imply that the majority of information for that MLS data point has come from the measurements, whereas lower values imply substantial contributions from a priori information. (Right) Horizontal averaging kernels (integrated in the vertical dimension) and resolution. The horizontal averaging kernels are shown scaled such that a unit averaging kernel amplitude is equivalent to a factor of 10 change in pressure.

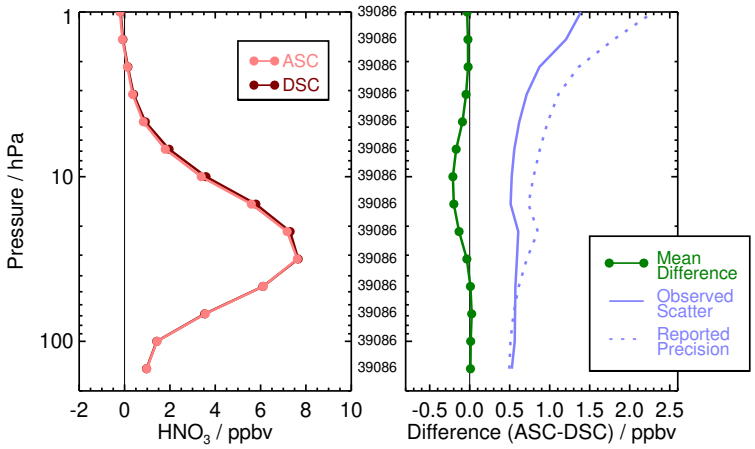

Figure 3.13.5: (left) Ensemble mean profiles for ascending (light red) and descending (dark red) orbit matching pairs of MLS v6.0*x* HNO_3 profiles averaged over several months of a representative year of data (2019). Symbols indicate MLS retrieval pressure levels. (right) Mean differences (ascending−descending) in pptv (green solid line). Also shown are the standard deviations about the mean differences (light blue solid line) and the root sum square (RSS) of the precisions calculated by the retrieval algorithm for the two sets of profiles (light blue dotted line). The observed scatter about the mean differences and the reported precision values have been scaled by $1/\sqrt{2}$ (to convert from standard deviations of differences into standard deviations of individual data points); hence the light blue solid line represents the statistical repeatability of the MLS measurements, and the light blue dotted line represents the expected 1σ precision for a single profile. The thin black lines mark zero in each panel. The number of crossing pairs of measurements being compared at each pressure level is noted in the space between the panels.

horizontal resolution. Smoothing, imposed on the retrieval system in both the vertical and horizontal directions to enhance retrieval stability and precision, reduces the inherent resolution of the measurements. Thus, although HNO_3 measurements are reported at six pressure levels per decade change in pressure (spacing of ~2.7 km), the vertical resolution of the v6.0*x* HNO_3 data as determined from the full width at half maximum of the rows of the averaging kernel matrix shown in Figure 3.13.4 varies from ~3.5 to 5 km over the useful vertical range (see Table 3.13.1 for estimates at individual levels). Substantial overlap in the averaging kernels for the 215 and 316 hPa retrieval surfaces (which both peak at 215 hPa) indicates that the 316 hPa retrieval provides little independent information. Figure 3.13.4 also shows horizontal averaging kernels, from which the along-track horizontal resolution is determined to be ~250–500 km over most of the vertical range, degrading to 600–800 km at 1.5 and 1 hPa. The cross-track resolution, set by the widths of the fields of view of the 190-GHz and 240-GHz radiometers, is ~10 km. The along-track separation between adjacent retrieved profiles is 1.5° great circle angle (~165 km), whereas the longitudinal separation of MLS measurements, set by the Aura orbit, is 10°–20° over low and middle latitudes, with much finer sampling in the polar regions.

3.13.4 Precision

The precision of the MLS HNO_3 measurements is estimated empirically by comparing profiles measured at the intersections of ascending (mainly day) and descending (mainly night) portions of the orbit. Under ideal conditions (i.e., a quiescent atmosphere), the standard deviation about the mean differences between such matched profile pairs provides a measure of the precision of the individual data points. In practice, however, real changes in the atmosphere may occur over the 12 h interval between the intersecting measurement points, in which case the observed scatter provides an upper limit on the estimate of precision, assuming that the a priori has a negligible influence on the retrieval (a reasonable assumption throughout the retrieval range for HNO_3). The precision estimates were found to be essentially invariant with time; results for a representative year of data are shown in Figure 3.13.5. Mean differences between paired crossing profiles are negligible over most of the profile, indicating the absence of significant systematic ascending / descending biases; small differences in the middle and upper stratosphere may be largely related to photochemical effects. The ob-

served standard deviation values are ~0.6 ppbv or less throughout most of the vertical domain, increasing to ~0.9 ppbv at 2.1 hPa and ~1.4 ppbv at 1 hPa. An alternative method of computing the standard deviation of the profiles in the 20°-wide latitude band centered around the equator yields very similar precision estimates (not shown).

The observational determination of the precision is compared in Figure 3.13.5 to the theoretical precision values reported by the Level 2 data processing algorithms. Although the two estimates compare very well at the bottom of the recommended vertical range, at pressures smaller than 30 hPa the predicted precision substantially exceeds the observed scatter, indicating that the a priori information and the vertical smoothing (regularization) applied to stabilize the retrieval system and improve the precision are influencing the results at the higher retrieval levels. Because the theoretical precisions take into account occasional variations in instrument performance, the best estimate of the precision of an individual data point is the value quoted for that point in the L2GP files, but it should be borne in mind that this approach overestimates the actual measurement noise at pressures less than 30 hPa.

The single-profile precision estimates cited here are, to first order, independent of latitude and season. However, large geographic variations in HNO_3 abundances give rise to a wide range of signal-to-noise ratios; thus at some latitudes and altitudes and in some seasons, HNO_3 abundances are smaller than the single-profile precision, necessitating the use of averages for scientific studies. In most cases, precision can be improved by averaging, with the precision of an average of N profiles being $1/\sqrt{N}$ times the precision of an individual profile (note that this is not the case for averages of successive along-track profiles, which are not completely independent because of horizontal smearing).

3.13.5 Accuracy

The effects of various sources of systematic uncertainty (e.g., instrumental issues, spectroscopic uncertainty, and approximations in the retrieval formulation and implementation) on the MLS v6.0*x* HNO_3 measurements were quantified through a comprehensive set of retrievals of synthetic radiances; see *Santee et al.* [2007] for details of a similar analysis conducted on MLS v2.2*x* HNO_3 data. The overall systematic uncertainty, or accuracy, is calculated by combining (RSS) the contributions from both the expected biases and the additional scatter each source of uncertainty may introduce into the data. In aggregate, the factors considered in these simulations are estimated to give rise to a total systematic uncertainty in the MLS v6.0*x* HNO_3 data ranging from approximately 0.2 to 2.4 ppbv, depending on the level (see Table 3.13.1).

3.13.6 Comparisons with other datasets

Extensive comparisons of MLS v2.2*x* HNO_3 data with a variety of different platforms (ground-based, balloon-borne, aircraft, and satellite instruments) were presented by *Santee et al.* [2007]. Comparisons of v6.0*x* HNO_3 with correlative data have not been conducted but are expected to yield results similar to those for previous versions.

3.13.7 Data screening

General HNO_3 screening considerations

Pressure range: 215–1.5 hPa

Values outside this range are not recommended for scientific use. The HNO_3 data at 1.0 hPa and lower pressures may be useful under certain enhanced conditions but should not be analyzed in scientific studies without significant discussion with the MLS science team.

Estimated precision: Only use values for which the estimated precision is a positive number.

Values where the a priori information has a strong influence are flagged with negative or zero precision and should not be used in scientific analyses (see Section 1.5).

Upper troposphere / lower stratosphere (pressures of 22 hPa or greater)

The `Quality` and `Convergence` fields included in the `HNO3` swath in the standard `L2GP-HNO3` files are appropriate for use in screening the data at and below (i.e., at pressures greater than) 22 hPa. For those levels:

Quality: Only profiles whose `Quality` field is greater than 0.8 should be used.

In a typical month this threshold for `Quality` (unchanged from v5.0*x*) excludes ∼1–2% of HNO_3 profiles; it is a conservative value that potentially discards some "good" data points while not necessarily identifying all "bad" ones. As in previous versions, many HNO_3 profiles in v6.0*x* are characterized by a "notch", with unexpectedly low (often negative in the tropics) values at 100 and/or 147 hPa and higher values at the level below; although some of the oscillatory profiles are removed through filtering using the `Quality` field, in many cases mean profiles continue to display a prominent notch (e.g., see Figure 3.13.3).

Convergence: Only profiles whose `Convergence` field is less than 1.03 should be used.

In a typical month this threshold for `Convergence` (unchanged from v5.0*x*) discards few (0.2% or less) of the HNO_3 profiles, some of which show unphysical behavior.

Status flag: Only use profiles for which the `Status` field is zero.

Nonzero but even values of `Status` indicate that the profile has been marked as questionable, typically because the measurements may have been affected by the presence of thick clouds. In the UTLS, thick clouds can lead to spikes in the HNO_3 mixing ratios in the equatorial regions. Therefore, it is recommended that at and below (i.e., at pressures greater than) 68 hPa all profiles with nonzero values of `Status` be discarded because of the potential for cloud contamination. Globally ∼2–4% of profiles are identified as affected by clouds in v6.0*x*, with the fraction of profiles possibly impacted by clouds rising to ∼8–12% in the tropics. While this procedure rejects some profiles that are probably not significantly impacted by cloud effects, the majority of profiles rejected in this manner (some of which are unphysical) are not filtered by other criteria. See Section 1.6 for more information on the interpretation of the `Status` field.

Upper stratosphere (pressures of 15 hPa or less)

The above screening criteria *should not be used* for data at 15 hPa and higher altitudes (lower pressures). Rather, the appropriate indicators to be used in masking HNO_3 data at these altitudes are the `Quality` and `Convergence` values pertinent to the 190-GHz retrievals. To aid that screening, the `HNO3-190` swath is included in the standard HNO_3 files. The following screening criteria are based on the 190-GHz HNO_3 information:

Quality: Only profiles with a value of the `Quality` field for `HNO3-190` greater than 0.8 should be used.

In a typical month this threshold for `Quality` (unchanged from v5.0*x*) excludes ∼1–3% of HNO_3 profiles; it is a conservative value that potentially discards some "good" data points while not necessarily identifying all "bad" ones.

Convergence: Only profiles with a value of the `Convergence` field for `HNO3-190` less than 1.4 should be used.

In a typical month this threshold for `Convergence` (unchanged from v5.0*x*) discards ∼1–4% of the HNO_3 profiles. Some profiles thus flagged show unphysical behavior, especially at the highest altitudes in the recommended range.

Status flag: Only use profiles for which the `Status` field is an even number.

Clouds generally have little influence on the stratospheric HNO_3 data at these altitudes, thus profiles for which the `HNO3-190` `Status` field is a nonzero even number can be used without restriction.

3.13.8 Artifacts

A persistent "notch" in the profile, with low values at 100 and/or 147 hPa and higher values at the level below, is most pronounced in the tropics and midlatitudes but is also apparent at high latitudes in some seasons (Figure 3.13.3). The origin of this oscillatory signature in the retrievals is unclear; it is reduced but by no

Table 3.13.1: Summary of Aura MLS v6.0*x* HNO_3 Characteristics

Pressure hPa	Resolution[a] V × H km	Single-Profile Precision[b] ppbv	Accuracy[c] ppbv	Comments
0.68–0.001	—	—	—	Unsuitable for scientific use
1.0	4.5 × 800	±1.4	±0.3	Caution, averaging recommended
1.5	4.5 × 600	±1.2	±0.3	Caution, averaging recommended
2.2	5 × 500	±0.8	±0.5	
3.2	4.5 × 400	±0.6	±0.2	
4.6	4 × 300	±0.6	±0.5	
6.8	4 × 300	±0.6	±0.4	
10	4 × 250	±0.6	±0.5	
15	4 × 250	±0.6	±0.6	
22	4.5 × 500	±0.6	±2.4	
32	4 × 450	±0.6	±1.3	
46	3.5 × 400	±0.6	±1.0	
100–68	3.5 × 400	±0.6	±0.8	Consult MLS team for use in tropical UTLS
147	4 × 450	±0.6	±1.0	Consult MLS team for use in tropical UTLS
215	4.5 × 500	±0.6	±1.1	Consult MLS team for use in tropical UTLS
316	—	—	—	Unsuitable for scientific use
1000–464	—	—	—	Not retrieved

[a]Vertical and along-track horizontal resolutions; cross-track horizontal resolution is 7–9 km.
[b]Precision on individual profiles, determined from observed scatter in the data in a region of minimal atmospheric variability.
[c]Values should be interpreted as 2σ estimates of the probable magnitude.

means eliminated through application of the recommended screening procedures. Users of the MLS HNO_3 data are cautioned that retrieved abundances can be strongly negative in the tropical UTLS, even for mean profiles, and are advised to consult with the MLS science team before undertaking scientific studies of that region relying on the v6.0*x* HNO_3 data.

3.13.9 Desired improvements should another data version be produced

Further work to diagnose and eliminate the persistent unphysical oscillations at the lowest retrieval levels will be undertaken should an opportunity to produce an updated MLS data version arise.

3.14 Peroxy Radical (HO_2)

Swath name: HO2

Useful range: 22–0.046 hPa

Product lead: Luis Millán <Luis.F.Millan@jpl.nasa.gov>

3.14.1 Introduction

MLS observes HO_2 emission lines within the 640-GHz radiometer. A description of HO_2 data quality, precision, systematic errors, and validation for an earlier version, v2.2*x*, is given by *Pickett et al.* [2006a]. An early validation using v1.5 software is also described by *Pickett et al.* [2006a]. The estimated uncertainties, precisions, and resolution for v6.0*x* HO_2 are summarized below in Table 3.14.1.

An algorithm to retrieve daily zonal means of HO_2 over an extended vertical range by first averaging the radiances has been developed by the MLS team [*Millán et al.*, 2015]. This alternative dataset provides daytime and nighttime HO_2 measurements across the stratosphere and mesosphere. This dataset and associated documentation is available from the GSFC DISC with the product short name "ML3DZMHO2".

3.14.2 Resolution

Figure 3.14.1 shows the HO_2 averaging kernel for daytime at 70°N and the Equator. The latitudinal variation in the averaging kernel is very small. The vertical resolution for pressures greater than 0.1 hPa is generally about 5 km.

3.14.3 Precision

A typical HO_2 profile and the associated precisions (for both v5.0*x* and v6.0*x*) are shown in Figure 3.14.2. The profile is shown in both volume mixing ratio (vmr) and density units. All MLS data are reported in vmr for consistency with the other retrieved molecules. However, use of density units (10^6 cm^{-3}) reduces the apparent steep gradient of the HO_2 vertical profile, allowing one to see the profile with more detail. The nighttime HO_2 profile is expected to exhibit a narrow layer near the altitudes of the nighttime OH layer at ~82 km [*Pickett et al.*, 2006b], which is not shown in Figure 3.14.2 since MLS HO_2 data are not recommended for altitudes above 0.046 hPa (~70 km). Precisions are such that an HO_2 zonal average within a 10° latitude bin can be determined with better than 10% relative precision with 20 days of data (~2000 samples) for most pressure levels over 22–0.046 hPa.

3.14.4 Accuracy

Table 3.14.1 summarizes the accuracy expected for v6.0*x* HO_2. The effect of each identified source of systematic error on MLS measurements of radiance has been quantified and modeled [*Read et al.*, 2007]. These quantified effects correspond to either 2σ estimates of uncertainties in each MLS product or an estimate of the maximum reasonable uncertainty based on instrument knowledge and/or design requirements. The HO_2 bias can be minimized by taking day/night differences over the entire recommended pressure range. The overall uncertainty is the square root of the sum of squares of the precision and accuracy.

3.14.5 Data screening

Pressure range: 22–0.046 hPa

Values outside this range are not recommended for scientific use.

Estimated precision: Only use values for which the estimated precision is a positive number.

Values where the a priori information has a strong influence are flagged with negative or zero precision and should not be used in scientific analyses (see Section 1.5).

Status flag: Only use profiles for which the `Status` field is an even number.

Odd values of `Status` indicate that the profile should not be used in scientific studies. See Section 1.6 for more information on the interpretation of the `Status` field.

Quality: MLS v6.0*x* HO_2 data can be used irrespective of the value of the `Quality` field.

Convergence: Only profiles whose `Convergence` field is less than 1.1 should be used.

3.14.6 Artifacts

Currently, there are no known artifacts in the HO_2 product. The primary limitations are its precision and its narrow recommended altitude range. That said, the alternative daily zonal mean dataset (short name: "`ML3DZMHO2`") offers three distinct improvements over the standard MLS HO_2 product: (1) an extended pressure range, enabling measurements of the mesospheric maximum that occurs near 0.02 hPa, (2) expanded latitudinal coverage, allowing measurement at the poles, where the HO_2 is located, and (3) nighttime HO_2 estimates.

3.14.7 Review of comparisons with other datasets

HO_2 data from MLS v2.2*x* software have been validated with two balloon-borne remote-sensing instruments. Details of the comparison are given by *Pickett et al.* [2006a]. Comparisons between v2.2*x* and v6.0*x* show no differences large enough to alter results of previous validation studies.

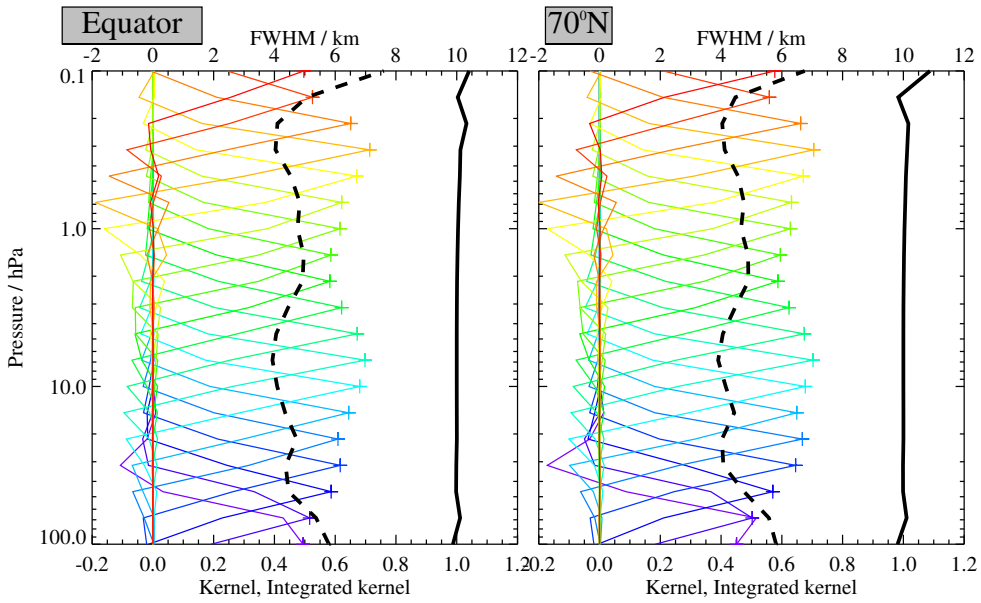

Figure 3.14.1: Typical vertical averaging kernels for the MLS v6.0*x* HO_2 data at the equator (left) and at 70°N (right); variation in the averaging kernels is sufficiently small that these are representative of typical profiles. Colored lines show the averaging kernels as a function of MLS retrieval level, indicating the region of the atmosphere from which information is contributing to the measurements on the individual retrieval surfaces, which are denoted by plus signs in corresponding colors. The dashed black line indicates the vertical resolution, determined from the full width at half maximum (FWHM) of the averaging kernels, approximately scaled into kilometers (top axes). The solid black line shows the integrated area under each kernel; values near unity imply that the majority of information for that MLS data point has come from the measurements, whereas lower values imply substantial contributions from a priori information. The low signal to noise for this product necessitates the use of significant averaging (e.g., monthly zonal mean), making horizontal averaging kernels largely irrelevant.

Table 3.14.1: Summary of Aura MLS v6.0*x* HO_2 Characteristics

Pressure hPa	Vertical resolution km	Precision[a] 10^6 cm^{-3}	Day–night accuracy 10^6 cm^{-3}	Comments
< 0.03	—	—	—	Unsuitable for scientific use
0.046	10	4	0.01	Use day–night difference
0.10	7	8	0.3	Use day–night difference
1.0	5	11	0.5	Use day–night difference
10	4	56	15	Use day–night difference
> 22	—	—	—	Unsuitable for scientific use

[a]Precision for a single profile

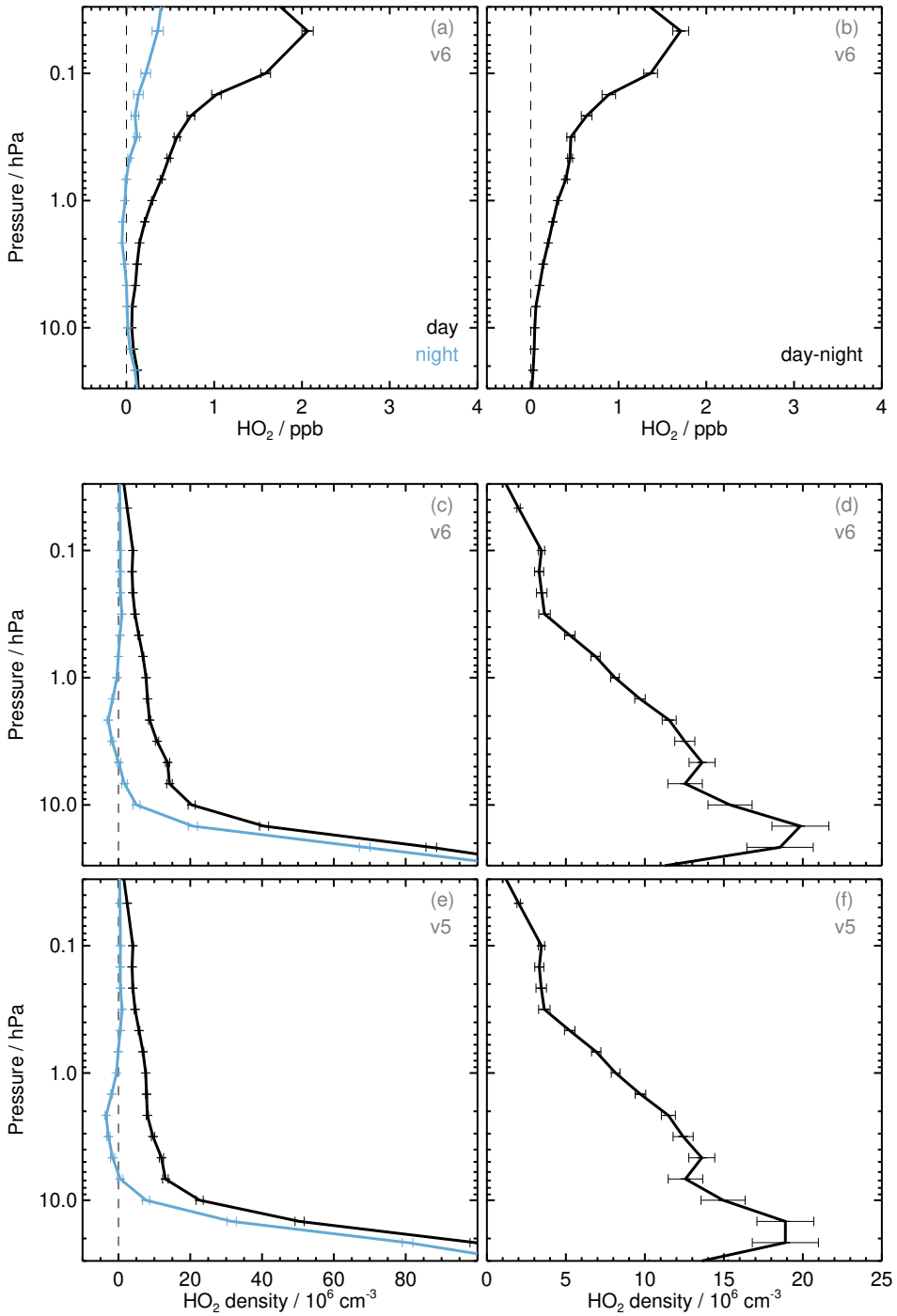

Figure 3.14.2: Monthly zonal mean of retrieved HO_2 and its estimated precision (horizontal error bars) for January 2005 averaged over 29°N to 39°N. Panel (a) shows v6.0*x* HO_2 vmr vs. pressure for day (black) and night (blue). Panel (b) shows the same data plotted as a day/night difference (note that a day/night difference is required for HO_2 for all pressure levels). Panel (c) shows the same data in (a) converted into density units. Panel (d) shows the day-night differences for the data in panel (c). Panels (e) and (f) are equivalent to (c) and (d) but using v5.0*x* data.

3.15 Hypochlorous Acid (HOCl)

Swath name: HOCl

Useful range: 10–2.2 hPa

Product lead: Lucien Froidevaux

Contact: Luis Millán <Luis.F.Millan@jpl.nasa.gov>

3.15.1 Introduction

MLS observes HOCl emission lines within the 640-GHz radiometer. The HOCl spectral signature in the MLS radiances is very small, resulting in poor signal-to-noise ratio for individual MLS observations. Thus, the HOCl retrievals are quite noisy for individual profiles. HOCl data therefore require some averaging (e.g., in 10°-latitude-resolution zonal means for one or more weeks) to achieve a useful precision of better than 10 pptv, compared with typical upper stratospheric HOCl abundances of 100–150 pptv. Table 3.15.1 summarizes the MLS HOCl resolution, precision, and accuracy estimates for the upper stratosphere. Further discussion and a brief validation summary are provided in the following sections, along with data screening recommendations. HOCl trend results in the upper stratosphere were reported by *Froidevaux et al.* [2022].

An algorithm to retrieve daily zonal means of HOCl by first averaging the radiances has been developed by the MLS team, building on the work described by *Millán et al.* [2012] and *Millán et al.* [2015] for BrO and HO_2, respectively. This alternative dataset slightly reduces the variability and is available, along with associated documentation, from the GSFC DISC. The product short name is "ML3DZMHOCl". It is expected to be very similar to the HOCl dataset used by *Froidevaux et al.* [2022].

Limb radiances measured by the MLS 640-GHz radiometer are affected by water vapor (and other species) in addition to HOCl. As noted in Section 1.10.2, as of May 2024, the 190-GHz radiometer, which is used to measure water vapor, is operated only intermittently. When that radiometer is turned off and H_2O measurements are not available, a priori information for H_2O (based on climatological values) is used in the HOCl retrievals, adversely affecting their quality; further details are given in Section 3.15.6.

3.15.2 Changes from v5.0*x*

There were no significant algorithmic changes relating directly to HOCl for the v6.0*x* retrievals. However, given the small level of HOCl spectral radiance signal, the retrieved HOCl abundances can be sensitive, indirectly, to even minor changes in the retrieval system, such as changes in temperature or tangent pressure. Figure 3.15.1 shows a comparison of upper stratospheric HOCl between v6.0*x* and v5.0*x* for April 2009. The average v6.0*x* HOCl abundances are slightly larger than they were in the v5.0*x* retrievals, typically by about 5 to 15 pptv (or 5 to 15%); this has removed some of the small negative values that often occurred in v5.0*x* HOCl averages at the highest southern latitudes between 5 and 10 hPa. The estimated precision values are essentially unchanged from those in v5.0*x*.

3.15.3 Resolution

Based on the width of the averaging kernels shown in Figure 3.15.2, the vertical resolution of upper stratospheric HOCl is ~6 km (significantly coarser than the 640-GHz radiometer vertical field-of-view width of 1.4 km). This reflects the choice of smoothing constraints for HOCl, which favor precision over vertical resolution.

3.15.4 Precision

The estimated single-profile precision is about 300 to 450 pptv in the upper stratosphere. A more useful number of 8.5 to 10 pptv is quoted in Table 3.15.1 for the typical precision of a 10° weekly zonal means.

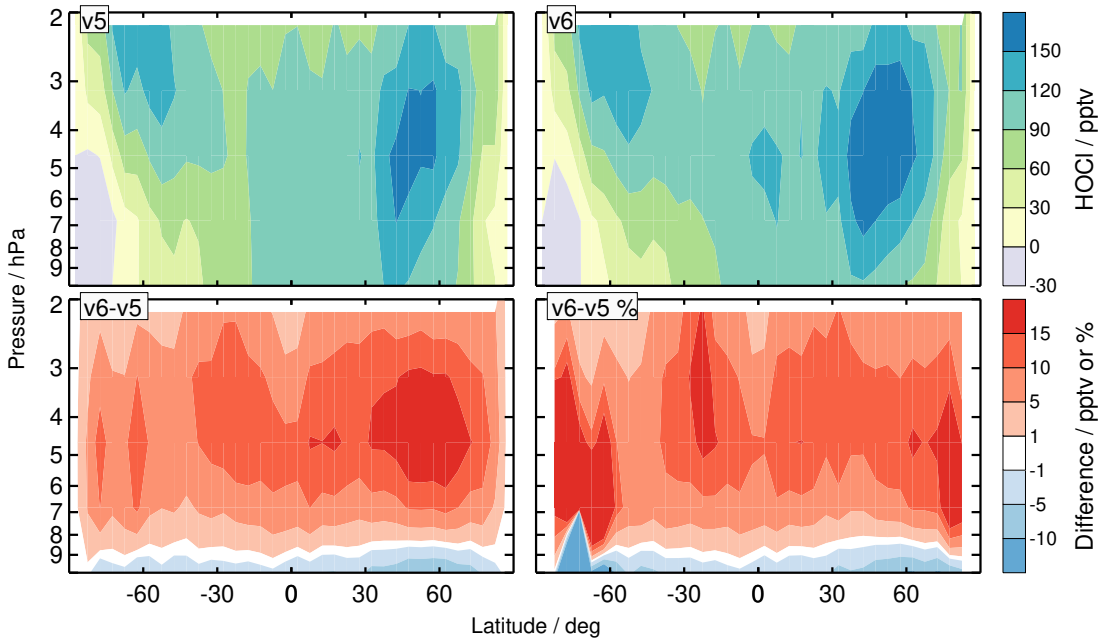

Figure 3.15.1: Zonal averages for upper stratospheric MLS HOCl profiles during April 2009 for v5.0*x* and v6.0*x*, and their differences in pptv and percent.

3.15.5 Accuracy

The accuracy estimates shown in Table 3.15.1 come from a formal quantification of the combined effects of possible systematic errors in MLS calibration, spectroscopy, etc. on the HOCl retrievals [*Read et al.*, 2007]. These values are intended to represent 2σ estimates of accuracy. The largest contributors to possible errors for HOCl are contaminant species, gain compression, and sideband ratio uncertainties. The average changes for upper stratospheric HOCl between v5.0*x* and v6.0*x* are well within the quoted accuracy estimates. The HOCl signal becomes too small compared to the systematic uncertainties to allow for reliable retrievals at pressures larger than 10 hPa.

3.15.6 Data screening

Pressure range: 10–2.2 hPa

Values outside this range are not recommended for scientific use. Artifacts (negative average abundances) for pressures larger than about 10 hPa make this product unsuitable for use in the lower stratosphere. Regarding the topmost altitude range, the sensitivity to a priori increases rapidly at pressures of 1 hPa or less; we continue to recommend the use of (average) HOCl values only up to 2.2 hPa.

Estimated precision: Only use values for which the estimated precision is a positive number.

Values where the a priori information has a strong influence are flagged with negative or zero precision and should not be used in scientific analyses (see Section 1.5).

Status flag: Only use profiles for which the `Status` field is an even number.

Odd values of `Status` indicate that the profile should not be used in scientific studies. See Section 1.6 for more information on the interpretation of the `Status` field.

Quality field: Only profiles with a value of the `Quality` field *greater* than 1.2 should be used.

This criterion removes profiles with the poorest radiance fits, typically less than 0.2% of the daily profiles. For HOCl, this screening correlates well with the poorly converged sets of profiles (see below);

we recommend the use of both the `Quality` and `Convergence` fields for data screening.

Convergence field: Only profiles with a value of the `Convergence` field *less* than 1.05 should be used.

For the vast majority of profiles (99% or more for most days), this field is less than 1.05. Nevertheless, on occasion, sets of profiles (typically one or more groups of ten profiles, retrieved as a 'chunk') have the `Convergence` field set to larger values and should be discarded.

Clouds: Profiles identified as being affected by clouds can be used with no restriction.

Additional screening on H_2O `Status`: As noted earlier, HOCl retrieval quality is degraded at some levels when the 190-GHz radiometer is turned off and H_2O measurements are not available. In these circumstances, biases in the retrieved HOCl values can reach more than 5 to 10% at 4.6 to 10 hPa, while the upper altitudes (pressures less than 4 hPa) are largely unaffected. These artifacts are not removed by the standard HOCl data filtering protocols. Thus, while the HOCl data on affected days are still useful for purely morphological or qualitative purposes, they cannot be quantitatively compared to measurements taken on surrounding days or in previous years when the 190-GHz radiometer was operational. The biases also have potential implications for the calculation of long-term trends. Therefore, for quantitative studies using HOCl data at the most affected retrieval levels noted above, an additional screening step is recommended, whereby the `Status` field in the colocated H_2O profile is examined to remove affected HOCl retrievals. That is, only HOCl profiles for which the `Status` flags of the corresponding H_2O profiles are an even number should be used in quantitative studies relying on HOCl measurements in the 4.6–10 hPa range (at lower pressures / higher altitudes, all HOCl data points passing the standard quality screening measures may be used). We also note, however, that measurements taken during time periods since May 2024 when the 190-GHz radiometer is turned off can be intercompared.

3.15.7 Review of comparisons with other datasets

The MLS HOCl retrievals exhibit the expected morphology in monthly mean latitude / pressure plots. For example, September MLS results compare favorably, to first-order, with results produced by the Michelson Interferometer for Passive Atmospheric Sounding (MIPAS) for September, 2002 [*von Clarmann et al.*, 2006]. MLS HOCl averages at midlatitudes are also consistent with balloon-borne infrared measurements. Favorable comparisons (within the error bars) have also been reported for the diurnal changes in upper stratospheric HOCl between Aura MLS (v3.3*x*/v3.4*x*), other satellite datasets, and a 1-D photochemical model [*Khosravi et al.*, 2013].

3.15.8 Artifacts

- The 640-GHz radiometer Bands 10 (for ClO) and 29 (for HOCl) were turned off for a few time periods in 2006 to investigate degradation issues that might affect these channels in the future. These bands were off on 8, 9, and 10 April 2006, and also for 17 April 2006 (after 19:52 UT) through 17 May 2006. There are essentially no useful HOCl (or ClO) data for these time periods. The v6.0*x* (as for previous data versions) software correctly flags these incidents with poor (odd) `Status` values (which should be screened out).
- There are significant artifacts in the mean abundances (large negative values) for HOCl in the lower stratosphere, where the use of this product is not recommended.
- Users should screen out the non-converged and poorest quality HOCl profiles, as such profiles (typically a very small number per day) tend to behave unlike the majority of the other MLS retrievals. See the criteria listed above.
- As discussed in Section 3.15.6, biases in HOCl values are present at some levels when coincident measurements from the 190-GHz radiometer are not available and H_2O a priori information is used in the HOCl retrieval. Depending on the specific goals of any study based on these measurements, additional HOCl data quality filtering may be necessary for days when the 190-GHz radiometer is off.

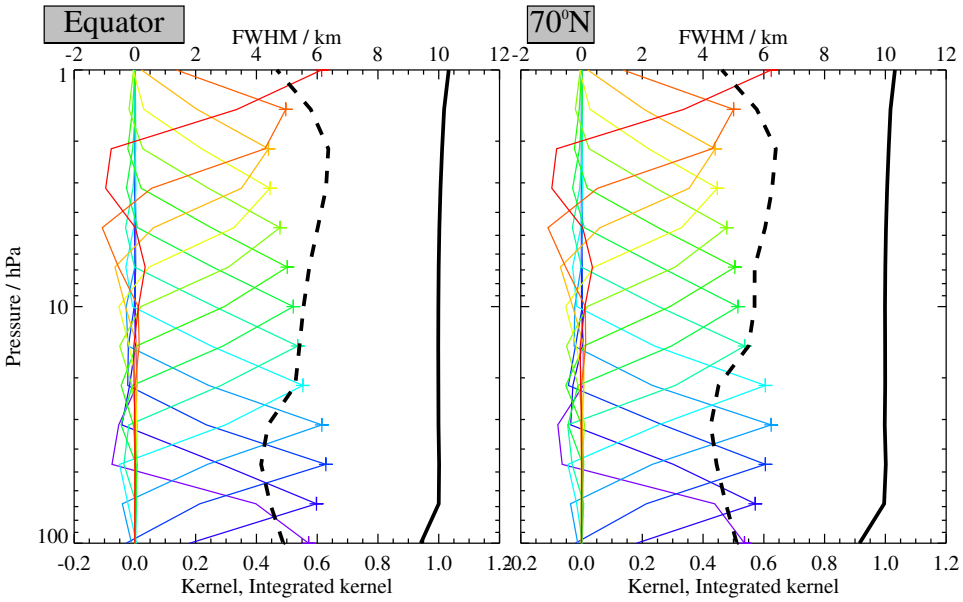

Figure 3.15.2: Typical vertical averaging kernels for the MLS v6.0*x* HOCl data at the equator (left) and at 70°N (right); variation in the averaging kernels is sufficiently small that these are representative of typical profiles. Colored lines show the averaging kernels as a function of MLS retrieval level, indicating the region of the atmosphere from which information is contributing to the measurements on the individual retrieval surfaces, which are denoted by plus signs in corresponding colors. The dashed black line indicates the vertical resolution, determined from the full width at half maximum (FWHM) of the averaging kernels, approximately scaled into kilometers (top axes). The solid black line shows the integrated area under each kernel; values near unity imply that the majority of information for that MLS data point has come from the measurements, whereas lower values imply substantial contributions from a priori information. The low signal to noise for this product necessitates the use of significant averaging (e.g., monthly zonal mean), making horizontal averaging kernels largely irrelevant.

Table 3.15.1: Summary Aura MLS v6.0*x* HOCl Characteristics

Pressure hPa	Vertical resolution km	Precision[a] pptv	Accuracy[b] pptv	Comments
< 1.5	—	—	—	Unsuitable for scientific use
10 to 2.2	5.5 – 6	8.5 – 10	60 – 90	Some averaging required
> 15	—	—	—	Unsuitable for scientific use

[a] Precision (1σ) for 1-week/10° zonal means or 2-week/5° zonal means
[b] 2σ estimate from systematic uncertainty characterization tests

3.16 Cloud Ice Water Content (IWC)

Swath name: IWC

Useful range: 215–83 hPa

Units: g/m^3

Product lead: Alyn Lambert <Alyn.Lambert@jpl.nasa.gov>

3.16.1 Introduction

The MLS IWC is retrieved from cloud-induced radiances (T_{cir}) of the 240-GHz window channel in a separate processing step after the atmospheric state (temperature and tangent point pressure) and important gaseous species (H_2O, O_3, HNO_3) have been finalized in the retrieval processing. The derived T_{cir} are binned onto the standard horizontal (1.5° along track) and vertical (12 surfaces per decade change in pressure) grids and converted to IWC using the modeled T_{cir}–IWC relations [*Wu et al.*, 2006]. The standard IWC profile has a useful vertical range of 215–83 hPa, although validation has only been conducted for a subset of the pressure range of IWC. IWC measurements beyond the value ranges specified in Table 3.16.1 are to be regarded as giving only qualitative information on cloud ice.

As noted in Section 1.10.2, as of May 2024, the 190-GHz radiometer, which is used to measure water vapor, is operated only intermittently. When that radiometer is turned off and H_2O measurements are not available, a priori information for H_2O (based on climatological values) is used in the derivation of the IWC data product, adversely affecting its quality. Therefore, we do not recommend the use of IWC data during the periods when the 190-GHz radiometer is deactivated. Further details are given in Section 3.16.5.

3.16.2 Resolution

In the IWC ranges specified in Table 3.16.1, each MLS measurement can be quantitatively interpreted as the average IWC for the volume sampled. This volume has an extent of ~3 km in the vertical and ~300 km and 7 km in the along- and cross-track directions, respectively.

3.16.3 Precision

The precision values quoted in the IWC files do not represent the true precision of the data. The precision for a particular measurement must be evaluated on a daily basis using the method described in Section 3.16.5. The precision listed in Table 3.16.1 reflects typical values obtained from the method described below.

3.16.4 Accuracy

The IWC accuracy values listed in Table 3.16.1 are estimates from comparisons of the earlier v2.2*x* MLS data product with CloudSat; detailed analyses of the v2.2*x* error budget are given by *Wu et al.* [2008].

3.16.5 Data screening

Pressure range (215–83 hPa): Values outside this range are not recommended for scientific use. The maximum detectable IWC is ~100 mg/m^3.

Use Temperature Status, Quality and Convergence: The user is advised to screen the IWC data using the `Status` field in the colocated temperature profile to exclude bad retrievals [*Schwartz et al.*, 2008]. In other words, only IWC profiles for which temperature `Status` is an even number should be used. Similarly, only use IWC profiles where the corresponding temperature profiles have (a) `Quality` of 0.9 or larger for 100 hPa and larger pressures or (b) `Quality` of 0.2 or larger for 83 hPa and smaller pressures. The temperature `Convergence` must be less than 1.03.

Other screening: The IWC product derives from differences between measured radiances and those predicted assuming cloud-free conditions. Spectroscopic and calibration uncertainties give rise to temporally and geographically varying biases in this difference, and hence the IWC product. These biases

must be iteratively identified and removed, using a "2σ, 3σ" screening method, as described below. Note that this screening step cannot provide an adequate correction for the lack of retrieved H_2O during the periods when the 190-GHz radiometer is turned off, and so the additional screening step on H_2O `Status` given below takes precedence.

1. Uncertainties in spectroscopy and atmospheric composition are manifested as residual biases in the IWC fields that should be identified and removed as follows. IWC data should be averaged in 10°-latitude bins and outliers rejected iteratively by excluding measurements greater than 2σ standard deviation about the mean (μ) of the bin. Repeat the σ and μ calculations after every new set of rejections. Convergence is usually reached within 5–10 iterations, and the final σ is the estimated precision for the IWC measurements.
2. Interpolate the final σ and μ to the latitude of each measurement, and subtract μ from IWC for each measurement.
3. Finally, apply the 3σ threshold to determine if an IWC measurement is statistically significant. In other words, it must have IWC $> \mu + 3\sigma$ in order to be considered as a significant cloud hit (where μ and σ are those resulting from step 1, i.e., computed excluding the identified rejected outliers). The 3σ threshold is needed for cloud detection since a small percentage of clear-sky residual noise can result in a large percentage of "false alarms" in cloud detection.

Additional screening on H_2O `Status`: As noted earlier, the quality of the IWC product is degraded when the 190-GHz radiometer is turned off, since only climatological H_2O is available in lieu of retrieved H_2O. In these circumstances, the IWC values cannot be quantitatively compared to measurements taken on surrounding days or in previous years when the 190-GHz radiometer was operational. Therefore, for quantitative studies, an additional screening step is recommended, whereby the `Status` field in the colocated H_2O profile is examined to remove affected IWC data. That is, only IWC profiles for which the `Status` flags of the corresponding H_2O profiles are an even number should be used in quantitative studies relying on IWC measurements.

3.16.6 Artifacts

At wintertime middle-to-high latitudes, strong stratospheric gravity waves may induce large fluctuations in the retrieved tangent pressure and cause false cloud detection with the "2σ, 3σ" screening method. The false cloud detections appear to occur more frequently at the lowest pressures, as a consequence of the increasing gravity wave amplitude with height.

3.16.7 Comparisons with other datasets

Scatter plots of v6.0*x* vs v2.2*x* IWC show mean biases of less than 10% in the pressure range 215–83 hPa, and histograms show that the random noise in v6.0*x* IWC is generally larger than that in v2.2*x* (see Figure 3.16.1 and Table 3.16.1). However, in localized regions, there can be substantial differences in IWC values between these versions that are driven by the response of the IWC retrieval to the changes in v6.0*x* UTLS H_2O. These effects are largest at pressures of 215 hPa and greater and have been verified by examining the negative correlations between the changes in H_2O and IWC.

Apart from the differences noted above, the MLS v6.0*x* IWC is similar to the MLS v2.2*x* product described and validated by *Wu et al.* [2008]. A revised validation paper for IWC is not planned, and users are encouraged to read *Wu et al.* [2008] for more information.

Comparisons between v2.2*x* MLS and CloudSat IWC showed good agreement, with probability density function (PDF) differences <50% for the IWC ranges specified in Table 3.16.1. Comparisons with AIRS, OMI, and MODIS suggest that in general MLS cloud tops are slightly higher by ~1 km than in the correlative data.

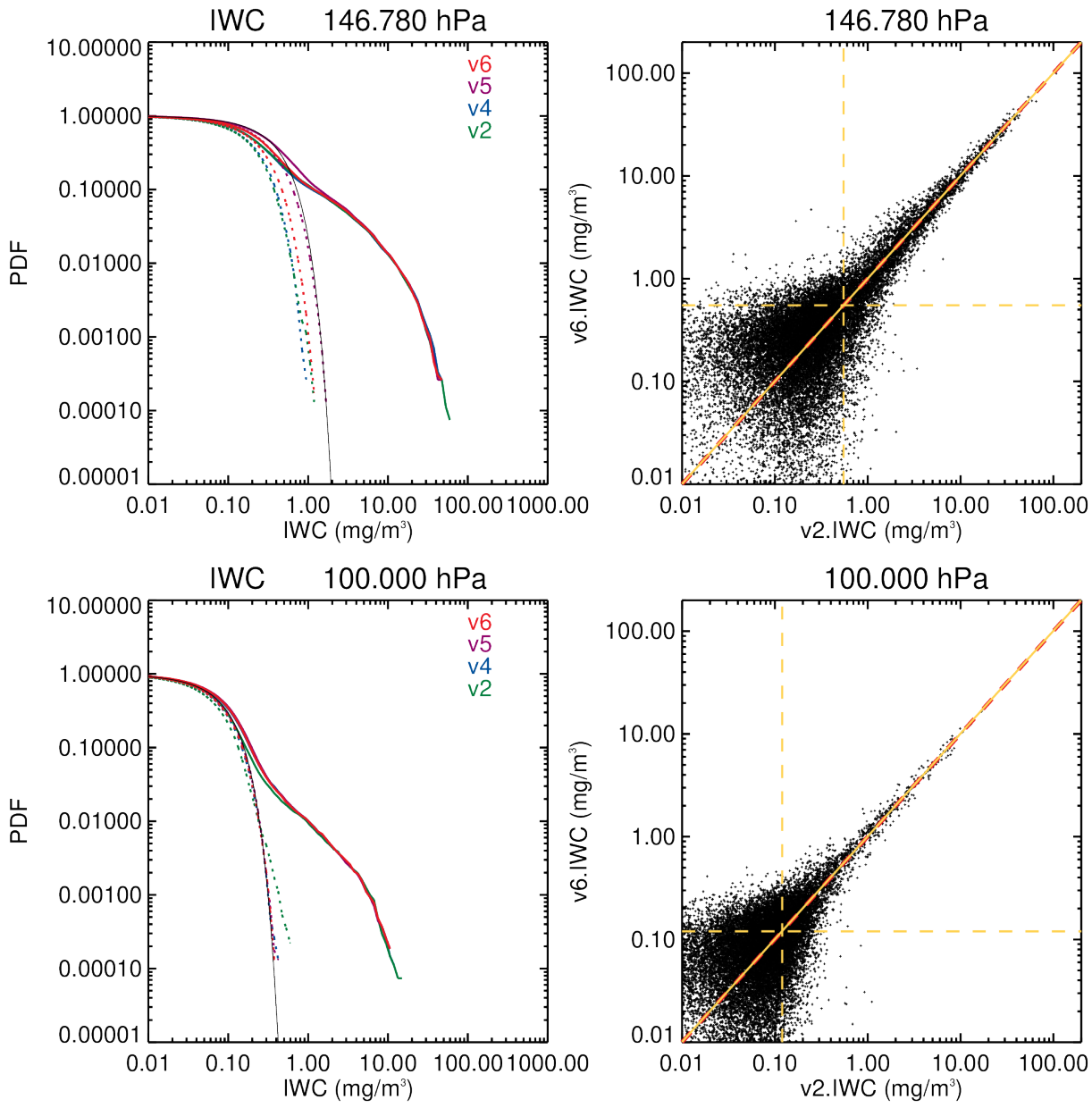

Figure 3.16.1: MLS v6.0*x*, v5.0*x*, v4.2*x*, and v2.2*x* IWC comparisons for June 2009 at 146 hPa and 100 hPa. (a) Left: Probability density functions (PDF) (v6.0*x*, red; v5.0*x*, purple; v4.2*x*, blue; and v2.2*x*, green), with dashed lines showing the corresponding noise levels (obtained by folding the negative IWC values about the origin) and the thin black lines representing the Gaussian error function. (b) Right: Scatter plots of IWC v6.0*x* vs. v2.2*x* (black points), with dashed red lines indicating the 1:1 line and dashed yellow lines the 1σ uncertainties. The solid yellow lines are linear fits to the data (which lie practically on the 1:1 line).

Table 3.16.1: Summary of Aura MLS v6.0*x* IWC precision, accuracy, and resolution.

Pressure	Resolution[a]	Typical precision[c]	Accuracy[b]		Valid IWC range[d]
hPa	km	mg/m^3	<10 mg/m^3	>10 mg/m^3	mg/m^3
p<70	Unsuitable for scientific use				
83	200×7×5	0.06–0.11	100%	—	0.02–50
100	200×7×5	0.07–0.13	100%	150%	0.02–50
121	250×7×4	0.09–0.19	100%	100%	0.04–50
147	300×7×4	0.20–0.45	100%	100%	0.1–50
177	300×7×4	0.5–1.7	150%	100%	0.3–50
215	300×7×4	0.5–4.5	300%	100%	0.6–50
p>260	Unsuitable for scientific use				

[a]The along-track, cross-track and vertical extent, respectively, of the atmospheric volume sampled by an individual MLS measurement.

[b]Estimated from comparisons with CloudSat.

[c]These are typical 1σ precisions where the better values are for the extratropics and the poorer values for the tropics. The precision for a particular measurement must be evaluated on a daily basis using the method described in the text.

[d]This is the range where the stated precision, accuracy, and resolution are applied. In this range, MLS measurements can be quantitatively interpreted as the average IWC for the volume sampled. IWC values above this range, currently giving qualitative information on cloud ice, require further validation for quantitative interpretation.

3.16.8 Desired improvements for future data version(s)

The IWC retrieval in v6.0*x* is a simple first-order conversion, applied independently to each T_{cir} measurement. Future development work on the MLS IWC retrieval should consider implementing a 2-D cloudy-sky radiative transfer model. This will allow IWC to be retrieved jointly with the T_{cir} measurements from adjacent scans.

3.17 Cloud Ice Water Path (IWP)

Swath name: `IWP` (stored as an additional swath in the `L2GP-IWC` file).

Useful range: MLS IWP is the ice water column above ~6 km

Units: g/m^2

Contact: Alyn Lambert <Alyn.Lambert@jpl.nasa.gov>

3.17.1 Introduction

MLS standard IWP is retrieved from cloud-induced radiances (T_{cir}) of the 240-GHz window channel at 650 hPa tangent pressure (see Figure 3.17.1). It represents a partial column above ~6 km and is stored in the v6.0*x* L2GP IWC file as a separate swath. For the IWP retrieval, T_{cir} is first converted to a near horizontal slant path (with a ~3° elevation angle) "hIWP", using the modeled T_{cir}–hIWP relation. The hIWP is then converted to the nadir IWP at the tangent point location and interpolated to the MLS standard horizontal grid.

As noted in Section 1.10.2, as of May 2024, the 190-GHz radiometer, which is used to measure water vapor, is operated only intermittently. When that radiometer is turned off and H_2O measurements are not available, a priori information for H_2O (based on climatological values) is used in the derivation of the IWP data product, adversely affecting its quality. Therefore, we do not recommend the use of IWP data during the periods when the 190-GHz radiometer is deactivated. Further details are given in Section 3.17.5.

3.17.2 Resolution

In the IWP ranges specified in the summary at the end of this section, each MLS measurement can be quantitatively interpreted as the average IWP for the volume sampled. The MLS IWP volume is a vertical column above ~6 km, with 60 km and 7 km along- and cross-track extent, respectively.

3.17.3 Precision

The precision values quoted in the IWP swaths do not represent the true precision of the data. The precision for a particular measurement must be evaluated on a daily basis using the method described in Section 3.17.5. The 3 g/m^2 precision given in the summary at the end of this section reflects *typical values* for MLS IWP measurements.

3.17.4 Accuracy

The IWP accuracy is ~50%, as estimated from comparisons of the earlier v2.2*x* MLS data with CloudSat; detailed analyses of the v2.2*x* error budget are given by *Wu et al.* [2009].

3.17.5 Data screening

Sensitivity: The standard IWP product has useful sensitivity up to 200 g/m^2; MLS measurements can be quantitatively interpreted as the average IWP for the volume sampled.

Use Temperature Status, Quality and Convergence: The user is advised to screen the IWP data using the `Status` field in the colocated temperature profile to exclude bad retrievals [*Schwartz et al.*, 2008]. In other words, only IWP values for which temperature `Status` is an even number should be used. Similarly, only use IWP values where the corresponding temperature profiles have `Quality` of 0.9 or larger. The temperature `Convergence` must be less than 1.03.

Other screening: The user is also recommended to screen the IWP data for significant cloud hits on a daily basis using the "2σ, 3σ" method described in the IWC section (3.16). The 3σ threshold is needed for cloud detection since a small percentage of clear-sky residual noise can result in a large percentage of "false alarms" in cloud detection. Note that this screening step cannot provide an adequate correction for the lack of retrieved H_2O during the periods when the 190-GHz radiometer is turned off, and so the additional screening step on H_2O `Status` given below takes precedence.

Additional screening on H_2O `Status`: As noted earlier, the quality of the IWP product is degraded when the 190-GHz radiometer is turned off, since only climatological H_2O is available in lieu of retrieved H_2O. In these circumstances, the IWP values cannot be quantitatively compared to measurements taken on surrounding days or in previous years when the 190-GHz radiometer was operational. Therefore, for quantitative studies, an additional screening step is recommended, whereby the `Status` field in the colocated H_2O profile is examined to remove affected IWP data. That is, only IWP values for which the `Status` flags of the corresponding H_2O profiles are an even number should be used in quantitative studies relying on IWP measurements.

3.17.6 Artifacts

High-latitude high-land surface can be mistakenly detected as a cloud when the atmosphere is very dry, allowing MLS 240-GHz radiances to penetrate down to the surface. Surface emission/scattering can then reduce brightness temperature. Surface effects (e.g., over the Antarctic Plateau) may introduce artificial IWP values as large as 10 g/m^2. In addition, the geographical location of MLS IWP is currently registered at the tangent point, which is ~2 profiles away from the actual location of the IWP column as shown in Figure 3.17.1. The user needs to correct this offset by replacing the IWP location with the one for two profiles earlier.

3.17.7 Comparisons with other datasets

Compared to v2.2*x* IWP, the v6.0*x* IWP values are similar and the random noise is slightly smaller (see Figure 3.17.2). Apart from those differences, the MLS v6.0*x* IWP is similar to the MLS v2.2*x* product described and validated by *Wu et al.* [2009]. A revised validation paper for IWP is not planned, and users are advised to read *Wu et al.* [2009] for more information.

Comparisons between v2.2*x* MLS and CloudSat IWP showed good agreement, with probability density function (PDF) differences <50% for the IWP range specified in the summary at the end of this section.

3.17.8 Desired improvements for future data version(s)

The IWP retrieval in v6.0*x* is a simple first-order conversion, applied independently to each T_{cir} measurement. Future development work on the MLS IWP retrieval should consider implementing a 2-D cloudy-sky radiative transfer model. This will allow IWP to be retrieved jointly with the T_{cir} measurements from adjacent scans.

3.17.9 Summary of Aura MLS v6.0*x* IWP Characteristics.

IWP column bottom: 6 km (estimated from MLS radiative transfer model calculations).

The calculation of the bottom height of the IWP column depends on the tropospheric water vapor loading and on the IWP itself, as discussed by *Wu et al.* [2009].

Typical precision: 3 g/m^2 is the typical 1σ precision.

The precision for a particular measurement must be evaluated on a daily basis using the method described in the text.

Accuracy: 50% (estimated from comparisons with CloudSat)

Resolution: 60 km along track, 7 km across track (the volume of air sampled by MLS)

Valid IWP range: ≤200 g/m^2

This is the range where the stated precision, accuracy, and resolution are applicable. In this range MLS measurements can be quantitatively interpreted as the average IWP for the volume sampled. IWP values above this range, currently giving qualitative information on cloud ice, require further validation for quantitative interpretation.

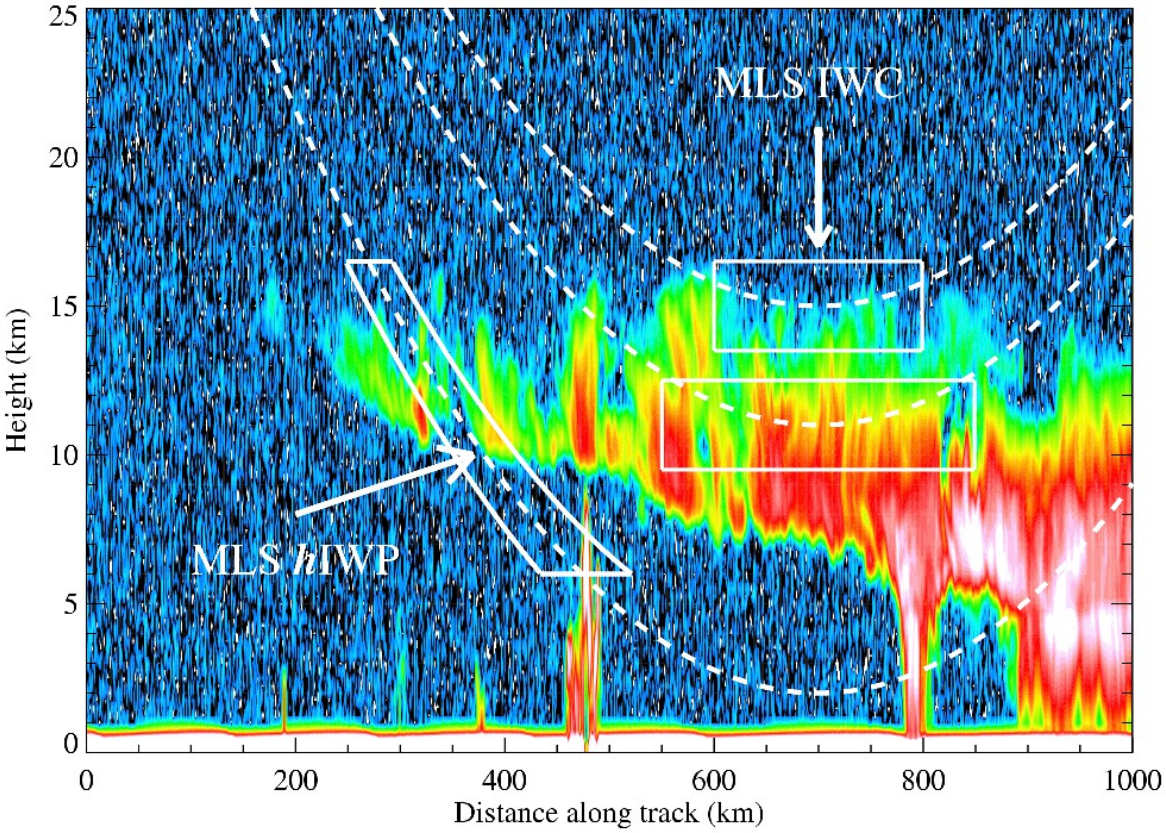

Figure 3.17.1: Diagram to illustrate the MLS IWC and IWP measurement. The dashed lines are the MLS tangential beams. At high tangent heights, the beams penetrate through the limb and become sensitive to a volume-averaged IWC, whereas, at low tangent heights, the MLS beams cannot penetrate through the limb due to strong gaseous absorption and become only sensitive to a partial slant column of IWP, with a shallow (~3°) angle, "hIWP". Note that the actual volume of the air represented by hIWP is centered ~300 km away from the tangent point, or ~2 profiles from the location of the nominal profile.

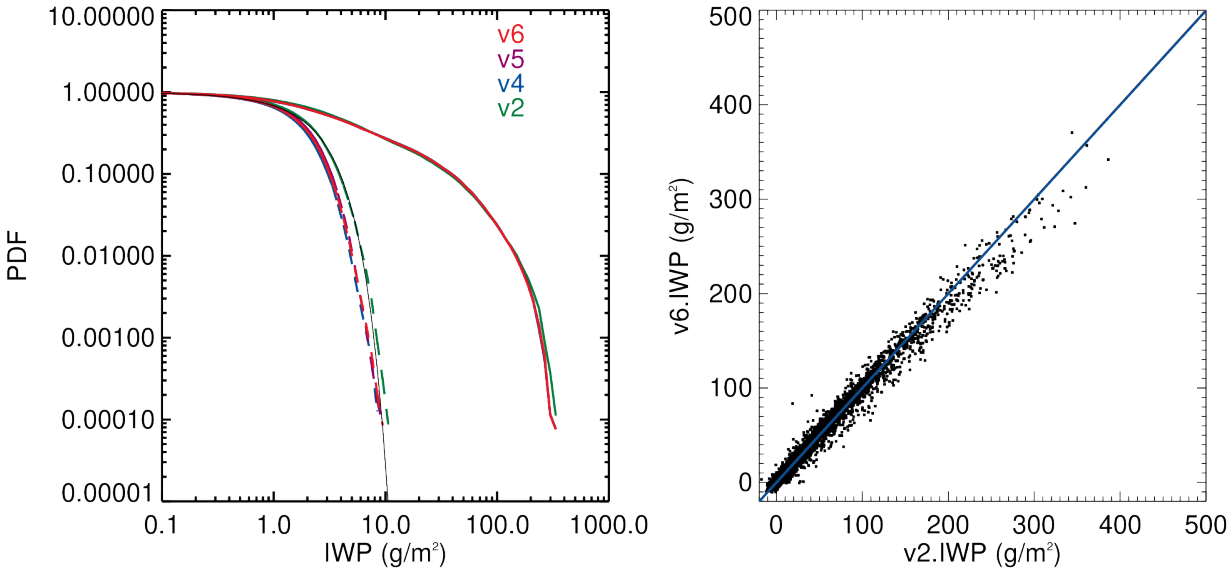

Figure 3.17.2: MLS v6.0*x*, v5.0*x*, v4.2*x* and v2.2*x* IWP comparisons for June 2009. (a) Left: Probability density functions (PDF) (v6.0*x* (red), v5.0*x* (purple), v4.2*x* (blue) and v2.2*x* (green)), with dashed lines showing the corresponding noise levels (obtained by folding the negative IWP values about the origin) and the thin black lines representing the Gaussian error function. (b) Right: Scatter plot of IWP v6.0*x* vs. v2.2*x* (black points), with a linear fit to the data shown as a blue line lying practically along the 1:1 line.

3.18 Nitrous Oxide (N_2O)

Swath name: N20

Useful range: 100–0.46 hPa

Product lead: Alyn Lambert <Alyn.Lambert@jpl.nasa.gov>

3.18.1 Introduction

The standard product for v6.0*x* N_2O is retrieved in the `CorePlusR2` phase, which also retrieves water vapor and other 190-GHz products, and replaces the customized v5.0*x* N_2O `NitrousOxide` retrieval phase. Improvements in the treatment of the N_2O retrieval in the v6.0*x* `CorePlusR2` phase are described in detail in Sections 1.4.1 and 2.8.

The decision to use the MLS "Band 3" 190-GHz radiances in preference to the "Band 12" 640-GHz measurements for v4.2*x* and later versions was undertaken in order to provide a continuous data product (`N2O-190`) for the entire mission. Earlier versions (prior to v4.2*x*) of the N_2O standard product relied on the "Band 12" 640-GHz (`CorePlusR4B`) retrieval; however, a noticeable reduction in quality of the Band 12 radiance signals became evident during June–August 2013. Band 12 was finally turned off on 6 August 2013, and the data collected on and after 7 June 2013 for `N2O-640` are not recommended for scientific use.

The 190-GHz N_2O data product in general shows slightly worse precision and resolution compared to those of the 640-GHz retrievals, although the 190-GHz precision is substantially better at 100–68 hPa. Data from `N2O-190` and `N2O-640` have been compared from launch until the end of Band 12 operations. A persistent, latitude-dependent, low bias over the pressure range 100 to 15 hPa is seen in the `N2O-190` product compared to `N2O-640` (see Figure 3.18.1). Other significant differences between the v6.0*x* `N2O-190` and `N2O-640` data, such as the resolution, precision, recommended pressure levels, and quality and convergence criteria, are noted below. The secondary v6.0*x* N_2O 640-GHz product is available for the period from launch until 6 June 2013 and is stored in the `L2GP-DGG` files in the `N2O-640` swath. Details of the retrieval method and validation results are presented by *Lambert et al.* [2007].

3.18.2 Resolution

The spatial resolution reported by the averaging kernel matrices is shown in Figure 3.18.2 for the 190-GHz measurements and Figure 3.18.3 for the 640-GHz measurements. For `N2O-190`, the vertical resolution is 5–7 km, and the horizontal along-track resolution is 330–525 km. For `N2O-640`, the vertical resolution is 4–6 km, and the horizontal along-track resolution is 330–600 km over most of the useful range of the retrievals.

The horizontal cross-track resolution is set by the 7 km width of the MLS 190-GHz field of view for all pressures. Note that the higher-frequency MLS 640-GHz measurements have a narrower 3 km field of view. The longitudinal separation of the MLS measurements is 10°– 20° over middle and lower latitudes, with much finer sampling in polar regions.

3.18.3 Precision

Precision as defined here is the 1σ uncertainty in the retrieved value calculated by the Level 2 algorithms and has been validated against the scatter about the mean of coincident ascending/descending MLS profile differences. The estimated precision on a single retrieved profile given in Tables 3.18.1 and 3.18.2 varies with height over ~15–20 ppbv for `N2O-190` and ~12–24 ppbv for `N2O-640`.

3.18.4 Accuracy

The accuracy values given in Table 3.18.2 were obtained for both v6.0*x* N_2O products by employing the same analysis approach as described by *Lambert et al.* [2007] for MLS `N2O-640` v2.2*x* data. These analyses quantify the systematic uncertainties associated with the MLS instrument calibration, spectroscopic uncertainty, and approximations in the retrieval formulation and implementation.

3.18.5 Data screening

Pressure range (`N2O-190`): 100–0.46 hPa

Pressure range (`N2O-640`): 100–0.46 hPa

Values outside this range are not recommended for scientific use. In the upper stratosphere and lower mesosphere, v6.0*x* N_2O requires significant averaging in order to obtain a scientifically useful signal-to-noise ratio, but see the note under "Artifacts" for issues at pressures smaller than 0.1 hPa.

Estimated precision: Only use values for which the estimated precision is a positive number.

Values where the a priori information has a strong influence are flagged with negative or zero precision and should not be used in scientific analyses (see Section 1.5).

Status flag: Only use profiles for which the `Status` field is an even number.

Odd values of `Status` indicate that the profile should not be used in scientific studies. See Section 1.6 for more information on the interpretation of the `Status` field.

Quality (`N2O-190`): Only profiles whose `Quality` field is greater than 0.8 should be used.

A small fraction of `N2O-190` profiles (typically less than 1.5%) will be discarded via this screening.

Convergence (`N2O-190`): Only profiles whose `Convergence` field is less than 2.0 should be used.

A small fraction of `N2O-190` profiles (typically less than 0.5%) will be discarded via this screening.

Quality (`N2O-640`): Only profiles whose `Quality` field is greater than 1.4 should be used.

A small fraction of `N2O-640` profiles (typically less than 1.5%) will be discarded via this screening.

Convergence (`N2O-640`): Only profiles whose `Convergence` field is less than 1.01 should be used.

A small fraction of `N2O-640` profiles (typically less than 0.5%) will be discarded via this screening.

Clouds: Clouds have little impact on the N_2O products at the recommended pressure levels. N_2O data can be used regardless of the value of the `Status` bits 16 (high cloud) or 32 (low cloud) used to indicate the presence of clouds. See "Artifacts" for more details.

3.18.6 Artifacts

There are occasional outliers at the largest pressures (lowest altitudes) in the `N2O-190` and `N2O-640` products. As with v5.0*x*, very thick clouds in the tropics produce a low rate of artifacts in the v6.0*x* N_2O products since improvements in the handling of radiances affected by clouds have reduced the frequency of outliers compared to older versions. The cloud bits of the `Status` field are too blunt a tool to identify these rare cases; rejecting profiles flagged with these bits would needlessly discard reasonable data. Screening using the `Convergence` and `Quality` fields (see above) is recommended to remove the majority of these data points.

The retrieval restricts N_2O values to be greater than −40 ppbv (approximately three times the retrieval noise level in the recommended pressure range) in order to prevent problems in the minimization search process. The low bound is applied at all levels, but it is only evident in the data for pressures less than 0.1 hPa, where the vertical smoothing is relaxed and the retrieval noise becomes comparable to the magnitude of the low-bound value. Accordingly, statistical averaging of the data (zonal means or longer time periods) cannot be applied successfully for pressures of or less than 0.1 hPa, as the −40 ppbv hard limit introduces a positive bias in any average.

3.18.7 Review of comparisons between MLS N_2O versions and other datasets

The v6.0*x* N_2O product shows significantly larger abundances (by up to 20%) in the lower stratosphere (100–10 hPa) than v5.0*x*, especially in the tropics (see Figure 3.18.4), improving agreement with expectations and other observations. Averaged monthly vertical profiles of v5.0*x* and v6.0*x* 190-GHz N_2O have been compared to matching ACE-FTS v5.2 profiles, and an example is shown for April 2019 in Figure 3.18.5, where

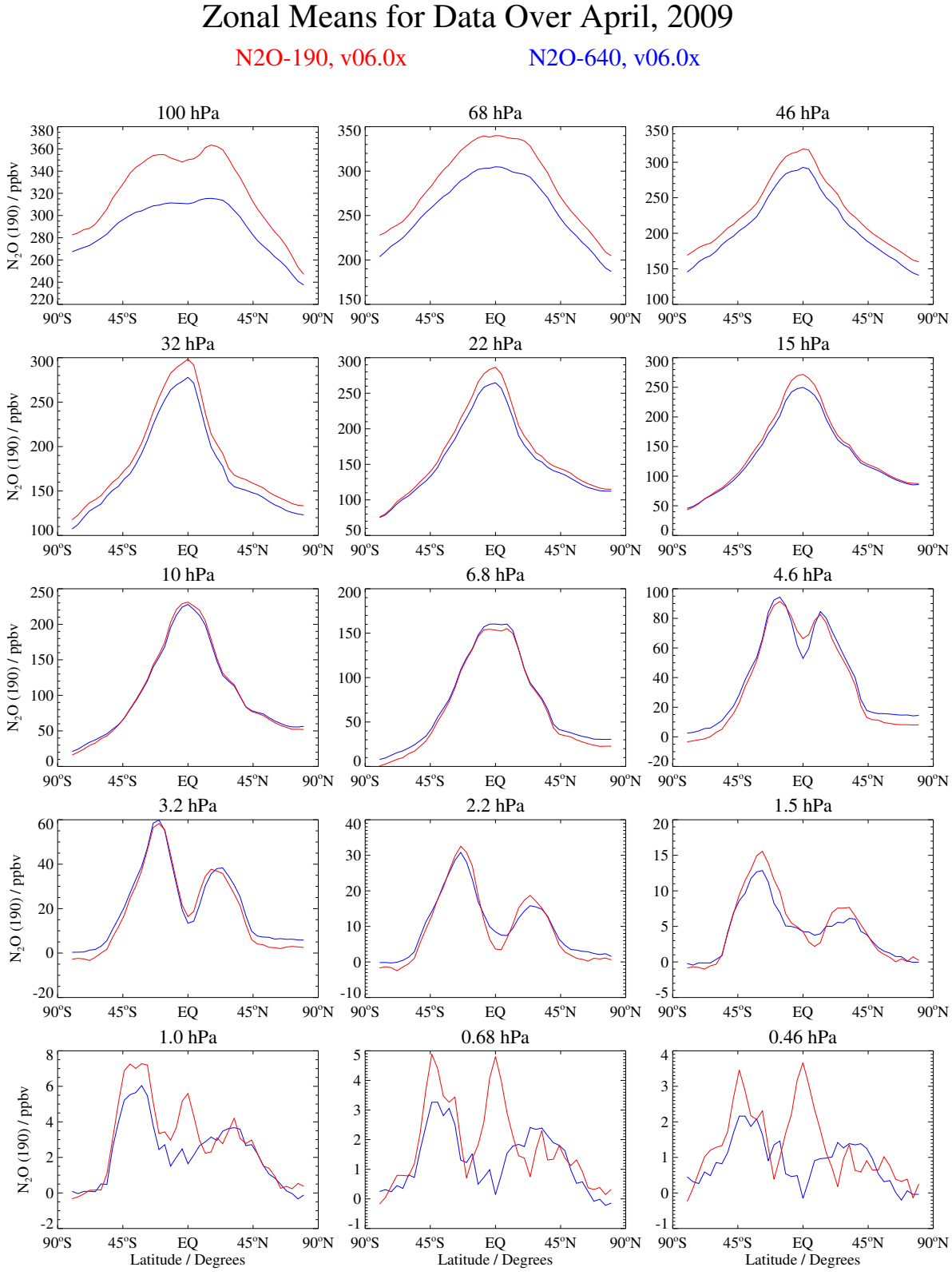

Figure 3.18.1: MLS v6.0*x* N20-190 and N20-640 comparison for April 2009

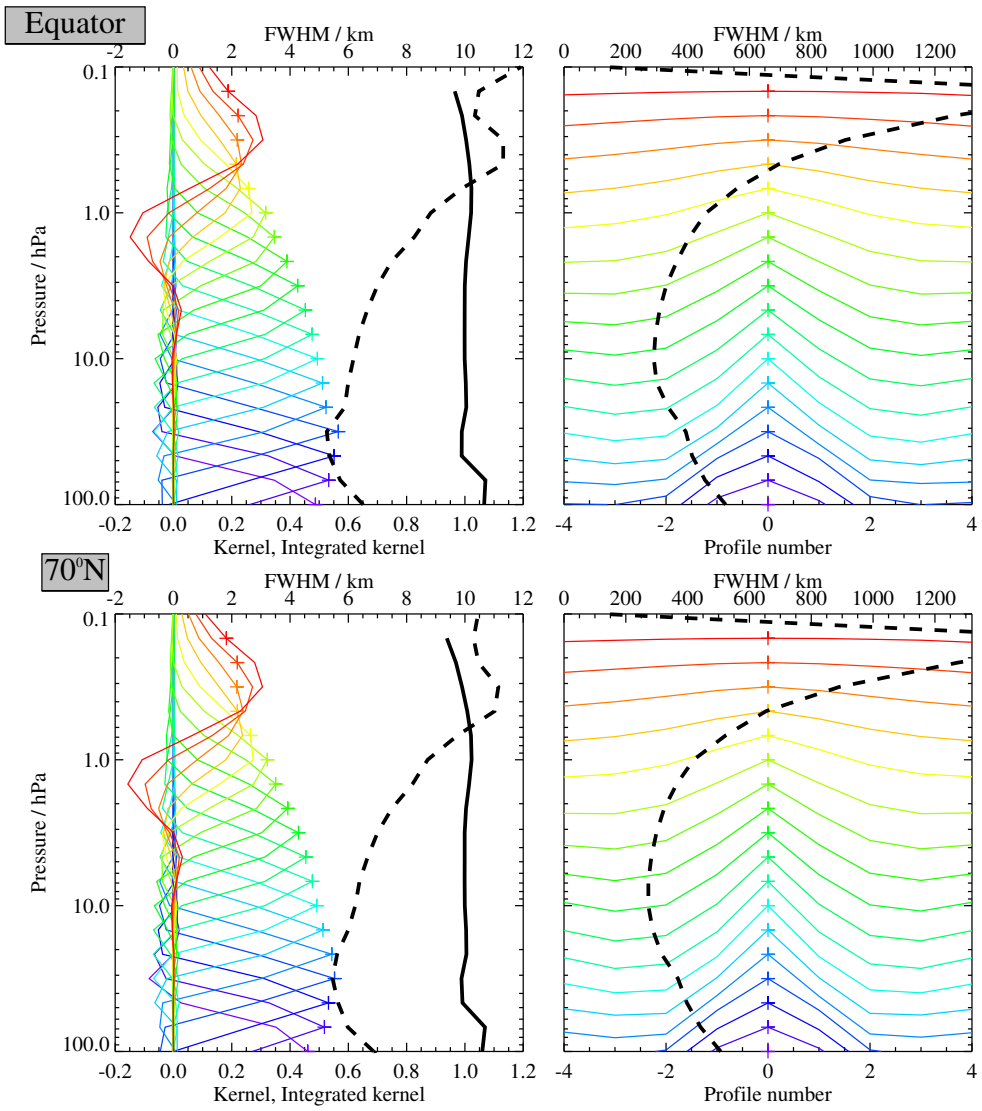

Figure 3.18.2: Typical two-dimensional (vertical and horizontal along-track) averaging kernels for the MLS v6.0*x* 190 GHz N_2O data at the equator (upper) and at 70°N (lower); variation in the averaging kernels is sufficiently small that these are representative of typical profiles. Colored lines show the averaging kernels as a function of MLS retrieval level, indicating the region of the atmosphere from which information is contributing to the measurements on the individual retrieval surfaces, which are denoted by plus signs in corresponding colors. The dashed black line indicates the resolution, determined from the full width at half maximum (FWHM) of the averaging kernels, approximately scaled into kilometers (top axes). (Left) Vertical averaging kernels (integrated in the horizontal dimension for five along-track profiles) and resolution. The solid black line shows the integrated area under each kernel (horizontally and vertically); values near unity imply that the majority of information for that MLS data point has come from the measurements, whereas lower values imply substantial contributions from a priori information. (Right) Horizontal averaging kernels (integrated in the vertical dimension) and resolution. The horizontal averaging kernels are shown scaled such that a unit averaging kernel amplitude is equivalent to a factor of 10 change in pressure.

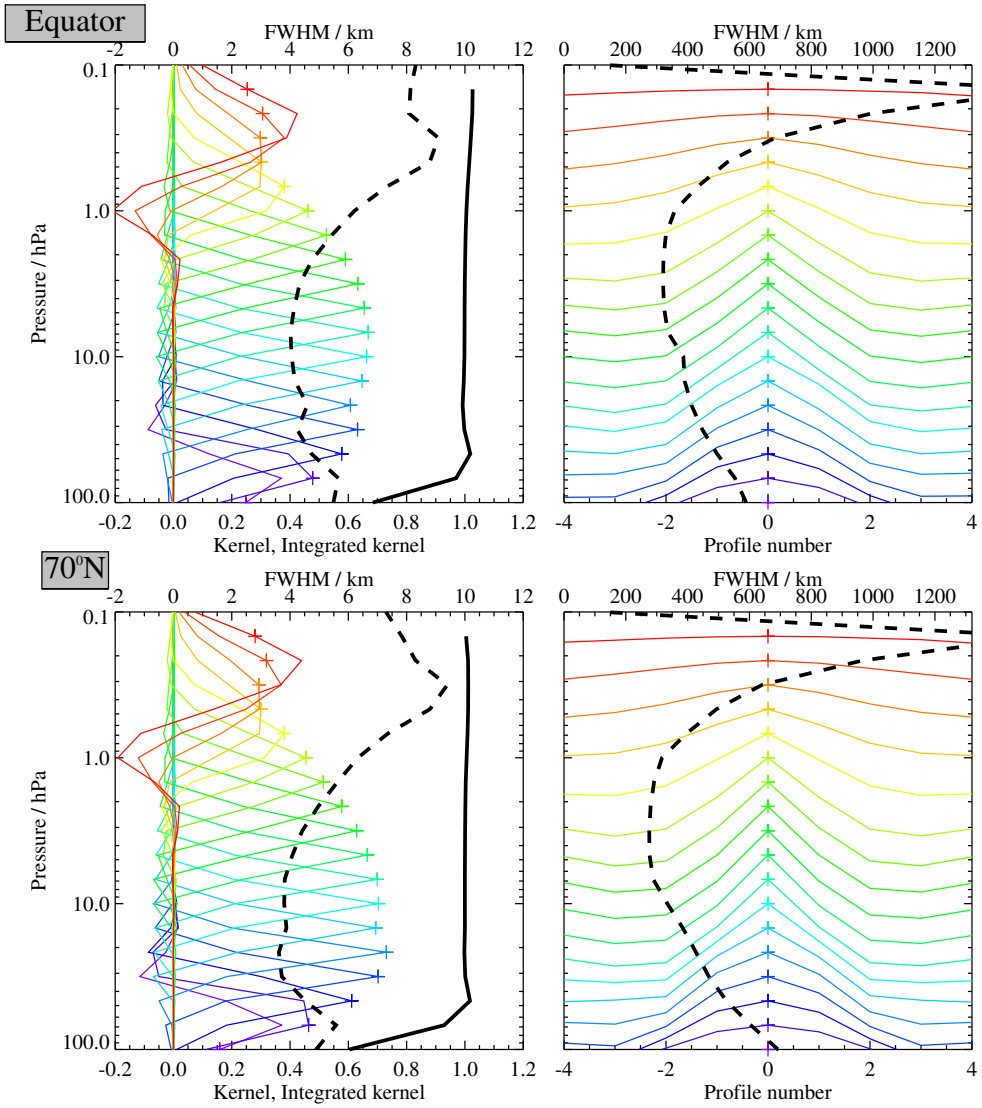

Figure 3.18.3: Typical two-dimensional (vertical and horizontal along-track) averaging kernels for the MLS v6.0*x* 640 GHz N_2O data at the equator (upper) and at 70°N (lower); variation in the averaging kernels is sufficiently small that these are representative of typical profiles. Colored lines show the averaging kernels as a function of MLS retrieval level, indicating the region of the atmosphere from which information is contributing to the measurements on the individual retrieval surfaces, which are denoted by plus signs in corresponding colors. The dashed black line indicates the resolution, determined from the full width at half maximum (FWHM) of the averaging kernels, approximately scaled into kilometers (top axes). (Left) Vertical averaging kernels (integrated in the horizontal dimension for five along-track profiles) and resolution. The solid black line shows the integrated area under each kernel (horizontally and vertically); values near unity imply that the majority of information for that MLS data point has come from the measurements, whereas lower values imply substantial contributions from a priori information. (Right) Horizontal averaging kernels (integrated in the vertical dimension) and resolution. The horizontal averaging kernels are shown scaled such that a unit averaging kernel amplitude is equivalent to a factor of 10 change in pressure.

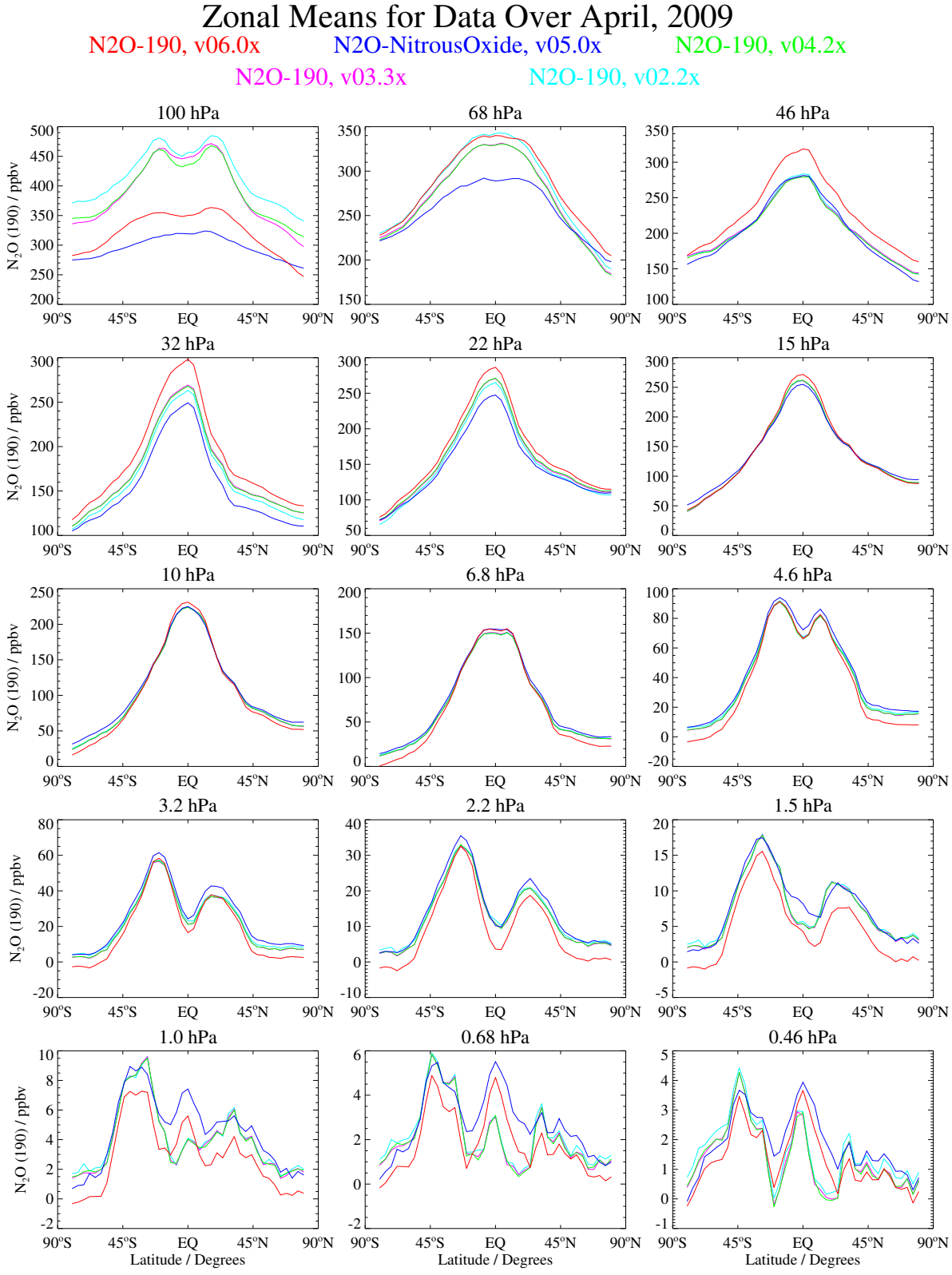

Figure 3.18.4: MLS v6.0*x* 190-GHz N_2O compared to v2.2*x*, v3.3*x*/v3.4*x*, v4.2*x*, and v5.0*x* for April 2009

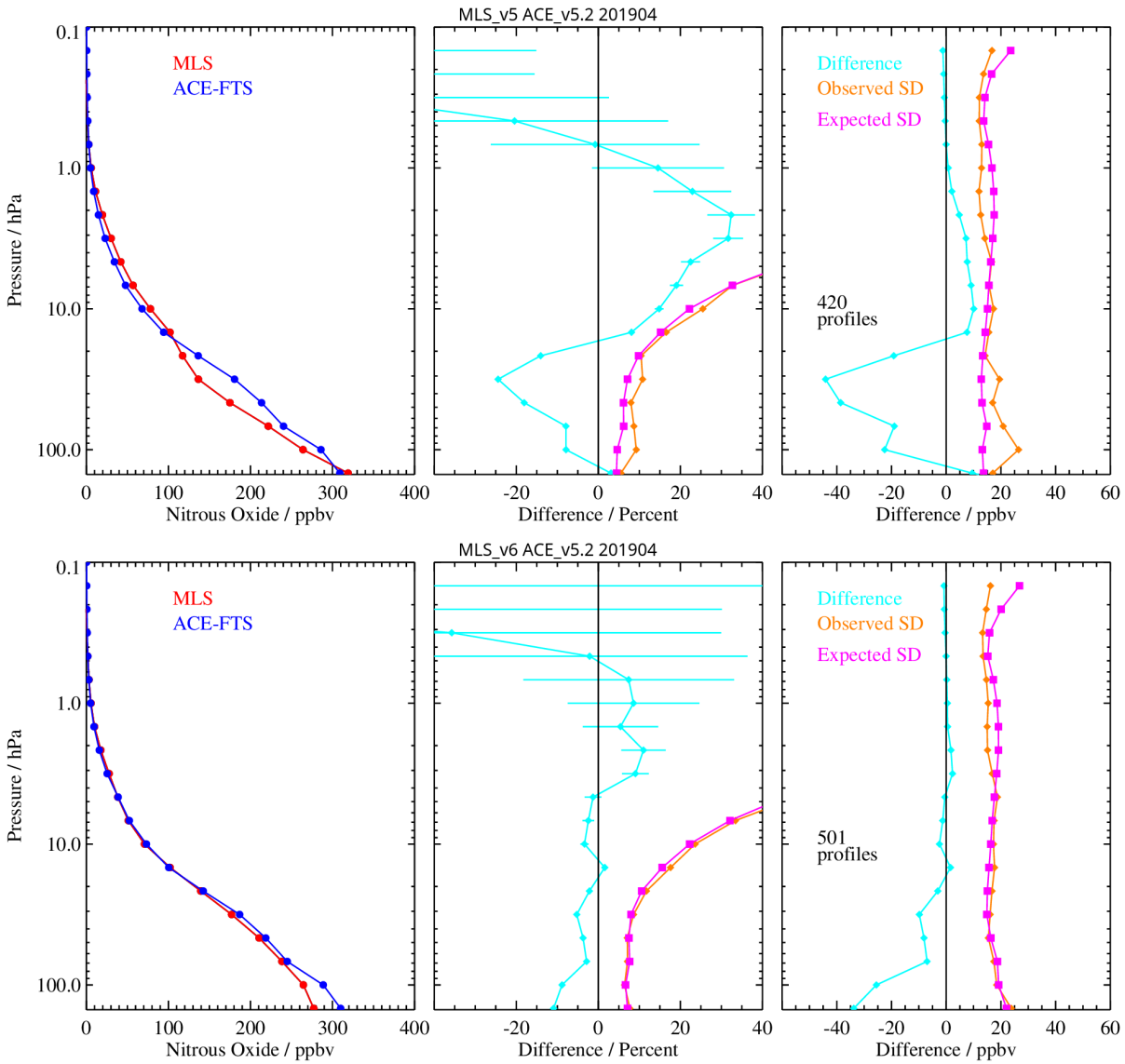

Figure 3.18.5: MLS v5.0*x* (upper) and v6.0*x* (lower) 190-GHz standard product N_2O compared to matching profiles for ACE-FTS v5.2 in April 2019. Left: MLS and ACE-FTS averaged matching profiles. Middle: percent differences, observed standard deviation (SD) of the differences, and expected SD based on the retrieval uncertainties. Right: same as for the middle panel but in mixing ratio units. The matching criteria are ±1° in latitude, ±8° in longitude, and ± 12 hours in time.

the MLS v6.0*x* N_2O values are seen to be in much better agreement with those from ACE-FTS throughout the stratosphere. These improvements for v6.0*x* 190-GHz N_2O are a result of the work described in Sections 1.4.1 and 2.8.

Average values for v6.0*x* 640-GHz N_2O are 20% larger than in v2.2*x* for the 100 hPa pressure level, up to 10% smaller at the 46–32 hPa levels, and within 5% for pressures greater than 22 hPa (see Figure 3.18.6). Differences between v6.0*x* and v5.0*x* 640-GHz N_2O are less than 10% at all levels. Apart from the differences noted above, the MLS v6.0*x* 640-GHz N_2O is similar to the MLS v2.2*x* product described and validated by *Lambert et al.* [2007]. Comparisons of v2.2*x* 640-GHz N_2O with coincident measurements by ACE-FTS, Odin/SMR, and Envisat/MIPAS, as well as balloon-borne observations, are shown by *Lambert et al.* [2007]. A revised validation paper for N_2O is not planned, and users are encouraged to read *Lambert et al.* [2007] for

more information.

3.18.8 Desired improvements for future data version(s)

Given the demonstrated utility of N_2O as a long-lived tracer in the lowermost stratosphere, should future development work on the 190-GHz MLS N_2O retrieval be undertaken, a priority will be to attempt to extend the retrievals to pressures greater than 100 hPa.

Table 3.18.1: Summary of Aura MLS v6.0*x* N_2O (N20-190) Characteristics.

Pressure	Resolution[a] V × H	Single-Profile Precision		Accuracy		Comments
hPa	km	ppbv	%	ppbv	%	
≤0.33	—	—	—	—	—	Unsuitable for scientific use
0.46	11.3 × 695	16	70	3	28	
0.68	9.9 × 560	18	75	3	18	
1.0	8.8 × 460	19	95	3	15	
2.2	7.5 × 365	20	95	5	12	
4.6	6.7 × 310	18	60	6	9	
10	6.2 × 290	16	24	8	7	
22	5.9 × 335	15	11	12	7	
46	5.4 × 415	15	7	27	11	
68	5.7 × 455	16	6	31	12	
100	6.5 × 525	18	6	33	12	
147	—	—	—	—	—	Unsuitable for scientific use
≥215	—	—	—	—	—	Unsuitable for scientific use

[a]Vertical and along-track horizontal resolutions; cross-track horizontal resolution is ~9 km.

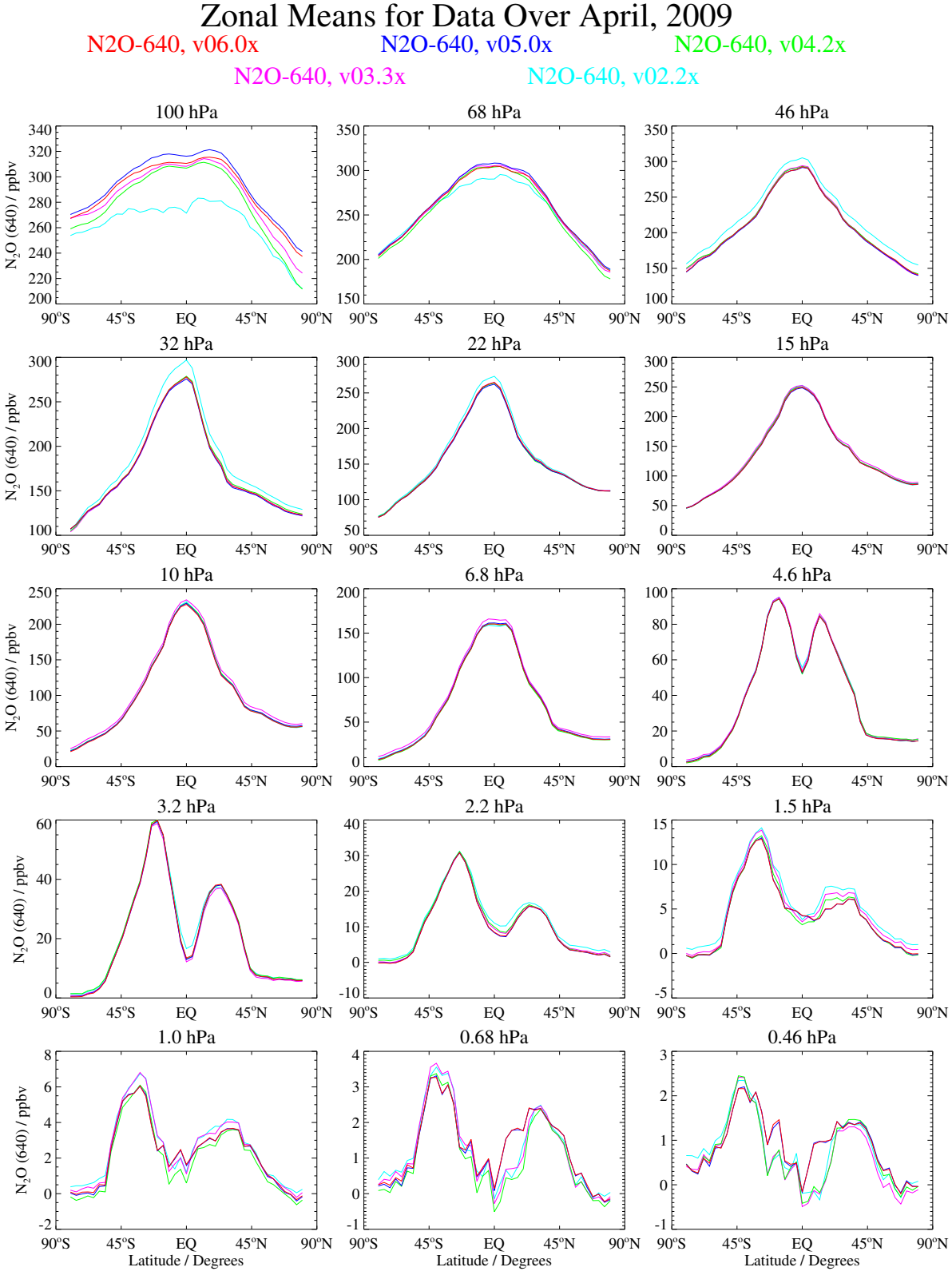

Figure 3.18.6: MLS v6.0*x* 640-GHz N_2O compared to v2.2*x*, v3.3*x*/v3.4*x*, v4.2*x*, and v5.0*x* for April 2009

Table 3.18.2: Summary of Aura MLS v6.0*x* N_2O (N20-640) Characteristics.

Pressure	Resolution V × H[a]	Single-Profile Precision		Accuracy		Comments
hPa	km	ppbv	%	ppbv	%	
≤0.33	—	—	—	—	—	Unsuitable for scientific use
0.46	8.8 × 550	12	80	2	23	
0.68	7.4 × 450	13	85	2	16	
1.0	6.3 × 370	14	105	3	12	
2.2	4.8 × 330	15	90	4	9	
4.6	4.2 × 335	14	40	5	8	
10	4.0 × 390	13	19	11	9	
22	4.6 × 410	13	10	24	13	
46	4.8 × 495	16	8	35	15	
68	5.8 × 555	20	8	32	12	
100	5.7 × 590	24	9	43	15	
147	—	—	—	—	—	Unsuitable for scientific use
≥215	—	—	—	—	—	Not retrieved

[a]Vertical and along-track horizontal resolutions; cross-track horizontal resolution is ~3 km.

3.19 Ozone (O_3)

Swath name: 03

Useful range: 261–0.001 hPa

Product leads: Lucien Froidevaux (stratosphere/mesosphere), Michael Schwartz (upper troposphere)

Contacts: Alyn Lambert (stratosphere/mesosphere) <Alyn.Lambert@jpl.nasa.gov>
Michael Schwartz (upper troposphere) <Michael.J.Schwartz@jpl.nasa.gov>

3.19.1 Introduction

In v6.0*x*, there are only minor changes in the standard O_3 product in comparison to v5.0*x*, with some impacts at the highest altitudes arising from small differences in temperature and/or tangent pressure. Generally, the retrievals and the resulting data for the standard ozone product have not changed significantly. As in previous versions, recommended v6.0*x* data screening is based on thresholds for `Status`, `Quality`, and `Convergence`.

Previously, the most significant improvement made between v4.2*x* and v5.0*x* MLS ozone was the use of a more accurate non-linear radiative transfer model (in place of an approximate linear model) for the digital autocorrelator (DAC) channels covering the center of the 236-GHz ozone line. This changed the ozone retrieval results for pressures less than about 0.02 hPa. While there is no comprehensive validation of global MLS ozone at this higher altitude range, there is clearly sensitivity to the nighttime ozone maximum mixing ratio near 0.001 hPa. The work of *Lee and Wu* [2020] had demonstrated that the v4.2*x* ozone retrieval (and by implication v6.0*x*) has enough radiance sensitivity in this altitude range to show strong dependence on the 11-year solar cycle variations (as for carbon monoxide).

As was the case for previous data versions, the v6.0*x* standard O_3 product is taken from a retrieval using 240-GHz radiances, providing sensitivity from the upper troposphere to high altitudes (and into the thermosphere, with v5.0*x* and v6.0*x* retrievals). In v6.0*x*, as in v5.0*x* and v4.2*x*, there is an optimized retrieval phase for the generation of the O_3 standard product prior to the phase that uses 240-GHz radiances to produce the standard carbon monoxide and nitric acid products. Table 3.19.1 summarizes typical O_3 resolution, precision (random uncertainty), and accuracy (systematic uncertainty) estimates versus pressure. Papers describing detailed validation of the MLS v2.2*x* ozone product and comparisons with other data sets were published in a special Aura validation issue of the *Journal of Geophysical Research*, see [*Froidevaux et al.*, 2008a; *Jiang et al.*, 2007; *Livesey et al.*, 2008].

Vertical oscillations in the UTLS and sensitivity to thick clouds were reduced in the development of v4.2*x* ozone through changes in the spectral form used to model cloud impacts on MLS radiances, through tightening of vertical smoothing at pressures greater than 67 hPa, and through retrieval of a spectrally flat atmospheric extinction over the ozone band for each limb view to better account for cloud inhomogeneity. No further reduction of the persistent oscillations in UTLS ozone has been achieved for the v6.0*x* ozone product.

In addition to the swath `03`, which gives the O_3 profile on 55 pressure surfaces, the `L2GP-03` files contain a swath, `03 column`, which is the integrated stratospheric column down to the thermal tropopause (WMO definition) calculated from MLS temperatures. The MLS temperature profiles from which the WMO tropopause is determined are used in the column calculation without regard to the screening rules given in Section 3.23; users may wish to reject ozone columns for which standard screening rejects (a small fraction of) the corresponding temperature profiles.

3.19.2 Comparison of v6.0*x* with past data versions

The vertical retrieval grid for the v6.0*x* ozone product is the same as that of v5.0*x*; between 316 hPa and 1 hPa, v6.0*x* ozone profiles are retrieved on 12 surfaces per decade, with a coarser retrieval grid at higher altitudes.

Figure 3.19.1 shows zonally averaged stratospheric and mesospheric ozone field comparisons between

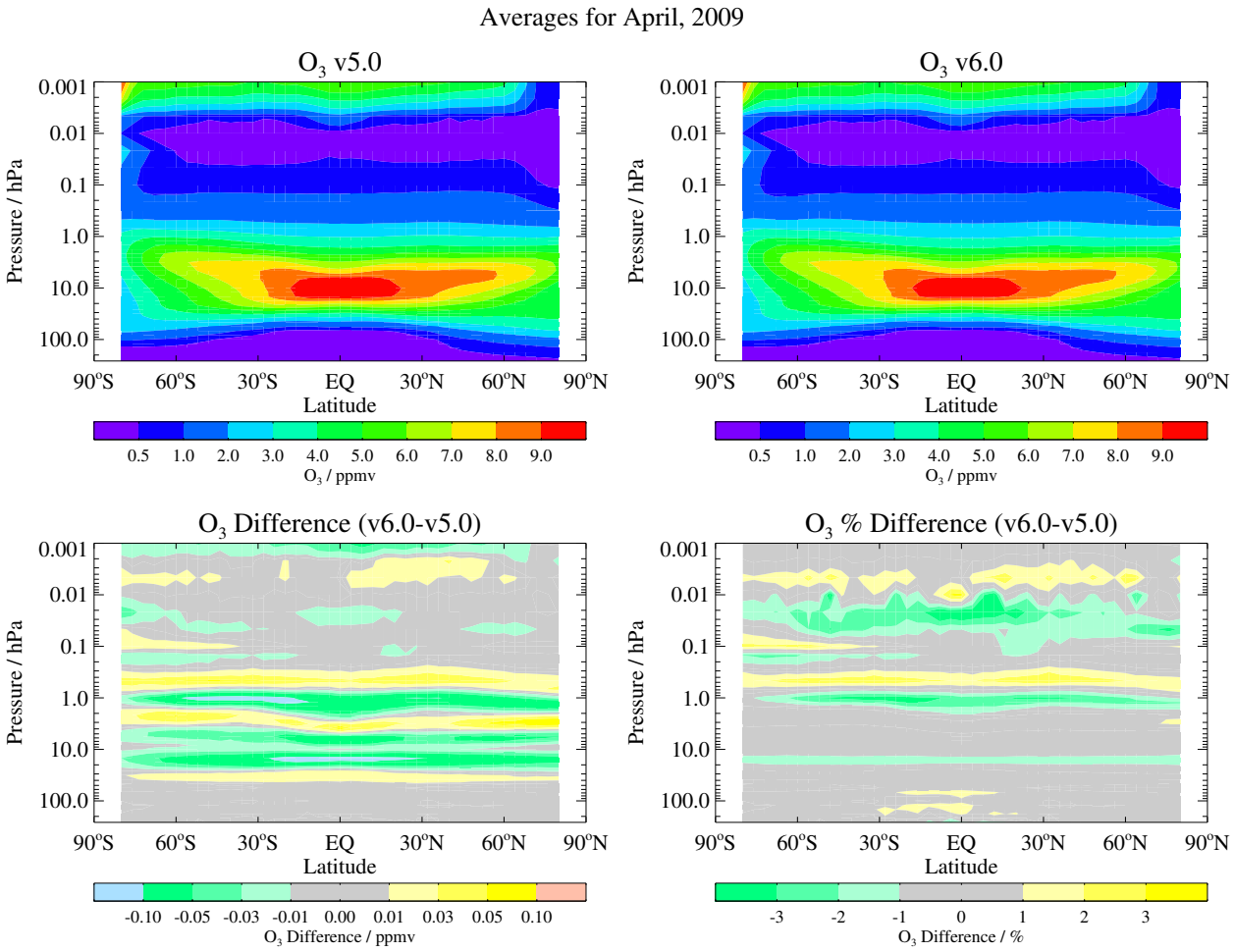

Figure 3.19.1: Zonal averages for stratospheric and mesospheric MLS ozone profiles during April 2009, showing the MLS v5.0*x* ozone mixing ratio contours versus latitude (top left panel), the v6.0*x* contours (top right panel), and their differences in ppmv (v6.0*x* minus v5.0*x*, bottom left panel) and percent (v6.0*x* minus v5.0*x* versus v5.0*x*, bottom right panel). Similar differences are seen in other months and years (not shown).

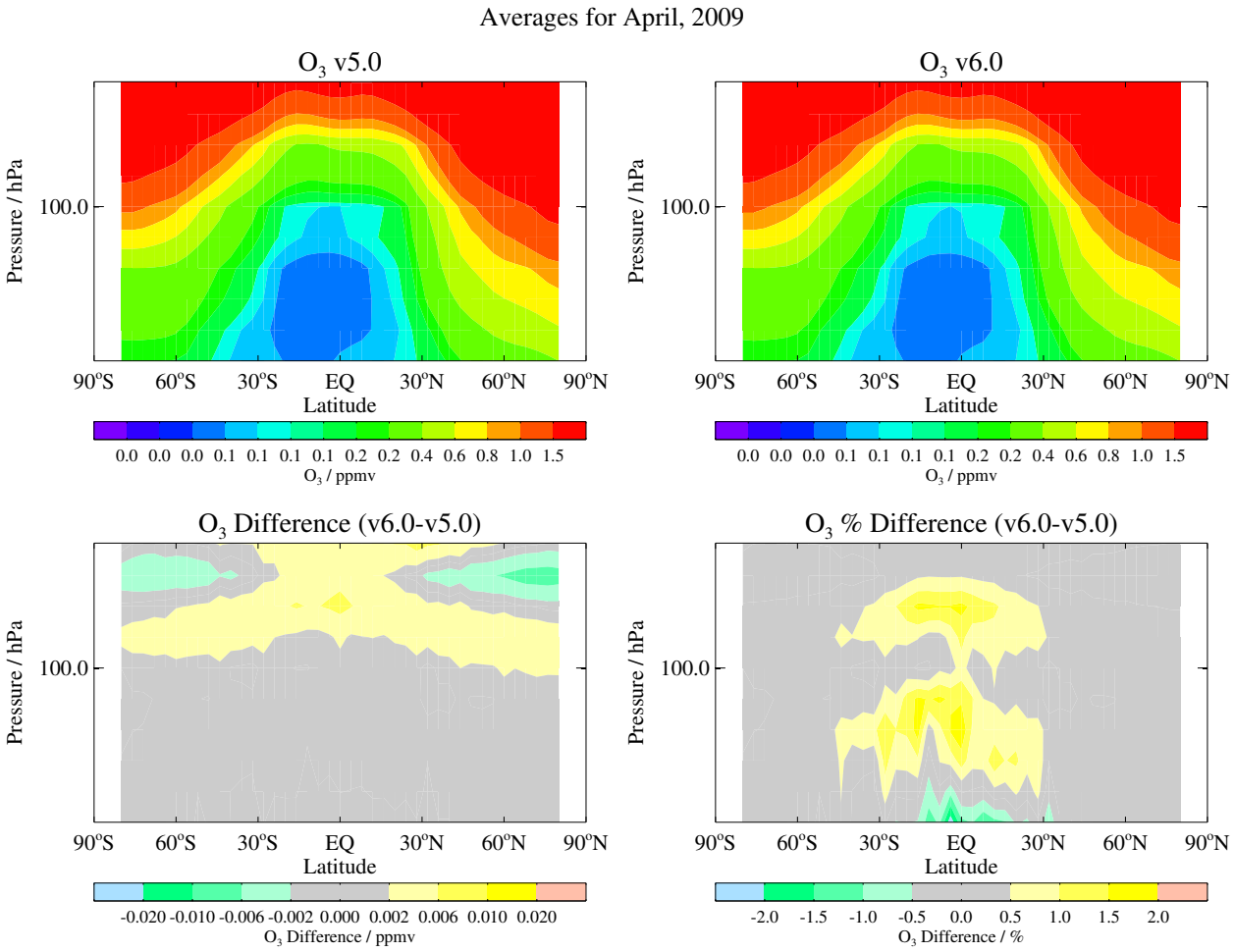

Figure 3.19.2: As Figure 3.19.1, but for the UTLS region, plotted here from 261 to 46 hPa. Similar differences are seen in other months and years (not shown).

v5.0*x* and v6.0*x* for the (full) month of April 2009, for properly screened profiles only; mean differences (ppmv and percent) are also shown. Similar plots focusing on the UTLS are provided in Figure 3.19.2. The absolute values of the differences between v5.0*x* and v6.0*x* above the tropopause for this year and month (but also for various other periods that we have checked) are typically less than 1 to 2%, and under 0.1 ppmv for the upper troposphere. In the UTLS, differences between the two versions are usually smaller than 2 ppbv, and less than 1 to 2%. There are some small differences between v5.0*x* and v6.0*x* versions regarding the locations of cloud-flagged profiles, as a result of an updated cloud characterization methodology (see Section 1.4.3).

Changes in the MLS stratospheric ozone columns between v5.0*x* and v6.0*x* are very small and not significant; daily zonal average column differences are typically less than one percent.

3.19.3 Resolution

Typical resolution values are provided in the summary Table 3.19.1, as derived from the full width at half maximum of typical averaging kernels in the vertical and horizontal (along-track) coordinates, shown in Figures 3.19.3 and 3.19.4 for the whole vertical range and the UTLS, respectively. The cross-track resolution is set by the 7-km width of the MLS 240-GHz field of view. Daily longitudinal separation of MLS measurements, set by the Aura orbit, is 10°–20° over middle and lower latitudes, with much finer sampling at the highest latitudes sampled in each hemisphere.

3.19.4 Precision

As found previously, the Level 2 precision values (Table 3.19.1) are often slightly smaller than the scatter observed in a narrow latitude band centered around the equator (where atmospheric variability is expected to be small) or obtained from a comparison between ascending and descending coincident MLS profiles.

Negative precision values for ozone sometimes occur at the largest and smallest pressure values within the recommended range. Precision values are flagged negative to indicate that retrieved values are strongly influenced by the a priori, although some geophysical information may also be present.

The typical precision of the MLS stratospheric column ozone product is 2–3%.

3.19.5 Accuracy

The accuracy estimates shown in Table 3.19.1 are from an analysis that propagates estimated systematic errors in MLS calibration, spectroscopy, etc., through the MLS measurement system, as described for v2.2*x* by *Read et al.* [2007]. The values shown here are intended to represent 2σ estimates of accuracy. Comparison of MLS O_3 with well-established data sets shows no evidence of significant biases overall, although the oscillations in the UTLS at low latitudes lead to some systematic effects that can reach 20–40%, depending on the pressure level. For more details, refer to the MLS validation papers by *Froidevaux et al.* [2008a], *Jiang et al.* [2007], and *Livesey et al.* [2008], and references therein; see also the comprehensive assessment of the long-term stability of MLS ozone measurements by *Hubert et al.* [2016].

3.19.6 Data screening

Pressure range: 261–0.001 hPa.

Values outside this range are not recommended for scientific use. Data at 0.00046 hPa represent a total column at and above that pressure level. Scientific use of these 0.00046 hPa data may be possible but requires consultation with the MLS team.

Estimated precision: Only use values for which the estimated precision is a positive number.

Values where the a priori information has a strong influence are flagged with negative or zero precision and should not be used in scientific analyses (see Section 1.5).

Status flag: Only use profiles for which the `Status` field is an even number.

Odd values of `Status` indicate that the profile should not be used in scientific studies. See Section 1.6 for more information on the interpretation of the `Status` field.

Quality: Only profiles whose `Quality` field is greater than 1.0 should be used.

Convergence: Only profiles whose `Convergence` field is less than 1.03 should be used.

Clouds: Scattering from thick clouds can lead to more systematic effects in the UTLS.

Most of the affected profiles are removed by the `Quality` and `Convergence` screening recommendations (although `Convergence` issues occur only rarely).

In summary, profiles with odd `Status` *or* `Convergence` above the convergence threshold *or* `Quality` below the quality threshold should be *rejected*. These criteria typically remove 1 to 2% of global daily data, with tropical latitudes showing somewhat larger data removal fractions of about 5%. This screening generally maintains sufficient coverage for a near-complete daily map (for any given day), even in the UTLS.

3.19.7 Review of comparisons with other datasets

Latitudinal and temporal variability observed in various correlative datasets are well reproduced by the MLS ozone product. Intercomparisons of a large variety of ozone measurements by satellite instruments were provided by *Tegtmeier et al.* [2013], as part of the analyses conducted by the SPARC Data Initiative. In that study, the Aura MLS ozone values compare quite favorably to the multi-instrument mean values as well as to SAGE II ozone. The temporal stability of the Aura MLS ozone dataset has been shown to be very good, in comparison to lidar datasets [*Nair et al.*, 2012]. The work by *Hubert et al.* [2016] includes both the lidar network and the ozonesonde network as references for a comprehensive satellite data intercomparison study. The latter authors show that average biases between MLS and latitudinally binned data from lidar and ozonesonde sites across the globe are typically within 5% or better, with poorer behavior (e.g., vertical oscillations) at low latitudes in the UTLS. In terms of drifts, the Aura MLS ozone dataset is shown (in the work by *Hubert et al.* [2016]) to be "very stable". MLS exhibits drifts with respect to data from the ground-based networks of about 1.5–2% per decade, with zero drift encompassed by the error bars (i.e., non-significant drifts), at least in the middle stratosphere. Notably, the Aura MLS ozone dataset has been used to assess the stability of other measurement systems, including ozonesondes [*Stauffer et al.*, 2022], OMPS [*Kramarova et al.*, 2018], and other satellite-derived datasets. The Aura MLS data, in combination with earlier datasets, provides a critical tool for the study of global ozone in a changing climate and during the ozone recovery period, as the total abundance of anthropogenic ozone depleting substances continues to decline.

3.19.8 Artifacts

Oscillations in UTLS ozone: While significant reduction in vertical oscillations in the UT ozone retrieval was accomplished in a previous version, oscillations are still evident in v6.0*x*, particularly at low latitudes. We have performed studies with different a priori values and have not found a satisfactory resolution of this issue. It is possible that the retrieval grid is slightly too fine; also, we are likely reaching the limit of possible retrieval remedies to the net impact of (known and unknown) systematic uncertainties on the MLS ozone retrievals. These oscillations are not expected to significantly impede studies of long-term trends.

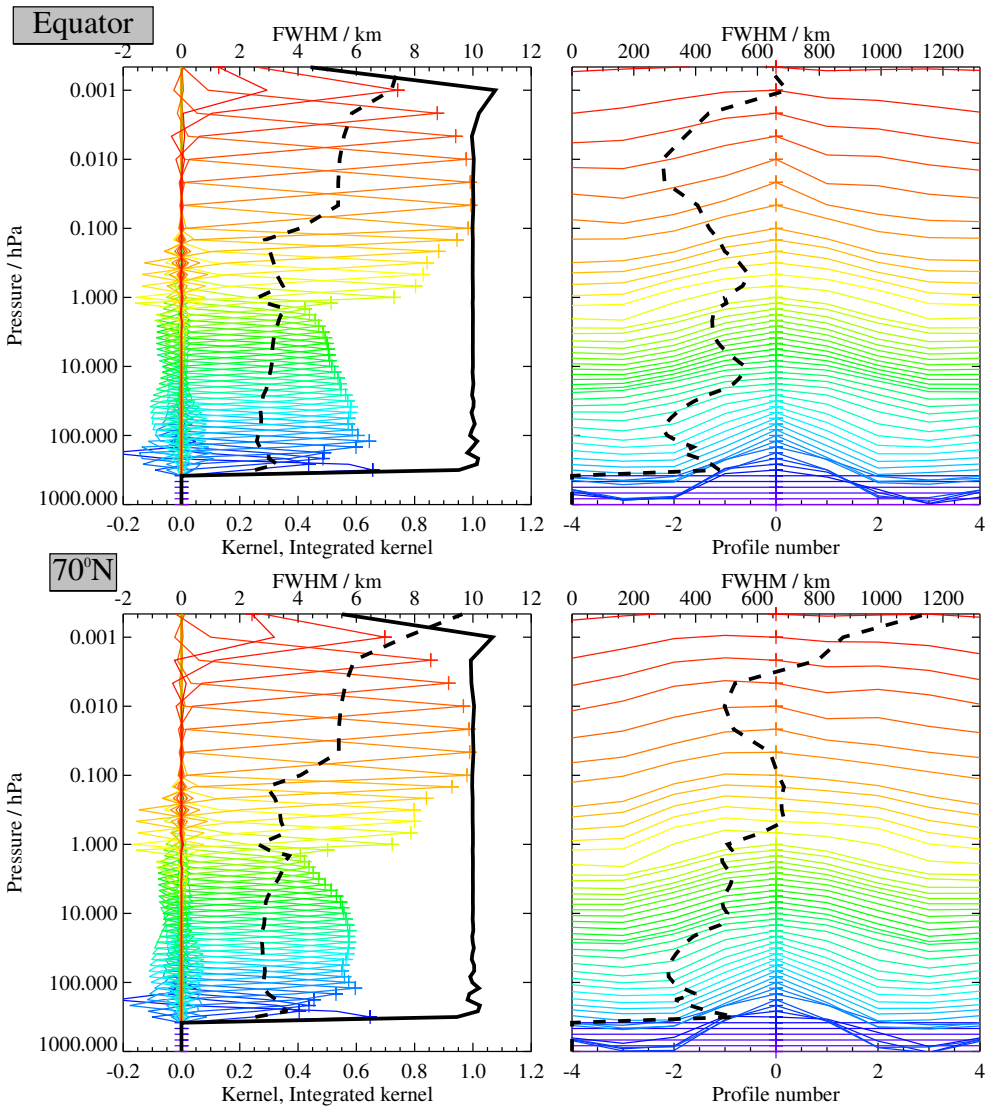

Figure 3.19.3: Typical two-dimensional (vertical and horizontal along-track) averaging kernels for the MLS v6.0*x* O_3 data at the equator (upper) and at 70°N (lower); variation in the averaging kernels is sufficiently small that these are representative of typical profiles. Colored lines show the averaging kernels as a function of MLS retrieval level, indicating the region of the atmosphere from which information is contributing to the measurements on the individual retrieval surfaces, which are denoted by plus signs in corresponding colors. The dashed black line indicates the resolution, determined from the full width at half maximum (FWHM) of the averaging kernels, approximately scaled into kilometers (top axes). (Left) Vertical averaging kernels (integrated in the horizontal dimension for five along-track profiles) and resolution. The solid black line shows the integrated area under each kernel (horizontally and vertically); values near unity imply that the majority of information for that MLS data point has come from the measurements, whereas lower values imply substantial contributions from a priori information. (Right) Horizontal averaging kernels (integrated in the vertical dimension) and resolution. The horizontal averaging kernels are shown scaled such that a unit averaging kernel amplitude is equivalent to a factor of 10 change in pressure.

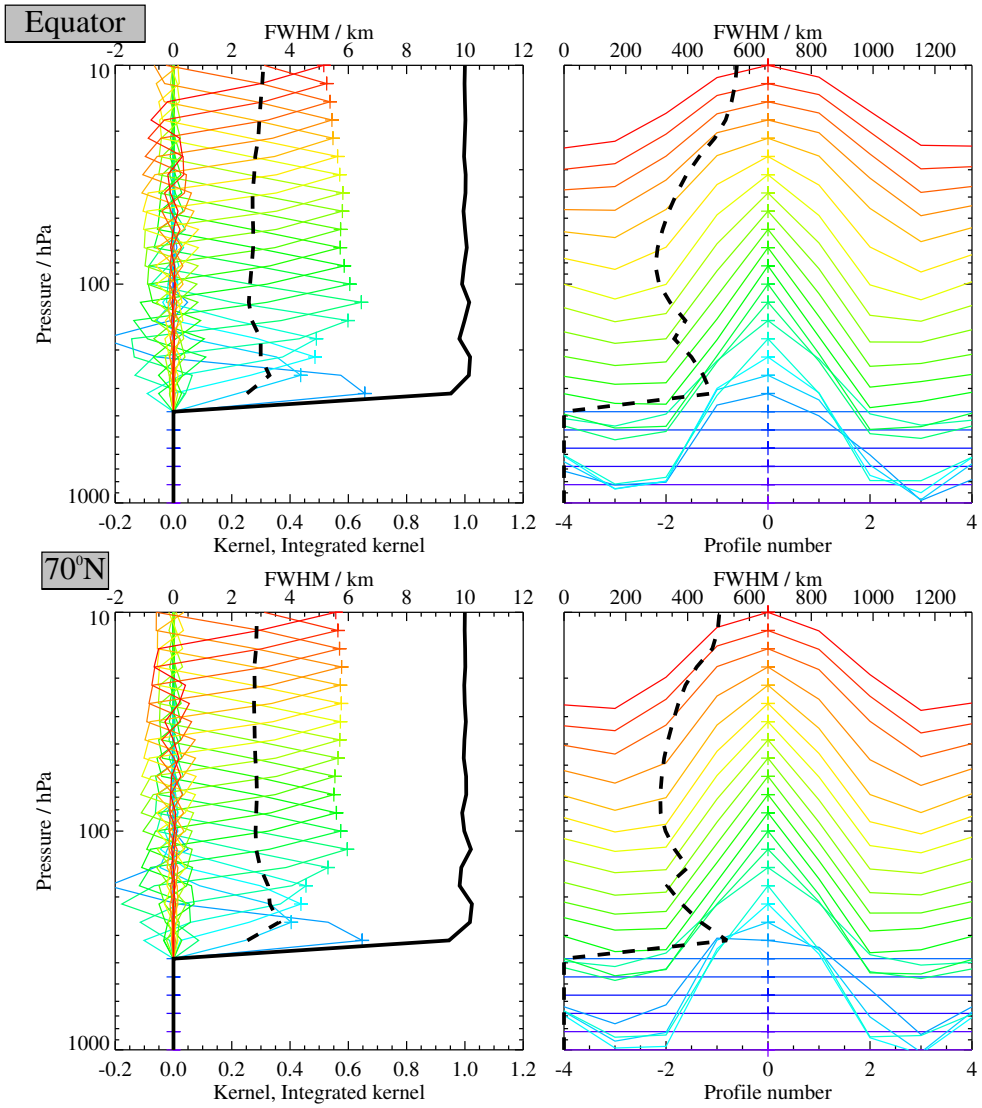

Figure 3.19.4: As for Figure 3.19.3 but for the upper troposphere and lower stratosphere region.

Table 3.19.1: Summary of Aura MLS v6.0*x* Ozone Characteristics

Pressure	Resolution[a] V × H	Single-Profile Precision		Accuracy[b]		Comments
hPa	km	ppmv	%	ppmv	%	
≤ 0.0005	—	—	—	—	—	Unsuitable for scientific use
0.001	7 × 650	3.4	> 40	0.9	30	Requires averaging
0.002	6 × 450	2.5	> 40	0.4	15	Requires averaging
0.005	5.5 × 350	1.7	> 200	0.3	25	Requires averaging
0.01	5.5 × 300	1.1	> 500	0.1	120	Requires averaging
0.02	5.5 × 300	0.7	> 100	0.15	40	Requires averaging
0.05	5.5 × 400	0.4	50	0.08	15	
0.10	4 × 450	0.4	40	0.09	8	
0.21	3 × 500	0.4	30	0.07	5	
0.46	3.5 × 600	0.3	20	0.1	6	
1	3 × 500	0.2	7	0.2	7	
2	3.5 × 500	0.15	3	0.2	5	
4.6	3 × 500	0.15	2	0.3	6	
10	3 × 500	0.1	2	0.4	6	
21	2.5 × 400	0.1	2	0.2	5	
46	2.5 × 350	0.06	3	0.2	8	
68	2.5 × 350	0.04	4	0.1	6	
100	2.5 × 300	0.04	20–30	[+0.005 + 7%][c]		
150	2.5 × 400	0.03	5–100	[+0.005 + 7%][c]		
215	3 × 400	0.02	5–100	[+0.01 + 10%][c]		
261	3.5 × 450	0.03	5–100	[+0.02 + 10%][c]		See note[d]
316	2.5 × 500	0.04	—	—	—	Not recommended
1000–464	—	—	—	—	—	Not retrieved

[a] Vertical and along-track horizontal resolutions; cross-track horizontal resolution is ~7 km.

[b] Primarily as estimated from systematic uncertainty characterization tests (based on a full day of retrieval perturbations). Stratospheric values are expressed in ppmv with a typical *equivalent* percentage value quoted.

[c] 261–100 hPa accuracies are the *sum of the ppmv and percentage* uncertainties; the ppmv terms arise from observed average positive biases in the MLS values relative to climatological tropical sonde data.

[d] Positive bias in the UT, but the mean annual variation is nevertheless well behaved versus tropical sonde data.

3.20 Hydroxyl Radical (OH)

Swath name: OH

Useful range: 32–0.0032 hPa

Product lead: Luis Millán <Luis.F.Millan@jpl.nasa.gov>

3.20.1 Introduction

The MLS THz radiometer is dedicated to measuring OH in the 2.5 THz spectral region. The methanol laser driving this radiometer, designed with an expected lifespan of 18 months, began to show signs of aging after five years of operation and was deactivated in December 2009. Between 2011 and 2014, the THz subsystem was reactivated annually for 30 days around August to capture data across an 11-year solar cycle. However, due to instrument aging, OH data from 2014 are notably noisier and have limited spatial coverage at middle to low latitudes. In September and October 2025, the THz subsystem was reactivated again; however, the limited data collected were of poor quality.

A description of OH data quality, precision, and systematic errors for an earlier version, v2.2*x*, is given by *Pickett et al.* [2006a]. The validation studies are described by *Pickett et al.* [2008] and *Wang et al.* [2008]. While the OH data quality is generally similar between v2.2*x* and v3.3*x*/v3.4*x*, there were significant improvements in v4.2*x* that have been carried into v5.0*x* and v6.0*x*. Prior to v4.2*x*, OH data near the mesospheric density peak, ~0.032 hPa, often showed a considerable amount of data flagged with negative precision, indicating the strong influence of a priori information, particularly in the summer hemisphere (or tropics for times near the equinox); this sometimes caused gaps in zonal mean time series. Starting with v4.2*x*, the software resolved this issue by fixing the overly tight a priori constraints. The resulting mesospheric OH data are less noisy and generally have somewhat larger values than previous versions for the problematic seasons/latitudes. Another improvement is the smaller bias at 10–15 hPa. Therefore, since v4.2*x*, applying a day-minus-night correction to reduce biases is only required at pressure levels of 21 and 32 hPa (v3.3*x*/v3.4*x* required such differences to be taken over a larger vertical range). Note that users may notice more zig-zags in nighttime mesospheric OH vertical profiles. This is a side effect of fixing the possible positive bias introduced by tight lower limits set in previous retrieval versions.

The estimated uncertainties, precisions, and resolution for v6.0*x* OH are summarized in Table 3.20.1.

3.20.2 Resolution

Figure 3.20.1 shows the OH averaging kernel for daytime and nighttime at 35°N. Daytime and nighttime kernels are shown separately as the largest natural variability in OH is diurnal. The vertical resolution is slightly different between day and night. The nighttime resolution is sufficient to allow the study of (for example) the "nighttime OH layer" around 82 km. The vertical width of the averaging kernel for pressures greater than 0.01 hPa is 2.5 km. The horizontal width of the averaging kernel is equivalent to a width of 1.5° (165 km distance) along the orbit. The changes in vertical resolution above 0.01 hPa are due mainly to use of a faster instrument vertical scan rate for tangent heights above 70 km. The horizontal resolution across track is 2.5 km. The averaging kernel and resolution for high and low latitudes are very similar to Figure 3.20.1 for most pressure levels. At the topmost two pressure levels, 0.0046 hPa and 0.0032 hPa, the vertical resolution is slightly better at the equator than at 70°N.

3.20.3 Precision

A typical OH profile and the associated precisions (for both v5.0*x* and v6.0*x*) are shown in Figure 3.20.2. The profile is shown in both volume mixing ratio (vmr) and density units. All MLS data are reported in vmr for consistency with the other retrieved molecules. However, use of density units (10^6 cm^{-3}) reduces the apparent steep gradient in the OH vertical profile, allowing one to see the profile with more detail, especially in the

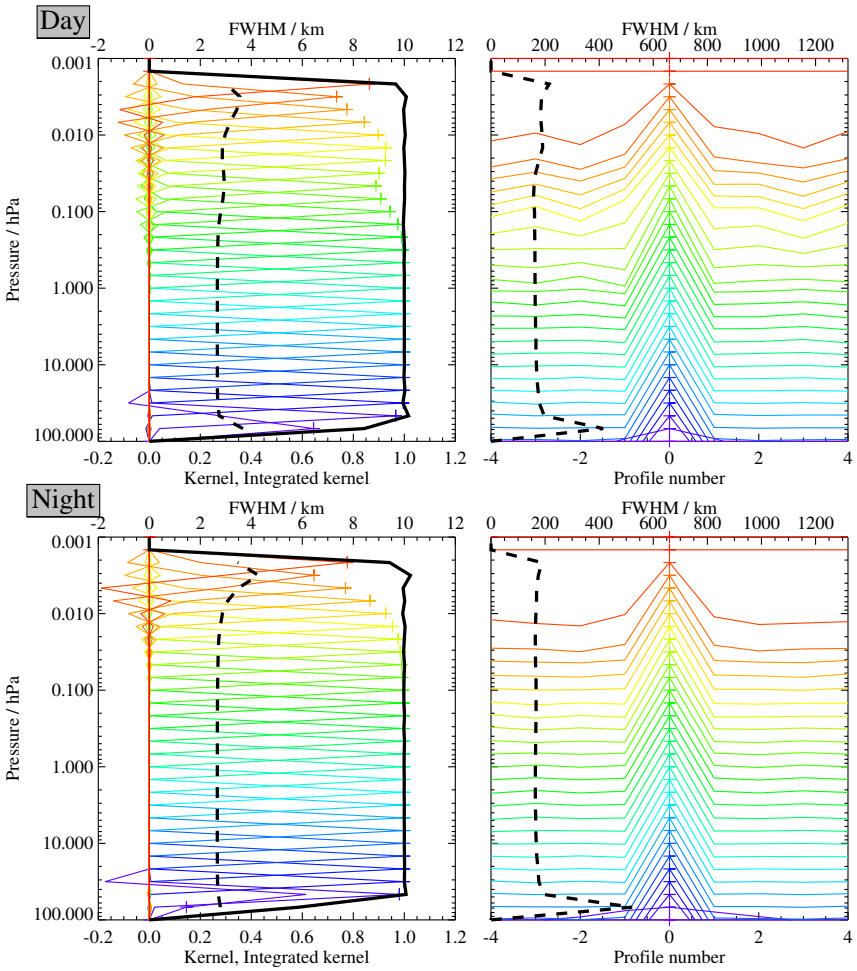

Figure 3.20.1: Typical two-dimensional (vertical and horizontal along-track) averaging kernels for the MLS v6.0*x* OH data at 35°N for daytime (upper) and nighttime (lower); variation in the averaging kernels is sufficiently small that these are representative of typical profiles. Colored lines show the averaging kernels as a function of MLS retrieval level, indicating the region of the atmosphere from which information is contributing to the measurements on the individual retrieval surfaces, which are denoted by plus signs in corresponding colors. The dashed black line indicates the resolution, determined from the full width at half maximum (FWHM) of the averaging kernels, approximately scaled into kilometers (top axes). (Left) Vertical averaging kernels (integrated in the horizontal dimension for five along-track profiles) and resolution. The solid black line shows the integrated area under each kernel (horizontally and vertically); values near unity imply that the majority of information for that MLS data point has come from the measurements, whereas lower values imply substantial contributions from a priori information. (Right) Horizontal averaging kernels (integrated in the vertical dimension) and resolution. The averaging kernels are scaled such that a unit change is equivalent to one decade in pressure.

stratosphere where most atmospheric OH is present. Additionally, at THz frequencies the collisional line width is approximately equal to the Doppler width at 1 hPa. Above 1 hPa, Doppler broadening is dominant and the peak intensity of OH spectral absorption is proportional to density, while below 1 hPa the peak intensity is proportional to vmr. The daytime OH density profile shows two peaks at ~45 km and ~75 km. The night OH profile exhibits the narrow layer at ~82 km [*Pickett et al.*, 2006b]. Precisions are such that an OH zonal average within a 10° latitude bin can be determined with better than 10% relative precision with one day of data (~100 samples) over 21–0.01 hPa. With 4 days of data, the 10% precision limits can be extended to 32–0.0046 hPa.

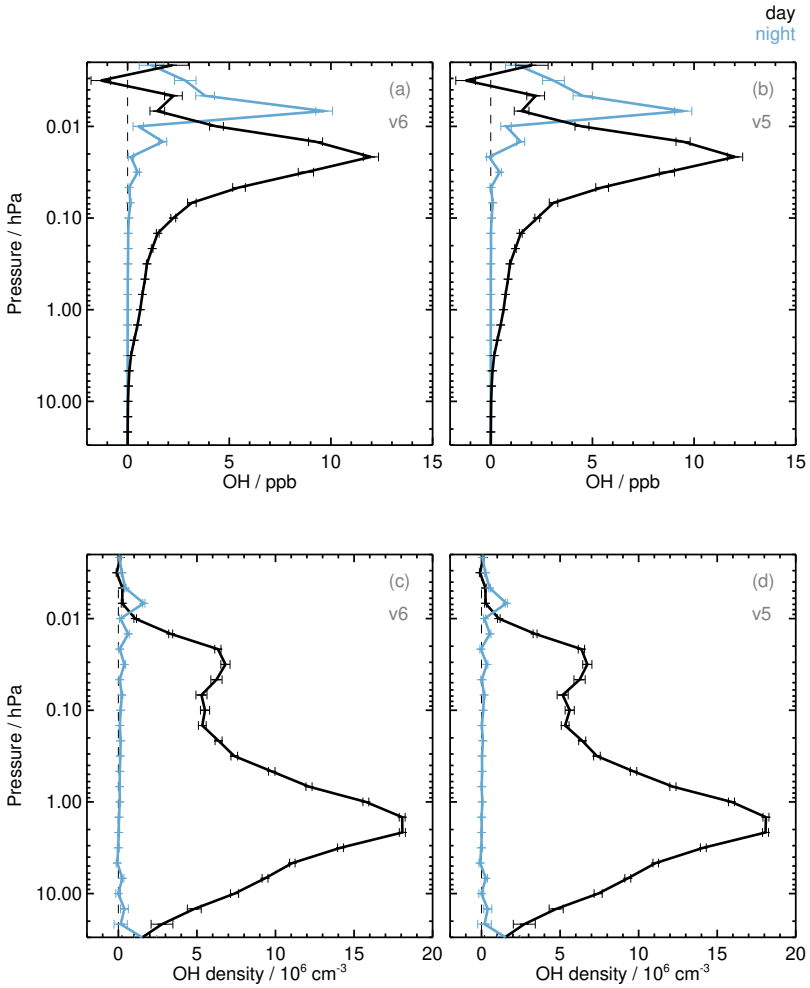

Figure 3.20.2: Zonal mean retrieved OH and its estimated precision (horizontal error bars) for 1 October 2005 averaged over 29°N to 39°N. The average includes ~100 profiles. Panel (a) shows v6.0*x* OH vmr vs. pressure for day (black) and night (blue). The retrieved night OH concentration is near zero for altitudes below 1 hPa. Note that a day/night difference is required for altitudes below 14 hPa. Panel (c) shows the same data in (a) converted into density units. Panels (b) and (d) are equivalent to (a) and (c) but using v5.0*x* OH data.

3.20.4 Accuracy

Table 3.20.1 summarizes the accuracy expected for OH. The effect of each identified source of systematic error on MLS measurements of radiance has been quantified and modeled [*Read et al.*, 2007]. These quantified effects correspond to either 2σ estimates of uncertainties in each MLS product or an estimate of the maximum reasonable uncertainty based on instrument knowledge and/or design requirements. Biases can be minimized by taking day/night differences at 32 and 21 hPa. For 14–0.1 hPa, the observed night OH concentration is small and day/night differencing is not ordinarily needed. The overall uncertainty is the square root of the sum of squares of the precision and accuracy.

3.20.5 Data screening

Pressure range: 32–0.0032 hPa.

Values outside this range are not recommended for scientific use.

Estimated precision: Only use values for which the estimated precision is a positive number.

Values where the a priori information has a strong influence are flagged with negative or zero precision and should not be used in scientific analyses (see Section 1.5).

Status flag: Only use profiles for which the `Status` field is an even number.

Odd values of `Status` indicate that the profile should not be used in scientific studies. See Section 1.6 for more information on the interpretation of the `Status` field.

Quality: MLS v6.0*x* OH data can be used irrespective of the value of the `Quality` field.

Convergence: Only profiles whose `Convergence` field is less than 1.1 should be used.

3.20.6 Artifacts

During some seasons, the Gas Laser Local Oscillator (GLLO) for the THz radiometer is automatically "relocked" as many as 5 times during a day, leading to data gaps. In these cases the `Status` flag is set to `257` and the profile is to be ignored. This can present a problem when compiling maps, because the missing data may appear at the same latitude and longitude on successive days.

3.20.7 Review of comparisons with other datasets

OH data from MLS v2.2*x* software were validated with two balloon-borne remote-sensing instruments and with ground-based column measurements. Details of the comparison are given by *Pickett et al.* [2008] and *Wang et al.* [2008]. Comparisons between v2.2*x* and v6.0*x* show no significant differences except for in the mesosphere, where v6.0*x* OH values are somewhat larger and less noisy in the summer hemisphere (or tropics when near equinox).

Table 3.20.1: Summary of Aura MLS v6.0*x* OH Characteristics

Pressure hPa	Resolution[a] V × H km	Precision[b] (day / night) 10^6 cm^{-3}	Accuracy 10^6 cm^{-3}	Comments
<0.003	—	—	—	Unsuitable for scientific use
0.003	4 × 200	0.4 / 0.4	0.5	
0.01	3 × 200	1.0 / 0.7	2	
0.1	3 × 200	3 / 0.5	1.0	
1.0	3 × 200	2 / 0.5	1.0	
10	3 × 200	3 / 2	1.0	
32–21	3 × 200	10 / 9	1.5	Use day/night difference
>32	—	—	—	Unsuitable for scientific use

[a]Vertical and along-track horizontal resolutions; cross-track horizontal resolution is ~3 km.
[b]Precision on an individual profile

3.21 Relative Humidity with respect to Ice (RHI)

Swath name: RHI

Useful range: Mean layer value for pressures greater than 383 hPa, vertically resolved profile from 316–0.001 hPa.

Product lead: William Read <william.g.read@jpl.nasa.gov>

3.21.1 Introduction

The vertical grid for the relative humidity with respect to ice (RHI) product is 12 levels per decade change in pressure for 1000–1.0 hPa, thinning to 6 levels per decade for 1.0–0.1 hPa, and finally 3 levels per decade for 0.1–10^{-5} hPa. The RHI product is a fusion of results from two separate retrievals. From 1000 hPa to the 383 hPa retrieval level, RHI is retrieved directly from optically thick radiances using measurement and retrieval principles similar to those employed for nadir sounding humidity instruments (e.g., TOVS). All grid levels between 1000–383 hPa are filled with a uniform value, representing the vertically weighted mean relative humidity of a broad layer (~4–6 km) that peaks between ~350 hPa (in the moist tropics) and ~650 hPa (typical for dry high latitudes). This humidity is used as a lower-altitude constraint and a priori for the vertically resolved H_2O product (for which 316 hPa is the lowest-altitude retrieval level). From the 316 hPa retrieval level to 10^{-5} hPa, RHI is derived from the standard products of water vapor mixing ratio and temperature using the Goff-Gratch ice humidity saturation formula. Validation of the v2.2*x* RHI product is presented by *Read et al.* [2007]. Table 3.21.1 summarizes the RHI precision, resolution, and accuracy. The precision and accuracy figures for v6.0*x* have been updated based upon error analysis following the methods described by *Read et al.* [2007]. The equivalent table for v5.0*x* in the previous edition of this document [*Livesey et al.*, 2022] included some analysis errors and footnote mislabeling that were discovered while performing this investigation. Those errors are corrected in Table 3.21.1 herein for v6.0*x*.

3.21.2 Changes from v5.0*x*

There are no changes between v5.0*x* and v6.0*x* for the single-layer 1000–383 hPa retrieval approach. RHI for the 316 hPa retrieval level and smaller pressures is a derived product, and any changes reflect those in the input H_2O (Section 3.10) and temperature (Section 3.23) products.

Figure 3.21.1 compares MLS v2.2*x*, v3.3*x*/v3.4*x*, v4.2*x* and v5.0*x* RHI to v6.0*x*. The changes seen reflect changes in temperature resulting from adjustments made to the filter shapes in the temperature-sounding channels and changes in H_2O resulting from an adjustment made to the MLS 190-GHz radiance observations in order to improve the N_2O product (see Sections 1.4.1, 2.8, and 3.18).

Relative humidity data at the 383 hPa retrieval level and greater pressures are derived from a retrieval of RHI over a single broad layer (using low-limb-viewing MLS wing channel radiances); a similar approach is employed by NOAA nadir-viewing operational humidity sounders such as TOVS. As noted by *Read et al.* [2007], the MLS v2.2*x* RHI retrievals at pressures greater than 383 hPa were likely to be ~30% too high, based on comparisons with AIRS. The accuracy of the low-altitude RHI retrieval is highly sensitive to the assumed transmission efficiency of the MLS optics system. In v3.3*x*/v3.4*x* (and later versions), the assumed value of the MLS antenna transmission efficiency was adjusted empirically (within the uncertainty range established from MLS pre-launch calibration) to give better agreement with version 4.0.9.0 of AIRS in the tropics. It should be noted that the changes to sideband fractions and pointing offsets detailed in Section 3.10 do not overwrite the transmission efficiency change implemented in v3.3*x*/v3.4*x* and should not impact the low-altitude RHI retrieval for either v5.0*x* or v6.0*x*. The results of this retrieval provide an a priori and profile constraint for the humidity profile at the 383 hPa retrieval level and at greater pressures, where the standard H_2O product is not retrieved.

The third column in Figure 3.21.1 shows the mean estimated single-profile precision and the measured

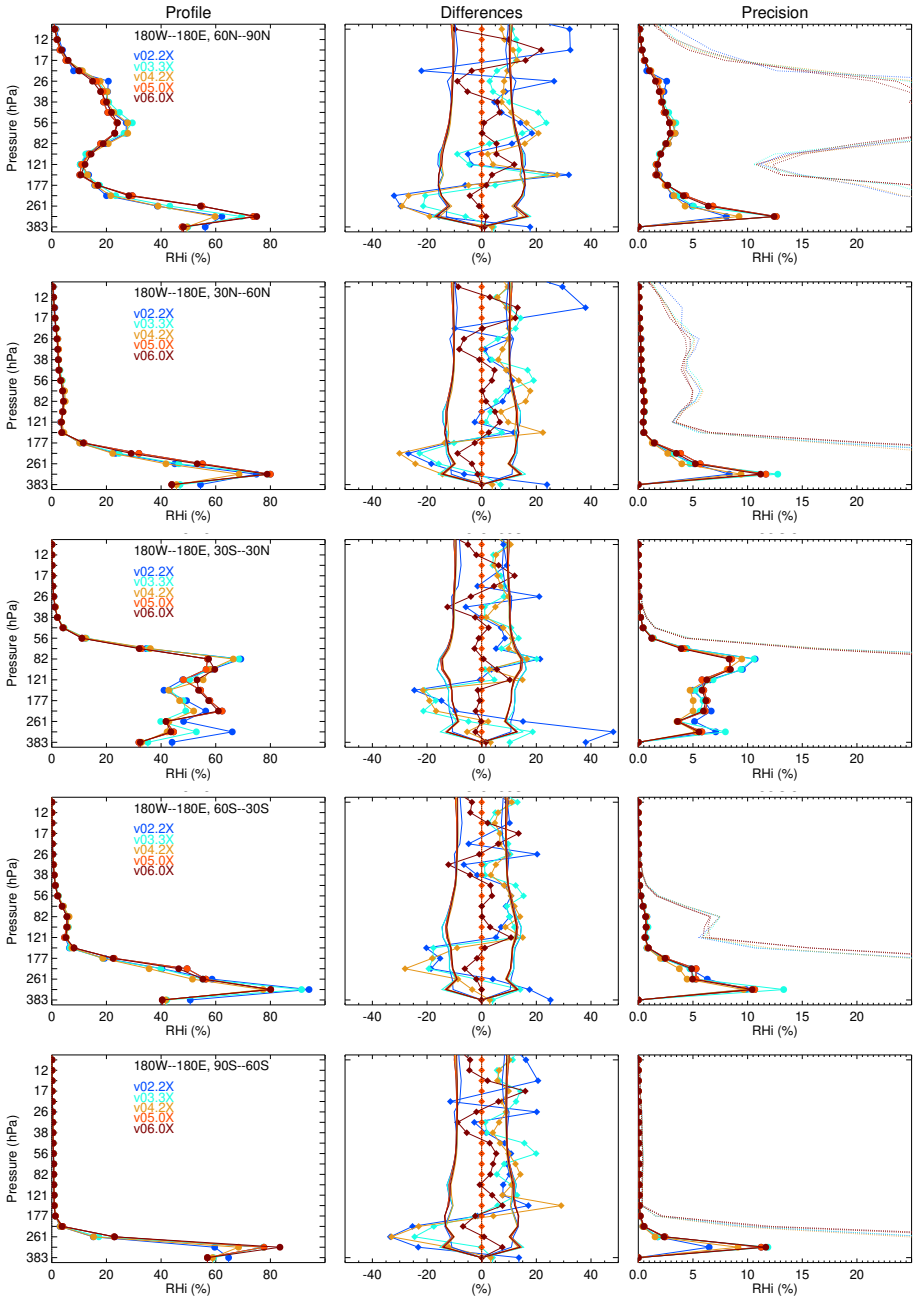

Figure 3.21.1: Comparisons of MLS v2.2*x* (blue), v3.3*x*/v3.4*x* (cyan), v4.2*x* (mustard), v5.0*x* (orange), and v6.0*x* (dark red) RHI profiles (in percent) for January-February-March 2005 in five latitude bands. Results for other time periods (not shown) are similar. Left panels show mean profiles, center panels show the mean differences from v5.0*x* (colored lines with diamonds) surrounded by each version's estimated precision (colored lines with no symbols), and right panels show the estimated retrieval precision (solid lines with bullets) and measured variability (which includes atmospheric variability about the mean profile; dotted lines).

variability (which reflects a combination of instrument noise and atmospheric variability). All versions show very similar precision, and in the upper troposphere and lower stratosphere these precision estimates are much smaller than the measured atmospheric variability. The precision for 383 hPa (and larger pressures) is reported in the L2GP RHI files as 0% by mistake. The actual precision is typically 0.2%.

3.21.3 Resolution

RHI for the 316 hPa retrieval level and smaller pressures is a derived product, and therefore a retrieval averaging kernel is not directly available. An estimate for the spatial resolution (vertical × along track) of this product is a combination of the temperature and H_2O resolutions. Typically H_2O has poorer horizontal resolution and temperature has poorer vertical resolution. Therefore, as a first-order estimate of spatial resolution, the horizontal resolution of the H_2O product should be assumed, along with the vertical resolution for temperature (see Sections 3.10 and 3.23). The cross-track resolution should be assumed to be 12 km, the larger of the temperature and H_2O cross-track resolutions. These estimated resolution values are only valid under the assumption that the mean log(H_2O) does not change appreciably over the broader temperature measurement volume. The longitudinal separation of the MLS measurements, set by the Aura orbit, is 10°–20° over middle and lower latitudes, with much finer sampling in polar regions.

RHI for the 383 hPa retrieval level and larger pressures represents the mean value over a broad layer (4–6 km) whose sensitivity peaks between ~350 hPa (in the moist tropics) and ~650 hPa (typical for dry high latitudes).

3.21.4 Precision

The values for precision are the root sum square (RSS) precisions for H_2O and temperature propagated through the Goff-Gratch relationship; see Sections 3.10 and 3.23 for more details. The precisions are set to negative values (or zero in some cases) in situations when the retrieved precision is larger than 50% of the a priori precision for either temperature or H_2O — an indication that the data are biased toward the a priori value. The precisions for all levels between 1000 and 383 hPa, which are erroneously reported as 0% in the RHI L2GP files, should typically be 0.2%.

3.21.5 Accuracy

The values for accuracy are the RSS accuracies for H_2O and temperature scaled into % RHI units; see Sections 3.10 and 3.23 for more details.

3.21.6 Data screening

Pressure range: The product describes a vertically resolved profile over the range from the 316 hPa retrieval level to 0.001 hPa; data for pressures larger than 383 hPa represent the mid-to-upper tropospheric column.

Values outside this range are not recommended for scientific use.

Estimated precision: Only use values for which the estimated precision is a positive number.

Values where the a priori information has a strong influence are flagged with negative or zero precision and should not be used in scientific analyses (see Section 1.5).

Status flag: Only use profiles for which the `Status` field is an even number.

Odd values of `Status` indicate that the profile should not be used in scientific studies. See Section 1.6 for more information on the interpretation of the `Status` field.

Clouds: Profiles flagged as being affected by high or low clouds (i.e., with `Status` bits corresponding to values of 16 and 32 set) can be used except in cases where the temperature product is rejected. Following Section 3.23.6 the RHI product between 316 and 100 hPa is to be rejected whenever the 215 hPa IWC product exceeds 0.005 g/m^3. See Section 3.21.7 for more details.

Quality field: The `Quality` fields for both the `L2GP-RHI` and `L2GP-Temperature` swaths need to be considered, as described below:

For pressures of 83 hPa and smaller: Only use profiles with RHI `Quality` *greater* than 0.7 and temperature `Quality` *greater* than 0.2.

For pressures of 100 hPa and larger: Only use profiles with RHI `Quality` *greater* than 0.7 and temperature `Quality` *greater* than 0.9.

Convergence field: Only profiles with a value of the RHI `Convergence` *less* than 2.0 and temperature `Convergence` *less* than 1.03 should be used in scientific studies.

Temperature precision: The `L2gpPrecision` field in the `L2GP-Temperature` file can be used to further eliminate outliers that are believed to be the result of thick clouds, primarily in the tropics. If careful screening of the troposphere is required, levels 261–178 hPa should be avoided if any of the following criteria are met:

At 316 hPa: `L2gpPrecision` > 1.1 K **and** latitude > −60° (i.e., this rule only applies at latitudes north of 60°S)

At 261 hPa: `L2gpPrecision` > 0.7 K

At 215 hPa: `L2gpPrecision` > 0.825 K

Additional screening for RHI based on H_2O: Any RHI profiles for which the corresponding H_2O profiles contain values less than 0.101 ppmv at any pressure greater than 1 hPa should be rejected. This step eliminates highly oscillatory RHI profiles.

3.21.7 Artifacts

See Section 3.10 for H_2O and Section 3.23 for temperature for specific issues related to these parent products. Effects of MLS temperature precision (∼1 to 2 K) must be considered if one wishes to use MLS RHI to study supersaturation. In simulation studies, sources of systematic error, in addition to introducing biases, also increase variability in differences with respect to a "truth" data set, particularly for pressures greater than 178 hPa. This will erroneously increase the frequency of occurrence of supersaturation in the tail of MLS RHI distributions. Therefore, MLS RHI is not recommended for studying statistics of supersaturation at pressures greater than 178 hPa. For smaller pressures, the contribution from temperature noise must be removed as part of the analysis, as described by *Buehler and Courcoux* [2003]. Clouds in the field of view degrade RHI measurement precision, increasing the scatter about the mean; nevertheless, comparisons with AIRS data show that the mean bias changes by less than 10%. In addition, the drift in MLS water vapor, discussed in Sections 1.10.1 and 3.10.2, also affects the RHI product.

3.21.8 Review of comparisons with other datasets

Figures 3.21.2 and 3.21.3 show comparisons between AIRS v7 and MLS v2.2*x*, v3.3*x*/v3.4*x*, v4.2*x*, v5.0*x*, and v6.0*x* RHI. Mapped features generally agree well, but MLS produces higher relative humidities in the moist regions of the tropics relative to AIRS. Two noteworthy features are that at high latitudes at 200 and 250 hPa, and at low latitudes at 150 hPa, v6.0*x* and v5.0*x* have higher relative humidity than previous versions. This difference likely reflects changes made to address a dry bias in the MLS H_2O retrieval discussed in Section 3.10.

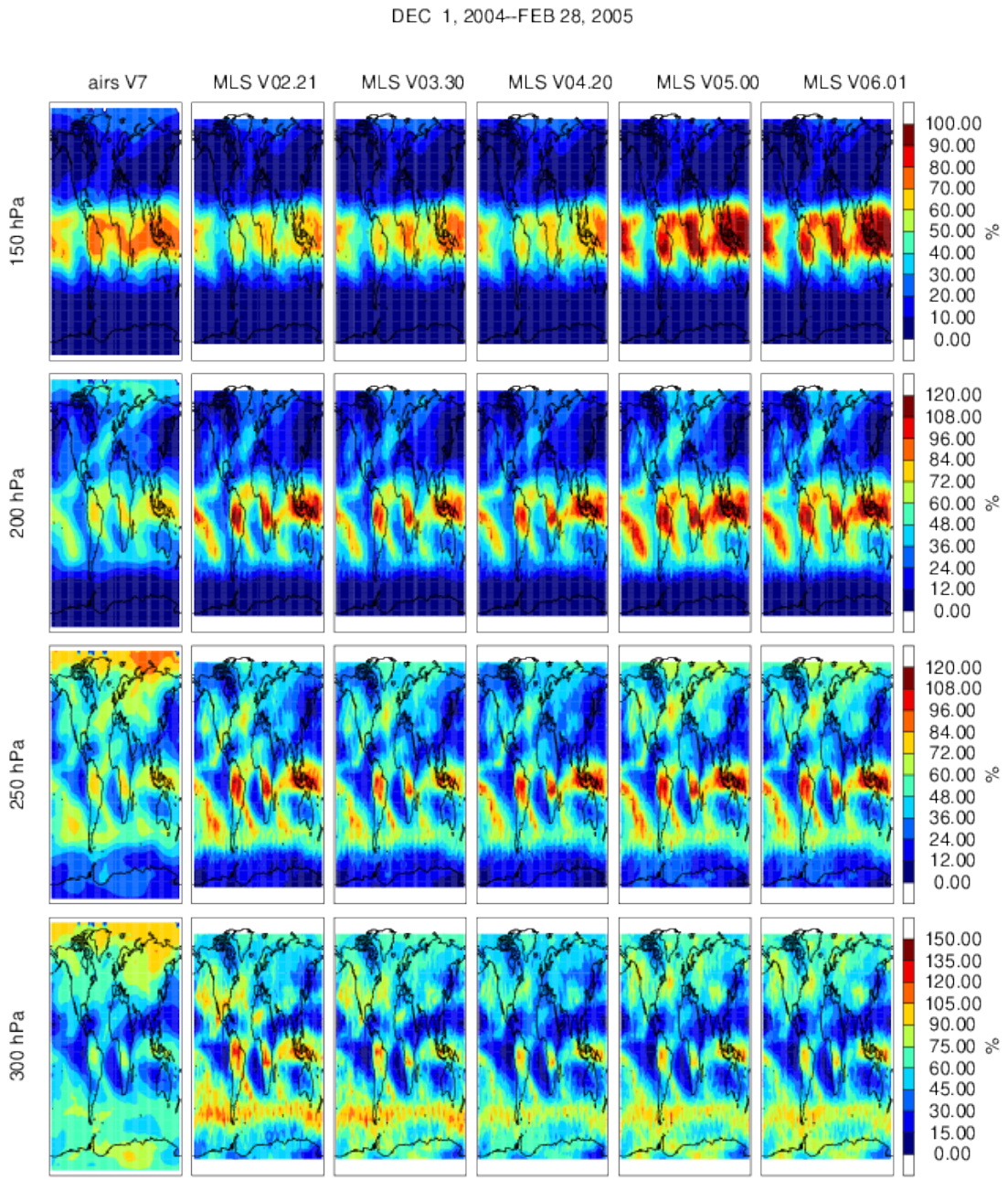

Figure 3.21.2: Mapped RHI fields from AIRS v7 and MLS v2.2*x*, v3.3*x*/v3.4*x*, v4.2*x*, v5.0*x*, and v6.0*x* at pressures between 300 and 150 hPa for December-January-February 2005.

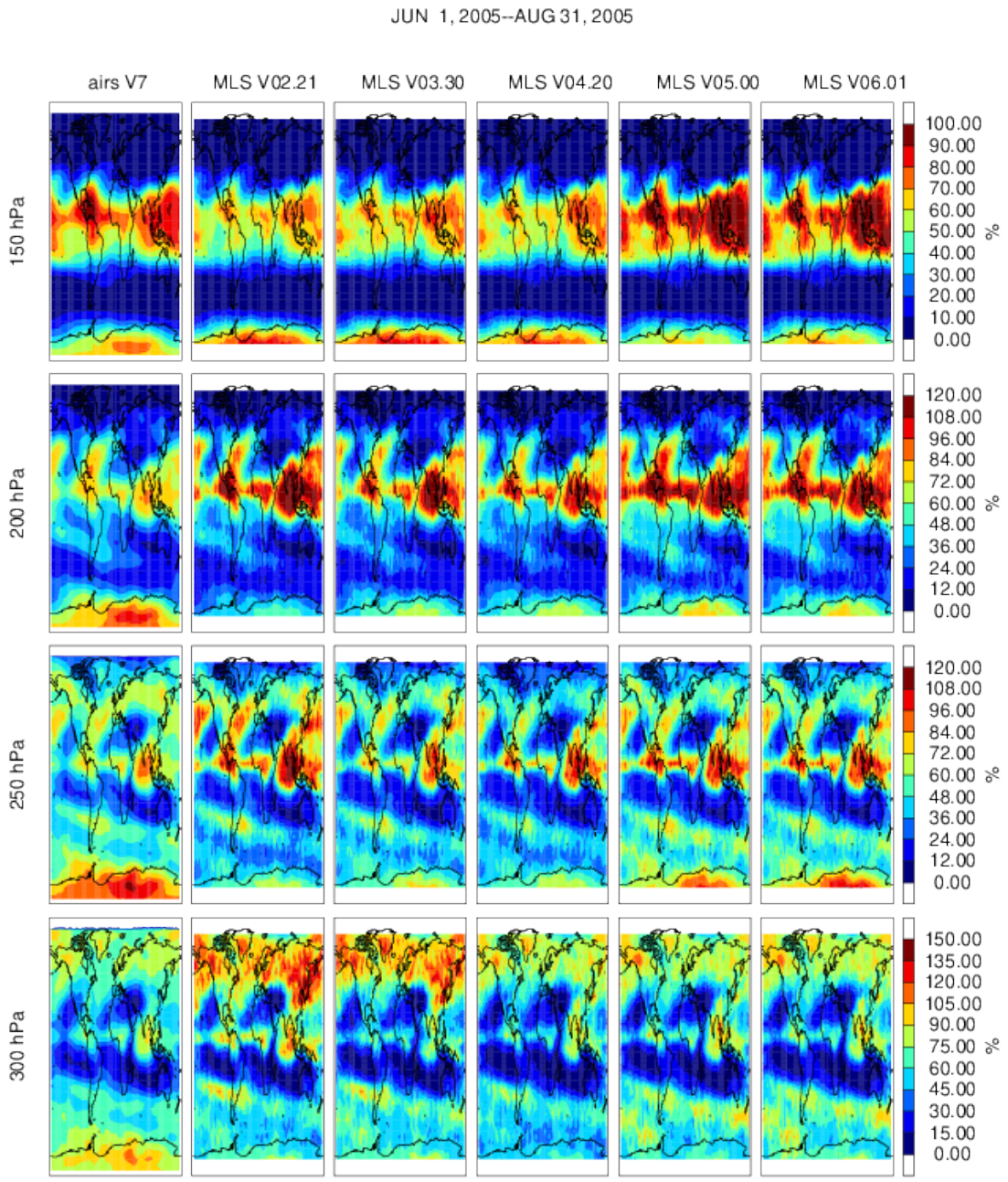

Figure 3.21.3: As in Figure 3.21.2 but for June-July-August 2005.

Table 3.21.1: Summary of Aura MLS v6.0*x* UTLS RHI Characteristics. Precision and accuracy values for the 1000–383 hPa single-layer retrievals are estimates.

Pressure	Resolution[a] V × H	Single-Profile precision[b]	Accuracy[b]	Comments
hPa	km	%	%	
0.00046	—	—	—	Unsuitable for scientific use
0.001	13.9 × 708	184	76	
0.002	14.0 × 508	145	74	
0.004	14.7 × 428	88	49	
0.010	13.8 × 398	66	37	
0.022	12.0 × 374	53	40	
0.046	10.6 × 318	42	41	
0.10	8.0 × 270	38	37	
0.22	8.2 × 262	28	26	
0.46	8.3 × 261	17	17	
1.00	7.2 × 316	12	11	
2.15	6.9 × 308	10	17	
4.64	6.1 × 295	10	18	
10	5.5 × 291	10	14	
22	5.3 × 275	11	33	
46	5.3 × 267	12	16	
68	5.4 × 248	12	23	
83	5.6 × 248	13	27	
100	5.8 × 251	12	30	
121	5.6 × 259	11	55	
147	5.1 × 259	11	51	
178	5.0 × 263	10	51	
215	4.5 × 263	10	61	See Table 3.10.1
261	4.7 × 253	9	80	See Table 3.10.1
316	4.4 × 253	13	167	See Table 3.10.1
1000–383	6 × 155	40 (est.)	10 (est.)	Single layer; peak height depends on atmospheric humidity

[a]Vertical and along-track horizontal resolutions; cross-track horizontal resolution is ~9 km.
[b]Fractional error ([error in RHI] / RHI) in percent

3.22 Sulfur Dioxide (SO_2)

Swath name: SO2

Useful range: 215–10.0 hPa

Product lead: William Read <william.g.read@jpl.nasa.gov>

3.22.1 Introduction

The standard SO_2 product is taken from the 240-GHz retrieval (`CorePlusR3`). MLS can only measure SO_2 when its concentrations are significantly enhanced above the nominal background, such as those from volcanic injections. Validation of v2.2*x* SO_2 was reported by *Pumphrey et al.* [2015].

3.22.2 Changes from v5.0*x*

Changes in the 240-GHz MLS products from v5.0*x* to v6.0*x* are minor. The standard SO_2 product is retrieved from the `CorePlusR3` phase that simultaneously retrieves tangent pressure, temperature, and its targeted species from 118- and 240-GHz signals. Changes made to improve the tangent pressure and temperature will have some impact on the SO_2 retrieval. Similarly, the new approach to cloud flagging discussed in Section 1.4.3 should be noted.

Figure 3.22.1 compares SO_2 in MLS v2.2*x*, v3.3*x*/v3.4*x*, v4.2*x*, v5.0*x*, and v6.0*x*. The atmosphere typically has ~0.1 ppbv SO_2, which is far smaller than the MLS SO_2 accuracy estimate. All versions (erroneously) report typical SO_2 abundances of the order of a few ppbv, due to systematic errors in the MLS measurement system. Changes from v2.2*x* through to v6.0*x* largely result from modifications in the handling of background radiance signals, which evolved from being modeled as an absorption continuum (v2.2*x*) to a continuum modeled as water vapor absorption retrieved as relative humidity (v3.3*x*/v3.4*x*) to an MLS limb-pointing-based absorption continuum with a frequency squared spectral dependence (v4.2*x* through v6.0*x*). Versions v4.2*x* through v6.0*x* also use improved cloud detection and radiance screening.

3.22.3 Resolution

Based on Figure 3.22.2, the vertical resolution for SO_2 is ~3 km, and the horizontal resolution is 170 km. The horizontal resolution perpendicular to the orbit track is 7 km, the full width at half maximum of the MLS antenna, for all pressures.

3.22.4 Precision

The estimated precision for SO_2 is ~4 ppbv for all heights between 215 and 10 hPa. The precisions are set to negative values (or zero in some cases) in situations when the retrieved precision is larger than 50% of the a priori precision — an indication that the data are biased toward the a priori value. The changes between v5.0*x* and v6.0*x* are minor and result in only small differences in the estimated precision. An example is shown in Figure 3.22.3 for 100 hPa on 14 February 2009, a day when no eruptions were detected by MLS. SO_2 precision estimates from v5.0*x* and v6.0*x* show much less variability and less latitude dependence than was present in v4.2*x*. Similar behavior is seen on other dates and at other stratospheric levels, as well as in other species retrieved from the 240-GHz radiances, such as HNO_3. This change in behavior occurred as a result of removing some approximations in the forward model in v5.0*x* and v6.0*x*.

3.22.5 Accuracy

Based on comparisons with coincident OMI total column SO_2 observations, the MLS SO_2 retrievals at 215 and 147 hPa occasionally exhibit spurious spikes and enhancements that are not reflected in the OMI measurements. Accordingly, although the formal MLS systematic error assessment approach described by *Read et al.* [2007] indicates smaller uncertainty, the MLS team recommends that the accuracy of the MLS SO_2 at these pressure levels be considered to be 20 and 10 ppbv at 215 and 147 hPa, respectively. Accuracies at other pressure levels are estimated using the approach taken by *Read et al.* [2007].

3.22.6 Data screening

Pressure range: 215–10.0 hPa

Values outside this range are not recommended for scientific use.

Estimated Precision: In general, as for other MLS species, retrieved SO_2 values for which the associated precision is negative should not be used. However, SO_2 data showing strong (>20 ppbv) enhancements that have negative precision may still be used.

Although it is generally recommended to not use values where precision is flagged negative, SO_2 is an exception, and it is appropriate to use values with negatively flagged precision (provided that the entire profile is not so flagged otherwise passes the `Status`, `Quality`, and `Convergence` criteria). High retrieved values of SO_2 at larger pressures (e.g., 215 and 147 hPa) also have larger (i.e., poorer) precision values that are sometimes large enough to trigger the "too much a priori influence" negative-precision flag. In such cases, the retrieved value will probably be smaller than the true abundance because the retrieval is being pulled towards the a priori value of zero ppbv. Nonetheless, greatly enhanced SO_2 is being observed, reflecting the detection of a volcanic plume. Profiles where the precision is set to zero, however, should be omitted from scientific analyses.

Status flag: Only use profiles for which the `Status` field is an even number.

Odd values of `Status` indicate that the profile should not be used in scientific studies. See Section 1.6 for more information on the interpretation of the `Status` field.

Quality field: Only profiles having `Quality` *greater* than 0.95 should be used.

As with water vapor, this value is where the quality versus yield sharply drops, indicating the transition from well-fit profiles toward more poorly fit ones, as shown in Figure 3.22.4.

Convergence field: Only profiles having `Convergence` *less* than 1.03 should be used.

3.22.7 Artifacts

High values of SO_2 accompanied by negative precisions are likely to be underestimated due to the influence of the a priori, which biases the retrieved abundances toward zero. The atmospheric background SO_2 (~0.1 ppbv) cannot be measured by MLS, even with extensive data averaging, as systematic errors will induce biases of a few ppbv.

3.22.8 Review of comparisons with other datasets

Figure 3.22.5 compares total column SO_2 measured by OMI and stratospheric column SO_2 calculated by MLS for two days following the Sarychev eruption. It is clear that MLS detects the main plume dispersal features. It also appears that MLS columns are often smaller than those from OMI. Interpreting the significance of this difference is not straightforward, given that OMI has to make assumptions regarding the profile shape and can observe SO_2 down to the boundary layer. The MLS column begins at 215 hPa and is integrated upward, thus neglecting tropospheric contributions. Another limitation is that OMI only makes measurements during the day, whereas MLS measures day and night. Since plumes generally move relatively quickly over the 12-hour MLS ascending/descending measurement separation time, MLS nighttime measurements often miss those seen by OMI during the day (12 hours apart) or detect plume features differently.

Figure 3.22.6 shows a comparison between v3.3*x*/v3.4*x*, v4.2*x*, v5.0*x*, and v6.0*x* for the portion of an MLS orbit with the maximum SO_2 measured on 16 June 2009. As expected, v5.0*x* and v6.0*x* show similar amounts of SO_2 at 215–68 hPa. The MLS retrieval shows that the SO_2 is concentrated between 147 and 100 hPa.

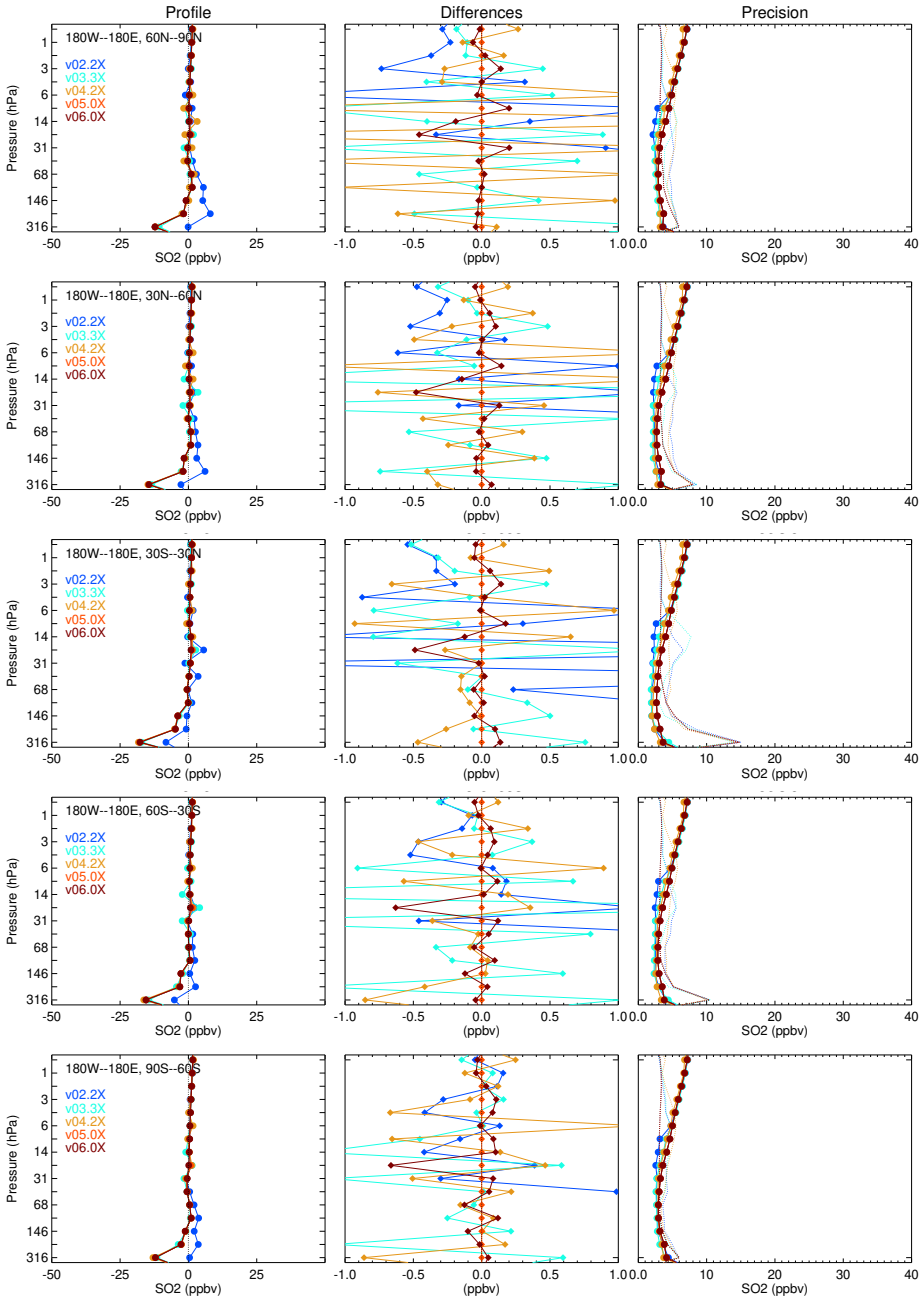

Figure 3.22.1: A comparison of v2.2*x* (blue), v3.3*x*/v3.4*x* (cyan), v4.2*x* (orange), v5.0*x* (orange), and v6.0*x* (dark red) SO_2 for January-February-March 2005 in five latitude bands. Results from other time periods are similar. The left panel compares mean profiles. The center panel shows each version's mean difference (diamonds) relative to v5.0*x*. The right panel shows the estimated retrieval precision (solid lines with bullets); measured variability (dotted lines), which includes atmospheric variability about the mean profile; and a priori precision (dashed lines).

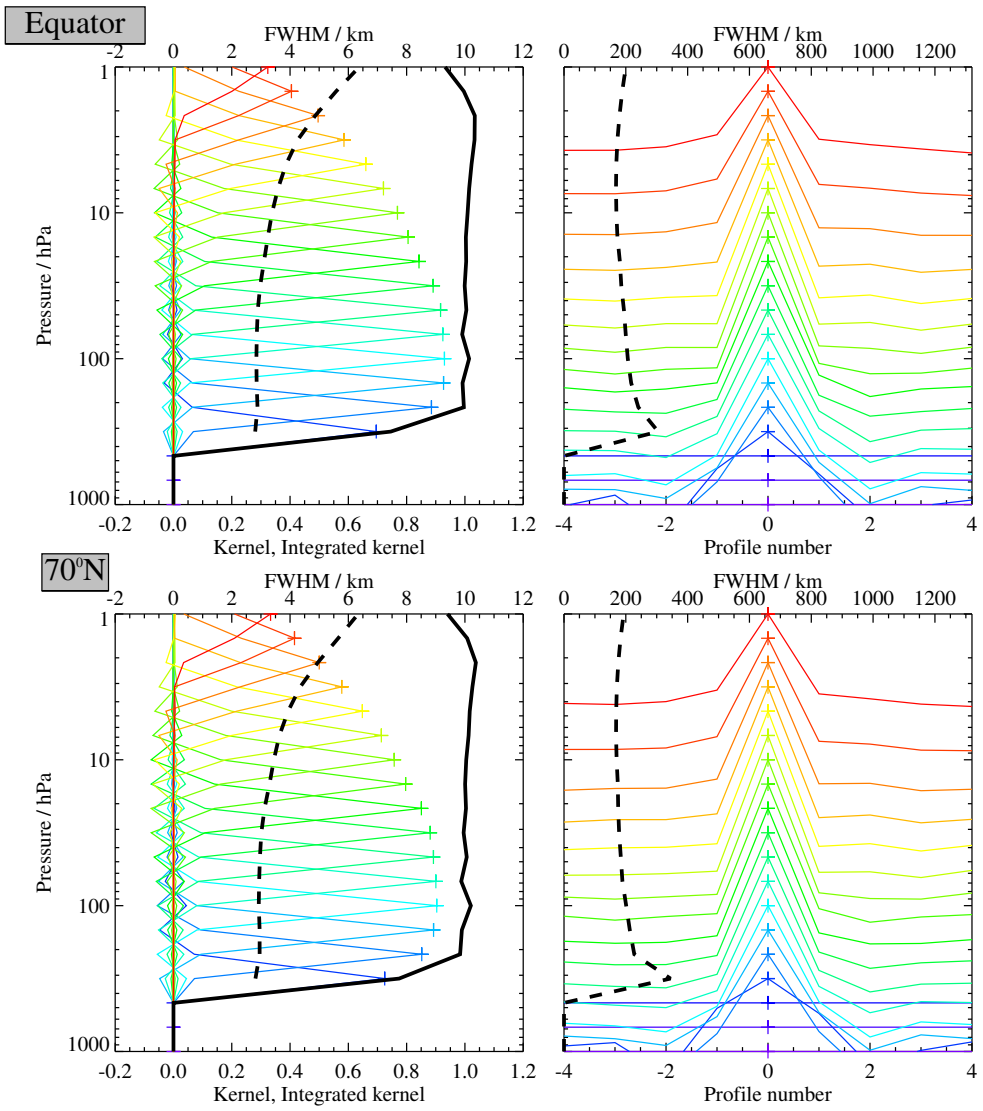

Figure 3.22.2: Typical two-dimensional (vertical and horizontal along-track) averaging kernels for the MLS v6.0*x* SO_2 data at the equator (upper) and at 70°N (lower); variation in the averaging kernels is sufficiently small that these are representative of typical profiles. Colored lines show the averaging kernels as a function of MLS retrieval level, indicating the region of the atmosphere from which information is contributing to the measurements on the individual retrieval surfaces, which are denoted by plus signs in corresponding colors. The dashed black line indicates the resolution, determined from the full width at half maximum (FWHM) of the averaging kernels, approximately scaled into kilometers (top axes). (Left) Vertical averaging kernels (integrated in the horizontal dimension for five along-track profiles) and resolution. The solid black line shows the integrated area under each kernel (horizontally and vertically); values near unity imply that the majority of information for that MLS data point has come from the measurements, whereas lower values imply substantial contributions from a priori information. (Right) Horizontal averaging kernels (integrated in the vertical dimension) and resolution. The horizontal averaging kernels are shown scaled such that a unit averaging kernel amplitude is equivalent to a factor of 10 change in pressure.

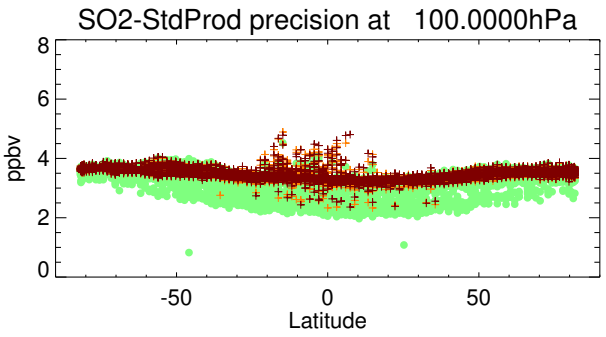

Figure 3.22.3: A comparison of estimated precision on 14 February 2009 (a date with no known detectable volcanic signatures) for SO_2 from v4.2*x* (green), v5.0*x* (orange), and v6.0*x* (dark red) at 100 hPa.

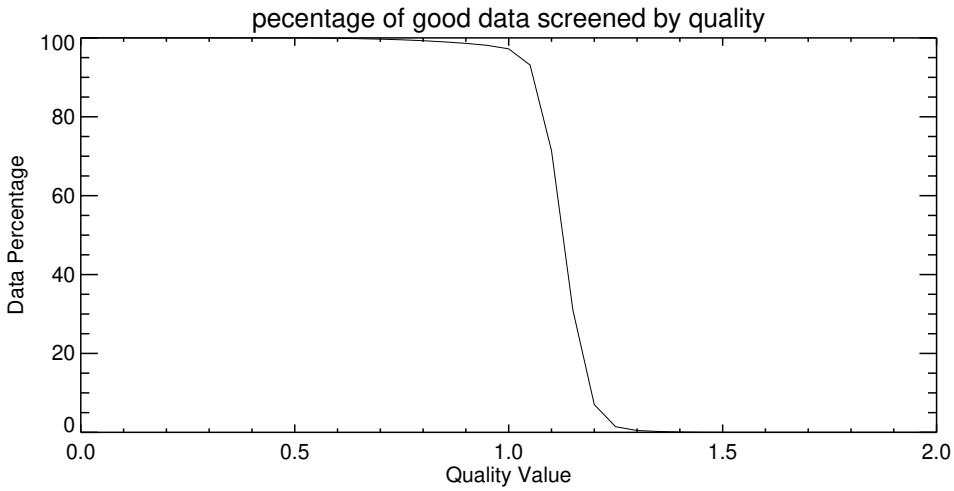

Figure 3.22.4: Reverse-cumulative distribution of v6.0*x* `Quality` values for June-July-August 2005.

Table 3.22.1: Summary of Aura MLS v6.0*x* SO_2 Characteristics.

Pressure	Resolution[a] V × H	Single-Profile Precision	Accuracy	Comments
hPa	km	ppbv	ppbv	
< 10	—	—	—	Unsuitable for scientific use
10	3.5 × 170	5.4	1	
15	3.4 × 170	5.0	1	
22	3.3 × 170	4.3	2	
32	3.0 × 170	3.7	3	
46	3.0 × 170	3.4	3	
68	2.9 × 170	3.3	3	
100	2.9 × 170	3.4	4	
147	2.9 × 170	3.5	10	
215	2.8 × 180	4.3	20	
>215	—	—	—	Unsuitable for scientific use

[a]Vertical and along-track horizontal resolutions; cross-track horizontal resolution is ~7 km.

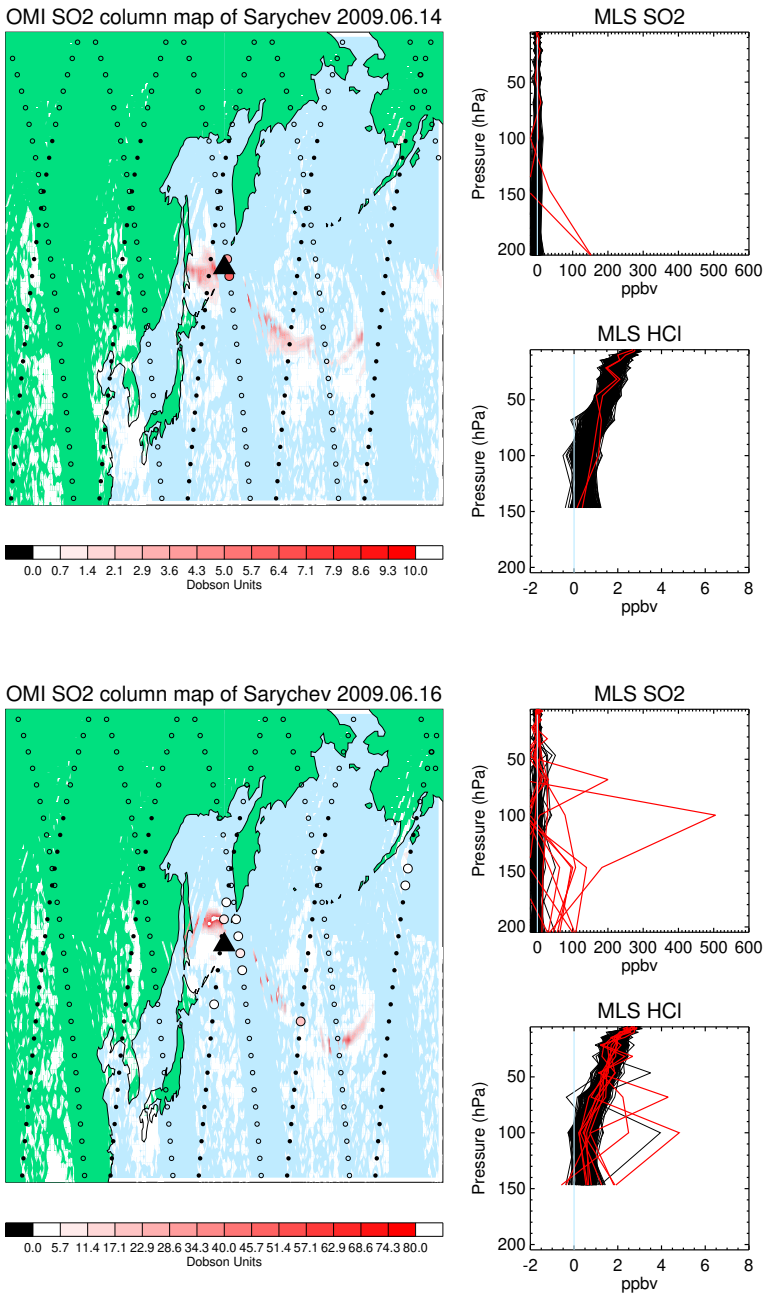

Figure 3.22.5: MLS measurement tracks overlaid on OMI SO_2 measurements from 14 and 16 June 2009 (separate maps) showing the dispersal of SO_2 from the Sarychev eruption (13 June 2009, black triangle). The OMI instrument has some non-operational pixels (known as the "row anomaly") in which measurements are not possible. It turns out that one of these row anomalies is perfectly aligned with the MLS track, and therefore there are no co-aligned OMI and MLS measurements. The color scale indicates the total SO_2 column measured by OMI. Daytime MLS tracks are depicted by small open circles; nighttime tracks are depicted by filled black circles. When the calculated stratospheric SO_2 column from MLS exceeds 2 DU, that data point is indicated by a larger open circle filled with the color of the column estimate as indicated by the color scale below (same as for OMI). The panels at right show all measured profiles covering the area shown in the maps for SO_2 and HCl. Profiles for which the MLS column calculation exceeds 2 DU are highlighted in red.

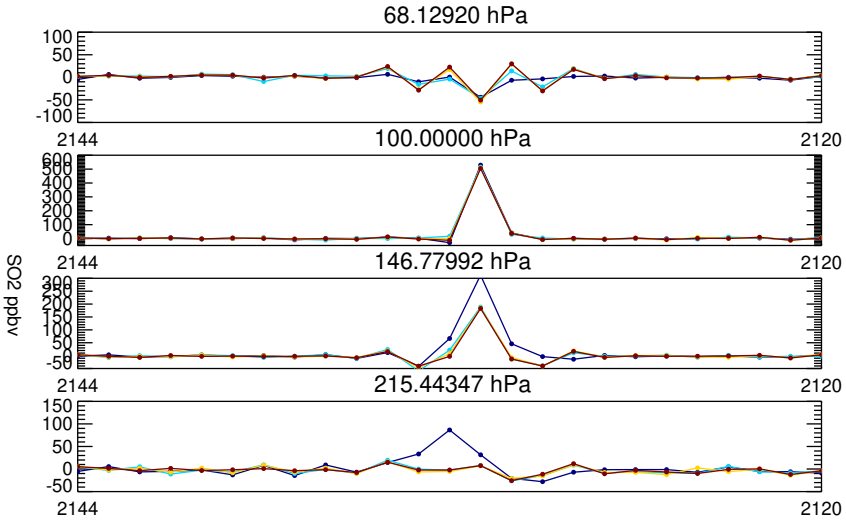

Figure 3.22.6: Time series comparisons of MLS SO_2 retrievals between several versions at 215, 147, 100, and 68 hPa where MLS measures more than 500 ppbv at 100 hPa from the Sarychev eruption (16 June 2009). Dark blue shows v3.3*x*/v3.4*x*, light blue shows v4.2*x*, yellow shows v5.0*x*, and red shows v6.0*x*.

3.23 Temperature (T)

Swath name: Temperature

Useful range: 261–0.00046 hPa

Units: K

Product lead: Michael J. Schwartz <Michael.J.Schwartz@jpl.nasa.gov>

3.23.1 Introduction

MLS temperature is retrieved primarily from bands near O_2 spectral lines at 118 GHz and 239 GHz that are measured with MLS radiometers R1A:118/R1B:118 and R3:240, respectively. The isotopic 239 GHz line is the primary source of temperature information in the troposphere, with information on temperature in the stratosphere and above deriving from the 118 GHz O_2 line. As a result of the work described in Section 1.4.2, the MLS v6.0*x* temperature product substantially improves upon the v5.0*x* product in the middle and upper stratosphere and lower mesosphere, with a reduction of vertical oscillations in the stratosphere, an up to 30% improvement in vertical resolution, and up to 20% improvement in measurement precision. In the upper troposphere and in the upper mesosphere and above, the v6.0*x* product is very similar that of v5.0*x*, and at those levels both versions are generally similar to the v3.3*x*/v3.4*x* product and to the v2.2*x* product described by *Schwartz et al.* [2008]. MLS v6.0*x* temperature has an approximately −1 K bias with respect to correlative measurements in the troposphere and lower stratosphere. Table 3.23.1 summarizes the measurement precision, resolution, and modeled and observed biases. The following subsections provide details.

3.23.2 Differences between v6.0*x* and v5.0*x*

The most significant differences between the v6.0*x* and v5.0*x* temperature products result from changes in the way radiances from the 25-channel filterbank centered on the 118.75 GHz O_2 line (Band 1) are used in the retrieval, as described in detail in Section 1.4.2. The general philosophy of the MLS science team is to avoid adjusting radiances to improve the consistency between MLS products and correlative data. As part of v6.0*x* development, Band-1 channel filter shapes were adjusted, not in order to obtain a "desired" retrieved temperature, but rather to make an off-line retrieval of O_2 (developed specifically for the purpose of investigating channel shifts) consistent with the known mixing ratio of O_2 in the stratosphere and lower mesosphere. These changes have the additional benefit of reconciling differences between the "radiometric" and "hydrostatic" information on temperature obtained from the 118-GHz observations (see the following paragraph and Section 1.4.2), allowing radiances from the central portion of Band 1 that had been excluded from recent retrieval versions to be used in v6.0*x*.

Figure 3.23.1(a) and (c) show, for v5.0*x* and v6.0*x*, respectively, differences between measured and fitted radiances in MLS Band 1. White dots in panel (a) indicate where radiances were excluded from the v5.0*x* and earlier retrievals. In some cases these daily averaged differences between observed and predicted radiances exceed ±5 K. Use of these channels/levels in v6.0*x* (Figure 3.23.1(c)) provides the retrieval with pressure information along the limb ray paths from the width of the pressure-broadened O_2 line. Saturated radiances from the bottom of the limb scan provide temperature information, much as do radiances from nadir-looking passive microwave temperature profilers. The improved pressure information of v6.0*x* combined with height information from the scan model provide additional temperature information through the assumption of hydrostatic balance, improving the vertical resolution of the v6.0*x* temperature retrieval relative to that of v5.0*x* by 20–30% in the upper stratosphere and lower mesosphere (10–0.1 hPa) while also improving the retrieval's estimated precision by 10–20% at these levels.

Figure 3.23.1(b) and (d) show typical "scan residual" histograms for v5.0*x* and v6.0*x*, respectively. The scan residual measures the difference between two estimates of limb tangent-point altitude, one derived from

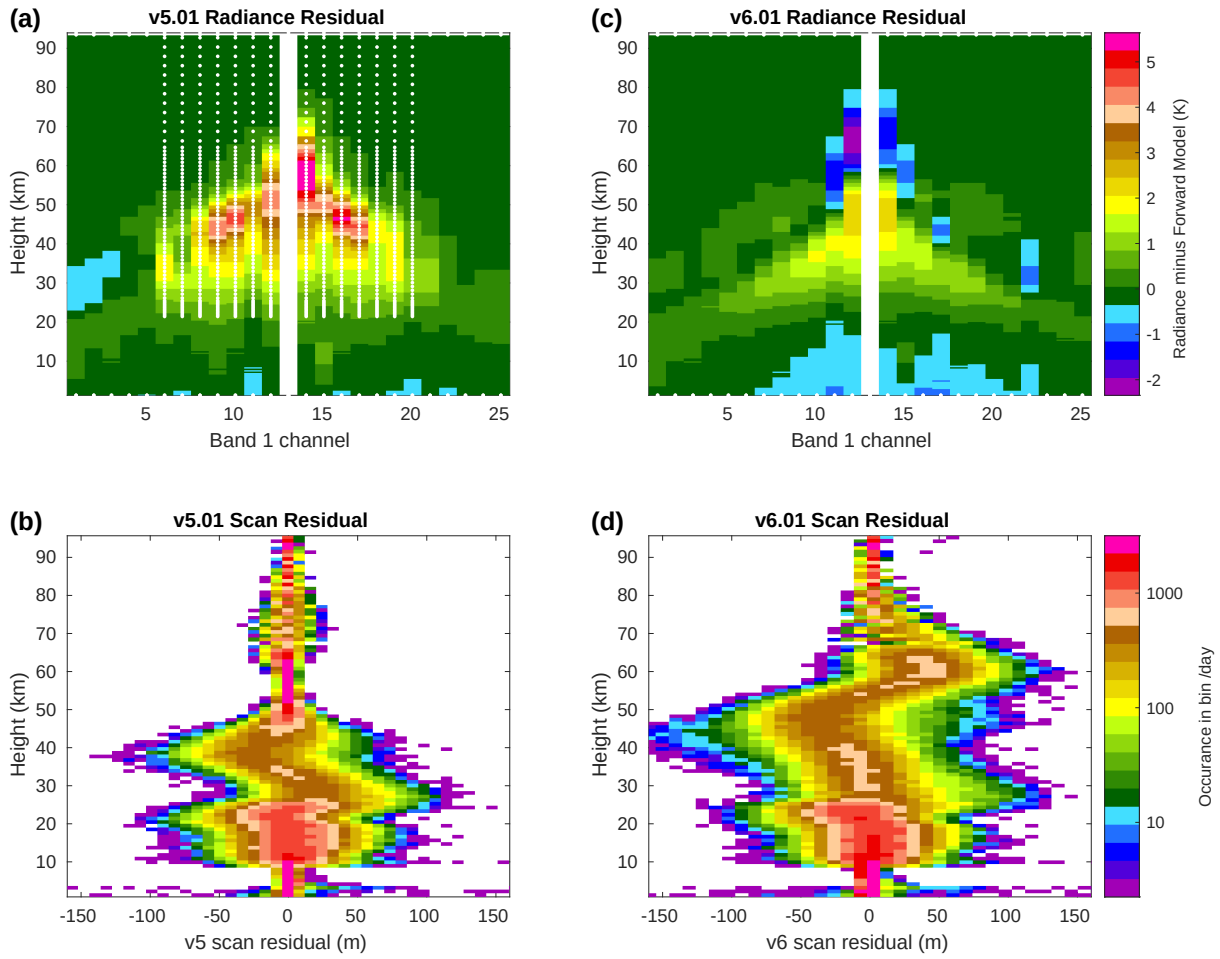

Figure 3.23.1: Panels (a) and (c) show daily averaged Band-1 radiance residuals (observed radiances minus retrieval forward model) for v5.0*x* and v6.0*x*, respectively, for day 2021d001. White dots on panel (a) indicate channels/levels that were excluded from the v5.0*x* and earlier retrievals (although a forward model estimate for these radiances was still calculated and is compared to here). Panels (b) and (d) show histograms of scan residuals vs. tangent height for v5.0*x* and v6.0*x*, respectively, also for day 2021d001. The height used to label the y-axis in all panels is taken from the instrument scan model and is the tangent height (daily averaged in (a) and (c)) of a given scan position minor frame.

instrument and spacecraft pointing information, the other from the temperature and tangent-point pressure retrievals, assuming hydrostatic balance applies in the atmosphere. The "optimal" solution is one that has these two measures agreeing to the degree expected given uncertainties in the quantities involved. Very small v5.0*x* scan residuals in the lower mesosphere (50–65 km) are consistent with the lack of line-width information provided to the v5.0*x* retrieval at these levels; the tangent-point pressure has a large uncertainty, so the retrieval cleaves to the pointing information. Higher in the mesosphere, the Band-22 high-resolution spectrometer centered on the 118-GHz O_2 line provides linewidth information in the altitude regions where pressure broadening dominates the line width. At the very top of the scan, Doppler broadening dominates, limiting the ability to measure pressure.

The v6.0*x* temperature retrieval uses Goddard Earth Observing System for Instrument Teams (GEOS-IT, `https://gmao.gsfc.nasa.gov/gmao-products/geos-it/`, system release GEOS-5.29.4) as its a priori in the upper troposphere and stratosphere, replacing the GEOS-5 "Forward Processing for Instrument Teams" (FP-IT) used as a priori in v5.0*x*. For both products, the same climatology is used above (at pressures smaller

than) 1 hPa. Throughout the rest of this section, "GEOS-5" without additional qualification refers to GEOS-IT. Zonal-mean differences between the GEOS versions are as large as 2.5 K in the upper stratosphere, with scatter as large as 4.5 K at 2 hPa, but zonal-mean differences in retrieved temperature due to the changed a priori are less than 0.5 K.

Figure 3.23.2 shows some of the major differences between the v6.0*x* and v5.0*x* temperature products. Panel (a) shows the globally and annually (2021) averaged v6.0*x* and v5.0*x* a priori and retrieved temperature products, while panel (b) show differences of these profiles from the v6.0*x* a priori. The v5.0*x* a priori is ∼1 K warmer in the uppermost stratosphere (1.4–2.2 hPa) than the v6.0*x* a priori (green line in panel (b)). This difference results from vertically sharp structure near the stratopause that can be seen to "leak" into the retrieved v5.0*x* product (red) of panel (b). A reduction in vertical oscillations in v6.0*x* (blue) in the middle and upper stratosphere and lower mesosphere (∼30–0.1 hPa) is evident, relative to the v5.0*x* profile (red), but v6.0*x* still has a global bias relative to a priori in the upper stratosphere that approaches −1 K. Figure 3.23.2 (c) and (d) show the more than 30% improvement in v6.0*x* vertical resolution relative to v5.0*x* in the upper stratosphere and lower mesosphere. Figure 3.23.2 (e) and (f) similarly show the ∼20% improvement in v6.0*x* retrieval precision relative to that of v5.0*x* in the upper stratosphere and lower mesosphere.

The standard v6.0*x* and v5.0*x* temperature products are both taken from the `CorePlusR3` phase, which uses radiances from the 240-GHz radiometer (`R3:240`) in addition to those from the 118-GHz radiometer (`R1A:118`/`R1B:118`). The 235-GHz $O^{18}O$ line in Band 8 provides upper-tropospheric temperature and tangent-point pressure information, supplementing that from the O_2 line at 118 GHz, the primary source of retrieved temperature and tangent-point pressure in the stratosphere and mesosphere. In addition to temperature, `CorePlusR3` simultaneously retrieves standard products for a number of atmospheric constituents. The `CorePlusR3` temperature and GPH, along with the accompanying tangent-point pressures, are used for all subsequent constituent retrievals, so standard temperature and GPH are internally consistent with the suite of constituent retrievals.

MLS is generally insensitive to the presence of thin clouds, but scattering in the cores of convective storms can produce significant perturbations in MLS retrieved quantities, including temperature. Indeed, a priori knowledge of temperature from analysis is often so good in the lower and middle atmosphere that perturbations of a few percent (an amount typically considered to be negligible for trace-gas constituent retrievals) are "significant" for temperature. In the troposphere, where a priori knowledge may be good to on the order of 1–2 K, temperatures from an analysis such as GEOS-5 (the retrieval a priori) may be more reliable than the MLS retrieval product, and differences between the MLS and GEOS-5 temperatures can be useful in the identification of retrieval artifacts. Cloud-induced perturbations generally occur in the tropics and midlatitudes (where convective storms occur) in both the v6.0*x* and v5.0*x* retrieval versions. In unscreened data at retrieval levels 316–178 hPa, clouds produce primarily positive outliers in v6.0*x* and v5.0*x*. The top panels of Figure 3.23.3 show this behavior at 215 hPa. Conversely, at 121 hPa, outliers are primarily positive in v6.0*x* and v5.0*x*.

Figure 3.23.4 shows unscreened and screened histograms of tropical (20°S–20°N) v6.0*x* and v5.0*x* temperature from 2021. Outlier behavior due to thick clouds is very similar in the two versions, and the screening recommended to ameliorate these effects is identical. Tails of low unscreened outliers are particularly evident from 316–147 hPa but are greatly reduced by recommended screening.

Temperature is retrieved, in both v5.0*x* and v6.0*x*, up to the 0.0001 hPa level, but the 0.00046 hPa level is typically near the top tangent point of the MLS scan, while the 0.00022 hPa surface is often above the height of the highest tangent point in the MLS limb scan (depending upon latitude). The estimated precision of the retrieval at both of those levels is less than half of the precision of the retrieval a priori. However, as can be seen from Figure 3.23.5 for both latitudes shown, the averaging kernel of the 0.00046 hPa retrieval level is sharply peaked at 0.00046 hPa, while the averaging kernel of the 0.00022 hPa retrieval level shows a larger contribution from 0.00046 hPa than from 0.00022 hPa. As was the case in v5.0*x*, the precision of the 0.00022 hPa level in v6.0*x* is set negative "by hand" to advise against its casual use, but the 0.00022 hPa level

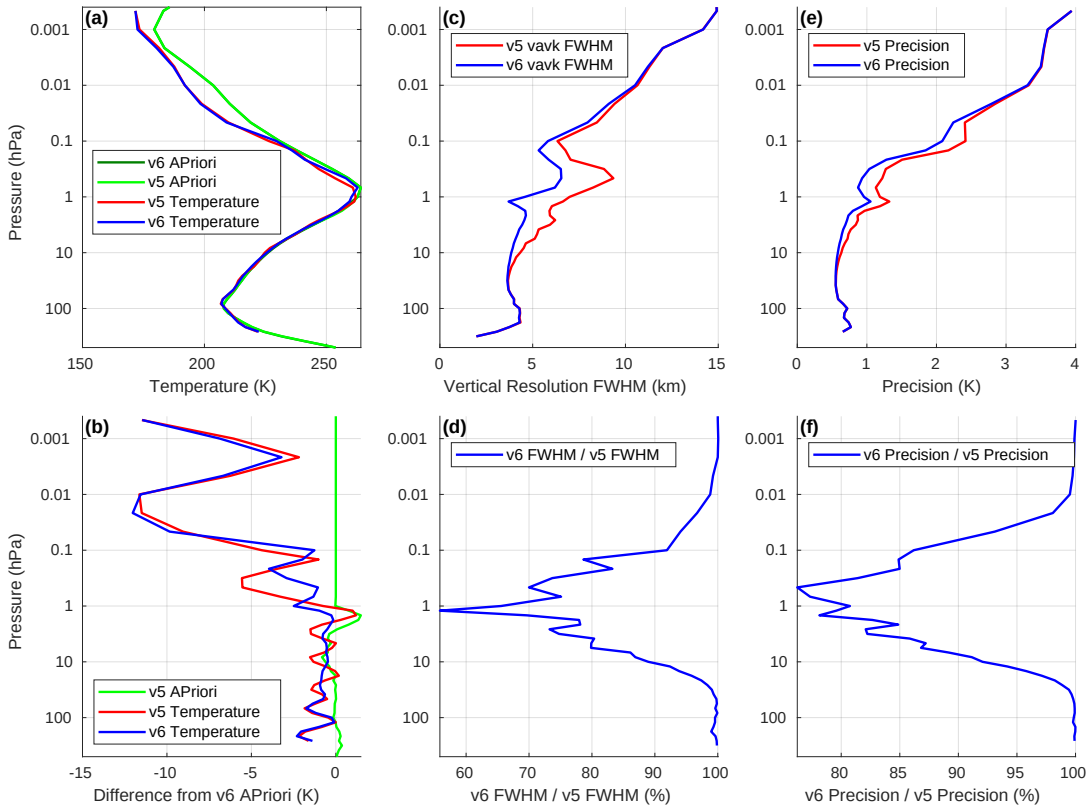

Figure 3.23.2: All panels are annual averages of 2021 data, which are typical of the mission as a whole. Screening, per the recommendation of this document, has been applied to retrieved products. (a) Global average a priori and retrieved v6.0*x* and v5.0*x* temperature profiles. (b) Differences from v6.0*x* a priori temperature of v5.0*x* a priori (green), as well as the v5.0*x* (red) and v6.0*x* (blue) standard temperature products. (c) Vertical resolution (full widths at half maxima of the vertical averaging kernels) of the v5.0*x* (red) and v6.0*x* (blue) temperature retrieval. (d) v6.0*x* vertical resolution divided by v5.0*x* vertical resolution. (e) Typical v5.0*x* and v6.0*x* estimated retrieval precision. (f) v6.0*x* estimated precision divided by v5.0*x* estimated precision.

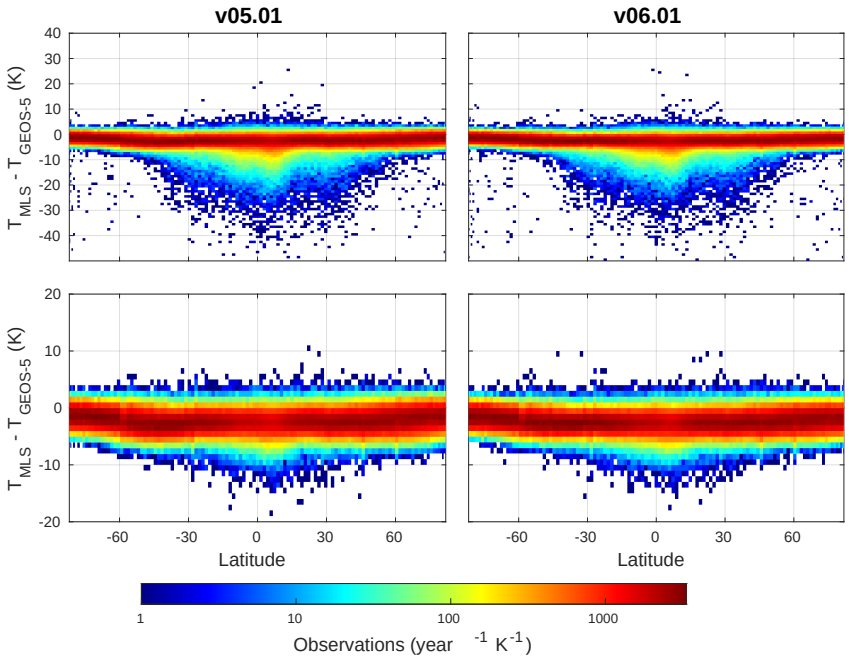

Figure 3.23.3: The top row shows histograms of unscreened v5.0*x* (left) and v6.0*x* (right) 215 hPa temperature differences from GEOS-5 temperature for 2021. The horizontal bin spacing is that of the ~1.5° latitudinal spacing of the MLS scans. The bottom panels show histograms of differences of the screened profiles on a finer vertical scale. Outliers beyond ±20 K have been almost completely eliminated and are not shown.

may have value for some scientific studies.

3.23.3 Resolution

The vertical and horizontal resolution of the MLS temperature measurement are defined to be the full width at half maximum (FWHM) of the vertically and horizontally collapsed retrieval averaging kernels. Averaging kernels are shown in Figure 3.23.5, and resolution is summarized in Table 3.23.1. Vertical resolution, shown on the left panel, is 3–4 km from 261 hPa to 10 hPa and degrades to 4–6 km at 1–0.1 hPa, 11 km at 0.01 hPa, and 13 km at 0.0001–0.00022 hPa. Along-track resolution is ~165 km from 261 hPa to 0.1 hPa and degrades to 280 km at 0.001 hPa and to 316 km at 0.00046 hPa. The cross-track resolution is set by the 6-km width of the MLS 240-GHz field of view in the troposphere and by the 12-km width of the MLS 118 GHz field of view in the stratosphere and above. The longitudinal separation of MLS measurements, which is determined by the Aura orbit, is 10°–20° over middle and low latitudes and finer in polar regions.

3.23.4 Precision

The precision of the MLS v6.0*x* temperature measurement is summarized in Table 3.23.1 and is shown in Figure 3.23.2(e) and (f). Precision quantifies the random uncertainty in the measurements, impacts of which can be assumed to be reduced when multiple profiles are averaged. The retrieval software returns an estimate of precision based upon the propagation of radiometric noise and a priori uncertainties through the measurement system. These values, which range from ~0.6 K in the lower stratosphere to ~2.5 K in the mesosphere and ~4 K at 0.00046 hPa, are given for selected levels. The "observed scatter" column gives the root mean square of differences of values from successive orbits (divided by the square root of two, as we are looking at the difference of two noisy signals) for latitudes and seasons where longitudinal variability is small and/or is a function only of local solar time. The smallest values found, which are in the tropics in the troposphere and in high-latitude summer in the stratosphere and mesosphere, are taken to be those least impacted by atmospheric variability and are what is reported in this column. These values are 0.5–0.8 K larger than those

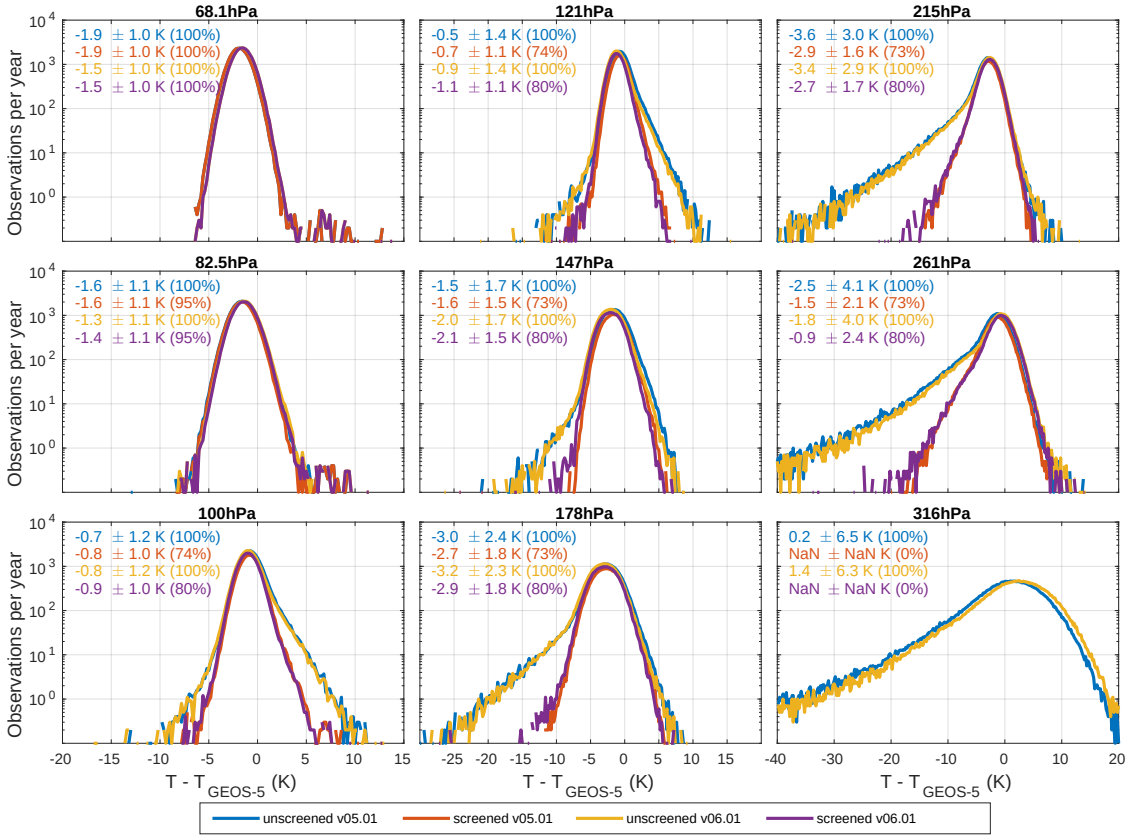

Figure 3.23.4: Panels show histograms of tropical (20°S–20°N) differences between MLS retrieved temperatures and GEOS-5 temperature for all of 2021. Blue and red lines are unscreened and screened v5.0*x*, respectively. Yellow and magenta are unscreened and screened v6.0*x*, respectively. Distribution means and standard deviations are given in the upper left of each panel, along with the percentage of points included after screening. Results at 316 hPa are shown for reference, although v6.0*x* temperature data at this level are not recommended for scientific studies.

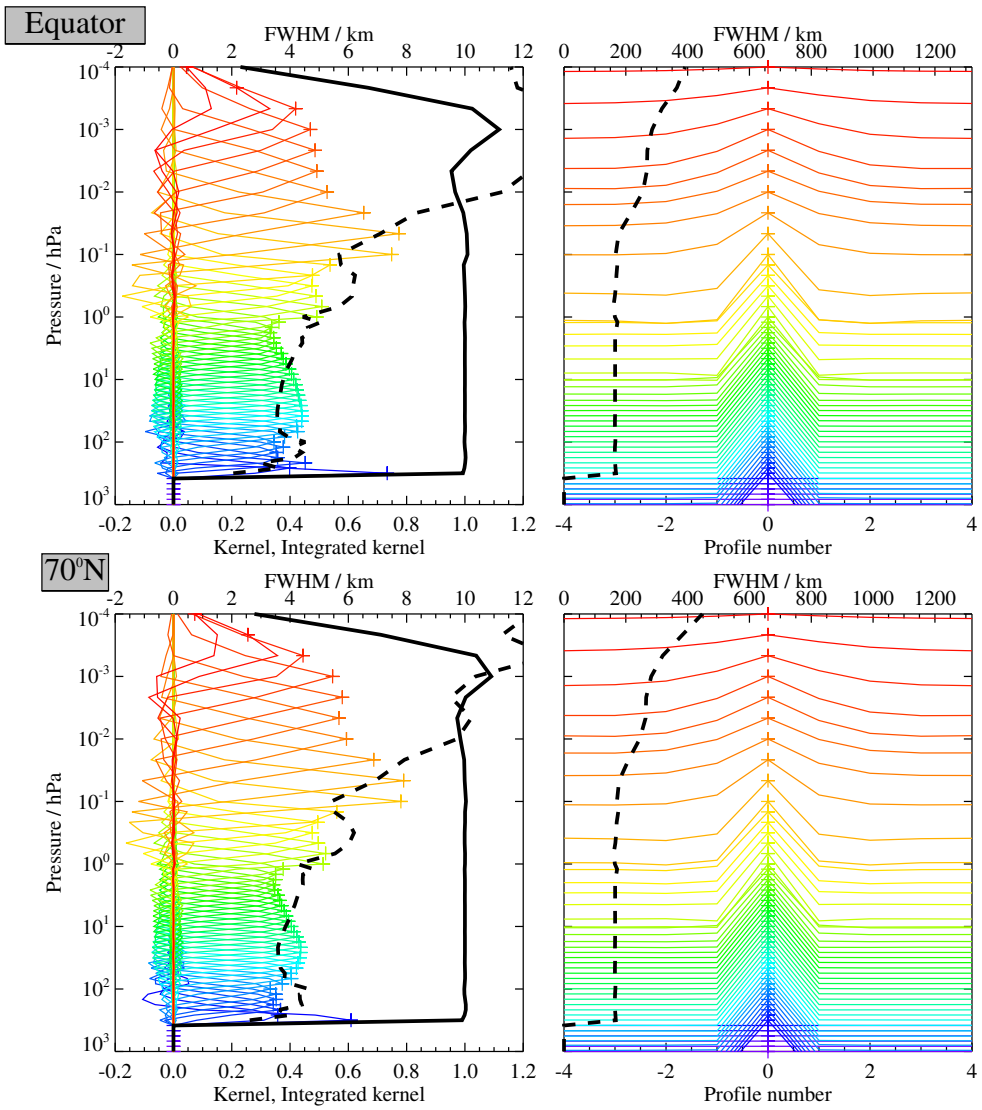

Figure 3.23.5: Typical two-dimensional (vertical and horizontal along-track) averaging kernels for the MLS v6.0*x* Temperature data at the equator (upper) and at 70°N (lower); variation in the averaging kernels is sufficiently small that these are representative of typical profiles. Colored lines show the averaging kernels as a function of MLS retrieval level, indicating the region of the atmosphere from which information is contributing to the measurements on the individual retrieval surfaces, which are denoted by plus signs in corresponding colors. The dashed black line indicates the resolution, determined from the full width at half maximum (FWHM) of the averaging kernels, approximately scaled into kilometers (top axes). (Left) Vertical averaging kernels (integrated in the horizontal dimension for five along-track profiles) and resolution. The solid black line shows the integrated area under each kernel (horizontally and vertically); values near unity imply that the majority of information for that MLS data point has come from the measurements, whereas lower values imply substantial contributions from a priori information. (Right) Horizontal averaging kernels (integrated in the vertical dimension) and resolution. The horizontal averaging kernels are shown scaled such that a unit averaging kernel amplitude is equivalent to a factor of 10 change in pressure.

estimated by the measurement system in the troposphere and lower stratosphere and a factor of ~1.4 larger from the middle stratosphere through the mesosphere.

3.23.5 Accuracy

A substantial study has been made of sources of systematic error in MLS v6.0*x* measurements, similar to that done as a part of the validation of MLS v5.0*x* and all previous versions back to v2.2*x*. Retrieval accuracy is estimated both by modeling the impact of uncertainties in measurement and retrieval parameters that could lead to systematic errors, and through comparisons of retrieved values with correlative data sets. The "modeled accuracy" column of Table 3.23.1 gives estimates from the propagation of parameter uncertainties, as discussed by *Schwartz et al.* [2008]. These combine estimates of sources of systematic uncertainty such as gain compression, spectroscopic parameters, retrieval numerics, and pointing. The resulting modeled accuracy estimates are ~2 K over most of the retrieval range, with spikes of 4 K at 3.16 hPa and 6 K at 0.1 hPa.

The "observed accuracy" column contains estimates of bias based upon comparisons with GEOS-5 and with other previously validated satellite-based measurements. A global average of those comparisons is shown in Figure 3.23.6 and is discussed in Section 3.23.8, below.

3.23.6 Data screening

Pressure range: 261–0.00046 hPa

Values outside this range are not recommended for scientific use.

Estimated precision: Only use values for which the estimated precision is a positive number.

Values where the a priori information has a strong influence are flagged with negative or zero precision and should not be used in scientific analyses (see Section 1.5).

Status flag: Only use profiles for which the `Status` field is an even number.

Odd values of `Status` indicate that the profile should not be used in scientific studies. See Section 1.6 for more information on the interpretation of the `Status` field.

Quality: Only use profiles with `Quality` greater than 0.2 for the 83 hPa level and smaller pressures, and profiles with `Quality` greater than 0.9 at 100 hPa and larger pressures. Profiles with `Quality` less than or equal to 0.9 comprise 1.4% of all data and 4.8% of profiles in the tropics.

Convergence: Only profiles whose `Convergence` field is less than 1.03 should be used.

This `Convergence` criterion rejects <0.1% of profiles, although chunks with convergence slightly over this target do not contain manifestly pathological profiles. The primary purpose of this criterion is to reject profiles with extremely poor convergence that may be expected to reflect poor retrieval behavior.

Cloud Screening: The "low cloud" bit of the temperature `Status` field does not contain useful information in v6.0*x*, so it cannot be used to screen temperature, in contrast with some earlier versions. Cloud impacts can instead largely be removed using the ice water content (IWC) product, rejecting profiles between 261–100 hPa for which the 215 hPa value of IWC is greater than 0.005 g/m^3. Implementation of this criteria requires loading the v6.0*x* IWC swath but accomplishes most of the rejection of cloud-induced outliers seen in Figure 3.23.4. This criterion removes 4.7% of UT profiles globally and 15% of profiles in the tropics (20°N–20°S).

Precision: The `L2gpPrecision` field can be used to further eliminate outliers that are believed to be the result of thick clouds, primarily in the tropics. If careful screening of the troposphere is required, levels 261–178 hPa should be avoided if any of the following criteria are met:

At 316 hPa: `L2gpPrecision` > 1.1 K **and** latitude > −60° (i.e., this rule only applies at latitudes north of 60°S)

At 261 hPa: `L2gpPrecision` > 0.7 K

At 215 hPa: `L2gpPrecision` > 0.825 K

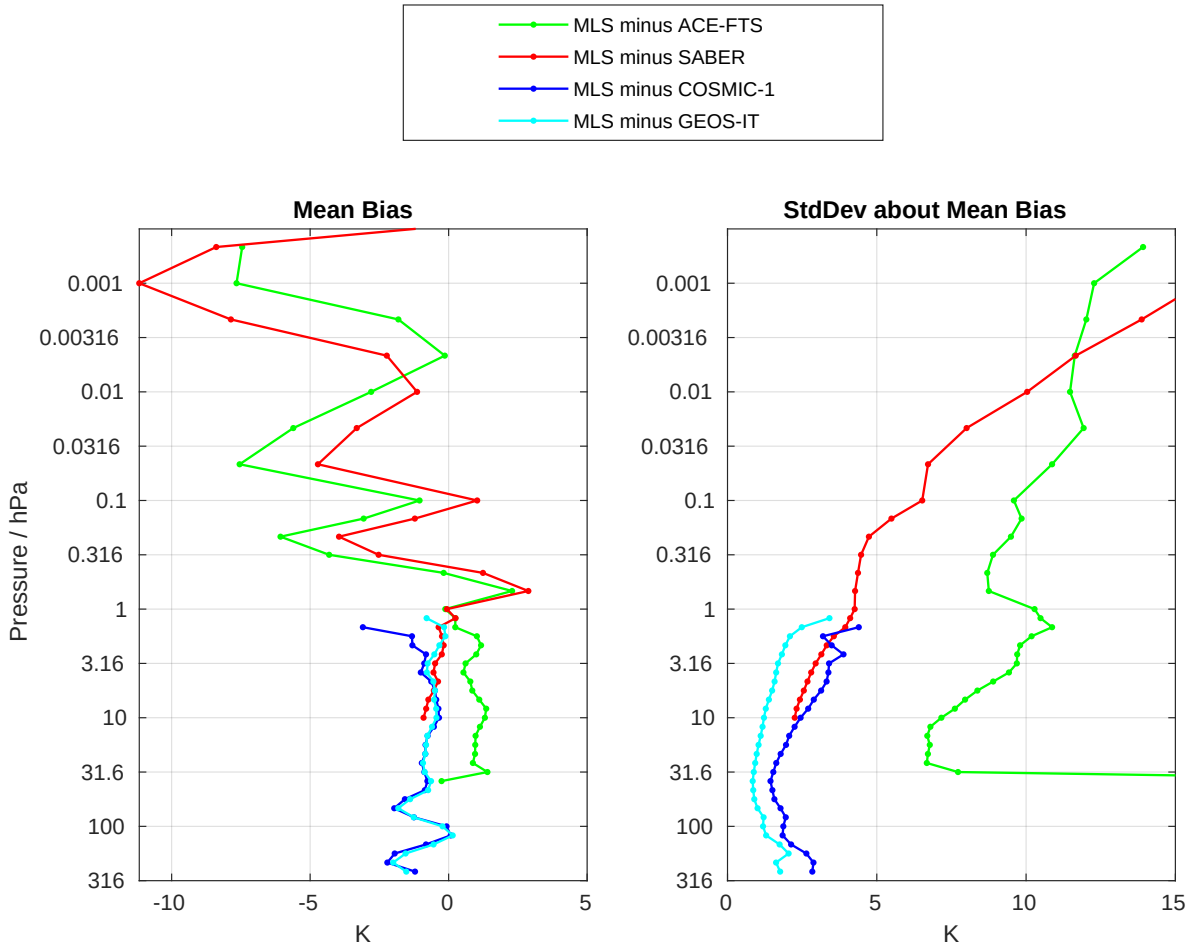

Figure 3.23.6: The left panel shows globally averaged mean differences between MLS temperature and four correlative data sets. ACE-FTS, SABER, and COSMIC-1 mean profiles are averages of pairs of coincident profiles, within 3 hours and 5 degrees of great circle from a corresponding MLS profile. Methods are described in detail by *Schwartz et al.* [2008]. The right panel shows the global standard deviations about the means.

3.23.7 Artifacts

Persistent vertically oscillating biases in v5.0*x* temperature with respect to analysis and correlative measurements have been greatly reduced in v6.0*x* in the stratosphere, but not completely eliminated in the lower stratosphere and upper troposphere. The impact of clouds is generally limited to tropospheric levels and to the tropics and, to a lesser extent, midlatitudes. After recommended screening, negative departures from a priori of greater than 10 K in the tropics (believed almost always to be cloud-induced artifacts) are seen in only 0.2% of tropical profiles. Flagging of clouds is discussed above. Further discussion of artifacts may be found in *Schwartz et al.* [2008].

3.23.8 Review of comparisons with other datasets

Schwartz et al. [2008] describe detailed comparisons of MLS v2.2*x* temperature with products from the Goddard Earth Observing System, version 5 [*Rienecker et al.*, 2007] (GEOS-5), the European Center for Medium-Range Weather Forecasts [e.g., *Simmons et al.*, 2005] (ECMWF), the CHAllenging Minisatellite Payload (CHAMP) [*Wickert et al.*, 2001], the combined Atmospheric Infrared Sounder / Advanced Microwave Sounding Unit (AIRS/AMSU), the Sounding of the Atmosphere using Broadband Radiometry (SABER) [*Mlynczak and Russell*, 1995], the Halogen Occultation Experiment [*Hervig et al.*, 1996] (HALOE), and the Atmospheric

Chemistry Experiment [*Bernath et al.*, 2005] (ACE), as well as to radiosondes from the global network. A similar validation effort is planned for v6.0*x* temperature, and this document will be updated with those results. Preliminary validation of v6.0*x* temperature has consisted of comparison with temperature from GEOS-5 and the Constellation Observing System for Meteorology, Ionsophere and Climate (COSMIC-1) [*Anthes et al.*, 2008] in the upper troposphere to the upper stratosphere and with SABER and ACE in the upper stratosphere, mesosphere, and lower thermosphere. Figure 3.23.6 shows the global-mean biases in the left panel and the 1σ scatter about the mean in the right panel for these comparisons. From 261 hPa to 68 hPa, MLS has a −2.5 K to 0 K vertically oscillating bias with respect to GEOS-5 and COSMIC-1, settling to a −0.5 K bias in the upper stratosphere. As was shown by *Schwartz et al.* [2008], there is generally agreement to ∼1 K between assimilation (ECMWF and GEOS-5) and AIRS, radiosondes, and radio-occultation instruments such as COSMIC-1 and CHAMP in the upper troposphere and stratosphere. Between 1 hPa and 0.001 hPa, MLS has generally consistent vertically oscillating biases with respect to SABER and ACE, with MLS-minus-SABER biases of +1 K to −5 K between 1 hPa and 0.01 hPa, increasing in magnitude to −10 K at 0.001 hPa. MLS-minus-ACE biases are ∼1 K more negative in the mesosphere and ∼2 K less negative in the lower thermosphere than MLS-minus-SABER biases.

Table 3.23.1: Summary of Aura MLS v6.0*x* Temperature Characteristics.

Pressure	Resolution[a] V × H	Single-Profile Precision	Observed Scatter[b]	Modeled accuracy	Observed accuracy	Comments
hPa	km	K	K	K	K	
<0.00022	—	—	—	—	—	Unsuitable for scientific use
0.00022	12 × 370	±4.8	—	—	—	Further validation needed. Generally not useful.
0.00046	13 × 316	±3.7	—	—	—	Further validation needed. Use with caution.
0.001	11.5 × 280	±3.5	±4.0	3.4	−9	
0.01	10.5 × 250	±3.2	±3.7	2.7	−2	
0.1	5.6 × 170	±2.1	±2.5	6.2	−1	
0.316	6.2 × 170	±1.0	±1.3	2.7	−4	
1	4.3 × 165	±1.0	±1.2	2.7	0	
3.16	4.3 × 165	±0.7	±1.0	4.2	−0.6	
10	3.8 × 165	±0.6	±0.9	2.3	−0.5	
14.7	3.7 × 165	±0.6	±0.9	2.1	−0.7	
31.6	3.6 × 165	±0.6	±0.8	1.8	−0.9	
56.2	3.7 × 165	±0.6	±0.8	2.1	−1.5	
100	4.6 × 165	±0.7	±1.3	2.5	−0.5	
215	3.3 × 165	±0.8	±2.3	1.9	−2.0	
261	3.8 × 167	±0.7	±3.3	2.5	−1.8	
1000–316	—	—	—	—	—	Unsuitable for scientific use

[a]Vertical and along-track horizontal resolutions; see text for a discussion of the (altitude dependent) cross-track horizontal resolution.

[b]Precision inferred from differences of individual profiles from successive orbits (v2.2*x* results shown)

Chapter 4
MLS Level 3 datasets

4.1 Introduction

The other chapters of this guide describe MLS "Level 2" data – geophysical products along the instrument observing track. This chapter describes MLS "Level 3" data – geophysical products binned onto regular grids. There is a wide array of techniques for transforming along-track observations into regular grids, including "kriging" approaches [e.g., *Cressie*, 2015], Fourier-series-based approaches [*Salby*, 1982], approaches using various windowing functions such as Hamming windows, and simple binning approaches. All methods have strengths and weaknesses, and the choice of which one to use is best made by the individual data user, based on the nature of the specific scientific question to be tackled. For this reason, until 2020, the MLS team had not produced any "official" Level 3 data products.

However, in order to facilitate certain studies by MLS data users, the MLS team is now producing and distributing a select set of Level 3 products derived using a straightforward "binning" approach (i.e., simply reporting the mean measured value within a given spatial/temporal "box"). As part of the generation of these data products, all the data screening rules described in Chapters 1 and 3 are applied (along with the ClO bias correction, see Section 3.6), providing a significant additional simplification to data users. Level 3 data are supplied for most MLS standard products. BrO and HO_2 are excluded, as they have a different Level 3 product available (see Sections 3.2 and 3.14). We also exclude CH_3CN and CH_3OH in light of the narrow range over which these products are recommended for scientific use.

Three sets of Level 3 products are provided:

Daily Binned Files: These are stored as one product per day of MLS data per file. The daily binned files contain the following datasets:

- Geodetic latitude and longitude maps on a pressure vertical coordinate (i.e., "3D" fields).
- Geodetic latitude and longitude maps on a potential-temperature vertical coordinate (i.e., "3D" fields).
- Geodetic latitude zonal means on a pressure vertical coordinate ("2D").
- Geodetic latitude zonal means on a potential-temperature vertical coordinate ("2D").
- Equivalent latitude[1] "zonal means" on a potential-temperature vertical coordinate ("2D").
- Vortex averages on a potential-temperature vertical coordinate ("1D").

Monthly Binned Files: These are stored as one product per year of MLS data per file. The monthly binned files contain the same datasets as the daily binned files, except with twelve monthly entries in each dataset instead of one daily one.

Zonal Mean Binned Files: These files contain "roll-ups" of all the datasets in the daily binned files, excluding the "3D" maps. These are provided with fields having 365 or 366 entries per dataset in each file.

For species with non-negligible diurnal variations over all or part of their vertical range (ClO, OH, HOCl, and O_3), the datasets described above are further subdivided into five different datasets containing:

- All valid profiles (as for all the non-diurnal products).

[1]Equivalent latitude is the geographical latitude that encloses the same area as an isoline of potential vorticity, giving a polar vortex-centered latitude [*Butchart and Remsberg*, 1986].

- All profiles measured on the ascending side of the orbit (mainly daytime observations, except in polar regions).
- All profiles measured on the descending side of the orbit (mainly nighttime observations, except in polar regions).
- All observations made with solar zenith angle less than 90° (i.e., daytime observations).
- All observations made with solar zenith angle greater than 110° (i.e., nighttime observations).

MERRA-2 [*Gelaro et al.*, 2017] reanalysis temperature fields (interpolated to each MLS observation point) are used to convert from pressure to potential temperature surfaces. Additionally MERRA-2 potential vorticity fields are used to construct equivalent latitude and vortex average information. The interpolated MERRA-2 fields used are taken from the MLS "Derived Meteorological Products" [*Manney et al.*, 2007, 2011]. Note that, for quantities on potential temperature surfaces, the MLS Level 3 profiles on pressure levels are first interpolated to the fixed potential temperature surfaces (from $\log[p]$ to $\log[\theta]$) before being binned (as opposed to directly binning Level 3 data points in potential temperature windows, which has the potential to introduce undesirable empty bins in the vertical). These interpolated values (and the interpolated `L2GPPrecision` field) are then used to construct all fields.

The vortex averages are defined using an altitude-dependent value of scaled potential vorticity (sPV) to demark the vortex edge. The values at each level are determined separately for each hemisphere, using the procedure described by *Lawrence et al.* [2018] wherein a constant sPV for each hemisphere and season is derived based on the climatological sPV value at the location of the maximum high-latitude sPV gradient. While there are numerous methods of estimating the location of the vortex edge, this simple method with a value that is constant in time has been shown to avoid some common pitfalls, such as large spurious day-to-day changes in vortex area and inappropriate values at the beginning and end of the cold season [see *Lawrence and Manney*, 2018, for a discussion of pros and cons of various vortex edge identification methods]. To estimate uncertainties in vortex edge definition, and to provide results for studies where more or less conservative estimates of the vortex edge are desirable, averages are also provided for "outer" and "inner" vortex edge values that are 0.2×10^{-4}s^{-1} less and more, respectively, than the determined value for the vortex edge "center" [this also follows *Lawrence et al.*, 2018].

4.2 Level 3 data files

Two different temporal resolutions of Level 3 data are provided—daily (`L3DB`) and monthly (`L3MB`). The `L3DB` files are one file per day per Level 3 data product (with one time entry in each dataset in the file), and the `L3MB` files are one file per year per Level 3 data product (with twelve time entries in each dataset in the file). Both of these files contain latitude × longitude grids, zonal means, and polar vortex averages on various vertical coordinates, as described in Section 4.1, above. To aid in the analysis of long-term datasets, the additional `L3DZ` files are a yearly rollup of all of the `L3DB` datasets except for the latitude × longitude grids, which are not included for file size considerations. The datasets in `L3DZ` files contain 365 or 366 time entries as appropriate. The filenames for these products use the following conventions, which differ mainly in the date format:

`MLS-Aura_L3DB-<product>_v04-20-c01_<yyyy>d<ddd>.nc`
`MLS-Aura_L3MB-<product>_v04-20-c01_<yyyy>.nc`
`MLS-Aura_L3DZ-<product>_v04-20-c01_<yyyy>.nc`
`MLS-Aura_L3MB-<product>_v04-20-c01_<yyyy>m<mm>.nc` (Mid-year forward processing only)
`MLS-Aura_L3DZ-<product>_v04-20-c01_<yyyy>m<mm>.nc` (Mid-year forward processing only)

Where
`<product>` is the MLS standard product: `CO`, `O3`, `Temperature`, etc.
`<yyyy>` is the four-digit year
`<ddd>` is a three-digit day of year (`001` = 1 January)
`<mm>` is an optional two-digit month for monthly files.

Files using the two-digit month will only be available during their current calendar year, as "forward processing" data are gathered; they will contain all data in the year up to and including the quoted month, with the remaining date entries present but consisting of values marked "bad" (i.e., with the netCDF `_FillValue`). Once all months are available, the complete dataset will be stored in the "`<yyyy>`" files.

Within each file, the datasets are stored in netCDF4 groups. The `L3DB` and `L3MB` files contain six types of datasets: latitude × longitude grids on both pressure and potential temperature vertical coordinates, zonal means on both pressure and potential temperature vertical coordinates, means within equivalent latitude contours on potential temperature surfaces, and polar vortex averages as a function of potential temperature. As noted above, the `L3DZ` files omit the latitude × longitude maps.

These datasets are named as follows (where `<product>` is the same as listed in the filename):

`<product> PressureGrid:`	4°×5° geodetic latitude × longitude grid on pressure surfaces (`L3DB` and `L3MB` only)
`<product> ThetaGrid:`	4°×5° geodetic latitude × longitude grid on potential temperature surfaces (`L3DB` and `L3MB` only)
`<product> PressureZM:`	4° geodetic latitude zonal mean on pressure surfaces
`<product> ThetaZM:`	4° geodetic latitude zonal mean on potential temperature surfaces
`<product> EqLZM:`	4° equivalent latitude zonal mean on potential temperature surfaces
`<product> VortexAvg:`	Polar vortex average values for each hemisphere on potential temperature surfaces. The values are calculated in accordance with the "outer", "center", and "inner" vortex edge criteria documented in *Lawrence et al.* [2018].

Diurnal product files have all of these groups repeated for day, night, ascending profiles only, and descending profiles only (with `Day`, `Night`, `Asc`, `Desc`, respectively, added to the group name).

Each group contains the following data fields:

`lon:`	The longitude at the center of the grid cell (`PressureGrid` and `ThetaGrid` groups only)
`lon_bnds:`	The longitude at the boundaries of the grid cell (`PressureGrid` and `ThetaGrid` groups only)
`lat:`	The latitude at the center of the grid cell
`lat_bnds:`	The latitude at the boundaries of the grid cell
`time:`	The date of the grid cell (days since 1950-01-01)
`time_bnds:`	The boundaries of the time period (days since 1950-01-01)
`lev:`	The vertical coordinate (i.e., pressure/potential temperature values)
`value:`	The average value for each bin
`nvalues:`	The number of valid data points found in each bin
`rms_uncertainty:`	The root mean square of all the Level 2 `L2GPPrecision` values that contributed to each bin (note that this has *not* been divided by $\sqrt{\texttt{nvalues}}$)
`minimum:`	The minimum value in each bin
`maximum:`	The maximum value in each bin
`std_dev:`	The standard deviation of the data in each bin

4.3 Guidance for users of Level 3 data

As discussed above, these Level 3 products are generated using only the Level 2 data points that meet all the screening criteria described in the earlier chapters of this document, providing a significant simplification for users. In cases where there are no good Level 2 data available to populate a Level 3 data point, the `nvalues`

field is set to zero and the other data fields are set to the `_FillValue` (bad data flag) for the given netCDF variables.

When considering Level 3 data, as with every geophysical measurement, attention should be paid to the associated uncertainties. The averaging inherent in generating Level 3 data will act to reduce "precision"-related errors, those due to random noise in the MLS radiance measurements, by $1/\sqrt{n}$, where n is the number of Level 2 data points in the average (which is given by the `nvalues` field). We have chosen not to divide by $\sqrt{n}$ in the files in order to make it easier for users who wish to perform further averaging. For example, when creating weekly averages from the daily L3 data, the final precision can be computed as the root mean square of the daily precisions divided by the square root of the total of the daily `nvalues` entries.

In contrast, the "accuracy"-related errors, those due to biases in the MLS measurement system, will in most cases be propagated through the averaging process unchanged and should be assumed to apply to the Level 3 values in the same manner as they do to the values in the underlying Level 2 datasets.

Appendix A
Embedded data files

In part to comply with journal requirements for data availability and also to help assure long-term preservation of key datasets beyond the lifetime of the MLS project, selected data files are embedded in the PDF file for this document. Not all PDF readers support the file-extraction capability. At the time of writing, the "Adobe Reader" software provides the needed functionality. File extraction can be accomplished through a "right click" (or some similar action, such as "option-click") on the 🖫 icons below and selecting the "Save Embedded File to Disk…" option.

At the time of writing, all the datasets embedded herein are also available from the MLS website at `https://mls.jpl.nasa.gov/eos-aura-mls/data-products/averaging-kernels`. They are also available from Zenodo at `https://zenodo.org/records/18988586`.

A.1 Averaging kernels

The averaging kernels described in Section 1.8 can be extracted using the icons in the table below.

	70°S	35°S	Equator	35°N	70°N
1D kernels	🖫	🖫	🖫	🖫	🖫
2D kernels	🖫	🖫	🖫	🖫	🖫

A.2 ClO bias correction

Per the discussion in Section 3.6, biases in lower-stratospheric ClO can be corrected to first order by subtracting the values given in this file 🖫. The file is also available from the MLS website at `https://mls.jpl.nasa.gov/data/MLS-Aura_ClO-BiasCorrection_v06.txt` and from Zenodo at `https://zenodo.org/records/18988847`.

Appendix B References

Anthes, R. A., D. Ector, D. C. Hunt, Y.-H. Kuo, C. Rocken, W. S. Schreiner, S. V. Sokolovskiy, S. Syndergaard, T.-K. Wee, et al. The COSMIC/FORMOSAT-3 mission: Early results. *Bull. Amer. Meteorl. Soc.*, 89(3):313–333. doi: 10.1175/bams-89-3-313. 2008.

Bernath, P. D. et al. Atmospheric Chemistry Experiment (ACE): mission overview. *Geophys. Res. Lett.*, 32:L15S01. doi: 10.1029/2005gl022386. 2005.

Buehler, S. A. and N. Courcoux. The impact of temperature errors on perceived humidity supersaturation. *Geophys. Res. Lett.*, 30(14). doi: 10.1029/2003gl017691. 2003.

Butchart, N. and E. E. Remsberg. The area of the stratospheric vortex as a diagnostic for tracer transport on an isentropic surface. *J. Atmos. Sci.*, 43:1319–1339. 1986.

Cofield, R. and P. Stek. Design and field-of-view calibration of 114–660-GHz optics of the Earth Observing System Microwave Limb Sounder. *IEEE Trans. Geosci. Remote Sens.*, 44(5):1166–1181. doi: 10.1109/tgrs.2006.873234. 2006.

Craig, C., K. Stone, D. Cuddy, S. Lewicki, P. Veefkind, P. Leonard, A. Fleig, and P. Wagner. HDF-EOS Aura file format guidelines. Technical report, National Center For Atmospheric Research. 2003.

Cuddy, D. T., M. Echeverri, P. A. Wagner, A. Hanzel, and R. A. Fuller. EOS MLS science data processing system: A description of architecture and capabilities. *IEEE Trans. Geosci. Remote Sens.*, 44(5):1192–1198. 2006.

Filipiak, M. J., N. J. Livesey, and W. G. Read. Precision estimates for the geophysical parameters measured by EOS MLS. Technical report, University of Edinburgh, Department of Meteorology. doi: 10.5067/aura/mls/doc/atbd.04. URL `https://zenodo.org/records/15547506`. 2004.

Froidevaux, L., Y. B. Jiang, A. Lambert, N. J. Livesey, W. G. Read, J. W. Waters, E. V. Browell, J. W. Hair, M. A. Avery, et al. Validation of Aura Microwave Limb Sounder stratospheric and mesospheric ozone measurements. *J. Geophys. Res.: Atmos.*, 113:D15S20. doi: 10.1029/2007jd008771. 2008a.

Froidevaux, L., Y. B. Jiang, A. Lambert, N. J. Livesey, W. G. Read, J. W. Waters, R. A. Fuller, T. P. Marcy, P. J. Popp, et al. Validation of Aura Microwave Limb Sounder HCl measurements. *J. Geophys. Res.: Atmos.*, 113(D15):D15S25. doi: 10.1029/2007jd009025. 2008b.

Froidevaux, L., D. E. Kinnison, M. L. Santee, L. F. Millán, N. J. Livesey, W. G. Read, C. G. Bardeen, J. J. Orlando, and R. A. Fuller. Upper stratospheric ClO and HOCl trends (2005–2020): Aura Microwave Limb Sounder and model results. *Atmos. Chem. Phys.*, 22(7):4779–4799. doi: 10.5194/acp-22-4779-2022. 2022.

Froidevaux, L., D. E. Kinnison, R. Wang, J. Anderson, and R. A. Fuller. Evaluation of CESM1 (WACCM) free-running and specified dynamics atmospheric composition simulations using global multispecies satellite data records. *Atmos. Chem. Phys.*, 19(7):4783–4821. doi: 10.5194/acp-19-4783-2019. 2019.

Fujinawa, T., T. O. Sato, T. Yamada, S. Nara, Y. Uchiyama, K. Takahashi, N. Yoshida, and Y. Kasai. Validation of acetonitrile (CH_3CN) measurements in the stratosphere and lower mesosphere from the SMILES instrument on the International Space Station. *Atmos. Meas. Tech.*, 13:2119–2129. doi: 10.5194/amt-13-2119-2020. 2020.

Gelaro, R., W. McCarty, M. J. Suárez, R. Todling, A. Molod, L. Takacs, C. A. Randles, A. Darmenov, M. G. Bosilovich, et al. The Modern-Era Retrospective Analysis for Research and Applications, Version 2 (MERRA-2). *J. Climate*, 30(14):5419–5454. doi: 10.1175/jcli-d-16-0758.1. 2017.

Harrison, J. J. and P. F. Bernath. ACE-FTS observations of acetonitrile in the lower stratosphere. *Atmos. Chem. Phys.*, 13:7405–7413. 2013.

Hervig, M. E., J. M. Russell III, L. L. Gordley, S. R. Drayson, K. Stone, R. E. Thompson, M. E. Gelman, I. S. McDermid, A. Hauchecorne, et al. Validation of temperature measurements from the Halogen Occultation Experiment. *J. Geophys. Res.: Atmos.*, 101(10):10 277–10,286. 1996.

Hubert, D., J.-C. Lambert, T. Verhoelst, J. Granville, A. Keppens, J.-L. Baray, A. E. Bourassa, U. Cortesi, D. A. Degenstein, et al. Ground-based assessment of the bias and long-term stability of 14 limb and occultation ozone profile data records. *Atmos. Meas. Tech.*, 9(6):2497–2534. doi: 10.5194/amt-9-2497-2016. 2016.

Hurst, D. F., W. G. Read, H. Vömel, H. B. Selkirk, K. H. Rosenlof, S. M. Davis, E. G. Hall, A. F. Jordan, and S. J. Oltmans. Recent divergences in stratospheric water vapor measurements by frost point hygrometers and the Aura Microwave Limb Sounder. *Atmos. Meas. Tech.*, 9(9):4447–4457. doi: 10.5194/amt-9-4447-2016. 2016.

Jarnot, R. F., V. S. Perun, and M. J. Schwartz. Radiometric and spectral performance and calibration of the GHz bands of EOS MLS. *IEEE Trans. Geosci. Remote Sens.*, 44(5):1131–1143. 2006.

Jiang, Y. B., L. Froidevaux, A. Lambert, N. J. Livesey, W. G. Read, J. W. Waters, B. Bojkov, T. Leblanc, I. S. McDermid, et al. Validation of the Aura Microwave Limb Sounder ozone by ozonesonde and lidar measurements. *J. Geophys. Res.: Atmos.*, 112:D24S34. doi: 10.1029/2007jd008776. 2007.

Khosravi, M., P. Baron, J. Urban, L. Froidevaux, A. I. Jonsson, Y. Kasai, K. Kuribayashi, C. Mitsuda, D. P. Murtagh, et al. Diurnal variation of stratospheric and lower mesospheric HOCl, ClO and HO_2 at the equator: comparison of 1-D model calculations with measurements by satellite instruments. *Atmos. Chem. Phys.*, 13(15):7587–7606. doi: 10.5194/acp-13-7587-2013. 2013.

Khosrawi, F., S. Lossow, G. P. Stiller, K. H. Rosenlof, J. Urban, J. P. Burrows, R. P. Damadeo, P. Eriksson, M. García-Comas, et al. The SPARC water vapour assessment II: comparison of stratospheric and lower mesospheric water vapour time series observed from satellites. *Atmos. Meas. Tech.*, 11(7):4435–4463. doi: 10.5194/amt-11-4435-2018. 2018.

Kiefer, M., D. F. Hurst, G. P. Stiller, S. Lossow, H. Vömel, J. Anderson, F. Azam, J.-L. Bertaux, L. Blanot, et al. The SPARC water vapour assessment II: biases and drifts of water vapour satellite data records with respect to frost point hygrometer records. *Atmos. Meas. Tech.*, 16(19):4589–4642. doi: 10.5194/amt-16-4589-2023. 2023.

Kleinböhl, A., G. C. Toon, B. Sen, J.-F. L. Blavier, D. K. Weisenstein, and P. O. Wennberg. Infrared measurements of atmospheric CH_3CN. *Geophys. Res. Lett.*, 32:L23807. doi: 10.1029/2005gl024283. 2005.

Kovalenko, L. J., N. L. Livesey, R. J. Salawitch, C. Camy-Peyret, M. P. Chipperfield, R. E. Cofield, M. Dorf, B. J. Drouin, L. Froidevaux, et al. Validation of Aura Microwave Limb Sounder BrO observations in the stratosphere. *J. Geophys. Res.: Atmos.*, 112(D24). doi: 10.1029/2007jd008817. 2007.

Kramarova, N. A., P. K. Bhartia, G. Jaross, L. Moy, P. Xu, Z. Chen, M. DeLand, L. Froidevaux, N. Livesey, et al. Validation of ozone profile retrievals derived from the OMPS LP version 2.5 algorithm against correlative satellite measurements. *Atmos. Meas. Tech.*, 11(5):2837–2861. doi: 10.5194/amt-11-2837-2018. 2018.

Lambert, A., W. G. Read, N. J. Livesey, M. L. Santee, G. L. Manney, L. Froidevaux, D. L. Wu, M. J. Schwartz, H. C. Pumphrey, et al. Validation of the Aura Microwave Limb Sounder stratospheric water vapor and nitrous oxide measurements. *J. Geophys. Res.: Atmos.*, 112(D24):D24S36. doi: 10.1029/2007jd008724. 2007.

Lawrence, Z. D. and G. L. Manney. Characterizing stratospheric polar vortex variability with computer vision techniques. *J. Geophys. Res.: Atmos.*, 123(3):1510–1535. doi: 10.1002/2017jd027556. 2018.

Lawrence, Z. D., G. L. Manney, and K. Wargan. Reanalysis intercomparisons of stratospheric polar processing diagnostics. *Atmos. Chem. Phys.*, 18(18):13547–13579. doi: 10.5194/acp-18-13547-2018. 2018.

Lee, J. N. and D. L. Wu. Solar cycle modulation of nighttime ozone near the mesopause as observed by MLS. *Earth & Space Sci.*, 7(4). doi: 10.1029/2019ea001063. 2020.

Livesey, N. J., M. J. Filipiak, L. Froidevaux, W. G. Read, A. Lambert, M. L. Santee, J. H. Jiang, J. W. Waters, R. E. Cofield, et al. Validation of Aura Microwave Limb Sounder O_3 and CO observations in the upper troposphere and lower stratosphere. *J. Geophys. Res.: Atmos.*, 113:D15S02. doi: 10.1029/2007jd008805. 2008.

Livesey, N. J. and W. G. Read. Direct retrieval of line-of-sight atmospheric structure from limb sounding observations. *Geophys. Res. Lett.*, 27(6):891–894. doi: 10.1029/1999gl010964. 2000.

Livesey, N. J., W. G. Read, L. Froidevaux, A. Lambert, G. L. Manney, H. C. Pumphrey, M. L. Santee, M. J. Schwartz, S. Wang, et al. EOS MLS version 3.3 and 3.4 Level 2 data quality and description document. Technical report, Jet Propulsion Laboratory. Available from https://mls.jpl.nasa.gov/. 2013.

Livesey, N. J., W. G. Read, L. Froidevaux, A. Lambert, M. L. Santee, M. J. Schwartz, L. F. Millán, R. F. Jarnot, P. A. Wagner, et al. Investigation and amelioration of long-term instrumental drifts in water vapor and nitrous oxide measurements from the Aura Microwave Limb Sounder (MLS) and their implications for studies of variability and trends. *Atmos. Chem. Phys.*, 21(20):15409–15430. doi: 10.5194/acp-21-15409-2021. 2021.

Livesey, N. J., W. G. Read, P. A. Wagner, L. Froidevaux, A. Lambert, G. L. Manney, L. F. M. Valle, H. C. Pumphrey, M. L. Santee, et al. EOS MLS version 4.2x Level 2 data quality and description document (revision e). Technical report, Jet Propulsion Laboratory. URL `https://mls.jpl.nasa.gov/eos-aura-mls/data-documentation`. 2020.

Livesey, N. J., W. G. Read, P. A. Wagner, L. Froidevaux, A. Lambert, M. L. Santee, M. J. Schwartz, A. Lambert, L. F. M. Valle, et al. EOS MLS version 5.0x Level 2 and 3 data quality and description document (revision b). Technical report, Jet Propulsion Laboratory. URL `https://mls.jpl.nasa.gov/eos-aura-mls/data-documentation`. 2022.

Livesey, N. J. and W. V. Snyder. EOS MLS retrieval processes algorithm theoretical basis. Technical report, Jet Propulsion Laboratory. doi: 10.5067/aura/mls/doc/atbd.03. URL `https://zenodo.org/records/15547464`. D-16159. 2004.

Livesey, N. J., W. V. Snyder, W. G. Read, and P. A. Wagner. Retrieval algorithms for the EOS Microwave Limb Sounder (MLS). *IEEE Trans. Geosci. Remote Sens.*, 44(5):1144–1155. doi: 10.1109/tgrs.2006.872327. 2006.

Livesey, N. J., J. W. Waters, R. Khosravi, G. P. Brasseur, G. S. Tyndall, and W. G. Read. Stratospheric CH_3CN from the UARS Microwave Limb Sounder. *Geophys. Res. Lett.*, 28(5):779–782. doi: 10.1029/2000gl012144. 2001.

Lossow, S., F. Khosrawi, M. Kiefer, K. A. Walker, J.-L. Bertaux, L. Blanot, J. M. Russell, E. E. Remsberg, J. C. Gille, et al. The SPARC water vapour assessment II: profile-to-profile comparisons of stratospheric and lower mesospheric water vapour data sets obtained from satellites. *Atmos. Meas. Tech.*, 12(5):2693–2732. doi: 10.5194/amt-12-2693-2019. 2019.

Lossow, S., F. Khosrawi, G. E. Nedoluha, F. Azam, K. Bramstedt, J. P. Burrows, B. M. Dinelli, P. Eriksson, P. J. Espy, et al. The SPARC water vapour assessment II: comparison of annual, semi-annual and quasi-biennial variations in stratospheric and lower mesospheric water vapour observed from satellites. *Atmos. Meas. Tech.*, 10(3):1111–1137. doi: 10.5194/amt-10-1111-2017. 2017.

Mahieu, E., M. P. Chipperfield, J. Notholt, T. Reddmann, J. Anderson, P. F. Bernath, T. Blumenstock, M. T. Coffey, S. S. Dhomse, et al. Recent Northern Hemisphere stratospheric HCl increase due to atmospheric circulation changes. *Nature*, 515(7):104–107. doi: 10.1038/nature13857. 2014.

Manney, G. L., W. H. Daffer, J. M. Zawodny, P. F. Bernath, K. W. Hoppel, K. A. Walker, B. W. Knosp, C. Boone, E. E. Remsberg, et al. Solar occultation satellite data and derived meteorological products: Sampling issues and comparisons with Aura Microwave Limb Sounder. *J. Geophys. Res.: Atmos.*, 112(D24):D24S50. doi: 10.1029/2007jd008709. 2007.

Manney, G. L., M. I. Hegglin, W. H. Daffer, M. L. Santee, E. A. Ray, S. Pawson, M. J. Schwartz, C. D. Boone, L. Froidevaux, et al. Jet characterization in the upper troposphere/lower stratosphere (UTLS): Applications to climatology and transport studies. *Atmos. Chem. Phys.*, 11:6115–6137. doi: 10.5194/acp-11-6115-2011. 2011.

Millán, L., N. Livesey, W. Read, L. Froidevaux, D. Kinnison, R. Harwood, I. A. Mackenzie, and M. P. Chipperfield. New Aura Microwave Limb Sounder observations of BrO and implications for Br_y. *Atmos. Meas. Tech.*, 5(7):1741–1751. doi: 10.5194/amt-5-1741-2012. 2012.

Millán, L., M. L. Santee, A. Lambert, N. J. Livesey, F. Werner, M. J. Schwartz, H. C. Pumphrey, Y. Wang, G. L. Manney, et al. Hunga Tonga-Hunga Ha'apai hydration of the stratosphere. *Geophys. Res. Lett.*, 49(13). doi: 10.1029/2022gl099381. 2022.

Millán, L., S. Wang, N. Livesey, D. Kinnison, H. Sagawa, and Y. Kasai. Stratospheric and mesospheric HO_2 observations from the Aura Microwave Limb Sounder. *Atmos. Chem. Phys.*, 15(5):2,889–2,902. doi: 10.5194/acp-15-2889-2015. 2015.

Millán, L., W. G. Read, M. L. Santee, A. Lambert, G. L. Manney, J. L. Neu, M. C. Pitts, F. Werner, N. J. Livesey, et al. The evolution of the Hunga hydration in a moistening stratosphere. *Geophys. Res. Lett.*, 51(19). doi: 10.1029/2024gl110841. 2024.

Mlynczak, M. and J. M. Russell, III. An overview of the SABER experiment for the TIMED mission. *NASA Langley Research Center, Optical Remote Sensing of the Atmosphere*, 2. 1995.

Nair, P. J., S. Godin-Beekmann, L. Froidevaux, L. E. Flynn, J. M. Zawodny, J. M. I. Russell, A. Pazmino, G. Ancellet, W. Steinbrecht, et al. Relative drifts and stability of satellite and ground-based stratospheric ozone profiles at NDACC lidar stations. *Atmos. Meas. Tech.*, 5(6):1301–1318. doi: 10.5194/amt-5-1301-2012. 2012.

Niemeier, U., S. Wallis, C. Timmreck, T. van Pham, and C. von Savigny. How the Hunga Tonga–Hunga Ha'apai water vapor cloud impacts its transport through the stratosphere: Dynamical and radiative effects. *Geophysical Research Letters*, 50(24). doi: 10.1029/2023gl106482. 2023.

Pickett, H. M. Microwave Limb Sounder THz Module on Aura. *IEEE Trans. Geosci. Remote Sens.*, 44(5):1122–1130. 2006.

Pickett, H. M., B. J. Drouin, T. Canty, L. J. Kovalenko, R. J. Salawitch, N. J. Livesey, W. G. Read, J. W. Waters, K. W. Jucks, et al. Validation of Aura MLS HO_x measurements with remote-sensing balloon instruments. *Geophys. Res. Lett.*, 33(1):L01808. doi: 10.1029/2005gl024048. 2006a.

Pickett, H. M., B. J. Drouin, T. Canty, R. J. Salawitch, R. A. Fuller, V. S. Perun, N. J. Livesey, J. W. Waters, R. A. Stachnik, et al. Validation of Aura Microwave Limb Sounder OH and HO_2 measurements. *J. Geophys. Res.: Atmos.*, 113(D16):D16S30. doi: 10.1029/2007jd008775. 2008.

Pickett, H. M., W. G. Read, K. K. Lee, and Y. L. Yung. Observation of night OH in the mesosphere. *Geophys. Res. Lett.*, page L19808. doi: 10.1029/2006gl026910. 2006b.

Pumphrey, H. C., M. J. Filipiak, N. J. Livesey, M. J. Schwartz, C. Boone, K. A. Walker, P. Bernath, P. Ricaud, B. Barret, et al. Validation of middle-atmosphere carbon monoxide retrievals from the Microwave Limb Sounder on Aura. *J. Geophys. Res.: Atmos.*, 112:D24S38. doi: 10.1029/2007jd008723. 2007.

Pumphrey, H. C., C. J. Jimenez, and J. W. Waters. Measurement of HCN in the middle atmosphere by EOS MLS. *Geophys. Res. Lett.*, 33(8):L08804. doi: 10.1029/2005gl025656. 2006.

Pumphrey, H. C., W. G. Read, N. J. Livesey, and K. Yang. Observations of volcanic SO_2 from MLS on Aura. *Atmos. Meas. Tech.*, 8(1):195–209. doi: 10.5194/amt-8-195-2015. 2015.

Read, W. G., A. Lambert, J. Bacmeister, R. E. Cofield, D. T. Cuddy, W. H. Daffer, B. J. Drouin, E. Fetzer, L. Froidevaux, et al. EOS Aura Microwave Limb Sounder upper tropospheric and lower stratospheric humidity validation. *J. Geophys. Res.: Atmos.*, 112:D24S35. doi: 10.1029/2007jd008752. 2007.

Read, W. G., Z. Shippony, M. J. Schwartz, N. J. Livesey, and W. V. Snyder. The clear-sky unpolarized forward model for the EOS Microwave Limb Sounder (MLS). *IEEE Trans. Geosci. Remote Sens.*, 44(5):1367–1379. doi: 10.1109/tgrs.2006.873233. 2006.

Read, W. G., Z. Shippony, and W. V. Snyder. Microwave Limb Sounder forward model algorithm theoretical basis document. Technical report, Jet Propulsion Laboratory. doi: 10.5067/aura/mls/doc/atbd.05. URL `https://zenodo.org/records/15547533`. JPL D-18130. 2004.

Read, W. G., G. Stiller, S. Lossow, M. Kiefer, F. Khosrawi, D. Hurst, H. Vömel, K. Rosenlof, B. M. Dinelli, et al. The SPARC Water Vapor Assessment II: assessment of satellite measurements of upper tropospheric humidity. *Atmos. Meas. Tech.*, 15(11):3377–3400. doi: 10.5194/amt-15-3377-2022. 2022.

Rienecker, M. M., M. J. Suarez, R. Todling, J. Bacmeister, L. Takacs, H.-C. Liu, W. Gu, M. Sienkiewicz, R. D. Koster, et al. The GEOS-5 data assimilation system: A documentation of GEOS-5.0. Technical report, NASA. TM-104606, Technical report series on Global Modeling and Data Assimilation. 2007.

Rodgers, C. D. Retrieval of atmospheric temperature and composition from remote measurements of thermal radiation. *Rev. Geophys.*, 14(4):609–624. 1976.

Rodgers, C. D. *Inverse Methods for Atmospheric Science, Theory and Practice*. World Scientific. 2000.

Rodgers, C. D. and B. J. Connor. Intercomparison of remote sounding instruments. *J. Geophys. Res.: Atmos.*, 108(D3):4116. doi: 10.1029/2002jd002299. 2003.

Santee, M. L., A. Lambert, W. G. Read, N. J. Livesey, R. E. Cofield, D. T. Cuddy, W. H. Daffer, B. J. Drouin, L. Froidevaux, et al. Validation of the Aura Microwave Limb Sounder HNO_3 measurements. *J. Geophys. Res.: Atmos.*, 112:D24S40. doi: 10.1029/2007jd008721. 2007.

Santee, M. L., A. Lambert, W. G. Read, N. J. Livesey, G. L. Manney, R. E. Cofield, D. T. Cuddy, W. H. Daffer, B. J. Drouin, et al. Validation of the Aura Microwave Limb Sounder ClO measurements. *J. Geophys. Res.: Atmos.*, 113:D15S22. doi: 10.1029/2007jd008762. 2008.

Santee, M. L., N. J. Livesey, G. L. Manney, and W. G. Read. Methyl chloride from the Aura Microwave Limb Sounder: First global climatology and assessment of variability in the upper troposphere and stratosphere. *J. Geophys. Res.: Atmos.*, 118:13,532–13,560. doi: 10.1002/2013jd020235. 2013.

Schwartz, M. J., A. Lambert, G. L. Manney, W. G. Read, N. J. Livesey, L. Froidevaux, C. O. Ao, P. F. Bernath, C. D. Boone, et al. Validation of the Aura Microwave Limb Sounder temperature and geopotential height measurements. *J. Geophys. Res.: Atmos.*, 113:D15S11. doi: 10.1029/2007jd008783. 2008.

Schwartz, M. J., W. G. Read, and W. V. Snyder. Polarized radiative transfer for Zeeman-split oxygen lines in the EOS MLS forward model. *IEEE Trans. Geosci. Remote Sens.*, 44(5):1182–1190. 2006.

Schwartz, M. J., W. V. Synder, and W. G. Read. MLS mesosphere-specific forward model algorithm theoretical basis document. Technical report, Jet Propulsion Laboratory. doi: 10.5067/aura/mls/doc/atbd.07. URL `https://zenodo.org/records/15547668`. JPL D-28534. 2004.

Simmons, A., M. Hortal, G. Kelly, A. McNally, A. Untch, and S. Uppala. ECMWF analyses and forecasts of stratospheric winter polar vortex breakup: September 2002 in the southern hemisphere and related events. *J. Atmos. Sci.*, 62(3):668–689. 2005.

Singh, H. B., L. Salas, D. Herlth, R. Kolyer, E. Czech, W. Viezee, Q. Li, D. J. Jacob, D. Blake, et al. In situ measurements of HCN and CH_3CN over the Pacific Ocean: Source, sinks and budgets. *J. Geophys. Res.: Atmos.*, 108(D20):8795. doi: 10.1029/2002hd003006. 2003.

Stauffer, R. M., A. M. Thompson, D. E. Kollonige, D. W. Tarasick, R. Van Malderen, H. G. J. Smit, H. Vömel, G. A. Morris, B. J. Johnson, et al. An examination of the recent stability of ozonesonde global network data. *Earth and Space Science*, 9(10). doi: 10.1029/2022ea002459. 2022.

Tegtmeier, S., M. I. Hegglin, J. Anderson, A. Bourassa, S. Brohede, D. Degenstein, L. Froidevaux, R. Fuller, B. Funke, et al. SPARC Data Initiative: A comparison of ozone climatologies from international satellite limb sounders. *J. Geophys. Res.: Atmos.*, 118(2):12229. doi: 10.1002/2013jd019877. 2013.

Tinney, E. N. and W. J. Randel. Characterizing variability and vertical structure of water vapor in the extratropical lower stratosphere. *Atmos. Chem. Phys. Discus.*, In review. doi: 10.5194/egusphere-2026-412. 2026.

von Clarmann, T., N. Glatthor, U. Grabowski, M. Höpfner, S. Kellmann, A. Linden, G. M. Tsidu, M. Milz, T. Steck, et al. Global stratospheric HOCl distributions retrieved from infrared limb emission spectra recorded by the Michelson Interferometer for Passive Atmospheric Sounding (MIPAS). *J. Geophys. Res.: Atmos.*, 111:D05311. doi: 10.1029/2005jd005939. 2006.

Wang, S., H. M. Pickett, T. J. Pongetti, R. Cheung, Y. L. Yung, C. Shim, Q. Li, T. Canty, R. J. Salawitch, et al. Validation of Aura Microwave Limb Sounder OH measurements with Fourier Transform Ultra-Violet Spectrometer total OH column measurements at Table Mountain, California. *J. Geophys. Res.: Atmos.*, 113:D22301. doi: 10.1029/2008jd009883. 2008.

Waters, J. W., L. Froidevaux, R. S. Harwood, R. F. Jarnot, H. M. Pickett, W. G. Read, P. H. Siegel, R. E. Cofield, M. J. Filipiak, et al. The Earth Observing System Microwave Limb Sounder (EOS MLS) on the Aura satellite. *IEEE Trans. Geosci. Remote Sens.*, 44(5):1075–1092. doi: 10.1109/tgrs.2006.873771. 2006.

Waters, J. W., L. Froidevaux, R. F. Jarnot, W. G. Read, H. M. Pickett, R. S. Harwood, R. E. Cofield, M. J. Filipiak, D. A. Flower, et al. An overview of the EOS MLS experiment. Technical report, Jet Propulsion Laboratory. doi: 10.5067/aura/mls/doc/atbd.01. URL `https://zenodo.org/records/15547343`. D-15745. 2004.

Waters, J. W., W. G. Read, L. Froidevaux, R. F. Jarnot, R. E. Cofield, D. A. Flower, G. K. Lau, H. M. Pickett, M. L. Santee, et al. The UARS and EOS Microwave Limb Sounder (MLS) experiments. *J. Atmos. Sci.*, 56:194–217. doi: 10.1175/1520-0469(1999)056<0194:tuaeml>2.0.co;2. 1999.

Werner, F., N. J. Livesey, M. J. Schwartz, W. G. Read, M. L. Santee, and G. Wind. Improved cloud detection for the Aura Microwave Limb Sounder (MLS): training an artificial neural network on colocated MLS and Aqua MODIS data. *Atmos. Meas. Tech.*, 14(12):7749–7773. doi: 10.5194/amt-14-7749-2021. 2021.

Wickert, J., C. Reigber, G. Beyerle, R. Konig, C. Marquardt, T. Schmidt, L. Grunwaldt, R. Galas, T. Meehan, et al. Atmosphere sounding by GPS radio occultation: First results from CHAMP. *Geophys. Res. Lett.*, 28(17):3263–3266. 2001.

Wu, D. L., R. Austin, S. Durden, A. Heymsfield, J. H. Jiang, A. Lambert, J. Li, N. J. Livesey, G. McFarquhar, et al. Comparison of global cloud ice from MLS, CloudSat and correlative data sets. *J. Geophys. Res.: Atmos.*, 113:D00A24. doi: 10.1029/2008jd009946. 2009.

Wu, D. L. and J. H. Jiang. EOS MLS algorithm theoretical basis for cloud measurements. Technical report, Jet Propulsion Laboratory. doi: 10.5067/aura/mls/doc/atbd.06. URL `https://zenodo.org/records/15547619`. JPL D-19299. 2004.

Wu, D. L., J. H. Jiang, and C. P. Davis. Aura MLS cloud ice measurements and cloudy-sky radiative transfer model. *IEEE Trans. Geosci. Remote Sens.*, 44(5):1156–1165. 2006.

Wu, D. L., J. H. Jiang, W. G. Read, R. T. Austin, C. P. David, A. Lambert, G. L. Stephens, D. G. Vane, and J. W. Waters. Validation of Aura MLS cloud Ice Water Content (IWC) measurements. *J. Geophys. Res.: Atmos.*, 113:D15S10. doi: 10.1029/2007ld008931. 2008.

Zhang, S., J. Chen, J. S. Wright, S. M. Davis, J. Gao, P. Konopka, N. Li, M. Lu, S. Tegtmeier, et al. Covariability of dynamics and composition in the asian monsoon tropopause layer from satellite observations and reanalysis products. *Atmos. Chem. Phys.*, 25(17):10109–10139. doi: 10.5194/acp-25-10109-2025. 2025.